AWARD NUMBER: W81XWH-16-1-0448

TITLE: Translational Significance of p53 Loss of Heterozygosity in Breast Cancer

PRINCIPAL INVESTIGATOR: Natalia Marchenko

CONTRACTING ORGANIZATION: Stony Brook University

Stony Brook, NY 11794-3362

REPORT DATE: DECEMBER 2021

TYPE OF REPORT: Final progress report

PREPARED FOR: U.S. Army Medical Research and Development Command

Fort Detrick, Maryland 21702-5012

REPORT DOCUMENTATION PAGE

Form Approved
OMB No. 0704-0188

1. REPORT DATE	2. REPORT TYPE	3. DATES COVERED
DECEMBER 2021	Final progress report	1 SEPT 2016 - 31 AUG 2021

4. TITLE AND SUBTITLE

Translational Significance of p53 Loss of Heterozygosity in Breast Cancer

5a. CONTRACT NUMBER
W81XWH-16-1-0448

5b. GRANT NUMBER
BC151569

5c. PROGRAM ELEMENT NUMBER

6. AUTHOR(S)

Natalia Marchenko

Email: Natalia.marchenko@stonybrookmedicine.edu

5d. PROJECT NUMBER

5e. TASK NUMBER

5f. WORK UNIT NUMBER

7. PERFORMING ORGANIZATION NAME(S) AND ADDRESS(ES)

Stony Brook University
Department of Pathology
W5510 Melville Library
Stony Brook, NY 11794-3362

8. PERFORMING ORGANIZATION REPORT NUMBER

9. SPONSORING / MONITORING AGENCY NAME(S) AND ADDRESS(ES)

U.S. Army Medical Research and Development Command
Fort Detrick, Maryland 21702-5012

10. SPONSOR/MONITOR'S ACRONYM(S)

11. SPONSOR/MONITOR'S REPORT NUMBER(S)

12. DISTRIBUTION / AVAILABILITY STATEMENT

Approved for Public Release; Distribution Unlimited

13. SUPPLEMENTARY NOTES

14. ABSTRACT Mutations in one allele of the TP53 gene in early stages are frequently followed by the loss of the remaining wild-type p53 (wtp53) allele (p53LOH) during tumor progression. Despite the strong notion of p53LOH as a critical step in tumor progression, its oncogenic outcomes that facilitate the selective pressure for p53LOH occurrence were not elucidated. Using MMTV;ErbB2 mouse model of breast cancer carrying heterozygous R172H p53 mutation, we identified a novel gain-of-function (GOF) activity of mutant p53 (mutp53): the exacerbated loss of wtp53 allele in response to γ-irradiation. We show that wild-type p53 allele is partially transcriptionally competent and enables the maintenance of the genomic integrity under normal conditions in mutp53 heterozygous cells. In heterozygous cells γ-irradiation promotes mutp53 stabilization, which suppresses DNA repair and the cell cycle checkpoint allowing cell cycle progression in the presence of inefficiently repaired DNA, consequently increasing genomic instability leading to p53LOH. Hence, in mutp53 heterozygous cells, irradiation facilitates the selective pressure for p53LOH that enhances cancer cell fitness and provides the genetic plasticity for acquiring metastatic properties. As consequences of p53LOH in mutp53 heterozygous cells, we observed profound stabilization of mutp53 protein, the loss of p21 expression, upregulation of mTOR pathway, the abrogation of G2/M checkpoint, chromosomal instability, centrosome amplification, and transcriptional upregulation of mitotic kinase Nek2 involved in the regulation of centrosome function. To avoid the mitotic catastrophe in the absence of G2/M checkpoint, cells with centrosome amplification adapt Nek2-mediated centrosomes clustering as pro-survival mutp53 GOF mechanism enabling unrestricted proliferation and clonal expansion of cells with p53LOH. Thus, the clonal dominance of mutp53 cells with p53LOH may represent the mechanism of irradiation-induced p53LOH.

15. SUBJECT TERMS
p53 loss of heterozygosity is a critical prerequisite for mutant p53 stabilization and oncogenic activity

16. SECURITY CLASSIFICATION OF:			17. LIMITATION OF ABSTRACT	18. NUMBER OF PAGES	19a. NAME OF RESPONSIBLE PERSON
a. REPORT	b. ABSTRACT	c. THIS PAGE			USAMRDC
Unclassified	Unclassified	Unclassified	Unclassified	144	19b. TELEPHONE NUMBER *(include area code)*

Standard Form 298 (Rev. 8-98)
Prescribed by ANSI Std. Z39.18

Table of Contents

Page

1. INTRODUCTION:

Breast cancer is one of the leading causes of death in women worldwide. Currently, radiation therapy, coupled with breast-conserving surgery is the standard of care for the majority of breast cancer patients. However, a meta-analysis showed that radiation reduces 15-year breast cancer mortality risk only by 5%. At present, 30% of all breast cancer cases are considered to be overtreated by the administration of more aggressive therapies than is necessary or by overdiagnosis, where no treatment is required. An estimated one to three deaths from overtreatment occur for every one breast cancer death avoided [1]. Hence, the understanding of how to reliably identify which breast cancer patients will benefit from radiotherapy is needed to reduce the mortality risk and improve the quality of life.

Mutations in TP53 (p53) gene are common in breast cancer and are especially enriched in Her2 (human EGF receptor 2, ErbB2) positive breast cancer (72%) [2], and basal-like breast cancer (80%) [2]. Whereas wild-type p53 (wtp53) is an important determinant of the efficacy of DNA-damaging therapies, the p53 mutational status is not routinely used for cancer management. This is mainly due to inconsistent results of clinical studies [3], conceivably because in previous studies the predictive effect of p53 status in response to genotoxic modalities has not been assessed at the different stages and in the context of p53 heterozygosity. In some cancers, mutant p53 (mutp53) status was shown to predict poor patient outcome in response to genotoxic treatment. A prospective clinical trial in the early stages of non–small-cell lung cancer revealed that chemotherapy shortens the survival of patients with dual TP53/KRAS mutations, but not wild-type TP53/mutKRAS patients, compared to untreated cohorts [4], whereas other studies showed a better response of mutp53 tumors to chemotherapies [5]. Thus, knowing how mutp53 interacts with the specific oncogenic environment in the context of conventional therapies will facilitate the clinical utilization of the mutational status of p53.

Clinical data suggest that p53 behaves as a classic “two-hit” tumor suppressor where a point mutation in one allele of p53 at early stages is followed by loss of the wild-type allele (loss of heterozygosity (LOH)) later during tumor progression [6]. Albeit mutp53 in heterozygosity may exert dominant-negative (DN) effect [7], several *in vivo* studies showed that wtp53 retains its function in heterozygous tumors [8]. In support, ~80% of advanced-stage mutp53 breast cancer tumors have lost the wtp53 allele suggesting the high selective pressure for p53LOH during tumor progression [9]. These studies raise the question of why mutp53 exerts DN in some contexts, but not others, and what is the clinical relevance of these findings?

To address these questions, we generated MMTV-ErbB2 and mutp53 R172H (H thereafter) knock-in mouse model that faithfully recapitulates human Her2-positive breast cancer [10]. We found that wtp53 retains its transcriptional activity in both p53-/+;ErbB2 and p53H/+;ErbB2 heterozygous cancer cells. However, irradiation of premalignant mammary lesions aggravates mammary tumorigenesis that is associated with increased frequency of p53LOH mostly in mutp53 heterozygous mice. We propose that in response to irradiation, mutp53, via activation of several oncogenic pathways (mTOR, Nek2),

generates the selective pressure for wtp53 loss in heterozygous cells that is fueled by inactivation of ATM signaling and deficient DNA repair. Thus, p53LOH in the presence of mutp53 allele enhances cancer cell fitness, provides the genetic plasticity for acquiring metastatic properties that enables tumor progression.

2. KEYWORDS: p53, mutant p53, ErbB2, Her2, breast cancer, loss of heterozygosity (LOH), radiation, chemotherapy, Her2 positive breast cancer.

3. ACCOMPLISHMENTS:

The major goals of the project.

Major Task 1. Determine the effect of DNA-damaging therapeutics on p53 LOH and tumorigenesis in ErbB2-driven mutp53 mammary tumors in vivo (100% completion).

Subtask 1. Define the physiological consequences of p53 LOH in ErbB2-driven mammary tumorigenesis. Analyze histopathology, the ErbB2/HSF1 signaling by IHC and Western in the established collection of mammary tumors from irradiated and non-irradiated mice with different p53 LOH status.

Subtask 2. Evaluate the effect of different p53 mutations on p53 LOH in ErbB2-driven mammary tumorigenesis. Test whether similar to R172H, R248Q mutant p53 allele aggravates mammary tumorigenesis compared to p53 null counterparts and promotes p53 LOH after irradiation.

Subtask 3. Assess the effect of irradiation of established mutp53;ErbB2 tumors on p53 LOH (neoadjuvant setting). Test whether irradiation of established tumors induces LOH and accelerates mammary tumorigenesis in R172H/+;ErbB2 mice. (50%completion)

Local IRB/IACUC approval (100% completion)

HRPO/ACURO approval (100% completion)

Major Task 2. Mechanistically assess the physiological consequences of p53 LOH in heterozygous mutp53 mammary cells *in vitro.* (100% completion)

Subtask 1. Examine the frequency and time of p53 LOH onset in the existing collection of cell culture of primary mammary epithelial cells and mammary tumors culture derived from mice with different p53 genotypes. Serial

passaging of R172H/+ErbB2 vs p53-/+;ErbB2 vs p53+/+;ErbB2 MECs and mammary tumors cultured cells.

Subtask 2. Test the effect of irradiation on the frequency and time of p53 LOH onset in primary mammary epithelial cells (MECs) and mammary tumors culture derived from mice with different p53 genotypes. Serial passaging of R172H/+;ErbB2 vs p53-/+;ErbB2 vs p53+/+;ErbB2 MECs and mammary tumors cultured cells after single dose of irradiation *in vitro* at passage 1.

Subtask 3. Correlate the p53 LOH status of R172H/+;ErbB2 vs p53-/+;ErbB2 vs p53+/+;ErbB2 MECs and mammary tumors cultured cells with cellular properties (proliferation, chemoresistance, allografts) and with biochemical characteristics.

Major Task 3. Determine whether p53 LOH promotes metastatic behavior in ErbB2 cancer cells. (50% completion)

Subtask 1. Establish whether p53 LOH enhances the motility and invasion of cancer cells *in vitro*.
Test the motility and invasive properties of primary mammary epithelial cells and tumor cultures derived from H/+;ErbB2 and p53-/+;ErbB2 mice before and after LOH *in vitro*. Boyden chamber assay, wound healing assay, metastases in allografts.

Subtask 2. Determine whether p53 LOH enhances the ability of tumor cells to metastasize *in vivo.* Isolate metastatic cells from lungs of irradiated and non-irradiated of R172H/+;ErbB2 vs p53-/+;ErbB2 vs p53+/+;ErbB2 mice. Assess p53 LOH status in metastases in comparison with primary tumors.

Major Task 1. Determine the effect of DNA-damaging therapeutics on p53 LOH and tumorigenesis in ErbB2-driven mutp53 mammary tumors in vivo. (100% completion)

Subtask 1. Define the physiological consequences of p53 LOH in ErbB2-driven mammary tumorigenesis. Analyze histopathology, the mutp53/ErbB2/HSF1 signaling by IHC and Western in the established collection of mammary tumors from irradiated and non-irradiated mice with different p53 LOH status.

1.1 Loss of heterozygosity is required for missense mutant p53 stabilization and GOF in vivo.

The translational significance of tumor-specific stabilization of mutant p53 was established previously. The purpose of this subtask is to 1) comprehensively evaluate mutant p53 protein levels in mammary tumors with regard to p53 LOH status; 2) correlate the mutant p53 levels/LOH status with physiological outcomes.

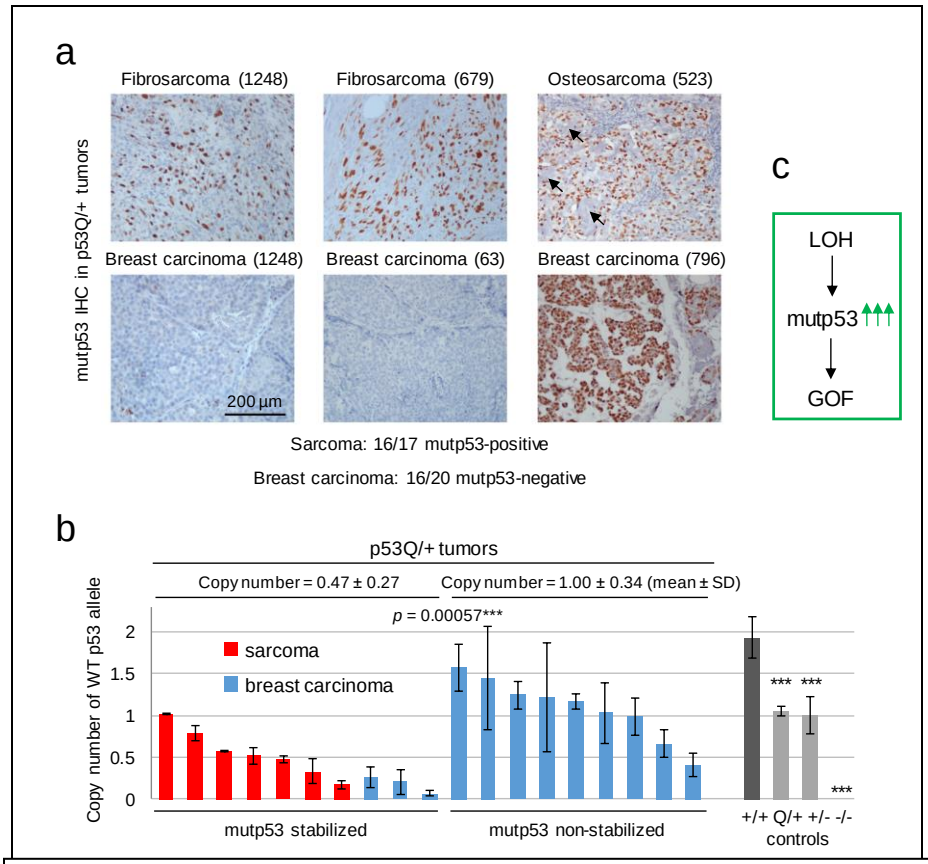

First, we evaluated the consequences of spontaneous LOH that occurs in the absence of genotoxic treatments. We analyzed histopathology and p53 IHC staining in non-irradiated tumors with the respect to p53 LOH status. For these experiments, we utilized the newly generated R248Q;Neu mouse model. We crossed the heterozygous breast cancer hotspot mutant p53 allele R248Q ('p53Q/+') with the MMTV-Neu ('Neu') mice expressing additional wild-type ErbB2 copies selectively in the mammary gland. Surprisingly, histopathological analysis revealed that about half of p53Q/+;Neu

Fig.1 Loss of wtp53 allele is required for missense mutant p53 stabilization and GOF. (a) The vast majority of sarcomas (16/17 cases, 94%) have stabilized mutp53. In contrast, the majority of breast carcinomas (16/20 cases, 80%) do not. Immunohistochemistry for mutp53. Mouse identity in parentheses. Arrows indicate the osteoid in osteosarcoma. (b) Analysis of wtp53 copy number in sarcomas and breast carcinomas of p53Q/+;Neu mice by quantitative genotyping. Tumors with mutp53 stabilization (all sarcomas and three breast cancers tested) have significantly higher LOH than tumors without mutp53 stabilization (majority of breast cancers). Note, as sarcomas have highnormal stroma contamination (top, blue mutp53-negative stromal cells, which do not have LOH), the actual LOH in sarcomas is most likely even higher because of dilution of the tumor genotype, causing LOH underestimation. For the same reason, copy numbers of the two highest sarcoma cases (two left red bars) are likely inflated. The wtp53 signal was normalized to the Rosa26 signal. Tail biopsies from p53+/+ (two wt alleles), p53Q/+, p53−/+ (one wt allele) and p53−/− mice (no wt alleles) were used as normal control tissues without LOH. Bars represent mean±S.D. of two technical replicas of individual cases. ***Po0.001. (c) Schematic diagram of the proposed mechanism for mutp53 stabilization and GOF in heterozygous tumors. Loss of the wtp53 allele (LOH) causes accumulation of highly stabilized mutp53 protein, which triggers tumor development and is the principle mechanism and prerequisite of GOF

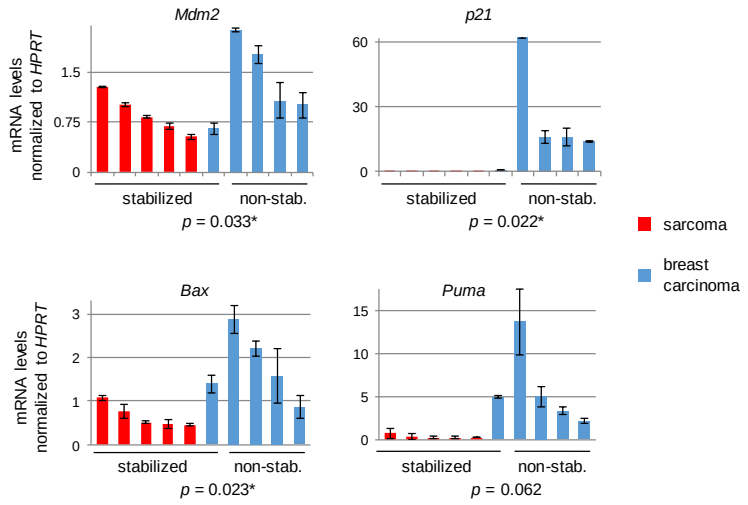

and p53− /+;Neu mice did not develop breast cancer but instead developed osteosarcomas and fibrosarcomas, which originate from mesenchymal tissues where MMTV-Neu is not expressed. This data suggests that presence of one mutp53 Q allele is sufficient to drive tumorigenesis even in the absence of ErbB2 in tissues of the mesenchymal origin. Strikingly, IHC analysis of tumors revealed mutp53 stabilization in nearly all

Fig.2 Real-time qPCR analysis of wtp53 target genes Mdm2, p21, Bax and Puma shows that their expression is largely decreased in samples with mutp53 stabilization

examined sarcomas (94%, 16/17), but only in rare breast carcinomas (20%, 4/20), even within the same animal (Figure 1a, e.g., animal #1248). Our previous work has established that a high level of mutant p53 in cancer cells is essential for its oncogenic activity. Thus, we asked whether mutant p53 stabilization in sarcomas is the result of wtp53LOH and whether sarcomas are more prone to p53 LOH than breast tumors. Indeed, qPCR of genomic DNA showed that p53 spontaneous LOH occurs in all sarcomas, but is less frequent in breast cancer (Fig. 1b). Moreover, the few breast tumors that did stabilize mutp53 also underwent p53 spontaneous LOH. Together, this strongly suggests that LOH is a critical prerequisite for mutp53 stabilization in cancer cells (Fig.1c). Importantly, LOH and its related stabilization of mutant p53 protein strongly correlate with the tumor onset and survival. We observed the oncogenic effect of mutant p53 only in sarcomas, where LOH and stabilization of mutant p53 are more profound that in breast carcinomas. Sarcoma onset is faster in p53Q/+;Neu compared with p53− /+;Neu mice (Fig. 3a).

The stability of mutant and wt p53 is maintained by Mdm2, p53-specific E3 ligase, which itself is the transcriptional target of wtp53. Hence, the low level of mutant p53 protein in heterozygous mammary tumors, most likely, is attributed to the transcriptional activity of wt53. There is a strong notion in the field, that in heterozygosity mutant p53 inactivates wtp53 via the dominant-negative mechanism. To test this idea in our model, we analyzed p53 target genes in tumors as a readout for the remaining wtp53 allele activity (Fig. 2). Indeed, all tumors with stabilized mutp53, including the single 'outlier' breast cancer tested, had reduced or undetectable Mdm2 and p21 levels, respectively, and sarcomas also had reduced Bax and Puma expression correlating with their LOH. Hence, our data suggest that in heterozygosity wt p53 retains its transcriptional activity and its tumor-suppressive function. While induced and/or spontaneous LOH would lead to complete loss of wtp53 function, the manifestation of mutant p53 gain-of-function (GOF) and, thus, augment tumor progression. First, we assessed mutp53 protein level through systematic IHC analysis of mammary tumors from irradiated and non-irradiated mice.

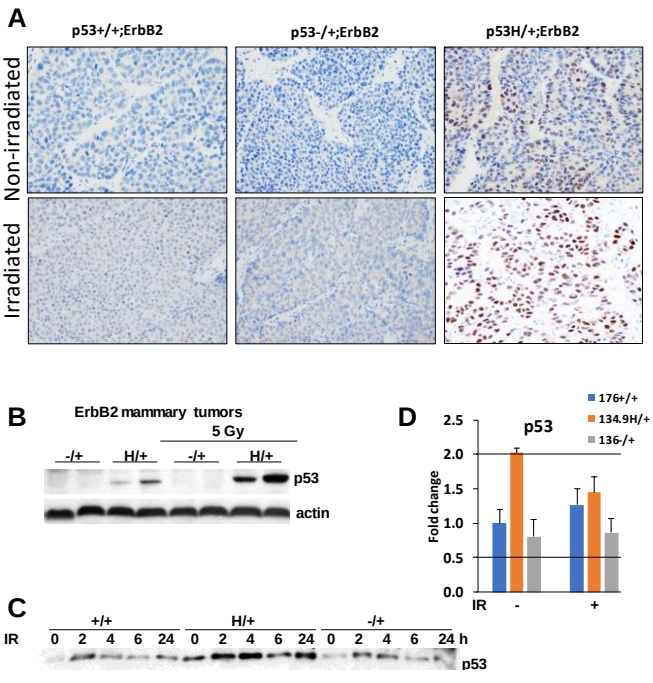

Fig. 3 Irradiation induces the accumulation of mutant p53 protein in heterozygous cancer cells. (A) The increase in p53LOH in H/+;ErbB2 mammary tumors are associated with the stabilization of mutp53 after irradiation of premalignant lesions, while irradiation did not affect wtp53 levels in +/+;ErbB2 and -/+;ErbB2 tumors. Representative images of p53 IHC of mammary tumors with indicated genotypes that were non-irradiated (upper panels) and irradiated (lower panels).4 tumors per genotype were analyzed. (B) irradiation stabilizes mutp53 protein in mutp53 heterozygous tumors, but not in -/+;ErbB2 tumors. Western blot 16h after irradiation *in vivo*. (C) wtp53 in +/+;ErbB2 cells was only transiently upregulated at 2h post-irradiation (9Gy), mutp53 shows much higher and continuous stabilization in H/+;ErbB2 cells. (D) No increase in p53 RNA was found in H/+;ErbB2 cells after irradiation *in vitro*. QRT-PCR.

1.2 Irradiation induces the accumulation of mutant p53 protein in heterozygous cancer cells.

Next, we tested whether our results on R248Q p53 mutant are reproducible for R172H p53 mutation in MMTV;ErbB2 mouse model. R172H mutation in murine p53 corresponds R175H mutation in humans and is highly prevalent in human ErbB2 positive breast cancer [2]. As radiotherapy is the most common genotoxic modality in human breast cancer, we tested the oncogenic function of R172/H (H thereafter) and driving forces for p53 LOH in the context of γ-irradiation. Consistent with our previous study on R248Q;MMTV-Neu mouse model[9], we found only 10-15% of p53 positive cells in H/+;ErbB2 mammary tumors, while no p53 staining was detected in p53-/+;ErbB2 and +/+;ErbB2 tumors (Fig. 3A, upper panel). The increase in p53LOH in H/+;ErbB2 mammary tumors was associated with stabilization of mutp53 after irradiation of premalignant lesions (Fig. 3A, lower panel). Conversely, irradiation did not affect wtp53 levels in +/+;ErbB2 and -/+;ErbB2 tumors (Fig. 3A, lower panel). As mutp53 stabilization in tumors was proposed to be essential for its oncogenic function [11], p53LOH with subsequent mutp53 stabilization may represent a key event in cancer progression *in vivo*.

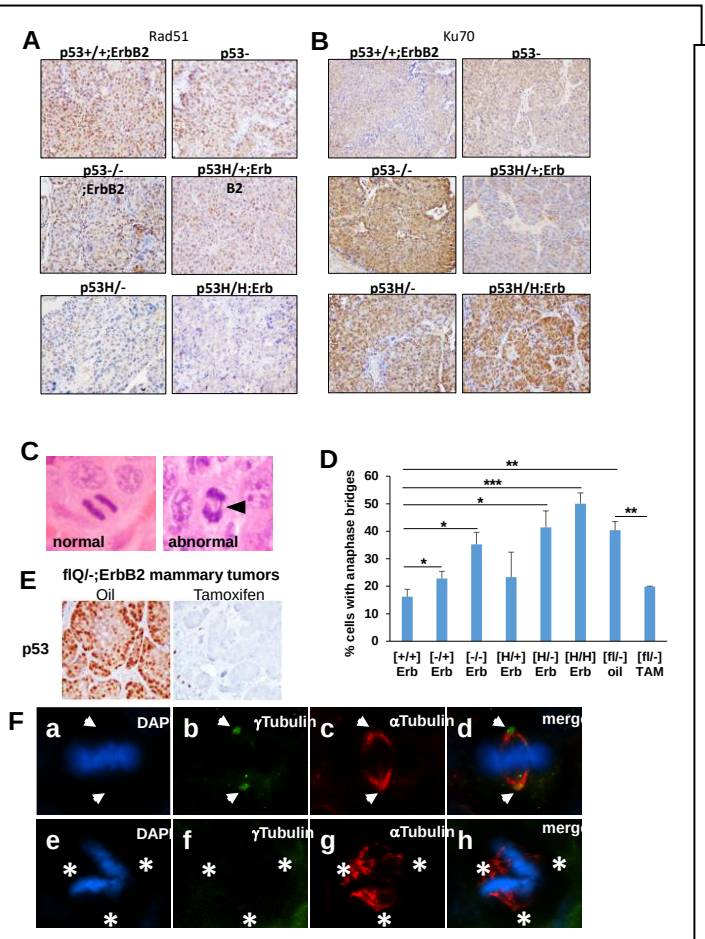

Fig.4 P53LOH is associated with the switch from homologous recombinational repair (HRR) to nonhomologous end joining (NHEJ) and genomic instability.

(A) Rad51(marker for HRR) IHC in ErbB2 mammary tumors of mice with indicated p53 genotypes. (B) Ku70 (a marker for NHEJ) in ErbB2 mammary tumors of mice with indicated p53 genotypes. Four mammary tumors per genotype were stained. Representative images. (C) H&E staining of normal anaphase showing the segregating masses of chromosomes and bridging (arrow) between the segregating masses of chromosomes during anaphase. (D) p53 IHC staining in the tumor from flR248Q/-;ErbB2 mouse injected with oil or following the depletion of p53 in the tumor from flR248Q/-;ErbB2 mouse after tamoxifen injection. The scale bars in A-D represent 50 μm. (E) Quantification of anaphase bridges (AB) in ErbB2 mammary tumors of mice with indicated p53 genotypes. N=3-4 tumors per genotype. *=p<0.05; **=p<0.01; ***=p<0.001. (F) Staining for mitotic spindles in a mitotic cell (metaphase) in p53H/-;ErbB2 mouse mammary tumor (a and e). Nuclear staining (DAPI), (b and f) centrosomes (γ-Tubulin), (c and g) mitotic spindles (α-Tubulin), (d and h) merge. (a-d) a mitotic cell with normal (2) spindle poles and 2 centrosomes. (e-h) a mitotic cell with no centrosomes (acentrosomal) and abnormal (>2) spindle poles. Arrows point to the position of the centrosomes in the mitotic cell. Asterisks indicate the 3 directions of the pull of the acentrosomal spindle poles.

To understand how irradiation affects mutp53 protein levels in heterozygosity, H/+;ErbB2 and -/+;Erbb2 mice were irradiated or not at the time of tumor onset (tumor volume-1cm^3). Western blot of tumors

16h after irradiation revealed that irradiation stabilizes mutp53 protein in heterozygous tumors significantly higher than wtp53, as p53 in -/+;ErbB2 tumors remained undetectable (Fig. 3B). Likewise, murine mammary tumor cell lines show different kinetic of wtp53 and mutp53 stabilization following irradiation (9Gy). While wtp53 in +/+;ErbB2 cells was only transiently upregulated at 2h post-irradiation, mutp53 shows much higher and continuous stabilization in H/+;ErbB2 cells (Fig. 3C).

As the previous study has shown upregulation of mutp53 RNA in response to genotoxic anthracyclines in human cell lines[12], we analyzed p53 mRNA in cells with different genotypes before and after irradiation. We found no increase in p53 RNA in H/+;ErbB2 cells (Fig. 3D), suggesting post-transcriptional regulation of mutp53 protein levels in heterozygosity in response to irradiation. Collectively our data led us to hypothesize that in heterozygous cells, irradiation stabilizes mutp53 over the threshold, which is sufficient to promote its oncogenic activities leading to p53LOH and tumor progression. Therefore, independently of the type of p53 mutation (R172H and R248Q) and tissue of origin (mammary epithelial or mesenchymal) LOH-mediated stabilization of mutp53 protein over threshold necessary for gain-of-function activity represents one of the major oncogenic outcome of p53LOH.

1.3 P53LOH is associated with the switch from HRR to NHEJ and genomic instability.

Mutp53 was shown to elicit its GOF activities through various mechanisms, including the hallmark of cancer cells- genomic instability. Genomic instability, such as chromosomal rearrangement caused mainly by failure in normal chromosome segregation during mitosis, has been regarded as one of the major causes of LOH in cancer [13, 14]. Mutations in a number of genes, e.g., p53 and PI3K, hinder normal mitosis leading to chromosomal aberrations [13]. Alternatively, the accumulation of various oncogenic mutations during cancer progression can be a result of inefficient DNA repair. Therefore, we assessed two major DNA repair mechanisms in ErbB2 mammary tumors with various p53 genotypes.

Wtp53 is activated in response to genotoxic treatments, eliciting cell-cycle arrest, DNA repair, and/or apoptosis [15, 16]. Depending on cell context and the extent of DNA damage, p53 may promote DNA repair by one or both of the two major repair pathways: 1) homologous recombinational repair (HRR) [17, 18], nonhomologous end-joining (NHEJ) [18-20]. HRR is relatively slow and less error-prone, while NHEJ is faster and more error-prone [21].

HRR (Rad51 as a marker) was activated in p53+/+;ErbB2, p53-/+;ErbB2, p53H/+;ErbB2 and p53-/-;ErbB2 but was suppressed in p53H/-;ErbB2 and p53H/H;ErbB2 mammary tumors (Fig. 4A). Conversely, wtp53 inhibited NHEJ (Ku70 as a marker), while higher Ku70 staining was only in tumors lacking wtp53 (Fig. 4B). Hence, in the context of p53 status, the presence of wtp53 allele may shift DNA repair mechanism towards HRR, whereas loss of wtp53 allele leads to switch to NHEJ repair with mutp53 actively suppressing HRR. Therefore, we hypothesized, that p53 LOH leads to the switch from HRR to NHEJ DNA repair mechanism, causing the acquisition of multiple mutations, mitotic abnormalities, and chromosomal aberrations.

Chromosomal aberrations can be measured by the frequency of 'anaphase bridges' (AB) in the anaphase of the cell cycle. AB are extended chromosome bridging between two spindle poles (Fig. 4C) and are a histologic hallmark of dicentric chromosomes [22]. High AB was shown to be associated with the increased frequency of Apc LOH in a colon cancer mouse model [14]. We found a marginal difference in AB scoring between p53+/+;ErbB2, p53-/+;ErbB2, and p53H/+;ErbB2 mammary tumors, whereas the absence of wtp53 allele markedly increased AB in ErbB2 mammary tumors (Fig. 4C). Additionally, p53H/-;ErbB2 tumors had higher AB compared to p53-/-;ErbB2 tumors and AB was further increased in p53H/H;ErbB2 tumors (Fig. 4E). Also, we analyzed another ErbB2 mouse model with conditional deletion of R248Q mutp53 allele (flQ/-;ErbB2) upon tamoxifen administration [11]. Genetic ablation of R248Qp53 *in vivo* significantly reduced the mutp53 expression in established ErbB2 tumors compared to

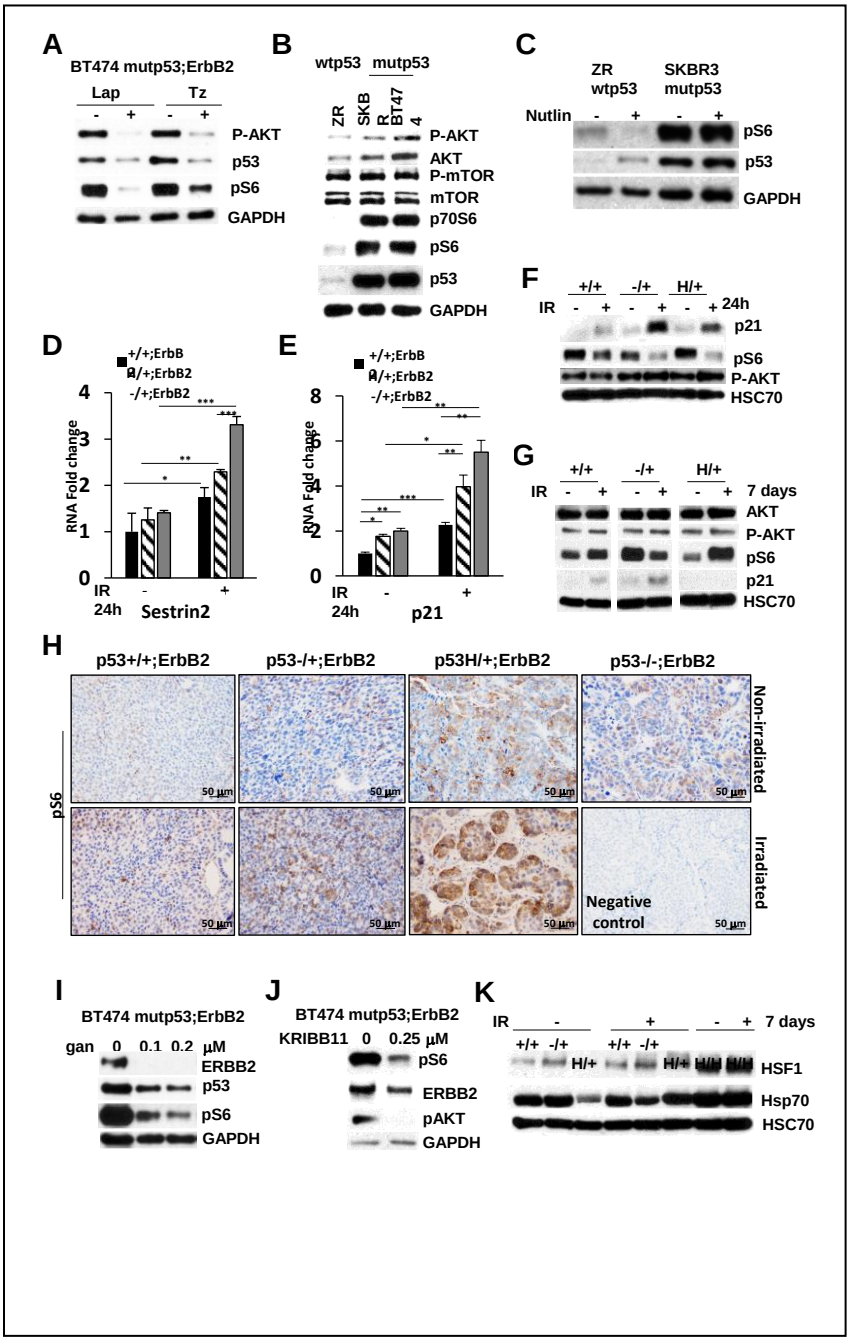

Figure 5. P53LOH is associated with the activation of the mTOR pathway.

(A) ErbB2 inhibition by lapatinib and trastuzumab inhibits mTOR (pS6) in human mutp53 (BT474) cells. (B) The mTOR (pS6) pathway is more activated in mutp53;ErbB2 (BT474 and SKBR3) than in wtp53 cells (ZR75-30). (C) Upregulation of wtp53 by nutlin suppresses mTOR signaling in wtp53;ErbB2 cells ZR 75-30, but not in mutp53;ErbB2 SKBR3 cells. (D and E) Irradiation induces RNA expression of p53 targets Sestrin 2 (D) and p21 (E) in all genotypes p53+/+;ErbB2, p53-/+;ErbB2 and p53H/+;ErbB2 cells. QRT-PCR 24h post-irradiation. N=3 independent experiments. *=p<0.05; **=p<0.01; ***=p<0.001. (F) The mTOR (pS6) pathway is downregulated in the presence of wtp53 allele 24h after irradiation that is concomitant with p21 upregulation. (G) irradiation-induced p53LOH in p53H/+;ErbB2 cells is associated with upregulation of mTOR and lack of detectable p21 in the long term. This is in contrast to p53+/+;ErbB2 and p53-/+;ErbB2 cells. Western blot 7 days post-irradiation. HSC70 as a loading control. (H) Irradiation-induced p53LOH is concomitant with the upregulation of mTOR signaling (He-g) that is more profound in mutp53 heterozygous tumors. The scale bar represents 50 □m. Hsp90 inhibition by ganetespib (I) and HSF1 inhibition by KRIBB11 (J) suppresses mTOR in mutp53 human BT474 cells. Western blot after 24h treatment with indicated concentrations. GAPDH as a loading control. (K) p53LOH after irradiation is associated with both mTOR and HSF1 activation (as indicated by elevated Hsp70) only in p53H/+;ErbB2 cells. Western blot 7 days after irradiation. HSC70 as a loading control.

vehicle-treated tumors (Fig. 4D) and was concomitant with a two-fold AB decrease (Fig. 4E). Thus, our results indicate elevated AB independently of the type of p53 mutation compared to p53-/- tumors (Fig. 4E).

Several studies have implicated centrosome abnormalities and mitotic multipolar spindle formation, as the origin of chromosome instability in a variety of human tumors [23-26]. P53 is required for proper centrosome duplication and was shown to localize to the centrosomes [27-30]. To identify centrosome aberrations (>2 or absence of centrosomes), we analyzed mitotic cells in mammary tumors for centrosome and spindle formation. Indeed, we observed acentrosomal multipolar polar spindles in p53H/-;ErbB2 tumors (Fig. 4F) only.
Collectively our data suggest that in heterozygosity wtp53 enables the maintenance of the genomic integrity in cancer cells. It is plausible that DNA damage via stabilization of mutp53 protein shifts the balance between mutant and wtp53 alleles and unveils the oncogenic power of mutp53, leading to increased genomic aberrations and p53LOH. Consequently, loss of wtp53 allele leads to further genome perturbations fueling tumor progression.

1.4 P53LOH is associated with the activation of the mTOR pathway.

The mTOR pathway is a key downstream component of ErbB2 signaling [31]. Indeed, specific inhibitors of ErbB2 (lapatinib and trastuzumab) effectively suppressed mTOR, as indicated by downregulation of pS6, a downstream target of mTOR, (Fig. 5A). The mTOR pathway plays an essential role in regulating many oncogenic processes – such as genomic instability in different cancer types [14, 32, 33], including breast cancer [32, 34]. The stimulation of the mTOR pathway followed by translational deregulation and accelerated G1-S transition was implicated in inducing genomic instability and Apc LOH in a colon cancer mouse model [14]. Hence, we asked whether the increased genomic instability and elevated p53LOH observed in the presence of mutp53 (Fig. 2) is attributed to increased mTOR signaling.

Several studies showed that wtp53 inhibits the mTOR pathway via inducing Sestrin 1 and 2 expressions, that interact and activate AMPK leading to mTOR inhibition [35, 36]. Our data show elevated mTOR signaling in mutp53;ErbB2 vs. wtp53;ErbB2 human cancer cells as indicated by high levels of downstream effectors of mTOR - p70S6 and pS6, whereas the level of mTOR and p-mTOR protein were comparable (Fig. 5B). Furthermore, upregulation of wtp53 by nutlin suppressed mTOR signaling in wtp53;ErbB2 cells, but not in mutp53;ErbB2 cells (Fig. 5C). Consistent with transcriptional activity of wtp53, Sestrin 2, and p21 (p53 targets) mRNA expression was upregulated 24h post-irradiation in all mouse cell lines genotypes (Fig. 5D-E), and this upregulation was associated with downregulation of mTOR activity (Fig. 5F). Importantly, irradiation did not alter pAKT, the upstream effector of mTOR, (Fig. 5F), indicating that wtp53-mediated induction of Sestrins is the main regulator of mTOR activity post-irradiation.

To investigate the effect of p53LOH on mTOR activity, we tested cells 7 days post-irradiation. Compared to p53+/+;ErbB2, the loss of wtp53 allele in p53H/+;ErbB2 cells was associated with mTOR upregulation and p21 suppression (Fig. 5G), while there were sustained mTOR inhibition and p21 upregulation in p53-/+;ErbB2

cells (Fig. 5G). Similarly, irradiation *in vivo* exacerbated p53LOH that is concomitant with significant upregulation of mTOR signaling in p53H/+;ErbB2 tumors (Fig. 5H).

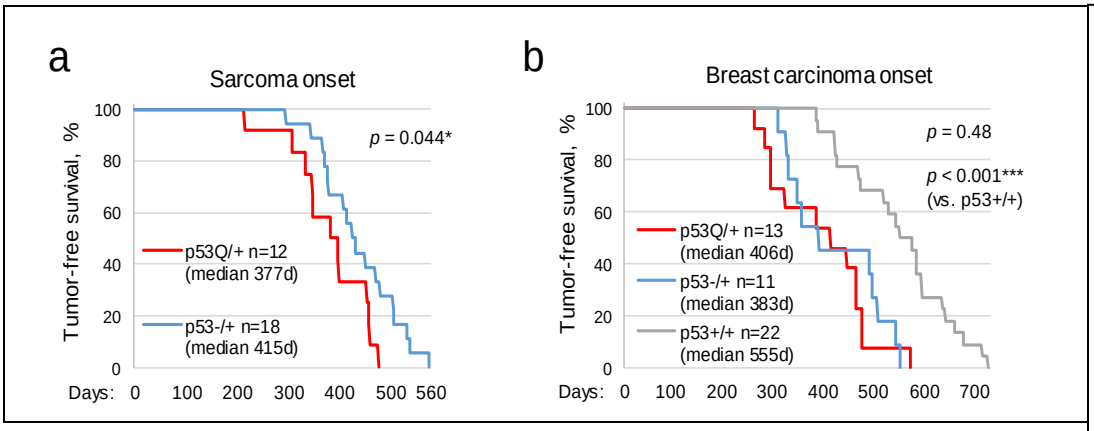

Fig.6 Survival curves analyzing tumor onset of sarcomas and breast carcinomas in p53Q/+;Neu, p53−/+;Neu and p53+/+;Neu mouse cohorts. (a) Sarcoma onset is faster in p53Q/+;Neu compared with p53−/+;Neu mice. This indicates either a DN effect over wtp53 or, alternatively, p53 LOH resulting in mutp53 GOF specifically in sarcoma. (b) Breast cancer latency in p53Q/+;Neu and p53−/+;Neu siblings is similar, reflecting that the majority of p53Q/+ breast tumors did not undergo LOH (see Figure 3b) in contrast to human breast cancer, and also did not exert a DN effect over wtp53 but simply behaved as a LOF allele. Kaplan–Meier analysis; n, number of mice; P, log rank statistics

Next, we asked whether mutp53 impacts the mTOR pathway through a gain-of-function (GOF) mechanism. We previously showed that mutp53 amplifies ErbB2 signaling via stimulation of HSF1 and its transcriptional target Hsp90, which, in turn, stabilizes numerous Hsp90 clients, such as ErbB2 and mutp53 itself [37]. The mTOR pathway components, which are Hsp90 clients (https://www.picard.ch/downloads/Hsp90interactors.pdf), may also be stabilized by mutp53-HSF1-Hsp90 loop. Indeed, both Hsp90 inhibitor (ganetespib) and HSF1 inhibitor (KRIBB11) efficiently suppressed mTOR signaling in mutp53;ErbB2 cell lines BT474 (Fig. 5I-J) and SKBR3. Furthermore, p53LOH post-irradiation was associated with the activation of both mTOR and HSF1 (as indicated by its elevated target, Hsp70) only in p53H/+;ErbB2 cells (Fig. 5K). Hence, in addition to the loss of wtp53 suppressive activity, p53LOH may lead to mTOR activation via stimulation of HSF1-ErbB2 axis in a mutp53-dependent manner, providing the survival advantage over p53+/+;ErbB2 and p53-/+;ErbB2 cells. Thus, the activation of the mTOR pathway associated with p53LOH may generate selective pressure for the loss of wtp53 allele in p53H/+;ErbB2 cells.

Previously we and others [38, 39] have shown that ErbB2 signals via the phosphoinositide-3-kinase (PI3K)–AKT– mTOR axis to phosphorylate HSF1 at pSer326 leading to transcriptional activation of HSF1. On the other hand, the specific inhibitor of mTOR, rapamycin, inhibits HSF1[38]. Therefore, we hypothesized that p53LOH via stimulation of the mTOR pathway leads to HSF1 activation. To test this hypothesis, we stained mammary tumors from irradiated/non-irradiated mice with different genotypes with HSF1 antibodies. However, all HSF1 antibodies, which showed highly specific IHC staining in human specimens[40], produced a substantial background staining in mouse tissues. As an alternative to the IHC study, we utilized *in vitro* approach to investigate how p53LOH affects mTOR and its downstream signaling (HSF1) (Major Task 2, Subtask 3).

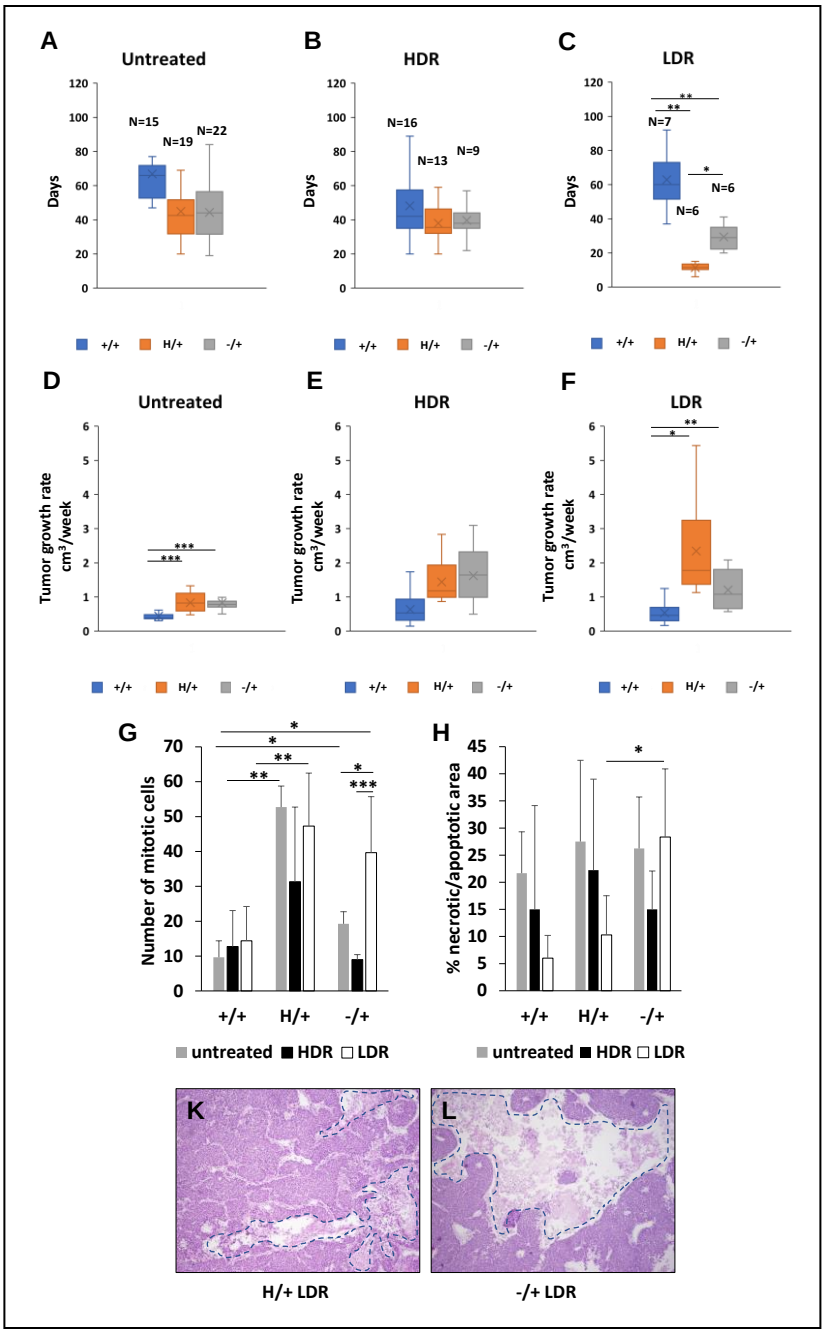

Fig.7 Increased growth rate of mutp53 heterozygous mammary tumors following low dose γ-radiation. A-C. Box plots of average survival days of +/+, H/+ and -/+ mice, untreated, or following HDR or LDR respectively. D-F. Box plots of average tumor growth rate of +/+, H/+ and -/+ mice, untreated, or following HDR or LDR respectively. G. Quantification of the number of mitotic cells in +/+, H/+ and -/+ tumors, untreated, or following HDR or LDR. H. Quantification of percent necrotic/apoptotic area in +/+, H/+ and -/+ tumors, untreated, or following HDR or LDR. K&L. H&E representative images of tumor with low necrosis/apoptosis area (K) and a tumor with high necrosis/apoptosis. Scale bar 200μm. Error bars represent ± SD. *=p<0.05;

Subtask 2. Evaluate the effect of different p53 mutations on p53 LOH in ErbB2-driven mammary tumorigenesis. Test whether similar to R172H, R248Q mutant p53 allele aggravates mammary tumorigenesis compared to p53 null counterparts and promotes p53 LOH after irradiation. (100% completion)

To test whether similar to R172H mutp53, R248Q p53 mutation in heterozygosity accelerates mammary tumorigenesis we generated and analyzed the survival of p53Q/+;Neu and p53− /+;Neu vs p53+/+;Neu mice.

Surprisingly, in contrast to R172H p53 mutation, breast cancer latency between p53Q/+;Neu and p53−/+;Neu siblings was similar (Fig.6), suggesting p53 mutation-specific effects on mammary cancer development and progression in ErbB2 context. Indeed, contrary to R172H p53 mutation, breast cancer latency, and the survival between p53R248Q/+;Neu and p53−/+;Neu siblings were similar. Nevertheless, loss or p53R248Q mutation of one wtp53 allele dramatically accelerated mammary tumorigenesis suggesting a strong wtp53 loss-of-function effect. Importantly, we found that the rate of spontaneous LOH is similar in both mouse models: H/+;ErbB2 mice (17%) and Q/+;ErbB2 mice (20%).

Fig.8 Low dose radiation drives dominant-negative effect in mutp53 heterozygous mammary tumors. A-C. Line graphs representations of average tumor volume measured per week in untreated, or following HDR or LDR respectively. D. Accelerated kinetics of growth in H/+ tumors following LDR but not HDR. Line graphs representations of average tumor volume measured per week in each genotype untreated or following HDR or LDR. E & F. PCR gel electrophoresis analysis of LOH in H/+ and -/+ tumors showing LOH in H/+ tumors following HDR (E) and lDR (F). Error bars represent ± SD.

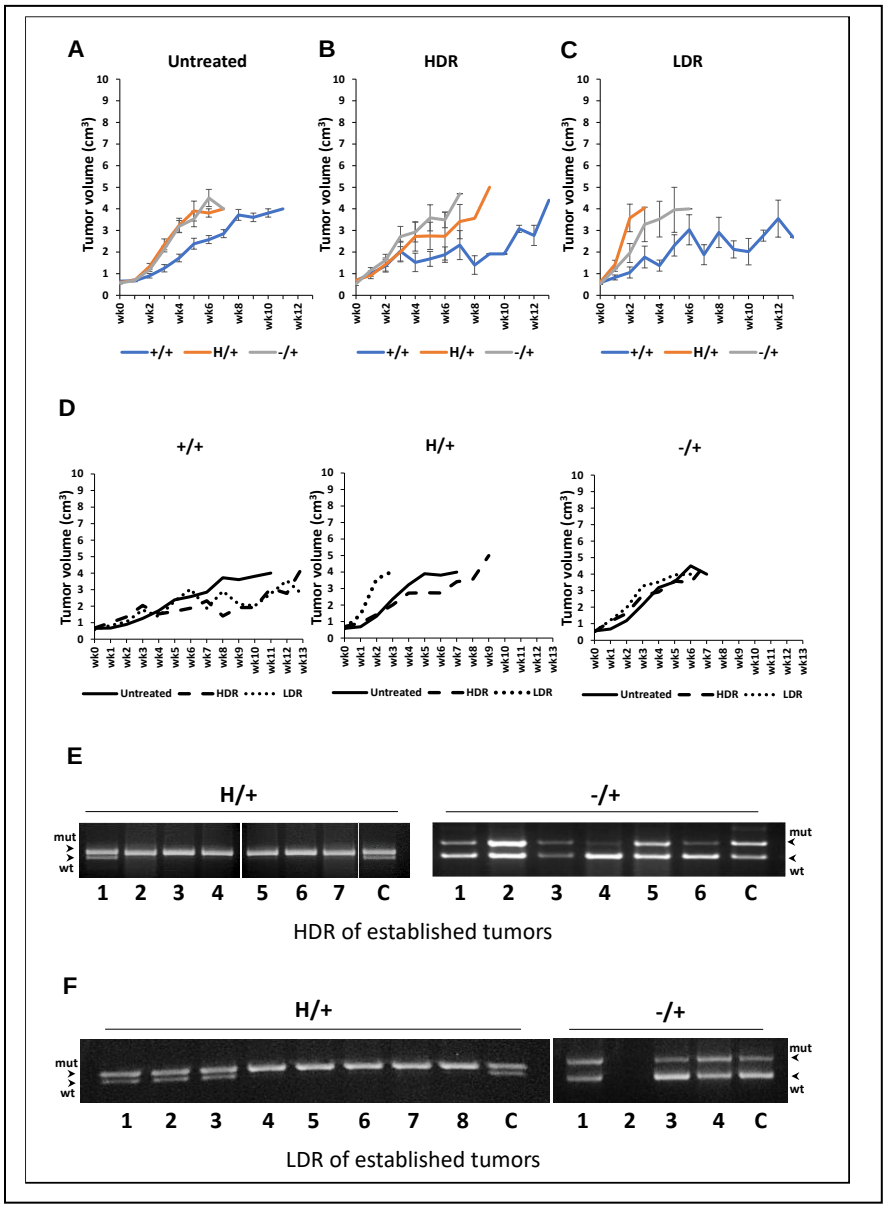

These results implicate p53 mutation-specific effects on mammary cancer development and progression in ErbB2 breast cancer. This data strongly suggests that physiological outcomes of irradiation in p53R248Q/+;Neu mice would be similar to -/+;ErbB2 mice. Therefore, throughout all study we focused on studying loss-of-function p53−/+;ErbB2 mice (see below), and cancer cells as a surrogate model for p53R248Q/+;ErbB2 cancer.

Subtask 3. Assess the effect of irradiation of established mutp53;ErbB2 tumors on p53 LOH. Test whether irradiation of established tumors induces LOH and accelerates mammary tumorigenesis in R172H/+;ErbB2 mice. (100% completion)

3.1. Low dose γ-radiation increases growth rate of mutp53 mammary tumors in MMTV-ErbB2 mouse model.

To complete this task we expanded the experimental design to test the effects of low (LDR) and high doses irradiation (HDR) of established tumors. We included low doses of irradiation in vivo in our study for the following reasons. The effects of low dose radiation (such as low doses used in mammography and other imaging modalities) on tumor cells have been largely overlooked, and in particular how mammary tumors harboring mutp53 behave in response to low radiation. TP53 is mutated in the majority of Her2 (human EGF receptor 2, ErbB2) positive breast cancer (72%), and basal-like breast cancer (80%). However, the p53 mutational status is not routinely used for cancer management. To

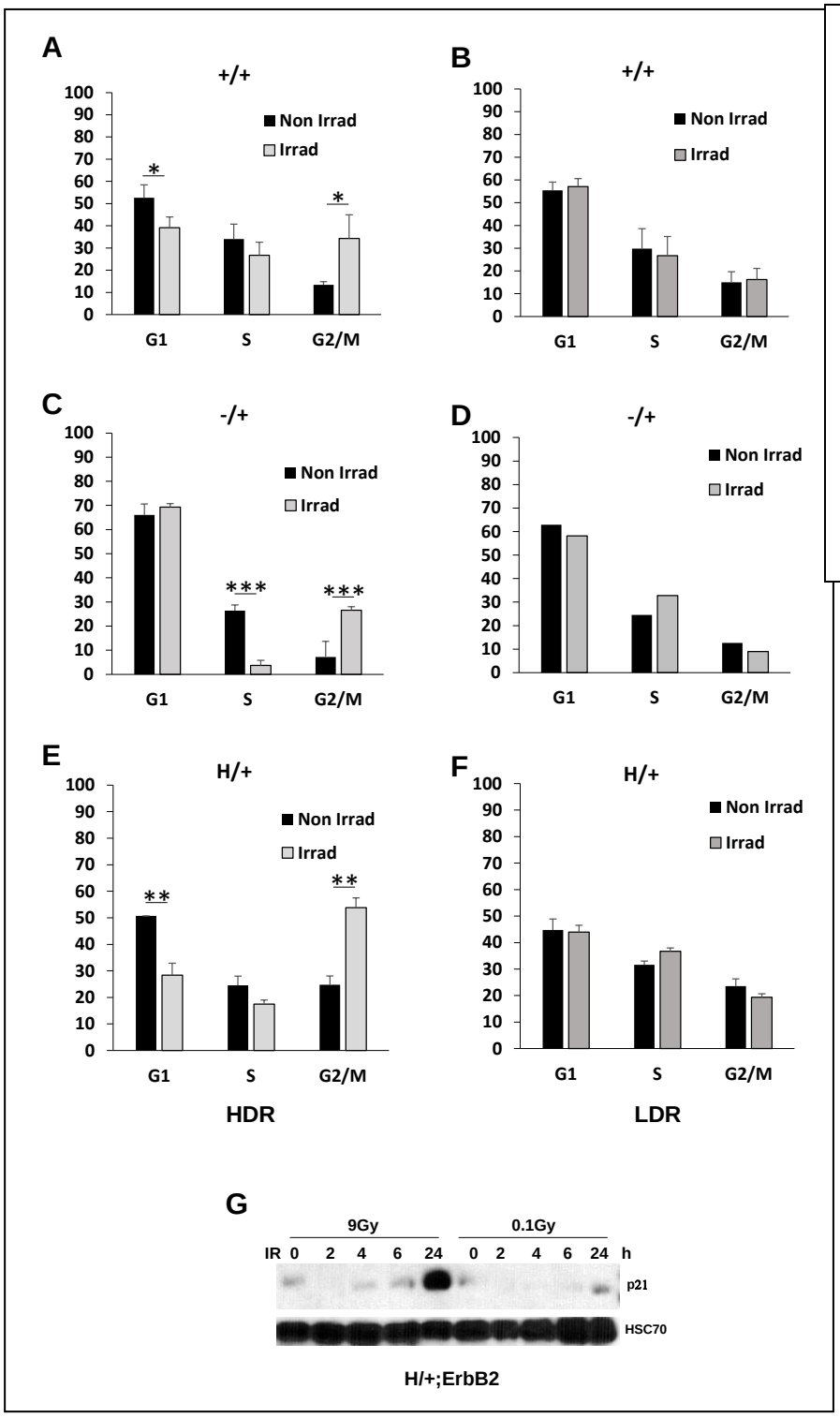

Figure 9. Differential cell cycle checkpoint in response to high dose radiation as compared to low dose radiation**.** A-F. Bar graphs showing cell cycle analysis of +/+, H/+, and -/+ cell lines irradiated (gray bars) or not (black bars). Aberrant cell cycle checkpoint following irradiation in H/+ cells following HDR, while LDR does not show any significant change in the cell cycle profile of the 3 genotypes. G. Western blot of p21 and H2AX level (representing cell cycle check point and DNA damage, respectively) post-irradiation, showing p21 response and H2AX elevation and resolution in H/+ in response to HDR, while no change in p21 and H2AX in response to LDR. HSC70 as a loading control. Error bars represent ± SD.

complete the task, mice with the following genotypes: p53H/+;ErbB2, p53+/+;ErbB2 and p53-/+;ErbB2 were irradiated, or not, with low (0.1Gy) and high (5Gy) irradiation when tumors reached 1 cm^3 in size. In untreated mice, we found no significant difference in p53H/+;ErbB2 mice survival, as compared to p53+/+;ErbB2 and p53-/+;ErbB2 mice, while p53+/+;ErbB2 tended to have slightly better survival (median survival 66 days) as compared to both p53H/+;ErbB2 and p53-/+;ErbB2 mice (median survival 42.5 and 44 days respectively) (Fig.7A). However, both p53H/+;ErbB2 and p53-/+;ErbB2 mice had significantly faster tumor growth rate as compared to p53+/+;ErbB2 mice (Fig.7D, 8A-C and 9A). In mice exposed to a single dose of HDR, we found no significant difference in survival of both p53H/+;ErbB2 and p53-/+;ErbB2 mice (median survival 35.5 and 38 days respectively), as compared to p53+/+;ErbB2 mice (median survival 42 days) (Fig. 7B). Though both p53H/+;ErbB2 and p53-/+;ErbB2 mice no significant difference in tumor growth rate as compared to p53+/+;ErbB2 mice. Yet, both genotypes tended to have a faster tumor growth rate as compared to p53+/+;ErbB2 mice (Fig. 7E, 8D-F and 9B). Interestingly, in mice exposed to a single dose of LDR, we found that in p53H/+;ErbB2 mice mammary tumor growth was aggravated compared to both p53+/+;ErbB2

and p53-/+;ErbB2 mice, as indicated by significantly shorter survival (median survival 11.5, 60 and 26 days respectively) (Fig. 7C) and significantly faster tumor growth rate (Fig. 7F, 8G-I, and 9C).

3.2. Both low and high dose γ-radiation of established tumors induces loss of heterozygosity in mutp53 mammary tumors in MMTV-ErbB2 mouse model.

We have previously shown that HDR promotes loss of heterozygosity (LOH) in p53H/+;ErbB2 and p53-/+;ErbB2 mouse mammary tumors when mice with premalignant lesions were irradiated [41]. Thus, to determine whether HDR- vs LDR of established tumors have any differential effect on LOH in mouse mammary tumors, we analyzed LOH in p53H/+;ErbB2 and p53-/+;ErbB2 mammary tumors from mice subjected to HDR vs LDR. As shown in figure 8D-E, following HDR, 86% (6/7) of p53H/+;ErbB2 tumors showed LOH while no LOH (0/6) was detected in p53-/+;ErbB2 tumors. Following LDR, 63% (5/8) of p53H/+;ErbB2 tumors and 25% (1/4) of p53-/+;ErbB2 tumors showed LOH. This result indicates that LDR is as effective as HDR in inducing LOH in mutp53 heterozygous setting, and that the significant increase in tumor growth rate observed in p53H/+;ErbB2 following LDR, as compared to HDR (Fig. 7) is not driven by LOH alone.

3.3. Differential cell cycle checkpoint to high dose γ–radiation as compared to low dose.

Our results on potentially deleterious effects of LDR on mammary tumor progression prompted us to investigate the mechanism underlying these observations. It is well established that upon genotoxic stress, wtp53 activates the transcription of genes involved in cell-cycle arrest and DNA repair or apoptosis, to protect the genome from the accumulation of mutations, while mutp53 may perturb these genome-guarding mechanisms and promote genomic instability [19,42]. Yet, how cells with mutp53 respond to DNA damage induced by HDR vs LDR is not fully understood. Hence, we irradiated cultured mouse mammary tumor cells with HDR (9 Gy) or with LDR (0.1 Gy) γ-radiation and we compared cell-cycle profiles of cells with various genotypes 24 h after γ-irradiation. Non-irradiated p53+/+;ErbB2 and p53−/+;ErbB2 cells exhibited comparable cell-cycle profiles, whereas p53H/+;ErbB2 cells showed cell-cycle profile with lower G1 and S and significantly higher G2/M indicating an increased rate of proliferation (Fig. 9A-F). Consistent with fast recovery from DNA-damage post HDR, p53+/+;ErbB2 cells did not significantly change G1 and S content and had a slight increase in G2/M arrest (Fig. 9A). In p53−/+;ErbB2 cells, HDR induced G1 and G2/M arrest, and significantly reduced S-phase (Fig. 9C). Conversely, p53H/+;ErbB2 cells treated with HDR continued cell cycling as indicated by the unchanged S-phase and increased G2/M (Fig. 9E). However, following, LDR, none of the cell genotypes showed any significant change in their cell cycle profile as compared to their non-irradiated controls (Fig. 9B, D & F). Western blot analysis for p21 (as an indicator of active cell cycle check point) and for γH2AX (as a marker of DNA double-strand breaks) in p53H/+;ErbB2 cells, for HDR and LDR, showed a peak for p21 by 24 hrs post HDR while there was no change in p21 level post-LDR (Fig. 9G). γH2AX showed a peak at 2-4 hrs post HDR and was still sustained (though at a lower level) by 24 hrs post HDR. However, no change in γH2AX level was detected

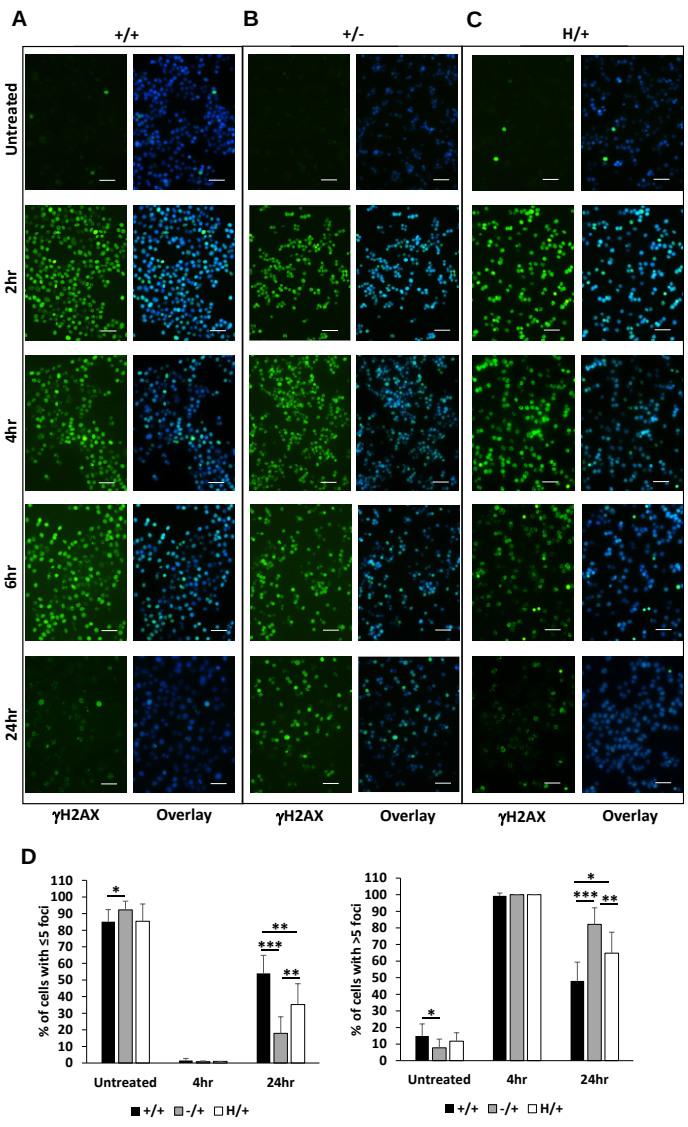

Fig. 10 DNA-damage repair response is activated response to high dose radiation in all genotypes. A-C. Staining of cells for H2AX in +/+, H/+, and -/+ cell lines, before and after HDR (2, 4, 6 and 24h post-irradiation). Scale bar 50μm. D) Quantification of cells with >5 and <5 H2AX foci/cell in +/+, H/+, and -/+ cell lines, before and after HDR (4 and 24h post-irradiation). Error bars represent ± SD. *=p<0.05; **=p<0.01; ***=p<0.001.

following LDR. These results suggested that there is differential sensitivity of the cells to HDR vs LDR for them to activate the cell cycle checkpoint.

3.4. Mutant p53 leads to defective DNA-damage repair response following low dose γ-radiation.

To confirm these findings, we stained the cells for the formation of γH2AX foci in response to HDR vs LDR. We analyzed the dynamics of γH2AX foci formation and resolve at different time points, at 0, 2, 4, 6 and 24 hrs, in response to HDR vs LDR in p53+/+;ErbB2, p53H/+;ErbB2 and p53-/+;ErbB2 cells. We counted the percent of cells with ≥5 foci post irradiation. Examples of γH2AX staining in untreated, HDR and LDR are shown in Figures 10 & 11, respectively. At the basal level, approximately 10% or less of untreated cells of the 3 genotypes had ≥5 γH2AX foci with no significant difference between them (Fig 10A&D). The percent of cells with ≥5 γH2AX foci was significantly increased to approximately 100% at 2 and 4 hrs post-HDR in all 3 genotypes and then returned to the basal level by 24 hrs post-HDR in p53+/+;ErbB2 and p53H/+;ErbB2 (Figure 10 A-D). However, in p53-/+;ErbB2 cells, the percent of cells with ≥5 γH2AX foci was significantly higher by 24 hrs post-HDR, as compared to its untreated control and to p53+/+;ErbB2 and p53H/+;ErbB2 cells (Figure 10 A-D). These results suggest that p53 haploinsufficiency leads to delayed DNA-damage response following HDR. Following LDR, the percent of cells with ≥5 γH2AX foci was significantly increased at 2 and 4 hrs to approximately 10% and 25% post-LDR in p53+/+;ErbB2 and p53-/+;ErbB2, respectively and then returned to the basal level by 24 hrs post-LDR (Fig. 11A-D). In contrast, p53H/+;ErbB2 cells showed no increase in the percent of cells with ≥5 γH2AX foci at any time point following LDR, as compared to its untreated control and to p53+/+;ErbB2 and p53-/+;ErbB2 cells (Fig. 11 A-D). These results suggest a differential sensitivity in DNA-damage response of p53H/+;ErbB2 to HDR vs LDR, and points to a potential gain of function of mutant p53 in suppressing DNA-damage response to LDR.

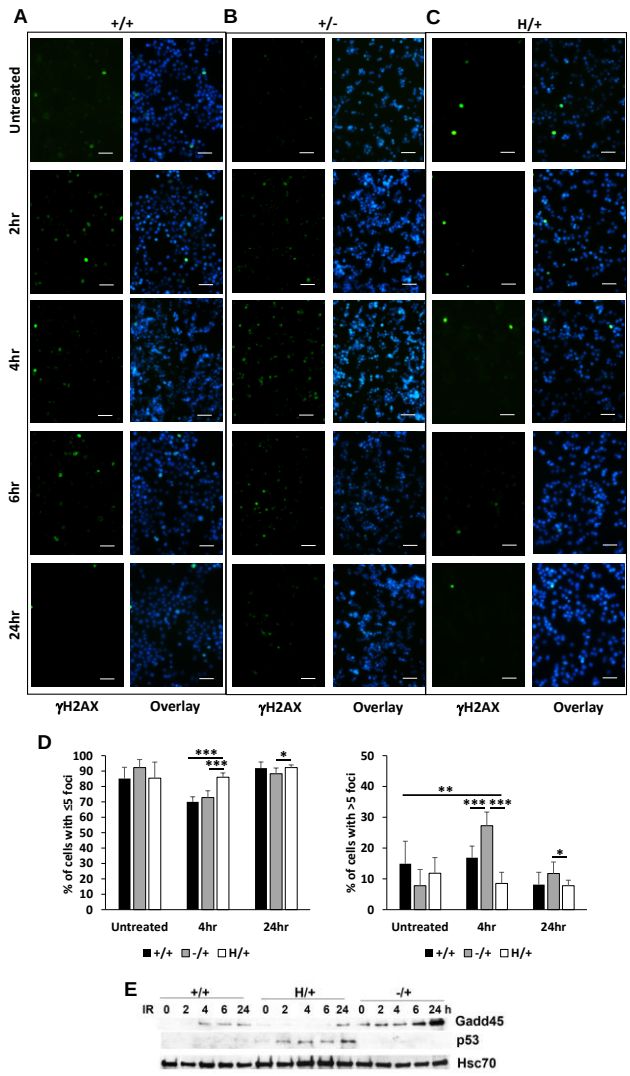

Fig.11 Mutant p53 abolishes DNA-damage repair response in a dominant-negative manner in response to low dose radiation. A-C. Staining of cells for H2AX in +/+, H/+, and -/+ cell lines, before and after LDR (2, 4, 6 and 24h post-irradiation), showing suppressed H2AX staining in H/+. Scale bar 50□m. D) Quantification of cells with >5 and <5 H2AX foci/cell in +/+, H/+, and -/+ cell lines, before and after LDR (4 and 24h post-irradiation). E. Western blot of Gadd45 (a downstream target of wtp53) and p53 level (representing cell cycle check point and DNA damage) post-irradiation, showing Gadd45 elevation in +/+ and -/+ in response to LDR, while no change in H/+ concomitant with elevation and stabilization of mutp53 in response to LDR. HSC70 as a loading control. Error bars represent ± SD. *=p<0.05; **=p<0.01;

3.5. Mutp53 is stabilized in response to LDR and exerts DNE as indicted by down-regulation of p53 target gene Gadd45.

To determine whether p53 protein level is affected in response to LDR, we subjected mouse cell lines p53+/+;ErbB2, p53H/+;ErbB2 and p53-/+;ErbB2 to LDR and analyzed p53 level at different time points up to 24 hrs, by WB. As shown Figure 11E, mutp53 level was increased and stabilized in p53H/+;ErbB2 cells but not in p53+/+;ErbB2 or p53-/+;ErbB2 cells. Also, the stabilization of mutp53 in p53H/+;ErbB2 showed a DNE as indicated by suppressed Gadd45 expression (a known wtp53 target), as compared to p53+/+;ErbB2 and p53-/+;ErbB2 cells.

3.6. ATM phosphorylation is suppressed in cells with mutant p53 following low dose radiation but not high dose radiation

In mammalian cells, the ATM (ataxia-telangiectasia mutated), ATR (ATM- and Rad3-Related), and DNA-PKcs (DNA-dependent protein kinase) kinases are the most upstream DNA-damage repair kinases. In response to DNA damage, many proteins are phosphorylated in an ATM- or ATR-dependent manner, whereas DNA-PKcs mainly regulate a smaller number of targets and play a role primarily in nonhomologous end joining (NHEJ) [28-32]. In vivo and in vitro studies suggest that the DNA-damage specificities and functions of ATM and ATR are distinct. ATM is primarily activated by double-stranded DNA breaks (DSBs) such as that induced by radiation [33], whereas ATR responds to a broad spectrum of DNA damage [34]. One of the first steps of sensing DSBs is the autophosphorylation of ATM (pATM) rendering it active [35-37]. pATM is required for the phosphorylation

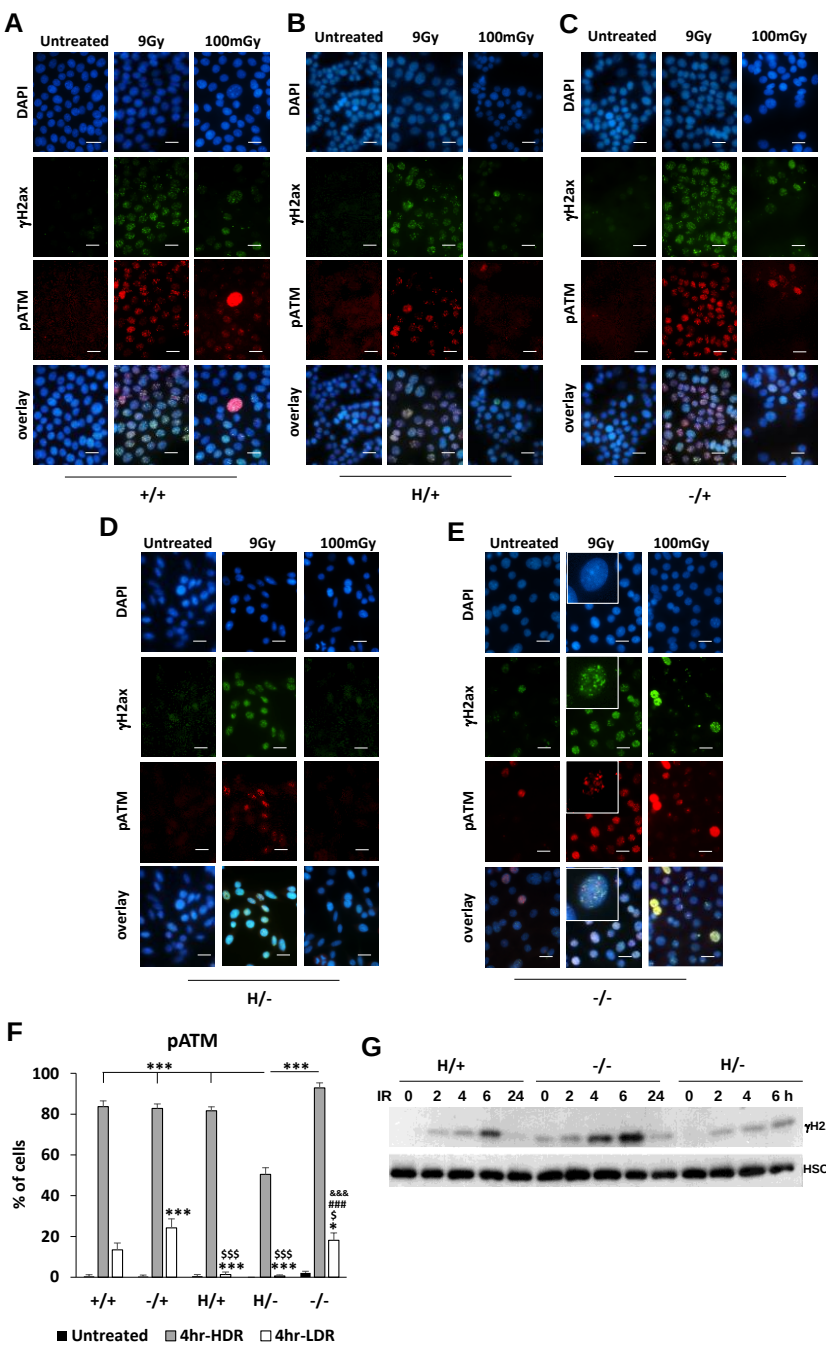

Figure 12. Mutant p53 suppresses ATM phosphorylation in response to low dose but not high dose radiation. A-E. Co-staining of cells for pATM and γH2AX in +/+, H/+, -/+, H/- and -/- cell lines, before and after HDR or LDR (4h post-irradiation), showing suppressed pATM and γH2AX staining in H/+ and H/-, but not in +/+, -/+ or -/- cells. Scale bar 20μm. F. Quantification of cells with pATM and γH2AX co-staining foci/cell in +/+, H/+, -/+, H/- and -/- cell lines, before and after HDR or LDR (4h post-irradiation). G. Western blot of γH2AX level (representing DNA damage) post-LDR, showing γH2AX elevation and resolution in -/- cells in response to LDR, while suppressed change in γH2AX in response to LDR in H/+ and H/-. HSC70 as a loading control. Error bars represent ± SD. All statistical significance is made to p53+/+ cells, unless otherwise indicated by cross bars, or indicated by ### and &&& on LDR -/- where comparison was made to LDR H/+ and LDR H/-, respectively. *=p<0.05; **=p<0.01; ***=p<0.001.

of H2AX converting it to γH2AX which then marks the DNA DSBs [38]. Additionally, pATM phosphorylates other substrates such as Chk2 [39-41] and p53 [42, 43]. Since we observed a defect in γH2AX foci in p53H/+;ErbB2 cells following LDR, we hypothesized that mutant p53 might be hampering the pATM-γH2AX axis in response to LDR-induced DSBs, in a potential GOF manner. To test this hypothesis, we stained for pATM and γH2AX in p53+/+;ErbB2, p53-/+;ErbB2 and in p53H/+;ErbB2 cells (Fig.12). We also included p53H/-;ErbB2 and p53-/-;ErbB2 cells as controls (Fig.12). Since the phosphorylation is of ATM is an early event in response to DSBs, we analyzed the cells for pATM foci at 4 hrs post HDR or LDR by counting the percent of cells with pATM foci that co-stained in cells with ≥5 γH2AX foci post-irradiation. Examples of pATM and γH2AX co-staining in untreated, HDR and LDR are shown in Figure 12. At the basal level, approximately 2% or less of untreated cells of all genotypes had pATM- γH2AX co-staining with no significant difference between them (Fig. 12 A-F). The percent of cells with pATM- γH2AX co-staining was significantly increased to approximately 80%

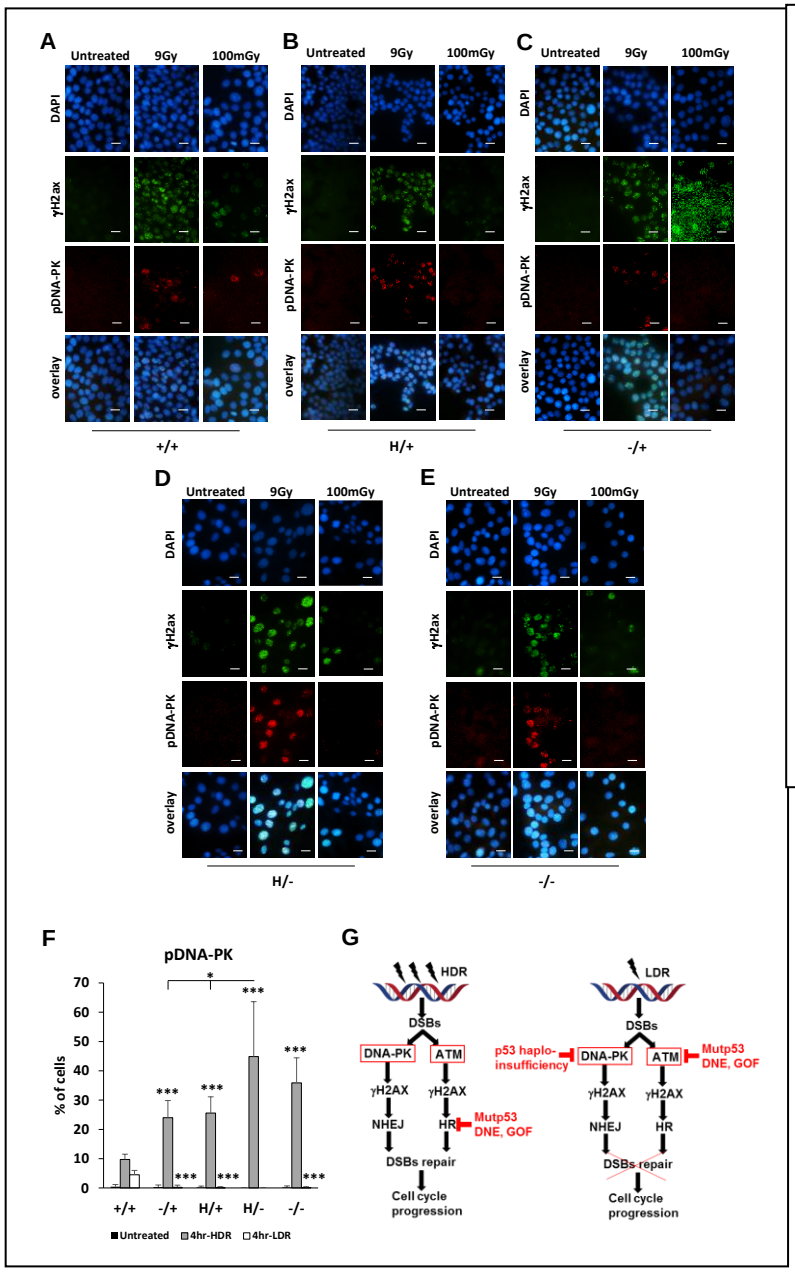

Figure 13. p53 haploinsufficiency suppresses DNA-PK mediated DNA damage repair in response to low dose but not high dose radiation. A-E. Co-staining of cells for pDNA-PK and γH2AX in +/+, H/+, -/+, H/- and -/- cell lines, before and after HDR or LDR (4h post-irradiation), showing suppressed pDNA-PK and γH2AX staining in all genotypes except +/+ cells. Scale bar 20μm. F. Quantification of cells with pDNA-PK and γH2AX co-staining foci/cell in +/+, H/+, -/+, H/- and -/- cell lines, before and after HDR or LDR (4h post-irradiation). G. Model comparing DNA damage repair (DDR) in response to HDR vs LDR in presence of mutp53. Following HDR, mutp53 suppresses ATM pathway (homologous recombination (HR) DDR), allowing DNA-PK pathway (non-homologous end joining (NHEJ) DDR) to take place. Following LDR, DNA-PK pathway is suppressed in wtp53 haploinsufficiency while mutp53 suppresses ATM pathway, with a net result ablation of DDR in cells with mutp53. Error bars represent ± SD. All statistical significance is made to p53+/+ cells, unless otherwise indicated by cross bars. *=p<0.05; **=p<0.01; ***=p<0.001.

at 4 hrs post-HDR in p53+/+;ErbB2, p53-/+;ErbB2, p53H/+;ErbB2 and p53-/-;ErbB2 (Fig. 12 A-C, E&F). However, though p53H/-;ErbB2 had a significant increase in pATM-□□H2AX co-staining, yet it was significantly lower than the other 4 genotypes, at approximately 50% (Fig. 12 D&F). Following LDR, the percent of cells with pATM- gH2AX co-staining was significantly increased to approximately 13%, 24% and 18% post-LDR in p53+/+;ErbB2, p53-/+;ErbB2 and p53-/-;ErbB2, respectively (Fig. 12 A, C, E&F). In contrast, both p53H/+;ErbB2 and p53H/-;ErbB2 cells showed no increase in the percent of cells with pATM- gH2AX co-staining following LDR, as compared to their untreated controls and to the other genotypes (Fig. 12B, D&F). Western blot for □□H2AX in p53H/+;ErbB2, p53-/-;ErbB2 and p53H/-;ErbB2 cells confirmed that in p53-/-;ErbB2 has higher □H2AX levels post LDR as compared to p53H/+;ErbB2 and p53H/-;ErbB2 cells (Fig. 12G). These results suggest that: 1) LDR can still activate ATM; 2) phosphorylation of ATM and consequently, H2AX are p53 independent events; 3) mutant p53 suppresses ATM phosphorylation and consequently H2AX phosphorylation in a GOF and/or DNE manner.

3.7. DNA-PK DDR pathway is suppressed in p53 haploinsufficiency-manner in response to low dose but not high dose □-radiation.

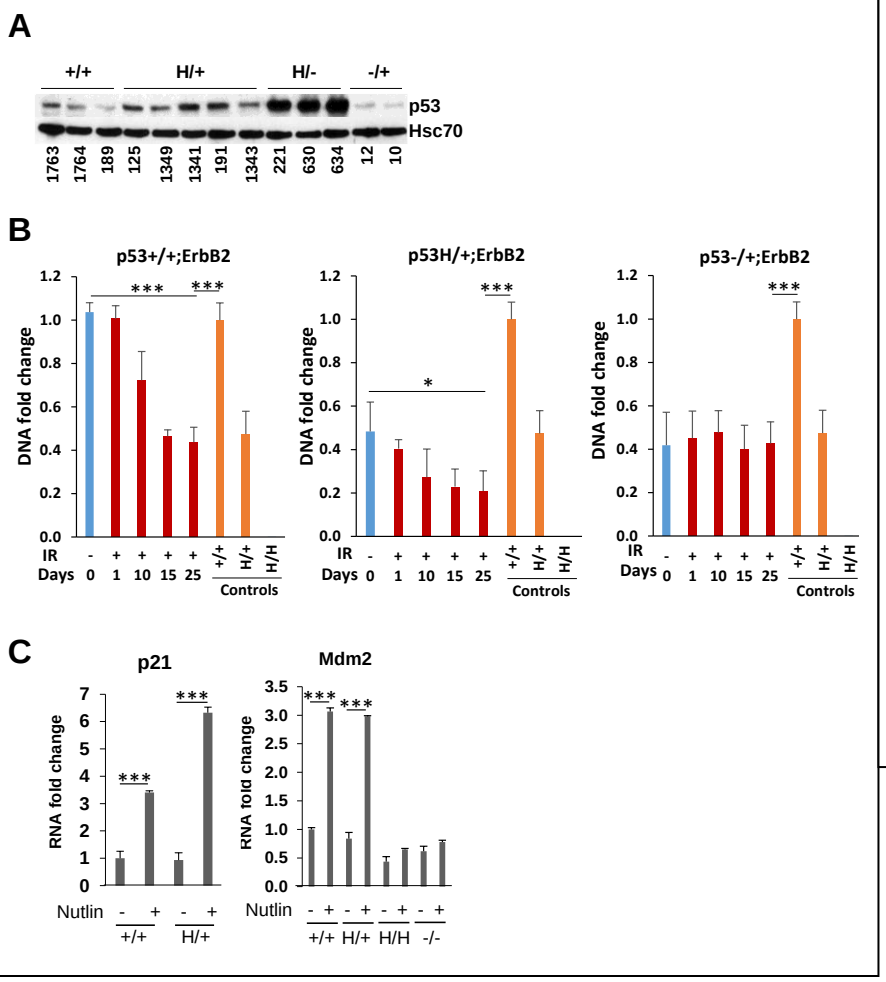

Figure 14. (A) P53 expression in a panel of cell lines established from mammary tumors of MMTV-ErbB2 mice with different p53 genotypes. HSC70 is a loading control. (B) Mutp53 enhances LOH following irradiation in cell culture (n=3 independent samples). Cultivated mammary tumors cells were irradiated (9Gy), or not, and grown up to 25 days post-irradiation. DNA was extracted at the indicated time points. The copy number of p53 wt and mut alleles was quantified by real-time PCR. DNA extracted from tail tissue samples of the corresponding genotype was used for copy number control. The experiment was repeated three times. Summary of a representative experiment. (D) Wtp53 retains transcriptional activity and, in response to Mdm2 inhibitor nutlin, induces its target p21 and Mdm2 in mutp53 heterozygous cells. Nutlin does not induce Mdm2 in p53H/H;ErbB2 and p53-/-;ErbB2 MECs. N=3 independent experiments.

We have previously shown that wtp53 promotes HR DNA damage repair mechanism in response to □-irradiation and that mutp53 diverts the DNA damage repair (DDR) mechanism to the more error-prone NHEJ pathway, leading to more aggressive tumors (Fig.4 A,B). Thus, we examined whether mutp53 would have any differential effect on HR vs NHEJ DNA damage repair in response to HDR vs LDR. We analyzed the cells for pDNA-PK foci at 4 hrs post HDR or LDR by counting the percent of cells with pDNA-PK foci that co-stained in cells with ≥5 □H2AX foci post-irradiation. Examples of pDNA-PK and □H2AX co-staining in untreated, HDR and LDR are shown in Figure 13. Indeed, our data show that DNA-PK (NHEJ DDR) is activated in all genotypes following HDR. (Fig. 13 A-F). However, following LDR, DNA-PK pathway was activated only in p53+/+ cells, but not in the other genotypes (Fig. 13A-F). Importantly, following HDR, H/+ and H/- cells showed the highest DNA-PK activation as compared to +/+, -/+ and -/- cells, indicating more active NHEJ DDR in cells with mutp53. This is in support of our previous finding (Fig.4 A,B) that mutp53 promotes NHEJ following HDR.

Major Task 2. Mechanistically assess the physiological consequences of p53 LOH in heterozygous mutp53 mammary cells *in vitro.(100% completion)*

Subtask 1. Examine the frequency and time of p53 LOH onset in the existing collection of cell culture of primary mammary epithelial cells (MECs) and mammary tumors culture derived from mice with different p53

genotypes. Serial passaging of R172H/+ErbB2 vs p53-/+;ErbB2 vs p53+/+;ErbB2 MECs and mammary tumors cultured cells.

Previously, we successfully established and passaged primary cultures of MECs derived from mammary epithelial of mice of following genotypes: H/H;ErbB2, -/-;ErbB2 and Q/-;ErbB2. Although, H/H;ErbB2 and -/-;ErbB2 MECs proliferate at a different rate, we were able to passage them indefinitely. Unexpectedly, in contrast to primary mouse embryo fibroblasts (MEFs) (Shetzer, Y. et al. The onset of p53 loss of heterozygosity is differentially induced in various stem cell types and may involve the loss of either allele. Cell death and differentiation 21, 1419-1431) we failed to passage MECs from H/+;ErbB2, -/+;ErbB2 and +/+;ErbB2 mice. All wtp53 expressing MECs undergo senescence following passage 3. This data is consistent with our observations that wtp53 in heterozygosity can exert its tumor suppressive function by inducing the transcription of a subset of wtp53 target genes. Therefore, now we mainly will focus on cell lines established from mammary tumors of H/+;ErbB2, -/+;ErbB2 and +/+; ErbB2 cells (Fig. 14A). We successfully established mammary tumor cell lines from different H/+;ErbB2, -/+;ErbB2 and +/+; ErbB2 mice that continuously retain wtp53 allele. Our initial analysis has shown, that tumor cell lines in contrast to wtp53 expressing MECs can be propagated for indefinite time, even in the presence of wt p53 allele.

Subtask 2. Test the effect of irradiation on the frequency and time of p53 LOH onset in primary mammary epithelial cells (MECs) and mammary tumors culture derived from mice with different p53 genotypes. Serial passaging of R172H/+;ErbB2 vs p53-/+;ErbB2 vs p53+/+;ErbB2 MECs and mammary tumors cultured cells after single dose of irradiation in vitro at passage 1.

Next, we determined whether the presence of mutp53 allele accelerates p53LOH after irradiation *in vitro*. Cell lines, generated from mouse tumors of different genotypes (Fig.14A) were irradiated, or not, and the copy number of wtp53 and mutp53 alleles were determined at different time points by qPCR (Fig. 14B). In agreement with *in vivo* data [41], we found 3-fold reduction of wtp53 allele post-irradiation in p53H/+;ErbB2 compared to untreated cells (a 5-fold reduction compared to control p53+/+;ErbB2 cells), but not in p53-/+;ErbB2 cells compared to non-irradiated cells (Fig.14B). Irradiation induced a 2-fold decrease in copy number of the wild-type allele in p53+/+;ErbB2 cells compared to control cells (Fig. 14B).

To evaluate the consequences of p53LOH *in vitro* with respect to the transcriptional activity of wtp53 in heterozygosity, we examined the expression of canonical p53 target genes Mdm2 and p21 in response to Mdm2 inhibitor, nutlin, by qPCR. Nutlin promotes p53 transcriptional activity without induction of DNA damage [42]. No significant difference in the expression of Mdm2 and p21 was observed between p53+/+;ErbB2 and p53H/+;ErbB2 cells at the basal level, while the expression of both was increased following nutlin addition (Fig. 14C). In contrast, nutlin failed to induce p53 targets in p53H/H;ErbB2 and p53-/-;ErbB2 mammary epithelial cells (MECs) (Fig. 14C). Hence, in heterozygosity, wtp53 at least partially preserves its transcriptional function, while p53LOH may abrogate tumor-suppressor activities of wtp53.

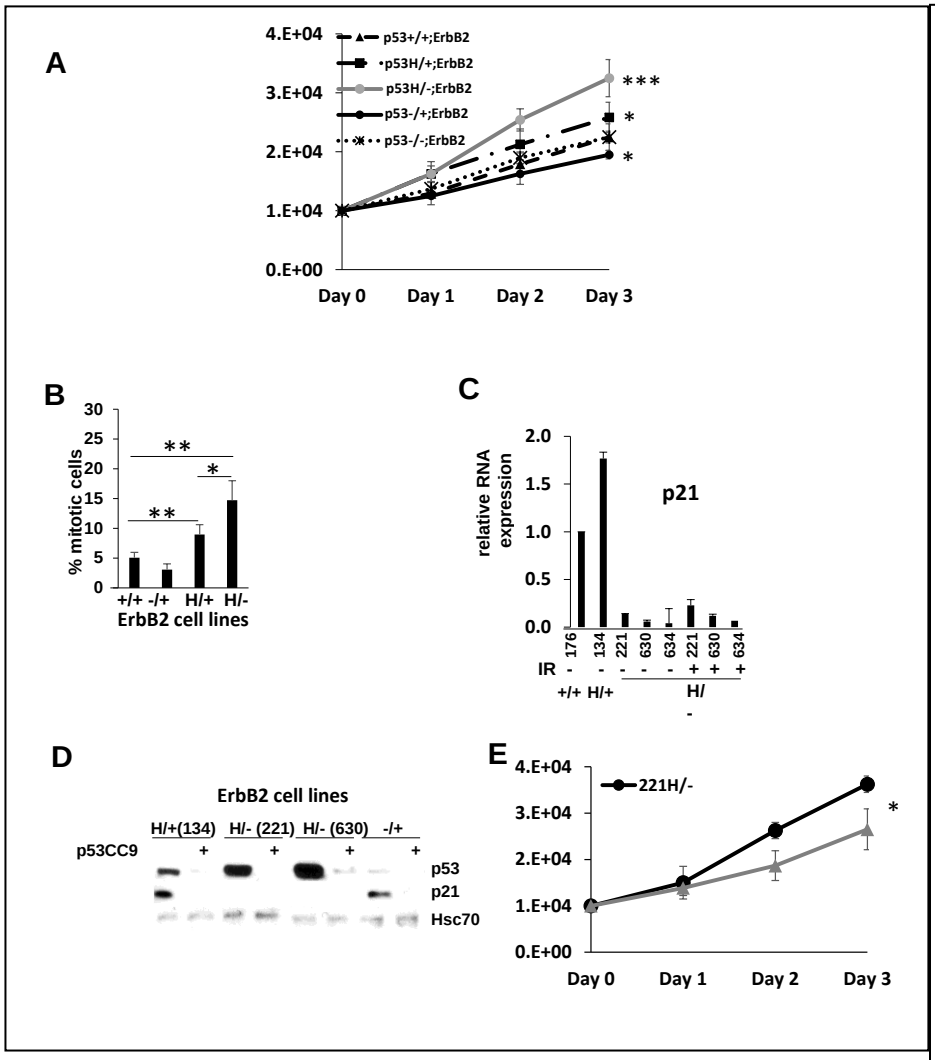

Figure 15. Mutp53 promotes cell proliferation. (A) Growth curve of mouse ErbB2 mammary epithelial tumor cell lines with different p53 status. n=3 independent experiments per genotype (one cell line per genotype except for p53+/+ and p53 H/- where 2 different cell lines derived from different tumors and result per genotype was averaged). (B) Bar graph showing percent mitotic cells in mouse ErbB2 mammary epithelial tumor cell lines with different p53 status. Each bar represents the average percent of mitotic per genotype counted from at least 5 randomly selected fields at x400 magnification (one cell line per genotype except for p53+/+ and p53 H/- where 2 different cell lines derived from different tumors and result per genotype was averaged). (C) Bar graph showing relative mRNA expression level of p21 in ErbB2 mammary epithelial tumor cell lines with different p53 status. n=3 independent experiments per cell line per genotype. (D) Western blot analysis of p53 and p21 levels in mouse ErbB2 mammary epithelial tumor cell lines with different p53 status before and after CRISPR/Cas9 p53 deletion (p53CC9). Hsc70 is loading control. (E) Growth curve of mouse ErbB2 mammary epithelial tumor cell line with mutp53, before and after CRISPR/Cas9 p53 deletion (p53CC9). n=3 independent experiments per cell line. Where applicable *=p<0.05; **=p<0.01; ***=p<0.001. Error bars represent ± SD.

Subtask 3. Correlate the p53 LOH status of R172H/+;ErbB2 vs p53-/+;ErbB2 vs p53+/+;ErbB2 MECs and mammary tumors cultured cells with cellular properties (proliferation, chemoresistance, allografts) and with biochemical characteristics.

3.1 p53LOH enhances cell proliferation.

To perform this task we characterized the following mouse genotypes: R172H/wtp53;ErbB2 (H/+;ErbB2), p53null/wtp53;ErbB2 (-/+;ErbB2) and wtp53/wtp53;ErbB2 (+/+;ErbB2). To evaluate the phenotypic effects of mutp53 in heterozygosity, we established stable cell lines from mouse mammary tumors of +/+;ErbB2, H/+;ErbB2, H/-;ErbB2 (R172H/p53null;ErbB2), -/+;ErbB2 and -/-;ErbB2 genotype (three biological replicas per genotype) (Fig. 14A). In contrast to the existing human breast cancer cell lines that are mutp53 homo- or hemizygous, our panel of cell lines (isogenic and non-isogenic) allows us to evaluate the pathological consequences of p53LOH in the well-controlled model.

We found that compared to p53+/+;ErbB2 and p53-/+;ErbB2 cells, the presence of mutp53 allele in heterozygous cells elevates the total p53 protein level, while p53LOH leads to further stabilization of mutp53

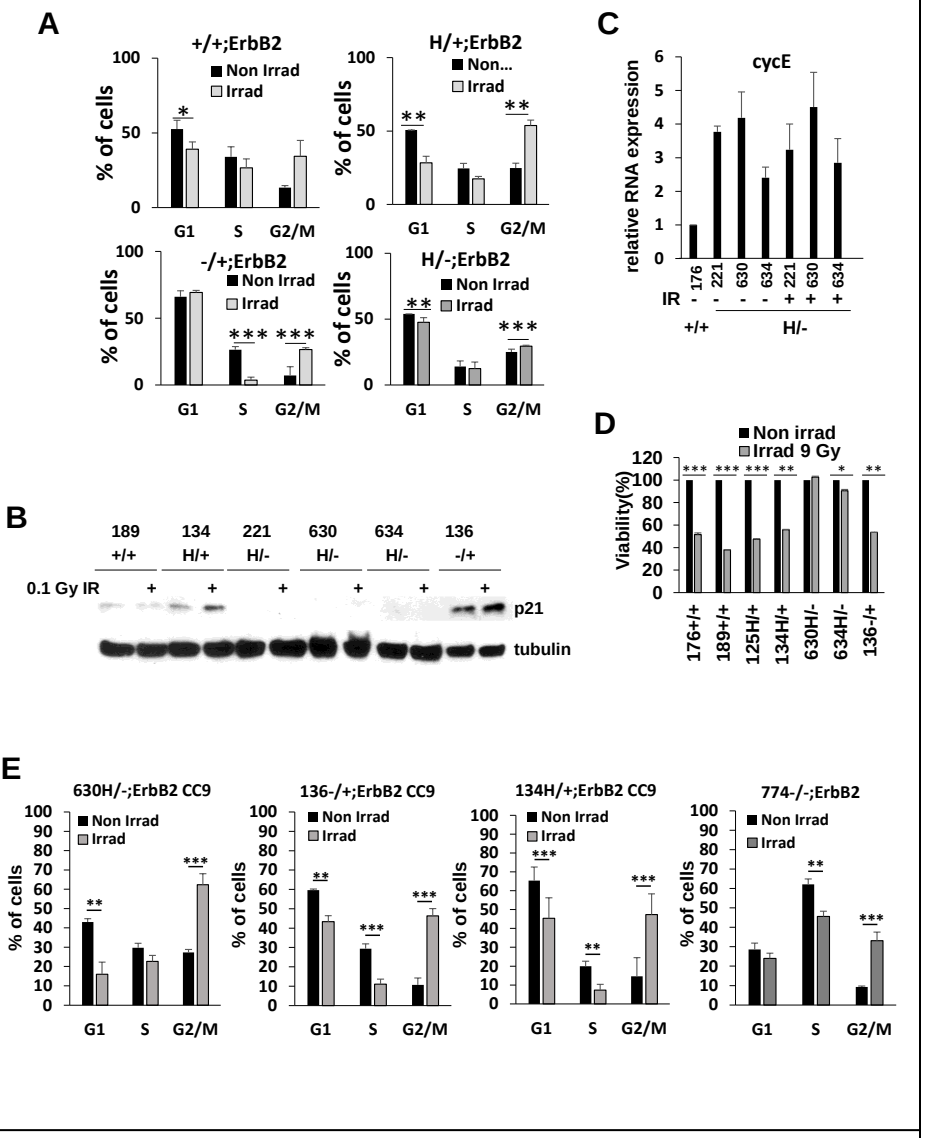

Figure 16. Mutp53 suppresses cell cycle checkpoint following irradiation. (A) Aberrant cell cycle checkpoint following irradiation in p53H/-;ErbB2 cells. Bar graphs showing cell cycle analysis of p53+/+;ErbB2, p53H/+;ErbB2, p53-/+;ErbB2 and p53H/-;ErbB2 cell lines irradiated (gray bars) or not (black bars). n=3 independent experiments per genotype (one cell line per genotype except for p53+/+ and p53 H/- where 2 different cell lines derived from different tumors and result per genotype was averaged). (B) Western blot analysis of p21 level before and 24h after □-irradiation (0.1Gy) in mouse ErbB2 mammary epithelial tumor cell lines with different p53 status. □-Tubulin is loading control. (C) Bar graph showing relative mRNA expression level of CycE before and 24h after □-irradiation in ErbB2 mammary epithelial tumor cell lines with different p53 status. n=3 independent experiments per cell line per genotype. (D) Bar graph showing percent viability before and 24h after irradiation in ErbB2 mammary epithelial tumor cell lines with different p53 status. n=3 independent experiments per cell line per genotype. (E) Restoration of cell cycle checkpoint 24h post □-irradiation p53-null cells. Bar graphs showing cell cycle analysis of p53H/-;ErbB2, p53H/+;ErbB2, p53-/+;ErbB2 following CRISPR/Cas9 p53 deletion (p53CC9) and in p53-/-;ErbB2 cell lines irradiated (gray bars) or not (black bars). n=3 independent experiments per genotype. (F) Bar graphs showing mitotic index in different cell lines irradiated (gray bars) or not (black bars) (result for each irradiated genotype was compared to its own control). n=3 independent experiments per genotype. Where applicable *=p<0.05; **=p<0.01; ***=p<0.001. Error bars represent ± SD.

protein (Fig. 1A). We have shown that γ–irradiation leads to the profound loss of wtp53 allele in p53H/+;ErbB2, but not in p53-/+;ErbB2 cell lines (Fig.14B). Hence, we utilized the established cell line panel to elucidate the mechanism of mutp53-mediated p53LOH.

Markedly, the cell growth analysis demonstrated that p53 LOH (H/-;ErbB2 cells) increases cell proliferation over cells with wtp53 allele (+/+;ErbB2, H/+;ErbB2 and -/+;ErbB2 cells) and over cells null for p53 (p53-/-;ErbB2) (Fig. 15A). Consistent with growth curves, loss of wtp53 allele in mutp53 heterozygous cells (H/-;ErbB2) shows the highest percentage of cells in mitosis compared to other p53 genotypes (Fig. 15B). Our previous results demonstrated that in H/+;ErbB2 cells, mutp53 does not exert a global DN effect over wtp53 allele in response to DNA damage (Fig.5D). In agreement with this data, here we show that the presence of wtp53 allele in H/+;ErbB2 cells is sufficient to induce canonical

p53 target p21 at the RNA (Fig. 15C) and protein level (Fig. 15D) under normal conditions. Loss of wtp53 allele in H/-;ErbB2 and p53-/-;ErbB2 cells abrogates p21 expression (Fig. 15C), which remains undetectable even after irradiation (Fig. 16B). Consistent with the transcriptional activity of wtp53 in heterozygous cells, CRISPR/Cas9-deletion of p53 (mutp53 and wtp53) obliterates the basal p21 expression in unstressed H/+;ErbB2 cells (Fig. 15D).

This finding suggests that the loss of wtp53-mediated p21 expression may enhance proliferation and provide a competitive advantage to cells with p53LOH over cells retaining wtp53 allele. Additionally, CRISPR/Cas9 deletion of mutp53 in H/-;ErbB2 cells decreased cell proliferation significantly (Fig. 15E), suggesting that mutp53 enhances cell proliferation in GOF manner.

These results led us to speculate that under normal conditions, spontaneous p53LOH in heterogeneous H/+;ErbB2 tumor population provides a competitive growth advantage to H/-;ErbB2 cells by two complementary mechanisms: the ablation of basal p21 expression via loss-of-function mechanism and stabilization of mutp53 protein enabling its GOF activities.

3.2 p53LOH abrogates the G2/M checkpoint after irradiation.

An increased incidence of p53LOH in the presence of mutp53 allele after irradiation (Fig.8E,F), set us to investigate the mechanism by which mutp53 promotes p53LOH. The cell cycle analysis demonstrated that p53LOH in mutp53 cells abrogates G2/M checkpoint, which is preserved in the presence of wtp53 allele in -/+;ErbB2 and is partially functional in H/+;ErbB2 (Fig. 16A). As p21 was shown to play a distinct role in the G2/M checkpoint [43, 44], we analyzed p21 protein level in response to irradiation. To avoid nonspecific effects of high dose irradiation, in subsequent experiments, we utilized the low dose irradiation (0.1 Gy). Consistent with the transcriptional activity of wtp53 allele in heterozygous cells (Fig. 15C), we found that irradiation induces p21 in H/+;ErbB2 cells, while the loss of wtp53 allele (H/-;ErbB2) correlates with a lack of detectable p21 protein even after irradiation (Fig. 16B).

Cyclin E is necessary for centrosome duplication in the S phase that precedes the G2/M transition [45]. Previously we demonstrated a significant reduction of cyclin E2 transcription after irradiation in the presence of wtp53 allele (p53H/+;ErbB2 and p53-/+;ErbB2), which is indicative of G2/M arrest [41]. Contrary, irradiation does not affect cyclin E2 transcription in H/-;ErbB2 (Fig. 16C) that was associated with the deficient G2/M checkpoint after irradiation (Fig. 16A). In agreement with defective G2/M checkpoint (Fig. 16A), the lack of p21 expression (Fig. 16B) and elevated cyclin E2 mRNA (Fig. 16C), H/-;ErbB2 cells sustain proliferation after irradiation (Fig. 16A, D). This is in stark contrast to continuous growth arrest of -/+;ErbB2 and H/+;ErbB2 cells after irradiation (Fig. 16A, D).

Importantly, we found that mutp53 CRISPR/Cas9 deletion in H/-;ErbB2 cells restored G2/M arrest after irradiation, as indicated by increased G2/M populations (Fig. 16E). A similar cell cycle profile was observed in H/+;ErbB2 and -/+;ErbB2 cells after p53 CRISPR/Cas9 deletion (Fig. 16E). Consistently, p53-/-;ErbB2 cells maintain functional G2/M checkpoint as indicated by increased G2/M population after irradiation (Fig. 16E), with

no mitotic slippage except in H/-;ErbB2 cells (Fig. 16F). Of note, the cell cycle profiles of H/-;CC9 and -/-;ErbB2 cells are slightly different. The -/-;ErbB2 line was established from -/+;ErbB2 tumor that lost its wtp53 allele through LOH, while the H/-;CC9 cells had mutp53 before CRIPSR depletion. The original presence of mutp53 in the H/-;ErbB2 cells may have led to genetic alterations that are persistent after p53 deletion leading to the differences in the cell cycle profile observed in H/-;CC9 line and -/-;ErbB2 cells. Most importantly, all CC9 (including 630H/-;CC9) and -/-;ErbB2 cells exhibit functional G2/M checkpoint post-irradiation. This data indicates wtp53 independent G2/M checkpoint; however, skipping the G2/M arrest is driven by mutp53 (Fig. 16A). These results strongly suggest that p53LOH in mutp53 heterozygous cells abrogates G2/M checkpoint in the mutp53 GOF manner leading to cell cycle progression after γ-irradiation in the presence of unrepaired DNA (Fig. 16E).

Together, our data indicate that γ-irradiation enhances the clonal expansion of mutp53 cells with p53LOH by providing the competitive growth advantage over cells retaining the wtp53 allele, which induces p21 and undergo G2/M arrest in response to irradiation. Therefore, the clonal dominance of cells with p53LOH may represent the mechanism of irradiation-induced p53LOH.

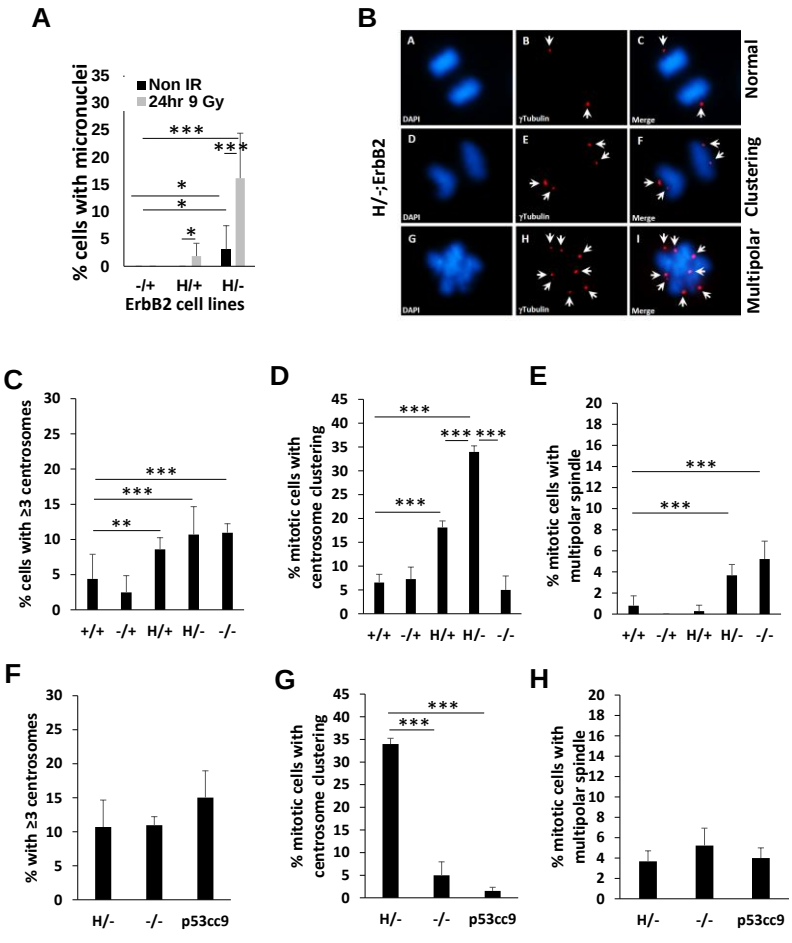

Figure 17. Mutp53 increases centrosomal aberrations and clustering. (A). Bar graph showing percent of cells with micronuclei before and 24h after irradiation in ErbB2 mammary epithelial tumor cell lines with different p53 status. n=3 independent experiments per cell line per genotype (one cell line per genotype except for p53+/+ and p53 H/- where 2 different cell lines derived from different tumors and p53CC9 3 different cell lines, and result per genotype was averaged). (B) Immunofluorescence staining showing centrosome clustering in mitotic p53H/-;ErbB2-mouse mammary epithelium tumor cell line. Centrosomes identified by γ-tubulin staining (red) and DNA by DAPI (blue). (BA-BC) Normal bipolar mitosis with one centrosome at each side. (BD-BF) Bipolar mitosis showing supernumerary centrosome (≥3) clustering, 2 centrosomes on each side. (BG-BI) Multipolar mitosis showing failure of supernumerary centrosomes to cluster. (C-E) Bar graphs showing percent of cells with ≥3 centrosomes, with centrosome clustering and with multipolar spindle, respectively, in ErbB2 mammary epithelial tumor cell lines with different p53 status. n=3 independent experiments per genotype. (F-H) Bar graphs showing percent of cells with ≥3 centrosomes, with centrosome clustering and with multipolar spindle, respectively, in p53H/-;ErbB2 cell line before and after CRISPR/Cas9 p53 deletion (p53CC9) and in p53-/-;ErbB2 cell line. n=3 independent experiments per genotype (For panels C-H, one cell line per genotype except for p53+/+ and p53 H/- where 2 different cell lines derived from different tumors and p53CC9 3 different cell lines, and result per genotype was averaged). Where applicable *=p<0.05; **=p<0.01; ***=p<0.001. Error bars represent ± SD.

3.3 p53LOH drives chromosomal instability in mutant p53 cancer cells.

While mutp53 was implicated as an essential driver of various forms of chromosomal instability - aneuploidy, translocation, and amplification [31, 35], the underpinning mechanism of how mutp53 induces chromosomal aberrations remains vague. Previously we demonstrated that p53LOH in the presence of mutp53 allele is associated with increased chromosomal instability *in vivo* indicated by the higher incidence of anaphase bridges in mammary tumors [41]. In addition, errors in chromosome segregation (chromosomal instability) during mitosis might be monitored by the formation of micronuclei [46, 47]. Consistent with our previous finding [41], we found that irradiation more profoundly drives chromosomal instability in the presence of a mutp53 allele that is further augmented by p53LOH, as indicated by micronuclei formation (Fig. 17A).

As chromosomal instability may arise from abnormal chromosome segregation in mitosis, we investigated centrosome aberration with respect to p53 status. During mitosis, two centrosomes form spindle poles and direct the formation of bipolar mitotic spindles, which is an essential event for the accurate segregation of chromosomes. The presence of more than two centrosomes (centrosome amplification) severely disturbs cytokinesis during mitosis via the formation of more than two spindle poles (Fig. 17B), resulting in an increased frequency of chromosome segregation errors, such as aneuploidy, amplifications, and deletions. These genetic events may further facilitate tumor progression and the acquisition of metastatic phenotype. Significantly, the presence of mutp53 allele in heterozygous cells increases centrosome amplification compared to -/+;ErbB2 cells (Fig. 17B, C) in an apparent DN fashion. Therefore, the elevated centrosome amplification in H/+;ErbB2 cells may increase the incidence of spontaneous p53LOH under normal conditions as compared to -/+;ErbB2 cells. Subsequently, p53LOH (H/-;ErbB2 and -/-;ErbB2 cells) slightly increases the abnormal centrosome number (Fig. 17B, C). On the other hand, the excessive centrosome amplification within tumor cells can be deleterious as it may lead to multipolar mitosis and generate sufficiently high levels of aneuploidy to pose a challenge for cell viability [48]. As a pro-survival mechanism, cancer cells adapt to avoid multipolar mitosis by clustering their extra centrosomes at the two poles of the spindle during mitosis, thus ensuring bipolar chromosome segregation [49]. However, pseudo-bipolar spindle formation through centrosome clustering causes slower mitosis. The latter leads to increased frequency of lagging chromosomes during anaphase and thus to chromosomal instability, thereby explaining the link between supernumerary centrosomes and chromosomal instability [50]. Although centrosome clustering occurs both *in vivo* [51, 52] and *in vitro* [53], its underpinning mechanism is not well understood. Thus, we set to determine whether the mutp53 cells ensure cell survival by evasion of multipolar mitosis via centrosome clustering at the expense of chromosomal instability. We observed mitotic cells with centrosome clustering in all mouse mammary tumor cell lines; however, the percent of mitotic cells with centrosome clustering was significantly higher in cells with mutp53 as compared to mitotic +/+;ErbB2, -/+;ErbB2 and -/-;ErbB2 cells (Fig. 17D). Furthermore, p53LOH (H/-;ErbB2 cells) significantly increased mitotic centrosome clustering compared to H/+;ErbB2 cells (Fig. 17D). Notably, the loss of protective wtp53 allele (-/-;ErbB2 and H/-;ErbB2) significantly elevated multipolar mitosis (Fig. 17E), but only H/-;ErbB2 cells adapt centrosome

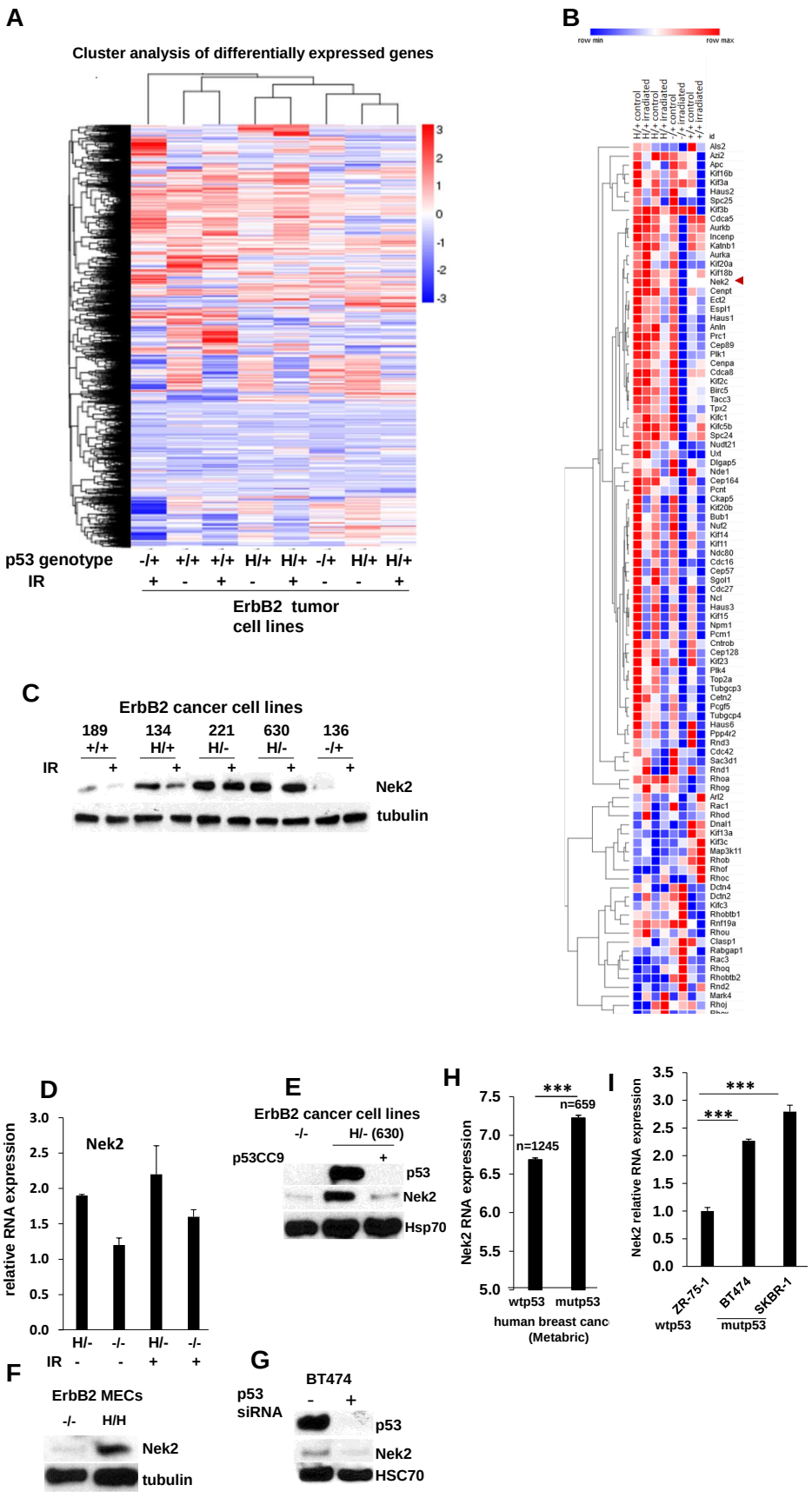

Figure 18. Mutp53 is associated with elevated mRNA and protein levels of NEK2. (A) Heat map showing cluster analysis of differentially expressed genes in p53+/+;ErbB2, p53H/+;ErbB2 and p53-/+;ErbB2 before and after irradiation (9Gy, 24h). (B) Heat map of RNAseq analysis showing differentially regulated centrosome proteins in p53+/+;ErbB2, p53H/+;ErbB2 and p53-/+;ErbB2 before and after irradiation (9Gy, 24h). Arrowhead indicates Nek2. (C) Western blot analysis of Nek2 level before and 24h after □-irradiation in mouse ErbB2 mammary epithelial tumor cell lines with different p53 status. □-tubulin is loading control. (D) Bar graph showing relative mRNA expression level of Nek2 in p53H/-;ErbB2 and p53-/-;ErbB2 cell lines before and after irradiation. n=3 independent experiments per genotype (one cell line per genotype except for p53 H/- where 2 different cell lines derived from different tumors and result was averaged). (E) Western blot analysis of p53 and Nek2 levels in p53-/-;ErbB2 cells and in p53H/-;ErbB2 cells before and after CRISPR/Cas9 p53 deletion. Hsp70 is loading control. (F) Western blot analysis of Nek2 level in p53-/- MECs and p53H/H MECs. □-Tubulin is loading control. (G) Western blot analysis of p53 and Nek2 levels in BT474 cells before and after p53 suppression with siRNA. HSC70 is loading control. (H) Bar graphs showing NEK2 relative mRNA expression in patients with wtp53 (n=1245) compared to with mutp53 (n=659) (all mutations combined vs different types of mutations) (DBD=DNA binding domain; TD=tetramerization domain). (I) Bar graph showing Nek2 relative mRNA expression in human breast cancer cell lines with different p53 status. n=3 experiments per genotype.

clustering as a pro-survival mechanism to avoid cell death due to mitotic catastrophe (Fig. 17D). In support of GOF mechanism of centrosome

clustering, deletion of mutp53 by CRISPR/Cas9 significantly reduced centrosome clustering but does not affect centrosome amplification or multipolar spindle formation Fig.17F-H.

Together our data identify centrosome clustering a novel pro-survival GOF mechanism that underlies an increased fitness of mutp53 cancer cells with p53LOH at the expense of chromosomal instability.

3.4 Mutant p53 allele is associated with the elevated Nek2 function*.*

Understanding how p53LOH enables the proliferation of mutp53 cells (Fig. 15A) and disrupts the mitotic checkpoint (Fig. 16A) in the presence of centrosomal and chromosomal aberrations (Fig. 17) would provide an essential insight into how to prevent the outgrowth of mutp53 cells with p53LOH.

To identify the putative mechanism, we performed RNAseq of mouse mammary tumor cell lines with various p53 genotypes, irradiated, or not (Fig. 18A). The expression analysis of genes involved in the regulation of mitosis identified Nek2 among the top 10 differentially up-regulated genes in the presence of mutp53. Neks (Never in Mitosis (NIMA) Kinases) are a family of serine/threonine kinases involved in the regulation of centrosome function and bipolar division during mitosis. Nek2 is overexpressed in various cancers, including Her2 positive breast cancer, where it predicts poor overall survival [54, 55]. RNAseq analysis showed upregulation of Nek2 at basal level in H/+;ErbB2 as compared to +/+;ErbB2 cells (Fig. 18B).

We focused on studying Nek2 for the following reasons: *i*) Nek2 plays an indispensable role for the entry into mitosis and G2/M progression, as it is required for centrosome assembly/maintenance, spindle formation, and chromosome segregation [56-59]. *ii*) Nek2 overexpression promotes centrosome amplification and aneuploidy by disrupting the mitotic checkpoint, leading to malignant transformation [60, 61]. *iii*) Silencing Nek2 with siRNA inhibited proliferation, induced cell death (due to mitotic errors), and dramatically increased the susceptibility of breast cancer cells to DNA-damaging modalities [60, 61]. *iv*) Wtp53–Nek2 autoregulatory feedback loop has previously been described [62-64], while no mutp53-Nek2 functional interaction has been investigated. *v*) Nek2 can be targeted by highly specific small-molecular inhibitor JH29525 that opens the opportunity for therapeutic intervention.

We validated the RNAseq data by Western (Fig. 18C). Consistent with wtp53 as a negative regulator of Nek2 expression [63], we observed the lowest level of Nek2 in +/+;ErbB2 and -/+;ErbB2 cells (Fig. 18C). Furthermore, irradiation downregulates Nek2 in cells carrying at least one p53 allele (Fig. 18C), while the loss of wtp53 allele (H/-;ErbB2) leads to Nek2 upregulation that is insensitive to irradiation on both protein (Fig. 18C) and RNA levels (Fig. 18D). In addition to the loss of wtp53 function, mutp53 in H/-;ErbB2 cells upregulates Nek2 expression in apparent GOF manner as stabilized mutp53 protein in H/-;ErbB2 cancer cells was associated with a higher level of Nek2 mRNA and protein levels compared to -/-;ErbB2 cancer cells (Fig. 18D) or following mutp53 ablation by CRISPR/Cas9 (Fig. 18E). Similarly, mammary epithelial cells (MECs) established from mammary of -/-;ErbB2 mice [10] express significantly lower levels of Nek2 protein compared to H/H;ErbB2 MECs (Fig. 18F). Importantly, mutp53 promotes Nek2 expression independently of the host and the type of p53

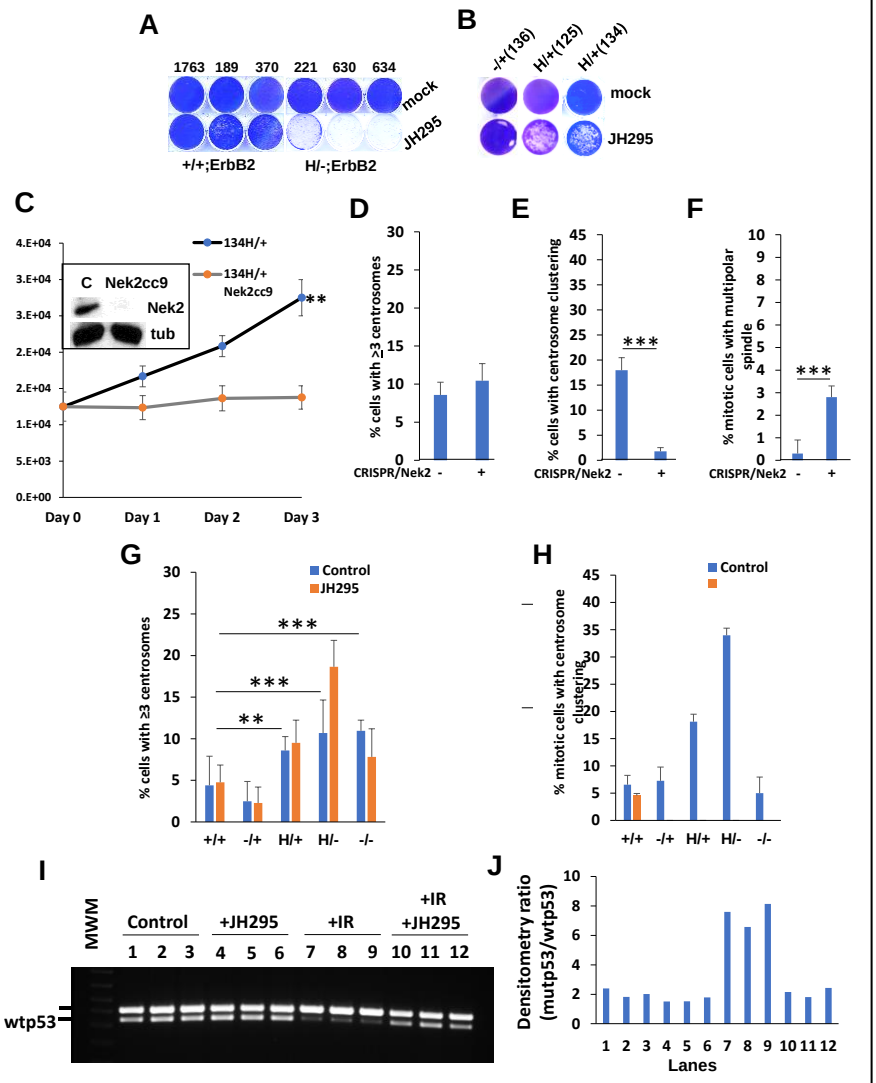

Figure 19. Nek2 ablation suppresses centrosome clustering and p53LOH. (A). Colony formation assay. JH295 suppresses proliferation of H/-;ErbB2 cells, as compared to +/+;ErbB2 cells and partially suppresses proliferation of H/+;ErbB2 cells, as compared to -/+;ErbB2 (B). (C) Growth curve showing suppressed proliferation in H/+;ErbB2 cells following CRISPR/Cas9 Nek2 deletion (Nek2cc9). Inset shows western blot for Nek2 before and after CRISPR/Cas9 Nek2 deletion. Tubulin is loading control. (D-F) Bar graphs showing percent of cells with ≥3 centrosomes, with centrosome clustering and with multipolar spindle, respectively, in H/+;ErbB2 cells before and following CRISPR/Cas9 Nek2 deletion. n=3 independent experiments per genotype. (G & H) Bar graphs showing percent of cells with ≥3 centrosomes and with centrosome clustering, respectively, in ErbB2 mammary epithelial tumor cell lines with different p53 status with and without treatment with Nek2 inhibitor JH295. n=3 independent experiments per genotype (one cell line per genotype) (I) Analysis of LOH in H/+;ErbB2 cell line. n=3 independent experiments per treatment. Non-irradiated cells (lanes 1-3) and cells treated with JH295 (lanes 4-6) are showing no LOH. Irradiated cells showing LOH (lanes 7-9). Cells irradiated and treated with JH295 are showing no LOH (lanes 10-12). (J) Densitometric analysis of band intensity ratio of PCR amplification product shown in (I).

mutation. Mutp53 depletion by siRNA decreases the Nek2 level in human cancer cell line BT474 (E285K) (Fig. 18G).

In further support of the mutp53-Nek2 association in human cancer, a retrospective analysis of the Metabric cohort of breast cancer patients (www.cbioportal.org) demonstrated a significantly higher median of Nek2 mRNA expression in mutp53 patients, regardless of the mutation type, as compared to patients with wtp53 (Fig. 18H). Furthermore, human mutp53 HER2-positive human breast cancer lines (BT474 (E285K), SKBR3 (R175H)) showed significantly higher expression of NEK2 mRNA as compared to ZR-75-1(wtp53) (Fig. 18I).

Together, these experiments indicate that mutp53 can affect Nek2 expression by two complementary mechanisms: the loss of wtp53 inhibitory function and mutp53 GOF upregulation of Nek2. Hence, mutp53-mediated Nek2 expression may reinforce G2/M transition, override G2/M checkpoints, and protect cancer cells from multipolar mitosis at the expense of chromosomal instability.

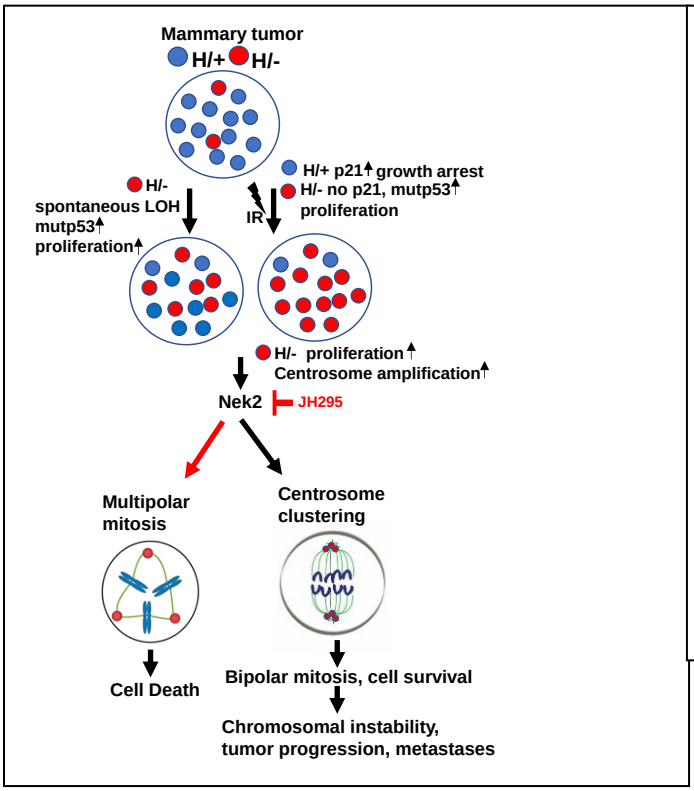

Figure 20. Proposed model for the role of mutp53 and Nek2 in promoting tumorigenesis. In tumors heterozygous for mutp53 there is a mixed population of heterozygous cells (H/+) and cells that underwent spontaneous LOH (H/-). Genotoxic stress, such as □-irradiation, leads to slow proliferation and expansion of H/+ population due to the presence of wtp53 that can induce cell cycle checkpoint and arrest. On the other hand, H/- cells continue unrestricted proliferation, taking over the H/+ population. In both cases, absence of wtp53 in H/- leads to increased cell proliferation and to centrosome amplification. To avoid multipolar mitosis and cell death of H/- cells with centrosome amplification, mutp53 utilizes Nek2 to induce centrosome clustering to promote bipolar mitosis and cell survival. Centrosome clustering process lengthens mitosis which then leads to increased chromosomal instability and thus enhancing tumor progression and metastasis. Our model proposes Nek2 as an Achilles heel, for tumor cells with mutp53, that can be used as a therapeutic target to prevent p53 LOH and cells that have

3.5 Nek2 inhibition prevents p53LOH in mutant p53 heterozygous cells.

We hypothesized that deficient checkpoints and the increased proliferation of H/-;ErbB2 cells confer a positive selection for p53LOH during tumor progression. Therefore, the identification of specific vulnerabilities of mutp53 cancer cells with p53LOH would provide the therapeutic opportunity to prevent p53LOH and, thus, the expansion of genetically unstable, more aggressive cancer cells population. As a mutp53-mediated upregulation of Nek2 (Fig. 18) may facilitate G2/M transition by reinforcing centrosome clustering, mutp53 cells with p53LOH may specifically be dependent on Nek2 expression for their survival to avoid multipolar mitosis and mitotic catastrophe.

To test this hypothesis, we investigated the effect of Nek2 inhibitors on mitotic spindle formation and centrosome clustering with respect to p53 genotypes. Several Nek2-specific inhibitors were described in the literature (JH 295, TOCRIS, or TAI-95, Probechem) [65]. In our study, we utilized JH295 (oxindole propynamide, IC50=770nM), which is a highly specific and irreversible Nek2 inhibitor that blocks Nek2 activity via alkylation of residue Cys22, and does not affect the activities of other mitotic kinases (CDK1, PLK1, Aurora B, or Mps1) [65]. Moreover, JH295 does not perturb bipolar spindle assembly or the spindle assembly checkpoint [65]. Given this selective profile, we thought that JH295 is as useful for identifying the biological roles of Nek2 as RNAi interference approach.

Strikingly, we observed a genotype-specific inhibitory effect of JH295 in mutp53 cells with p53LOH (H/-;ErbB2) as compared to cells with wtp53 allele (+/+;ErbB2, -/+;ErbB2, H/+ErbB2) as indicated by the colony formation assay (Fig. 19A, B). JH295 had an intermediate inhibitory effect on H/+ErbB2 cells (Fig. 19B). The specificity of JH295 was validated on cells where Nek2 was deleted using CRISPR/Cas9. Consistent with the requirement of Nek2 for the survival of mutp53 cancer cells, we were able to generate H/+;ErbB2/Nek2-/-, but not H/-;ErbB2/Nek2-/- cell lines by CRISPR/Cas9 technology. However, the genetic depletion of Nek2

significantly reduced the proliferation rate of H/+;ErbB2 cells in short term assay (Fig. 19C). The analysis of mitotic H/+;ErbB2/Nek2-/- cells revealed that the genetic ablation of Nek2 did not increase the proportion of cells with centrosome amplification (Fig. 19D), but dramatically reduced centrosome clustering (Fig. 5E) with a concomitant increase in cells carrying multipolar mitotic spindle (Fig. 19F). Consistent with the genetic depletion of Nek2, the sensitivity to JH295 correlates with the complete abrogation of centrosome clustering in H/+;ErbB2 and H/-;ErbB2 cells (Fig. 19H), while the proportion of mitotic cells carrying supernumerary centrosomes did not change (Fig. 19G). Importantly, JH295 most robustly affected H/-;ErbB2 cells, but not +/+;ErbB2 cells in any tested assays (Fig. 19A, G & H), suggesting an alternative Nek2-independent mechanism of centrosome regulation in wtp53 cells. In sum, our data identified the requisite function of Nek2 for centrosome clustering and, thus, survival of H/-;ErbB2 cells.

The increased sensitivity of H/-;ErbB2 cells to Nek2 inhibition set us to test whether JH295 prevents outgrowth mutp53 cells with p53LOH, thus preventing loss of wtp53 allele after irradiation. Hence, H/+;ErbB2 cells were irradiated (9 Gy), or not, and then treated with JH295, or not, for 10 days. DNA from surviving cells was analyzed for p53LOH by PCR. As shown in Fig. 19I & J, we observed p53LOH only in irradiated cells (lanes 7-9), but not in non-irradiated (lanes 1-3) or JH295-treated cells (lanes 4-6). Remarkably, Nek2 inhibition protects cells from irradiation-induced p53LOH (lanes 10-12).

In sum, our results suggest that Nek2 inhibition may alter the selective pressure for p53LOH in heterogeneous tumor population by contraction of specifically mutp53 population with p53LOH, thus, preventing the outgrowth of genetically unstable and metastatic cells (Fig.20) .

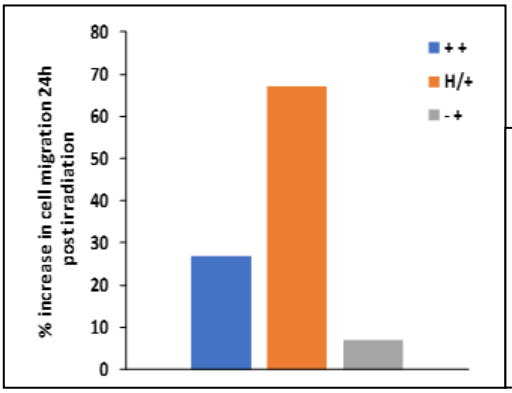

Figure 21. Mutp53 allele promotes migration in heterozygous cells after irradiation. Cells were □-irradiated (9Gy), or not, and 24h post-irradiation were assayed for migration using transwell assay. Cells were fixed and stained using crystal violet. Cell were counted in 4 random fields per treatment. For each cell genotype, the percent change in cell migration post irradiation as compared to non-irradiated controls was then calculated.

Major Task 3 Determine whether p53 LOH promotes metastatic behavior in ErbB2 cancer cells (50% completion).

Subtask 1. Establish whether p53 LOH enhances the motility and invasion of cancer cells in vitro.

Test the motility and invasive properties of primary mammary epithelial cells and tumor cultures derived from H/+;ErbB2 and p53-/+;ErbB2 mice before and after LOH in vitro. Boyden chamber assay, wound healing assay, metastases in allografts.

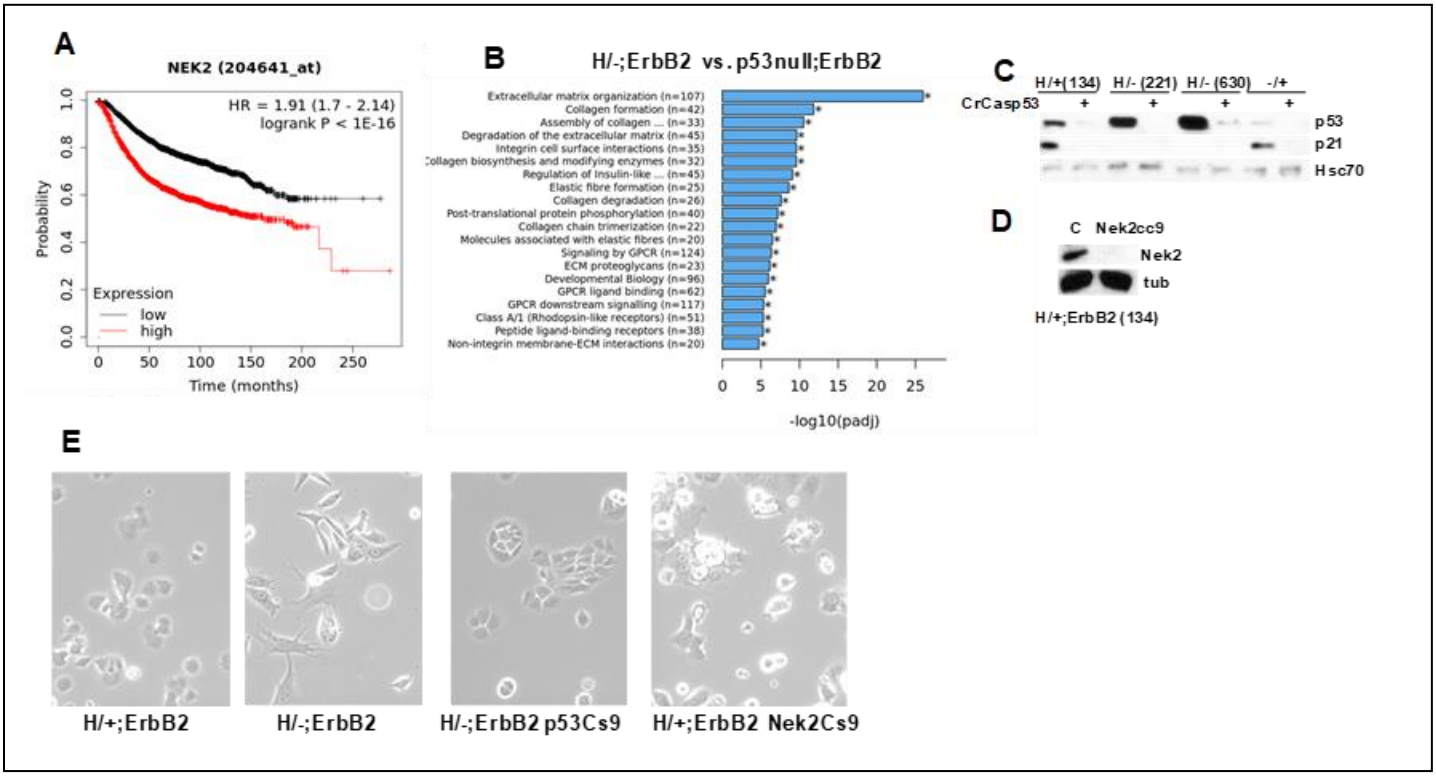

Figure 22. (A). high level of Nek2 expression is prognostic of poor survival of breast cancer patients (http://kmplot.com/). B. ECM-remodeling and integrin signaling are the most upregulated pathways in the presence of mutp53 allele. The transcriptome analysis of enriched gene sets differentially expressed in H/-;ErbB2 vs. p53null;ErbB2 cells. (C) Panel of isogenic CRISPR derivatives of murine ErbB2 tumor cell lines with depleted p53 (C) and Nek2 (D). (E) The loss of wtp53 allele shifts cells phenotype from epithelial (H/+;ErbB2) to mesenchymal (H/-;ErbB2). Panel 3: CRISPR-cas9 mediated depletion of mutp53 from H/-;ErbB2 cells revert mesenchymal (H/-;ErbB2) phenotype to epithelial. Panel 4: Nek2 CRISPR-cas9 depletion mitigate cells adhesion.

First, we assessed the short-term (p53LOH independent) effect of irradiation on cells motility in the context of p53 genotype. We tested migration 24h after irradiation. At this time point, we observed only marginal loss of wtp53 allele in H/+;ErbB2 cells. Strikingly, we found that irradiation induces migration in all genotypes, but more profoundly in H/+;ErbB2 cells (Fig. 21). Therefore, p53LOH independent effects may contribute to motility followed irradiation. We hypothesized that irradiation-induced mutp53 stabilization may impose mutp53 dominant-negative effect over wtp53 allele, inducing metastases that we observed *in vivo.* The dramatic difference in motility between H/+;ErbB2 and -/+;ErbB2 after irradiation supports this hypothesis.

As we previously reported, the main phenotype associated with p53LOH in mutp53 heterozygous cells is enhanced metastases *in vivo*. Also, we demonstrated that irradiation induces migration in all genotypes, but more profoundly in the presence of mutp53 allele (H/+;ErbB2 cells) *in vitro*. To identify the mechanism of mutp53-induced metastases, we performed the RNAseq analysis of cells with different genotypes (Fig. 18).

RNAseq analysis identified three top candidates which were highly overexpressed in H/+;ErbB2 (n=2) vs. -/+;ErbB2 cells: Cdh2 (N-cadherin), VEGFC, and MMP7. We validated the RNAseq data by qRT-PCR. N-cadherin (a member of the family of Ca2+ dependent cell-cell adhesion molecules) is involved in multiple processes including inducing invasion, migration, promoting survival of cancer cells, regulating adhesion, and,

ultimately, metastasis. N-cadherin and Her2 were found to be co-expressed in human invasive breast carcinomas, where they associated with lymph node-positive disease, distant metastases, and a high risk of metastatic brain relapse. Importantly, in the Her2 amplified subtype, the frequency of brain metastasis has been reported to be as high as 35% that representing a significant clinical problem[66].

Vascular endothelial growth factor (VEGF-C) overexpression in breast cancer cells is shown to be associated with increased intratumoral lymphangiogenesis, resulting in significantly enhanced metastasis to regional lymph nodes and to lungs *in vivo*. The expression of VEGF-C mRNA has recently been shown to correlate with the rate of metastasis to lymph nodes in human breast cancer[67].

Matrix metalloproteinase-7 (MMP-7) is a small secreted proteolytic enzyme with broad substrate specificity. Its expression is associated with tumor invasion, metastasis, and survival for a variety of cancers including metastatic breast cancer, where it is associated with metastasis, disease progression, and decreased survival[68].

Furthermore, our RNAseq data identified Nek2 as a novel putative target of mutp53 that promotes genomic and chromosomal instability. Genomic instability has long been proposed to be a mechanism by which a cell may acquire the necessary properties for invasion and metastasis. We performed extensive mechanistic studies on identifying the tumorigenic function of mutp53-Nek2 axis in breast cancer cells (Major Task 2). Although Cdh2 (N-cadherin), VEGFC, and MMP7 are promising potential leads, we focused on the mechanistic role of mutp53-Nek2 signaling in promoting breast cancer metastases.

The clonal diversity, produced by genomic instability, leads to intratumor clonal competition, clonal evolution, and acquisition of the necessary properties required for metastasis (Fig.20). Therefore, we hypothesized that mutp53-Nek2 axis mediates p53LOH that further produces genomic instability, generating a variety of genetically distinct clones with de novo genetic evolutionary changes that allow clones to metastasize. On the other hand, recent advances in understanding Nek2 biology suggest that Nek2 itself is an important regulator of cancer cell migration and metastasis beyond promoting genomic instability through the activation of a variety of oncogenic pathways. Consistently, our retrospective analysis of clinical data revealed that the high level of Nek2 expression is prognostic of poor survival of breast cancer patients (http://kmplot.com/) (Fig.22A). As metastatic disease remains the leading cause of cancer-related mortality in humans, this clinical observation confirms the association of the high Nek2 level and metastasis in humans.

To evaluate the impact of mutp53, p53LOH, and Nek2 on phenotypic characteristics related to metastatic dissemination, we utilized the panel cell lines from mammary tumors of mice with different p53 and LOH genotypes. The transcriptome analysis of differentially expressed gene sets revealed several pathways involved in ECM remodeling that were specifically enriched in the presence of mutp53 (Fig.22B). To build upon these observations, we generated isogenic CRISPR derivatives of murine tumor cell lines: with depleted p53 (Fig.22C) and Nek2 (Fig.22D). Consistent with our in vivo data, loss of wtp53 allele in cells shifts cells phenotype from

epithelial (H/+;ErbB2) to mesenchymal (H/-;ErbB2) (Fig.22E). Furthermore, CRISPR-cas9 mediated depletion of mutp53 from H/-;ErbB2 cells reverts mesenchymal (H/-;ErbB2) to epithelial phenotype (Fig.22E). Significantly, Nek2 CRISPR-cas9 depletion dramatically affects cell adhesion (Fig.22E, panel 4), indicating the interception of ECM-integrin signaling. In sum, our experiments imply that p53LOH in the presence of a mutp53 allele may promote metastases in mutp53 GOF manner via complementary mechanisms: 1) modulation ECM-integrin signaling; 2) upregulation Nek2 and its mediated metastatic properties; 3) inducing genomic instability. We hypothesize that after p53LOH mutp53-mediated upregulation of Nek may alter ECM-integrin signaling and, thus, metastases. As a future development of this project, we will determine whether genetic and pharmacological ablation of Nek2 prevents p53LOH associated metastases, which we observed *in vivo.*

Subtask 2. Determine whether p53 LOH enhances the ability of tumor cells to metastasize in vivo. Isolate metastatic cells from lungs of irradiated and non-irradiated of R172H/+;ErbB2 vs p53-/+;ErbB2 vs p53+/+;ErbB2 mice. Assess p53 LOH status in metastases in comparison with primary tumors.

We have made numerous attempts to isolate metastatic cells from the lungs of mice with different genotypes, as we designed in the original grant application (ErbB2 FACS sorting). We also attempted to dissect metastatic lesions from the paraffin-embedded section of lungs using a laser-capture microscope. However, the low yield of metastatic cells and contamination with normal tissues precluded the implementation of the proposed task in a reproducible and statistically appropriate manner. Therefore, this subtask was not completed as was originally designed due to technical issues.

Alternatively, currently, we are employing an established panel of isogenic cell lines with different p53 genotypes, which recapitulate p53LOH in p53 heterozygous cells (See subtask 1). We generated numerous isogenic loss-of-function mammary tumors cell lines (p53CRISPR and Nek2CRISPR). We employed these cell lines for the orthotopic mammary fat pad implantation in ongoing proof-of-principle experiments in vivo. Unfortunately, this is an ongoing experiment and we were unable to complete the final analysis in a statistically significant manner within the funding period.

Although this task was not completed within the funding period, we would like to point out that we completed mechanistic studies that were beyond proposed research that identified 1) differential mutp53-mediated suppression of ATM signaling in response to a high and low dose of irradiation; 2) new mutp53-Nek2 axis that governs p53LOH after genotoxic stress; 3) pharmacological inhibition of Nek2 prevents radiation-induced p53LOH in mutp53 dependent manner. These clinical questions could potentially have a significant clinical impact on the development of new diagnostic, prognostic, and therapeutic approaches for breast cancer management.

- What opportunities for training and professional development has the project provided?

Lucas Garcia, undergraduate student, Stony Brook University (September 2016-July 2017), Julia Rosenfeld, undergraduate student Binghamton University State University of New York, (June-July 2017) and Safia Mirza (high school student) have received professional on-hand training while working on this project. Lucas Garcia is the co-author on the manuscript submitted to Molecular Cancer Therapeutics. Partly as a result of this educational activity, Lucas Garcia was admitted to prestigious Graduate School of Boston Medical School. Malik Padellan, undergraduate student, Stony Brook University (September 2018-2019), and Boris Nekrasov (June18-August18, high school student) have received professional on-hand training while working on this project. Paige Brook, High School student, (June 2020- August 2020) has received professional on-hand training in literacy while working on this project.

- How were the results disseminated to communities of interest?
- Oral presentations:
- Stony Brook University Pathology Grand rounds (5/31/2018): Molecular mechanisms of p53 deregulation in HER2-positive breast cancer in response to radiation.
- VA, Northport Medical Center, NY, "Lunch and Learn" seminar series for medical residents (9/21/2018): P53 LOH in HER2-positive breast cancer in response to radiation: possible driver(s).
- Oral presentations: 8th International mutant p53 Workshop, Lyon, France, 15-18 May, 2019
- Poster presentation: “Molecular mechanisms of p53 loss of heterozygosity in breast cancer in response to irradiation”, Amr Ghaleb, Alisha Yallowitz, and Natalia Marchenko. 8th International mutant p53 Workshop, Lyon, France, 15-18 May, 2019.
- In May 2020 we planned to present our findings at the p53 International Workshop in Israel. The workshop was cancelled due to pandemic.
- Oral presentations: Amr Ghaleb “Centrosome clustering as a survival mechanism in breast cancer cells carrying mutant p53”. Stony Brook Cancer center, seminar (May 2021).

4.IMPACT

- Major innovative findings and achievements for this reporting period:

1) We completed generation and analysis of the novel mouse model for Her2 breast cancer R248Q;ErbB2. In contrast to previously generated R172H;ErbB2 mouse model, R248Q p53 mutation in heterozygosity does not accelerate mammary tumorigenesis. This data implies that cooperation of mutant p53 in ErbB2 occurs in p53

mutation type-specific manner. The survival analysis of newly generated heterozygous R248Q;ErbB2 mouse model indicates strong loss-of-function, but not gain-of-function effect of mutant p53.

2) Using MMTV;ErbB2 mouse model carrying heterozygous R172H p53 mutation, we show that under normal condition, transcriptionally competent wtp53 allele enables the genomic integrity and suppresses the mTOR pathway in mutp53 heterozygous ErbB2 cancer cells; As an early response in mutant p53 heterozygous cells, genotoxic stress promotes sustained mutant p53 stabilization, continuous DNA damage, and aberrant G1-S transition The main physiological outcomes of p53LOH are profound stabilization of mutant p53 protein, mTOR upregulation, enhanced genomic instability, and metastases.

3) We established that wtp53 in mutp53 heterozygous (H/+;ErbB2) tumors might be transcriptionally competent towards a subset of targets (p21, Mdm2) and/or mutp53 may exert dominant-negative effect and suppress subset of wtp53 targets (Gadd45) in response to irradiation. p53LOH leads to the loss of transcriptional activation of p21 and abrogation of G2/M checkpoint and aggravation centrosome aberrations leading to increased genomic and chromosomal instability; increased cells proliferation; 5) transcriptional upregulation of genes involved in mitosis, including Nek2 (member of Never in Mitosis (NIMA) Related Kinases family); the increased sensitivity of mutp53 cancer cells to Nek2 inhibition.

4) We identified Nek2 as a pharmacological target to prevent p53LOH onset in mutant p53 heterozygous cells. As a proof-of-principle, we demonstrate that Nek2-specific inhibitor JH295 precludes the loss of wtp53 allele in mutp53 heterozygous cells after irradiation. These findings may have a significant translational impact, as they may provide a foundation for developing a novel therapeutic strategy to curb tumor progression.

5) Using MMTV/ErbB2 mutant p53 (R172H) heterozygous mouse model we found differential p53 genotype-specific effect of low (LDR) and high (HDR) doses irradiation of established tumors on cancer progression. In mutant p53 tumors, LDR, but not HDR, causes p53 loss-of-heterozygosity. Following LDR, mutant p53 tumor cells exhibit aberrant ATM/DNA-PK signaling with defects in sensing of double-strand DNA brakes, leading to deficient DNA repair. In contrast, HDR-induced genotoxic stress is sufficient to reach the threshold of DNA damage that is necessary for wtp53 induced DNA repair and cell cycle arrest. As a result, LDR promotes genomic instability in mutant p53 cells leading to the selection of a proliferative death-resistant population, with negligible mutagenic effect on tumors carrying wtp53. Hence, our study suggest that early stages breast cancer patients carrying monoallelic p53 mutations are a potentially high-risk group for LDR exposure.

- What was the impact on the development of the principal discipline(s) of the project?
-

During the awarded period, the following studies were prepared for peer-reviewed publications:

1. Li D, Marchenko ND. ErbB2 inhibition by lapatinib promotes the degradation of mutant p53 protein in cancer cells. Oncotarget. 2017 Jan 24;8(4):5823-5833. (The study utilizes mouse models and cell lines generated for the DOD-funded project to explore how mutp53 affects ErbB2-HSF1 signaling)

2. Alexandrova EM, Mirza SA, Xu S, Schulz-Heddergott R, Marchenko ND, Moll UM. p53 loss-of-heterozygosity is a necessary prerequisite for mutant p53 stabilization and gain-of-function in vivo. Cell Death Dis. 2017 Mar 9;8(3). (In collaboration with Dr.Moll lab, we established that spontaneous p53LOH leads to stabilization of other mutp53 R248Q protein).

3. Yallowitz A, Ghaleb A, Garcia L, Alexandrova EM, Marchenko N. Heat Shock Factor 1 confers resistance to lapatinib in ErbB2 positive breast cancer cells. 2018, Cell Death Dis., 2018 May 24;9(6). (The study utilizes mouse models and cell lines generated for the DOD-funded project to test how mutp53 affects ErbB2 signaling).

4. Ghaleb A. Marchenko N. “Mutant p53-Hsp90 axis in human cancer”, book chapter, “Heat Shock Protein 90 in Human Diseases and Disorders”,2018, Springer Nature Publishers. In press. (The summary of our studies on how mutp53 affects ErbB2 signaling and cancer cells survival in response to proteotoxic stress and literature overview of the field).

5. Ghaleb A., Yallowitz A, Marchenko N. 2019. Irradiation induces p53 loss of heterozygosity in breast cancer expressing mutant p53. Commun Biol. 2(1):436.

6. Ghaleb A, Padellan M., Marchenko N. 2020. Mutant p53 drives the loss of heterozygosity by the upregulation of Nek2 in breast cancer cells. Breast Cancer Res. 2020 Dec 2;22(1):133.

7. Ghaleb A, Roa L, Marchenko N. Low-dose but not high-dose□□-irradiation elicits dominant negative effect of mutant p53 in vivo. Cancer Letters, 2021, under revision, # CANLET-S-21-03429-1

- What was the impact on other disciplines?

Nothing to Report.

- What was the impact on technology transfer?

Nothing to Report.

- What was the impact on society beyond science and technology?

Nothing to Report.

5. CHANGES/PROBLEMS:

As we described above, despite of our extensive expertise and numerous vigorous attempts we failed to establish continuous culture of MECs from H/+;ErbB2, -/+;ErbB2 and +/+;ErbB2 mice, likely due to transcriptional activity of wtp53 in heterozygosity. All wtp53 expressing MECs undergo senescence following passage 3. Therefore, now we mainly will focus on cancer cell lines established from mammary tumors of H/+;ErbB2, -/+;ErbB2 and +/+; ErbB2 mice.
Also, we encountered problem with the scoring of IHC staining for the implementation of Major Task1 Subtask 1, as ErbB2 staining produced overwhelmingly strong signal, while HSF1 staining was low and unspecific in mouse tumor tissues. To overcome these problems, we switched to analysis of mTOR that is a major downstream signaling target of ErbB2 and utilized in vitro studies to address genotype-specific effect of p53LOH on HSF1 signaling. In both cases, the alternative approaches helped us to solve initial problems.

Major Task3 Subtask 2. We have made numerous attempts to isolate metastatic cells from the lungs of mice with different genotypes, as we designed in the original grant application (ErbB2 FACS sorting). We also attempted to dissect metastatic lesions from the paraffin-embedded section of lungs using a laser-capture microscope. However, the low yield of metastatic cells and contamination with normal tissues precluded the implementation of the proposed task in a reproducible and statistically appropriate manner. Therefore, this subtask was not completed as was originally designed due to technical issues. We utilized the alternative approach as discussed above.

- Significant changes in use or care of human subjects, vertebrate animals, biohazards, and/or select agents

Nothing to Report.

- Significant changes in use or care of human subjects

Nothing to Report.

- Significant changes in use or care of vertebrate animals.

Nothing to Report.

- Significant changes in use of biohazards and/or select agents

Nothing to Report.

6. PRODUCTS:

During the awarded period, the following studies were prepared for peer-reviewed publications:

1. Li D, Marchenko ND. ErbB2 inhibition by lapatinib promotes the degradation of mutant p53 protein in cancer cells. Oncotarget. 2017 Jan 24;8(4):5823-5833. (The study utilizes mouse models and cell lines generated for the DOD-funded project to explore how mutp53 affects ErbB2-HSF1 signaling)

2. Alexandrova EM, Mirza SA, Xu S, Schulz-Heddergott R, Marchenko ND, Moll UM. p53 loss-of-heterozygosity is a necessary prerequisite for mutant p53 stabilization and gain-of-function in vivo. Cell Death Dis. 2017 Mar 9;8(3). (In collaboration with Dr.Moll lab, we established that spontaneous p53LOH leads to stabilization of other mutp53 R248Q protein).

3. Yallowitz A, Ghaleb A, Garcia L, Alexandrova EM, Marchenko N. Heat Shock Factor 1 confers resistance to lapatinib in ErbB2 positive breast cancer cells. 2018, Cell Death Dis., 2018 May 24;9(6). (The study utilizes mouse models and cell lines generated for the DOD-funded project to test how mutp53 affects ErbB2 signaling).

4. Ghaleb A. Marchenko N. “Mutant p53-Hsp90 axis in human cancer”, book chapter, “Heat Shock Protein 90 in Human Diseases and Disorders”,2018, Springer Nature Publishers. In press. (The summary of our studies on how mutp53 affects ErbB2 signaling and cancer cells survival in response to proteotoxic stress and literature overview of the field).

5. Ghaleb A., Yallowitz A, Marchenko N. 2019. Irradiation induces p53 loss of heterozygosity in breast cancer expressing mutant p53. Commun Biol. 2(1):436.

6. Ghaleb A, Padellan M., Marchenko N. 2020. Mutant p53 drives the loss of heterozygosity by the upregulation of Nek2 in breast cancer cells. Breast Cancer Res. 2020 Dec 2;22(1):133.

7. Ghaleb A, Roa L, Marchenko N. Low-dose but not high-dose□□-irradiation elicits dominant negative effect of mutant p53 in vivo. Cancer Letters, 2021, under revision, # CANLET-S-21-03429-1

All publications contain acknowledgement of DOD support.

- Other Products

Novel R248Q; ErbB2 mouse model recapitulating human Her2 positive breast cancer was generated.

7. PARTICIPANTS & OTHER COLLABORATING ORGANIZATIONS

Has there been a change in the active other support of the PD/PI(s) or senior/key personnel since the last reporting period?

Name:	Natalia Marchenko
Project Role:	PI
Researcher Identifier (e.g. ORCID ID):	
Nearest person month worked:	12 months
Contribution to Project:	Dr. Marchenko was responsible for the overall administration, data analysis, coordination and direction of the project and lab work. Dr. Marchenko performed breeding and mouse colony maintenance, tumor specimens analysis, mammary epithelial cells isolation, manuscript preparation.
Funding Support:	DOD # BC151569
Name:	Euvgenia Alexandrova
Project Role:	Collaborator
Researcher Identifier (e.g. ORCID ID):	
Nearest person month worked:	3 months
Contribution to Project:	As a collaborator Dr. Alexandrova was involved in generation, specimen tissue preparation and data analysis of R248Q;ErbB2 mice, manuscript preparation.
Funding Support:	NCI gran t# K22CA190653-01A1
Name:	Sulan Xu
Project Role:	Lab technician

Researcher Identifier (e.g. ORCID ID):	
Nearest person month worked:	3 months
Contribution to Project:	Sulan was responsible for breeding and mouse colony maintenance, mouse genotyping, performed tissue embedding, cutting and IHC staining.
Funding Support:	
Name:	Lucas Garcia
Project Role:	Undergraduate Student, Stony Brook University
Researcher Identifier (e.g. ORCID ID):	
Nearest person month worked:	11 months
Contribution to Project:	Lucas Garcia performed Western blot analysis of cell lines, mice genotyping and assessment of p53 LOH status in cell lines.
Funding Support:	none
Name:	Julia Rosenfeld
Project Role:	Summer Undergraduate Student, Binghamton University State University of New York
Researcher Identifier (e.g. ORCID ID):	
Nearest person month worked:	2 months
Contribution to Project:	Julia Rosenfeld performed Western blot analysis of cell lines.
Funding Support:	none
Name:	Ute Moll

Project Role:	Collaborator
Researcher Identifier (e.g. ORCID ID):	
Nearest person month worked:	1 month
Contribution to Project:	As a collaborator Dr. Moll participated in planning of experiments, discussions of data interpretations, manuscript preparation.
Funding Support:	NCI grant R01CA176647
Name:	Amr Ghaleb
Project Role:	investigator
Researcher Identifier (e.g. ORCID ID):	
Nearest person month worked:	12 months
Contribution to Project:	Amr was responsible for breeding and mouse colony maintenance, mouse genotyping, performed tissue embedding, cutting and IHC staining, QRT-PCR, in vitro experiments.

- What other organizations were involved as partners?

Nothing to Report

8. SPECIAL REPORTING REQUIREMENTS

Nothing to Report

1. Baum, M., *Harms from breast cancer screening outweigh benefits if death caused by treatment is included.* BMJ, 2013. **346**: p. f385.
2. Cancer Genome Atlas, N., *Comprehensive molecular portraits of human breast tumours.* Nature, 2012. **490**(7418): p. 61-70.
3. He, C., et al., *Mutant p53 Gain of Function and Chemoresistance: The Role of Mutant p53 in Response to Clinical Chemotherapy.* Chemotherapy, 2017. **62**(1): p. 43-53.
4. Shepherd, F.A., et al., *Pooled Analysis of the Prognostic and Predictive Effects of TP53 Comutation Status Combined With KRAS or EGFR Mutation in Early-Stage Resected Non-Small-Cell Lung Cancer in Four Trials of Adjuvant Chemotherapy.* J Clin Oncol, 2017. **35**(18): p. 2018-2027.
5. Bertheau, P., et al., *TP53 status and response to chemotherapy in breast cancer.* Pathobiology, 2008. **75**(2): p. 132-9.
6. Levine, A.J., J. Momand, and C.A. Finlay, *The p53 tumour suppressor gene.* Nature, 1991. **351**(6326): p. 453-6.
7. Petitjean, A., et al., *Impact of mutant p53 functional properties on TP53 mutation patterns and tumor phenotype: lessons from recent developments in the IARC TP53 database.* Hum Mutat, 2007. **28**(6): p. 622-9.
8. Jackson, J.G., et al., *p53-mediated senescence impairs the apoptotic response to chemotherapy and clinical outcome in breast cancer.* Cancer Cell, 2012. **21**(6): p. 793-806.
9. Alexandrova, E.M., et al., *p53 loss-of-heterozygosity is a necessary prerequisite for mutant p53 stabilization and gain-of-function in vivo.* Cell Death Dis, 2017. **8**(3): p. e2661.
10. Yallowitz, A.R., et al., *Mutant p53 Amplifies Epidermal Growth Factor Receptor Family Signaling to Promote Mammary Tumorigenesis.* Mol Cancer Res, 2015. **13**(4): p. 743-54.
11. Alexandrova, E.M., et al., *Improving survival by exploiting tumour dependence on stabilized mutant p53 for treatment.* Nature, 2015. **523**(7560): p. 352-6.
12. Bug, M. and M. Dobbelstein, *Anthracyclines induce the accumulation of mutant p53 through E2F1-dependent and -independent mechanisms.* Oncogene, 2011. **30**(33): p. 3612-24.
13. Rao, C.V. and H.Y. Yamada, *Genomic instability and colon carcinogenesis: from the perspective of genes.* Front Oncol, 2013. **3**: p. 130.
14. Aoki, K., et al., *Colonic polyposis caused by mTOR-mediated chromosomal instability in Apc+/Delta716 Cdx2+/- compound mutant mice.* Nat Genet, 2003. **35**(4): p. 323-30.
15. Hanel, W. and U.M. Moll, *Links between mutant p53 and genomic instability.* J Cell Biochem, 2012. **113**(2): p. 433-9.
16. Lane, D. and A. Levine, *p53 Research: the past thirty years and the next thirty years.* Cold Spring Harb Perspect Biol, 2010. **2**(12): p. a000893.
17. Linke, S.P., et al., *p53 interacts with hRAD51 and hRAD54, and directly modulates homologous recombination.* Cancer Res, 2003. **63**(10): p. 2596-605.
18. Menon, V. and L. Povirk, *Involvement of p53 in the repair of DNA double strand breaks: multifaceted Roles of p53 in homologous recombination repair (HRR) and non-homologous end joining (NHEJ).* Subcell Biochem, 2014. **85**: p. 321-36.
19. Akyuz, N., et al., *DNA substrate dependence of p53-mediated regulation of double-strand break repair.* Mol Cell Biol, 2002. **22**(17): p. 6306-17.
20. Lin, Y., B.C. Waldman, and A.S. Waldman, *Suppression of high-fidelity double-strand break repair in mammalian chromosomes by pifithrin-alpha, a chemical inhibitor of p53.* DNA Repair (Amst), 2003. **2**(1): p. 1-11.
21. Rodgers, K. and M. McVey, *Error-Prone Repair of DNA Double-Strand Breaks.* J Cell Physiol, 2016. **231**(1): p. 15-24.
22. Chin, K., et al., *In situ analyses of genome instability in breast cancer.* Nat Genet, 2004. **36**(9): p. 984-8.
23. Ghadimi, B.M., et al., *Centrosome amplification and instability occurs exclusively in aneuploid, but not in diploid colorectal cancer cell lines, and correlates with numerical chromosomal aberrations.* Genes Chromosomes Cancer, 2000. **27**(2): p. 183-90.
24. Lingle, W.L., et al., *Centrosome amplification drives chromosomal instability in breast tumor development.* Proc Natl Acad Sci U S A, 2002. **99**(4): p. 1978-83.
25. Pihan, G.A., et al., *Centrosome defects and genetic instability in malignant tumors.* Cancer Res, 1998. **58**(17): p. 3974-85.

26. Pihan, G.A., et al., *Centrosome abnormalities and chromosome instability occur together in pre-invasive carcinomas.* Cancer Res, 2003. **63**(6): p. 1398-404.
27. Fukasawa, K., et al., *Abnormal centrosome amplification in the absence of p53.* Science, 1996. **271**(5256): p. 1744-7.
28. Shinmura, K., et al., *Direct evidence for the role of centrosomally localized p53 in the regulation of centrosome duplication.* Oncogene, 2007. **26**(20): p. 2939-44.
29. Tarapore, P. and K. Fukasawa, *Loss of p53 and centrosome hyperamplification.* Oncogene, 2002. **21**(40): p. 6234-40.
30. Tarapore, P., et al., *Direct regulation of the centrosome duplication cycle by the p53-p21Waf1/Cip1 pathway.* Oncogene, 2001. **20**(25): p. 3173-84.
31. Porta, C., C. Paglino, and A. Mosca, *Targeting PI3K/Akt/mTOR Signaling in Cancer.* Front Oncol, 2014. **4**: p. 64.
32. Leonard, M.K., et al., *The PTEN-Akt pathway impacts the integrity and composition of mitotic centrosomes.* Cell Cycle, 2013. **12**(9): p. 1406-15.
33. Ghaleb, A.M., et al., *KLF4 Suppresses Tumor Formation in Genetic and Pharmacological Mouse Models of Colonic Tumorigenesis.* Mol Cancer Res, 2016. **14**(4): p. 385-96.
34. Wang, X., et al., *Overexpression of aurora kinase A in mouse mammary epithelium induces genetic instability preceding mammary tumor formation.* Oncogene, 2006. **25**(54): p. 7148-58.
35. Budanov, A.V. and M. Karin, *p53 target genes sestrin1 and sestrin2 connect genotoxic stress and mTOR signaling.* Cell, 2008. **134**(3): p. 451-60.
36. Vadysirisack, D.D., et al., *Feedback control of p53 translation by REDD1 and mTORC1 limits the p53-dependent DNA damage response.* Mol Cell Biol, 2011. **31**(21): p. 4356-65.
37. Workman, P., et al., *Drugging the cancer chaperone HSP90: combinatorial therapeutic exploitation of oncogene addiction and tumor stress.* Ann N Y Acad Sci, 2007. **1113**: p. 202-16.
38. Schulz, R., et al., *HER2/ErbB2 activates HSF1 and thereby controls HSP90 clients including MIF in HER2-overexpressing breast cancer.* Cell Death Dis, 2014. **5**: p. e980.
39. Chou, S.D., et al., *mTOR is essential for the proteotoxic stress response, HSF1 activation and heat shock protein synthesis.* PLoS One, 2012. **7**(6): p. e39679.
40. Li, D., et al., *A gain-of-function mutant p53-HSF1 feed forward circuit governs adaptation of cancer cells to proteotoxic stress.* Cell Death Dis, 2014. **5**: p. e1194.
41. Ghaleb, A., A. Yallowitz, and N. Marchenko, *Irradiation induces p53 loss of heterozygosity in breast cancer expressing mutant p53.* Commun Biol, 2019. **2**: p. 436.
42. Vassilev, L.T., et al., *In vivo activation of the p53 pathway by small-molecule antagonists of MDM2.* Science, 2004. **303**(5659): p. 844-8.
43. Maeda, T., et al., *Role of p21(Waf-1) in regulating the G1 and G2/M checkpoints in ultraviolet-irradiated keratinocytes.* J Invest Dermatol, 2002. **119**(2): p. 513-21.
44. Koyano, T., et al., *The p21 dependent G2 arrest of the cell cycle in epithelial tubular cells links to the early stage of renal fibrosis.* Sci Rep, 2019. **9**(1): p. 12059.
45. Aleem, E., H. Kiyokawa, and P. Kaldis, *Cdc2-cyclin E complexes regulate the G1/S phase transition.* Nat Cell Biol, 2005. **7**(8): p. 831-6.
46. Fenech, M., *Chromosomal biomarkers of genomic instability relevant to cancer.* Drug Discov Today, 2002. **7**(22): p. 1128-37.
47. Iarmarcovai, G., et al., *Genetic polymorphisms and micronucleus formation: a review of the literature.* Mutat Res, 2008. **658**(3): p. 215-33.
48. Kramer, A., B. Maier, and J. Bartek, *Centrosome clustering and chromosomal (in)stability: a matter of life and death.* Mol Oncol, 2011. **5**(4): p. 324-35.
49. Saunders, W., *Centrosomal amplification and spindle multipolarity in cancer cells.* Semin Cancer Biol, 2005. **15**(1): p. 25-32.
50. Ganem, N.J., S.A. Godinho, and D. Pellman, *A mechanism linking extra centrosomes to chromosomal instability.* Nature, 2009. **460**(7252): p. 278-82.
51. Basto, R., et al., *Centrosome amplification can initiate tumorigenesis in flies.* Cell, 2008. **133**(6): p. 1032-42.

52. Murphy, T.D., *Drosophila skpA, a component of SCF ubiquitin ligases, regulates centrosome duplication independently of cyclin E accumulation.* J Cell Sci, 2003. **116**(Pt 11): p. 2321-32.
53. Quintyne, N.J., et al., *Spindle multipolarity is prevented by centrosomal clustering.* Science, 2005. **307**(5706): p. 127-9.
54. Fang, Y. and X. Zhang, *Targeting NEK2 as a promising therapeutic approach for cancer treatment.* Cell Cycle, 2016. **15**(7): p. 895-907.
55. Hayward, D.G. and A.M. Fry, *Nek2 kinase in chromosome instability and cancer.* Cancer Lett, 2006. **237**(2): p. 155-66.
56. Bahe, S., et al., *Rootletin forms centriole-associated filaments and functions in centrosome cohesion.* J Cell Biol, 2005. **171**(1): p. 27-33.
57. Fry, A.M., et al., *C-Nap1, a novel centrosomal coiled-coil protein and candidate substrate of the cell cycle-regulated protein kinase Nek2.* J Cell Biol, 1998. **141**(7): p. 1563-74.
58. Man, X., T.L. Megraw, and Y.P. Lim, *Cep68 can be regulated by Nek2 and SCF complex.* Eur J Cell Biol, 2015. **94**(3-4): p. 162-72.
59. Rapley, J., et al., *Coordinate regulation of the mother centriole component nlp by nek2 and plk1 protein kinases.* Mol Cell Biol, 2005. **25**(4): p. 1309-24.
60. Muller, P.A. and K.H. Vousden, *p53 mutations in cancer.* Nat Cell Biol, 2013. **15**(1): p. 2-8.
61. Musacchio, A. and E.D. Salmon, *The spindle-assembly checkpoint in space and time.* Nat Rev Mol Cell Biol, 2007. **8**(5): p. 379-93.
62. Fischer, M., L. Steiner, and K. Engeland, *The transcription factor p53: not a repressor, solely an activator.* Cell Cycle, 2014. **13**(19): p. 3037-58.
63. Nabilsi, N.H., et al., *Local depletion of DNA methylation identifies a repressive p53 regulatory region in the NEK2 promoter.* J Biol Chem, 2013. **288**(50): p. 35940-51.
64. Tabach, Y., et al., *The promoters of human cell cycle genes integrate signals from two tumor suppressive pathways during cellular transformation.* Mol Syst Biol, 2005. **1**: p. 2005 0022.
65. Henise, J.C. and J. Taunton, *Irreversible Nek2 kinase inhibitors with cellular activity.* J Med Chem, 2011. **54**(12): p. 4133-46.
66. Qian, X., et al., *N-cadherin/FGFR promotes metastasis through epithelial-to-mesenchymal transition and stem/progenitor cell-like properties.* Oncogene, 2014. **33**(26): p. 3411-21.
67. Skobe, M., et al., *Induction of tumor lymphangiogenesis by VEGF-C promotes breast cancer metastasis.* Nat Med, 2001. **7**(2): p. 192-8.
68. Beeghly-Fadiel, A., et al., *Genetic polymorphisms in the MMP-7 gene and breast cancer survival.* Int J Cancer, 2009. **124**(1): p. 208-14.

COMMUNICATIONS BIOLOGY

ARTICLE

https://doi.org/10.1038/s42003-019-0669-y OPEN

Irradiation induces p53 loss of heterozygosity in breast cancer expressing mutant p53

Amr Ghaleb[1]*, Alisha Yallowitz[1,2] & Natalia Marchenko[1]*

Mutations in one allele of the TP53 gene in cancer early stages are frequently followed by the loss of the remaining wild-type allele (LOH) during tumor progression. However, the clinical impact of TP53 mutations and p53LOH, especially in the context of genotoxic modalities, remains unclear. Using MMTV;ErbB2 model carrying a heterozygous R172H p53 mutation, we report a previously unidentified oncogenic activity of mutant p53 (mutp53): the exacerbation of p53LOH after irradiation. We show that wild-type p53 allele is partially transcriptionally competent and enables the maintenance of the genomic integrity under normal conditions in mutp53 heterozygous cells. In heterozygous cells γ-irradiation promotes mutp53 stabilization, which suppresses DNA repair and the cell cycle checkpoint allowing cell cycle progression in the presence of inefficiently repaired DNA, consequently increases genomic instability leading to p53LOH. Hence, in mutp53 heterozygous cells, irradiation facilitates the selective pressure for p53LOH that enhances cancer cell fitness and provides the genetic plasticity for acquiring metastatic properties.

[1] Department of Pathology, Stony Brook University, Stony Brook, NY 11794-8691, USA. [2] Weill Cornell Medicine, 1300 York Avenue, LC-902, New York, NY 10065, USA. *email: amr.ghaleb@stonybrookmedicine.edu; natalia.marchenko@stonybrookmedicine.edu

Breast cancer is one of the leading causes of death in women worldwide. Currently, radiation therapy, coupled with breast-conserving surgery is the standard of care for the majority of breast cancer patients. However, a meta-analysis showed that radiation reduces 15-year breast cancer mortality risk only by 5%[1]. At present, 30% of all breast cancer cases are considered to be overtreated by the administration of more aggressive therapies than is necessary or by overdiagnosis, where no treatment is required[2]. An estimated one to three deaths from overtreatment occur for every one breast cancer death avoided[3]. Hence, the understanding of how to reliably identify which breast cancer patients will benefit from radiotherapy is needed to reduce the mortality risk and improve the quality of life.

Mutations in TP53 (p53) gene are common in breast cancer and are especially enriched in Her2 (human EGF receptor 2, ErbB2) positive breast cancer (72%)[4], and basal-like breast cancer (80%)[4]. Whereas wild-type p53 (wtp53) is an important determinant of the efficacy of DNA-damaging therapies, the p53 mutational status is not routinely used for cancer management. This is mainly due to inconsistent results of clinical studies[5], conceivably because in previous studies the predictive effect of p53 status in response to genotoxic modalities has not been assessed at the different stages and in the context of p53 heterozygosity. In some cancers, mutant p53 (mutp53) status was shown to predict poor patient outcome in response to genotoxic treatment[6], whereas other studies showed a better response of mutp53 tumors to chemotherapies[7]. Thus, knowing how mutp53 interacts with the specific oncogenic environment in the context of conventional therapies will facilitate the clinical utilization of the mutational status of p53.

Clinical data suggest that p53 behaves as a classic "two-hit" tumor suppressor where a point mutation in one allele of p53 at early stages is followed by loss of the wild-type allele (loss of heterozygosity (LOH)) later during tumor progression[8]. Albeit mutp53 in heterozygosity may exert dominant-negative (DN) effect[9], several *in vivo* studies showed that wtp53 retains its function in heterozygous tumors[10]. In support, ~80% of advanced-stage mutp53 breast cancer tumors have lost the wtp53 allele suggesting the high selective pressure for p53LOH during tumor progression[11]. These studies raise the question of why mutp53 exerts DN in some contexts, but not others, and what is the clinical relevance of these findings?

To address these questions, we generate MMTV-ErbB2 and mutp53 R172H (H thereafter) knock-in mouse model that faithfully recapitulates human Her2-positive breast cancer[12]. We find that wtp53 retains its transcriptional activity in both p53−/+;ErbB2 and p53H/+;ErbB2 heterozygous cancer cells. However, irradiation of pre-malignant mammary lesions aggravates mammary tumorigenesis that is associated with increased frequency of p53LOH mostly in mutp53 heterozygous mice. Importantly, p53LOH is concomitant with elevated genomic and chromosomal aberrations, inefficient DNA repair, activation of mTOR signaling and, as a result, increased metastases in mutp53 heterozygous compared to hemizygous cells. Hence, we propose that in response to irradiation, mutp53, via activation of the mTOR pathway, generates the selective pressure for wtp53 loss in heterozygous cells that is fueled by deficient DNA repair and abnormal cell-cycle progression.

Results

Survival of mutp53 breast cancer patients following radiotherapy is stage-dependent. To assess the predictive effect of TP53 overall mutations in response to γ-irradiation, we investigated publicly available databases of retrospective clinical data of Metabric cohort (2433 breast cancer patients, http://www.cbioportal.org). Analysis of all stages of breast invasive ductal carcinoma (BIDC) combined, showed that radiotherapy improved overall survival (OS) to all patients independently of the mutational profile (Fig. 1a, b). Stratification of BIDC patients by stage demonstrated a significant stage-dependent benefit of radiotherapy in stage 2 compared to stage 1 cohort (Fig. 1c, d). Strikingly, stratification by p53 status in ErbB2 cohort of BIDC showed that stage 1 patients with overall mutant TP53;ErbB2 tumors had significantly worse OS after radiotherapy as compared to untreated cohorts (Fig. 1e), while radiation significantly improved OS of stage 2 patients with overall mutant TP53;ErbB2 tumors (Fig. 1f). In contrast, radiotherapy marginally extended OS of patients with wild-type TP53 tumors independently of the stage (Fig. 1g, h). Hence, in ErbB2 breast cancer patients, overall mutant TP53 status might be predictive of a negative outcome from genotoxic modalities in stage 1, whereas it is significantly advantageous for stage 2. Similarly, patients with overall mutant TP53 BIDC tumors showed a worse outcome after chemotherapy in stage 1 (Supplementary Fig. 1a), but favorable outcome in stage 2 (Supplementary Fig. 1b). Although the number of cases limited the statistical significance, this trend was not observed for patients with wild-type TP53 breast cancer patients after chemotherapy (Supplementary Fig. 1c, d). Importantly, the frequency of p53LOH increased during tumor progression: 52% of stage 1 patients are heterozygous for p53, while only 20% of stage 2 patients retain wtp53 allele (Fig. 1i).

Therefore, we hypothesized that the p53LOH status might be an important determinant of the survival of patients carrying mutant TP53 tumors after genotoxic therapies.

γ-Irradiation aggravates mammary tumorigenesis and promotes p53LOH in MMTV-ErbB2 mouse model. To recapitulate the early stages of human ErbB2 breast cancer and study the impact of p53LOH in context of genotoxic therapies, we generated a genetic mouse model as described before[12]. The murine R172H (H thereafter) p53 mutation corresponds to human hotspot R175H mutation in ErbB2 breast cancer[4] and (http://www.cbioportal.org)). We found that ErbB2 mammary tumorigenesis was aggravated in p53H/+;ErbB2 mice, compared to p53 null counterparts, indicated by earlier tumor onset and shorter survival (Fig. 2, Table 1,[12]). Furthermore, a single dose of γ-irradiation at the time of pre-malignant lesions onset (5 Gy to 80-day-old mice) significantly shortened both tumor latency and overall survival by approximately 80 days, in both p53−/+;ErbB2 and p53H/+;ErbB2 genotypes (Fig. 2a), but not in p53+/+;ErbB2 mice (Fig. 2b). Notably, irradiation increased p53LOH in both p53H/+;ErbB2 (Fig. 2c) and p53−/+;ErbB2 (Table 1) tumors. Also, p53LOH occurred more frequently in the presence of mutp53 allele in both non-irradiated p53H/+;ErbB2 and p53−/+;ErbB2 (18 and 11%, respectively, Table 1) and this difference was exacerbated after irradiation (p53H/+;ErbB2 95% vs. p53−/+;ErbB2 38%, respectively, Table 1). Although we did not observe survival difference in p53H/+;ErbB2 vs. p53−/+;ErbB2, the main phenotype associated with enhanced p53LOH was the increased rate of metastases in the presence of mutp53 allele (p53H/+;ErbB2 100% vs. p53+/−;ErbB2 58%, Table 1). Contrary, irradiation of p53+/+;ErbB2 mice did not increase metastasis, and we were unable to detect loss of wtp53 allele in tumors after irradiation of p53+/+;ErbB2 mice (Table 1).

Next, we determined whether the presence of mutp53 allele accelerates p53LOH after irradiation in vitro. Cell lines, generated from mouse tumors of different genotypes (Fig. 2d and Supplementary Fig. 2a) were irradiated, or not, and the copy number of wtp53 and mutp53 alleles were determined at different

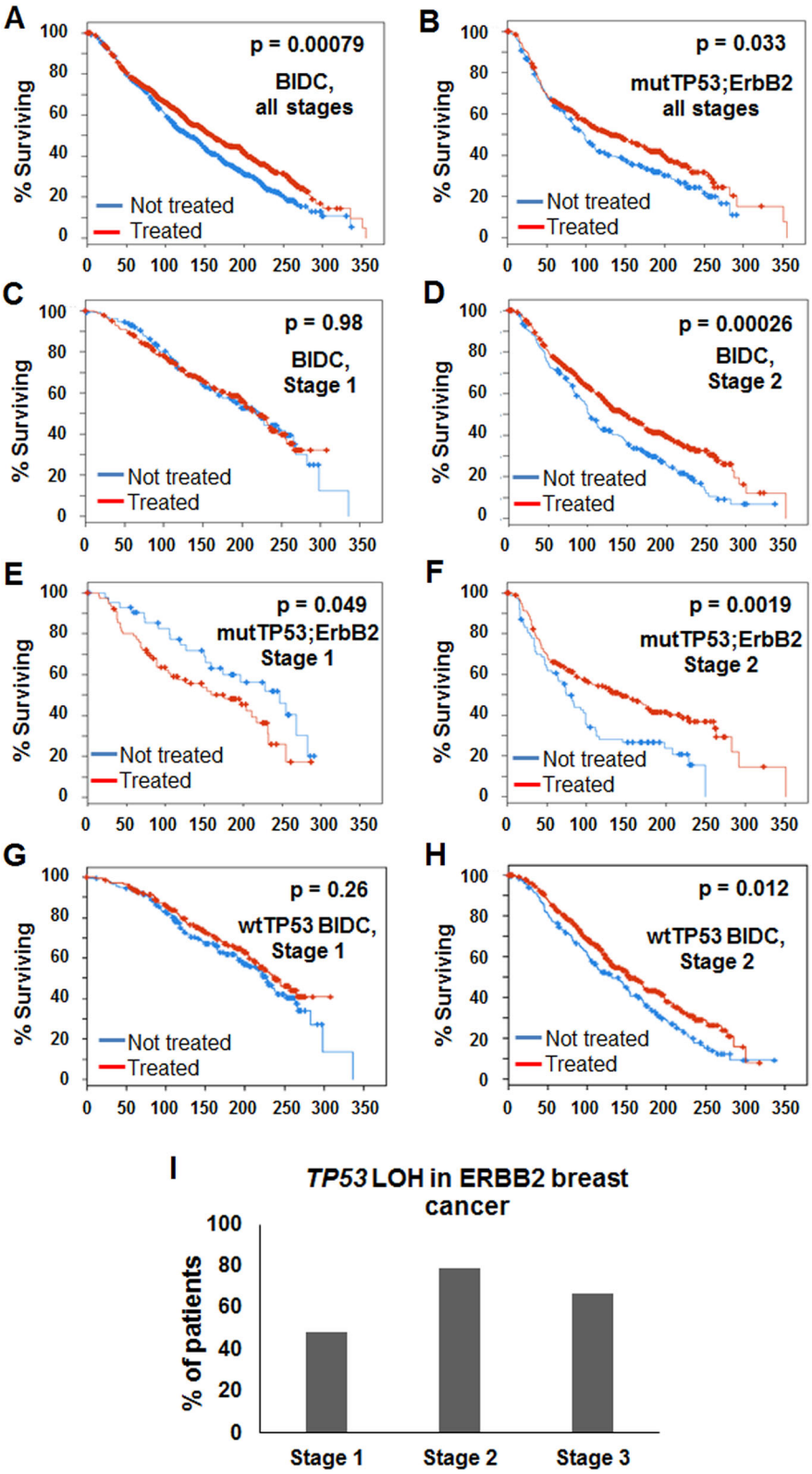

Fig. 1 The survival of mutp53 breast cancer patients following radiotherapy is stage-dependent. Kaplan-Meier survival curve for patients ($n = 2433$) with breast cancer receiving radiation therapy (red line) or untreated (blue line). **a** All breast cancer patients ($p = 0.00079$). **b** Patients with TP53 and ErbB2 mutations ($n = 193$, $p = 0.033$). **c** Stage 1, all breast cancer patients ($n = 440$, $p = 0.98$). **d** Stage 2, all breast cancer patients ($n = 759$, $p = 0.00026$). **e** Stage 1 patients with TP53 and ErbB2 mutations ($n = 35$, $p = 0.049$). **f** Stage 2 patients with TP53 and ErbB2 mutations ($n = 70$, $p = 0.0019$). **g** Stage 1 patients with wild-type p53 ($n = 302$, $p = 0.26$). **h** Stage 2 patients with wild-type p53 ($n = 458$, $p = 0.017$). **i** TP53 LOH in breast cancer patients is stage-dependent. 52% of stage I and only 20% stage II mutp53 tumors retain wtp53 allele.

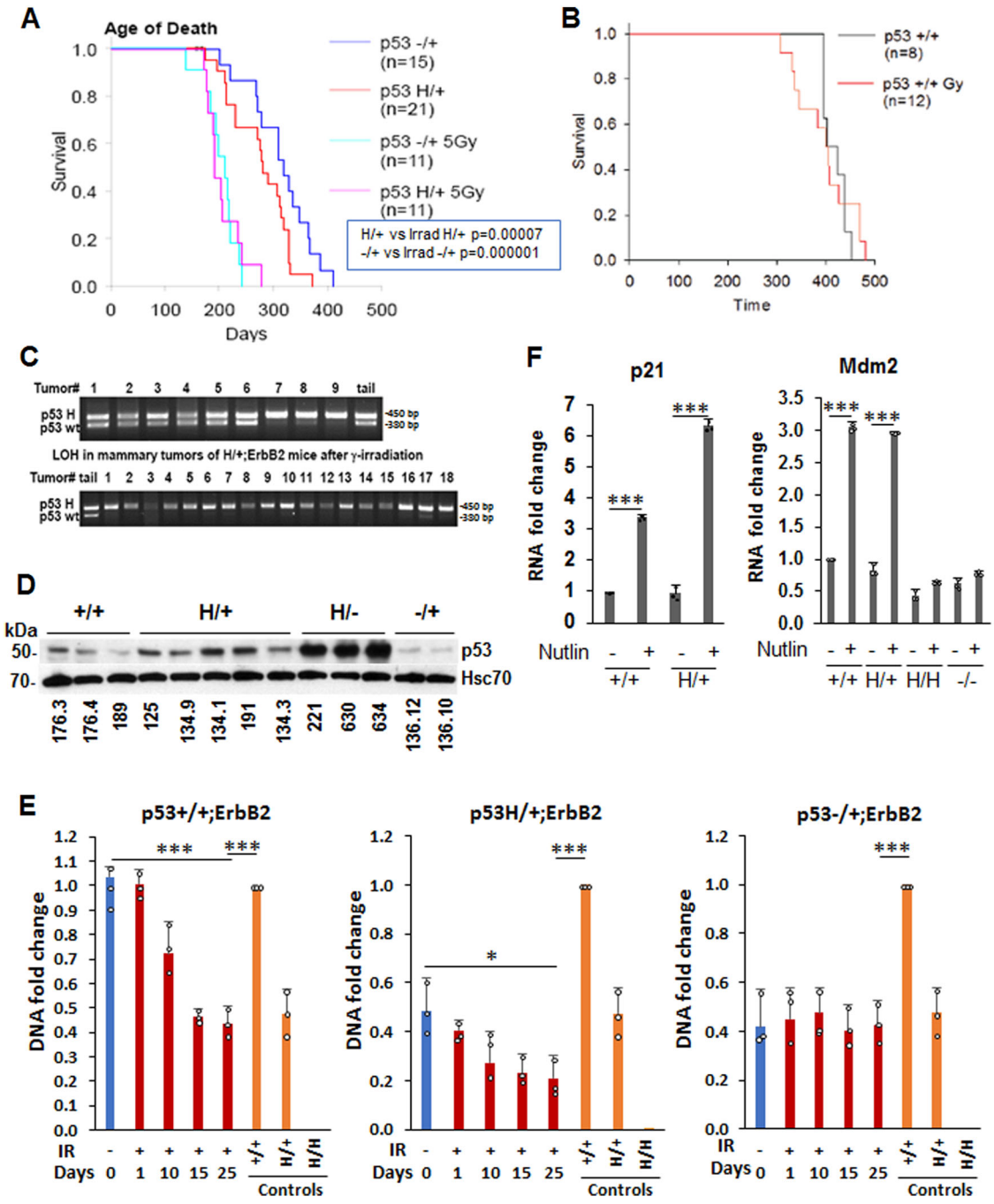

Fig. 2 γ-Irradiation aggravates mammary tumorigenesis and promotes p53LOH in MMTV-ErbB2 mouse model. **a**, **b** Kaplan-Meier survival curves of irradiated and non-irradiated MMTV-ErbB2 mouse model. Single-dose of 5 Gy γ-irradiation at the time of onset of pre-malignant lesions (80 days) aggravates mammary tumorigenesis in p53H/+;ErbB2 vs. p53−/+;ErbB2 ($p < 0.001$ and $p = 0.04$, respectively) (**a**), but not in p53+/+;ErbB2 mice ($p = 0.892$) (**b**). n values are indicated in the figure and represent the number of mice. **c** Example of LOH analysis in tumors from p53H/+;ErbB2 mice. Non-irradiated mice are showing LOH in few mice only (top lanes 7–9). Irradiated mice, showing LOH in all but 1 mouse (bottom lane 17). **d** P53 expression in a panel of cell lines established from mammary tumors of MMTV-ErbB2 mice with different p53 genotypes. HSC70 is a loading control. **e** Mutp53 enhances LOH following γ-irradiation in cell culture ($n = 3$ independent samples Error bars represent ± SD). Cultivated mammary tumors cells were irradiated (9 Gy), or not, and grown up to 25 days post-irradiation. DNA was extracted at the indicated time points. The copy number of p53 wt and mut alleles was quantified by real-time PCR. DNA extracted from tail tissue samples of the corresponding genotype was used for copy number control. The experiment was repeated three times. Summary of a representative experiment. **f** Wtp53 retains transcriptional activity and, in response to Mdm2 inhibitor nutlin, induces its target p21 and Mdm2 in mutp53 heterozygous cells. Nutlin does not induce Mdm2 in p53H/H;ErbB2 and p53−/−;ErbB2 MECs. $n = 3$ independent experiments. Error bars represent ± SD.

time points by qPCR (Fig. 2e). In agreement with *in vivo* data (Table 1), we found 3-fold reduction of wtp53 allele post-irradiation in p53H/+;ErbB2 compared to untreated cells (a 5-fold reduction compared to control p53+/+;ErbB2 cells), but not in p53−/+;ErbB2 cells compared to non-irradiated cells (Fig. 2e). Irradiation induced a 2-fold decrease in copy number of the wild-type allele in p53+/+;ErbB2 cells compared to control cells (Fig. 2e).

Table 1 Median survival, tumor spectrum and LOH in mice with indicated genotypes.

Tumor types				Irradiated		
	−/+;ErbB2 (*n* = 19)	H/+;ErbB2 (*n* = 22)	+/+;ErbB2 (*n* = 9)	−/+;ErbB2 (*n* = 16)	H/+;ErbB2 (*n* = 17)	+/+;ErbB2 (*n* = 16)
Mammary	86%	95%	100%	75%	59%	88%
Lymphoma	10%	0%	0	19%	24%	6%
Mammary + Lymphoma	0%	0	0	6%	0%	0%
Sarcoma	4%	5%	0	0%	24%	6%
tumor number per mouse	2.7	6.1	4.8	3.6	5.1	2.6
Median survival (days)	312	285	399	2.3	2.5	397
% of lung metastases	52%	58%	50%	58%	100%	54%
loss of wtp53 allele	11%	18%	0%	38%	95%	0%

To evaluate the consequences of p53LOH in vitro with respect to the transcriptional activity of wtp53 in heterozygosity, we examined the expression of canonical p53 target genes Mdm2 and p21 in response to Mdm2 inhibitor, nutlin, by qPCR. Nutlin promotes p53 transcriptional activity without induction of DNA damage[13]. No significant difference in the expression of Mdm2 and p21 was observed between p53+/+;ErbB2 and p53H/+;ErbB2 cells at basal level, while the expression of both was increased following nutlin addition (Fig. 2f). In contrast, nutlin failed to induce p53 targets in p53H/H;ErbB2 and p53−/−;ErbB2 mammary epithelial cells (MECs) (Fig. 2f). Hence, in heterozygosity, wtp53 at least partially preserves its transcriptional function, while p53LOH may abrogate tumor-suppressor activities of wtp53.

Irradiation induces the accumulation of mutant p53 protein in heterozygous cancer cells. Most homozygous mutp53 human cancers and cell lines accumulate high levels of mutp53 protein; however, little is known about how mutp53 protein levels are regulated in heterozygosity. Consistent with our previous study on R248Q;MMTV-Neu mouse model[11], we found only 10–15% of p53 positive cells in p53H/+;ErbB2 tumors, while p53 staining was undetected in p53−/+;ErbB2 and p53+/+;ErbB2 tumors (Fig. 3a and Supplementary Fig. 2b). Irradiation-mediated p53LOH in p53H/+;ErbB2 mammary tumors was associated with significant stabilization of mutp53 protein in vivo (Fig. 3a, and Supplementary Fig. 2b) and in cell lines generated from mammary tumors that underwent p53LOH in vivo (Fig. 2d, lanes 9–11 and Supplementary Fig. 2a). Conversely, irradiation did not affect wtp53 levels in p53+/+;ErbB2 and p53−/+;ErbB2 tumors (Fig. 3a and Supplementary Fig. 2b). These results are consistent with Li et al. report that irradiation stabilizes mutp53 protein in MDA231 cells and, thus, promotes proliferation[14]. As mutp53 protein stabilization in tumors was proposed to be essential for its oncogenic function[15], p53LOH with subsequent mutp53 stabilization may represent a key event in cancer progression in vivo.

Western blot of mouse tumors 16 h post-irradiation revealed that in irradiated p53H/+;ErbB2 tumors mutp53 protein was stabilized to a higher level than non-irradiated p53H/+;ErbB2 tumors, while p53 in p53−/+;ErbB2 tumors remained undetectable (Fig. 3b). Likewise, wtp53 in p53+/+;ErbB2 cell line was only transiently upregulated 2 h post-irradiation, but mutp53 showed much higher level in p53H/+;ErbB2 cell line up to 24 h after irradiation (Fig. 3c and Supplementary Fig. 2c).

It was previously shown that mutp53 mRNA is upregulated in response to genotoxic anthracyclines in human cell lines[16]. Analysis of p53 mRNA level showed no increase in p53 mRNA in p53H/+;ErbB2 cells after irradiation (Fig. 3d), suggesting post-transcriptional regulation of mutp53 protein levels in heterozygosity post-irradiation. Hence, we hypothesized that, in heterozygous cells, irradiation stabilizes mutp53 over the threshold that is sufficient to promote its oncogenic activities leading to p53LOH and tumor progression.

P53LOH is associated with the switch from HRR to NHEJ and genomic instability. Genomic instability, such as chromosomal rearrangement caused mainly by failure in normal chromosome segregation during mitosis, has been regarded as one of the major causes of LOH in cancer[17,18]. Mutations in a number of genes, e.g., p53 and PI3K, hinder normal mitosis leading to chromosomal aberrations[17]. Alternatively, the accumulation of various oncogenic mutations during cancer progression can be a result of inefficient DNA repair. Therefore, we assessed two major DNA repair mechanisms in ErbB2 mammary tumors with various p53 genotypes.

Wtp53 is activated in response to genotoxic treatments, eliciting cell-cycle arrest, DNA repair, and/or apoptosis[19,20]. Depending on cell context and the extent of DNA-damage, p53 may promote DNA repair by one or both of the two major repair pathways: (1) homologous recombinational repair (HRR)[21,22], and (2) nonhomologous end-joining (NHEJ)[22–24]. HRR is relatively slow and less error-prone, while NHEJ is faster and more error-prone[25].

HRR (Rad51 as a marker) was activated in p53+/+;ErbB2, p53−/+;ErbB2, p53H/+;ErbB2 and p53−/−;ErbB2 but was suppressed in p53H/−;ErbB2 and p53H/H;ErbB2 mammary tumors (Fig. 4a and Supplementary Fig. 3a). Conversely, wtp53 inhibited NHEJ (Ku70 as a marker), while higher Ku70 staining was only in tumors lacking wtp53 (Fig. 4b and Supplementary Fig. 3b). Hence, we hypothesized that, in the context of p53 status, the presence of wtp53 allele may shift DNA repair mechanism towards to HRR, whereas loss of wtp53 allele (LOH) leads to switch to NHEJ repair with mutp53 actively suppressing HRR, and causing the acquisition of multiple mutations, mitotic abnormalities, and chromosomal aberrations.

Chromosomal aberrations can be measured by the frequency of 'anaphase bridges' (AB) in the anaphase of the cell-cycle. AB are extended chromosome bridging between two spindle poles (Fig. 4c) and are a histologic hallmark of dicentric chromosomes[26]. High AB was shown to be associated with the increased frequency of Apc LOH in a colon cancer mouse model[18]. We found a marginal difference in AB scoring between p53+/+;ErbB2, p53−/+;ErbB2 and p53H/+;ErbB2 mammary tumors, whereas the absence of wtp53 allele markedly increased AB in ErbB2 mammary tumors (Fig. 4c). Additionally, p53H/−;ErbB2 tumors had higher AB compared to p53−/−;ErbB2 tumors and AB was further increased in p53H/H;ErbB2 tumors (Fig. 4e). Also, we analyzed another ErbB2 mouse model with conditional-

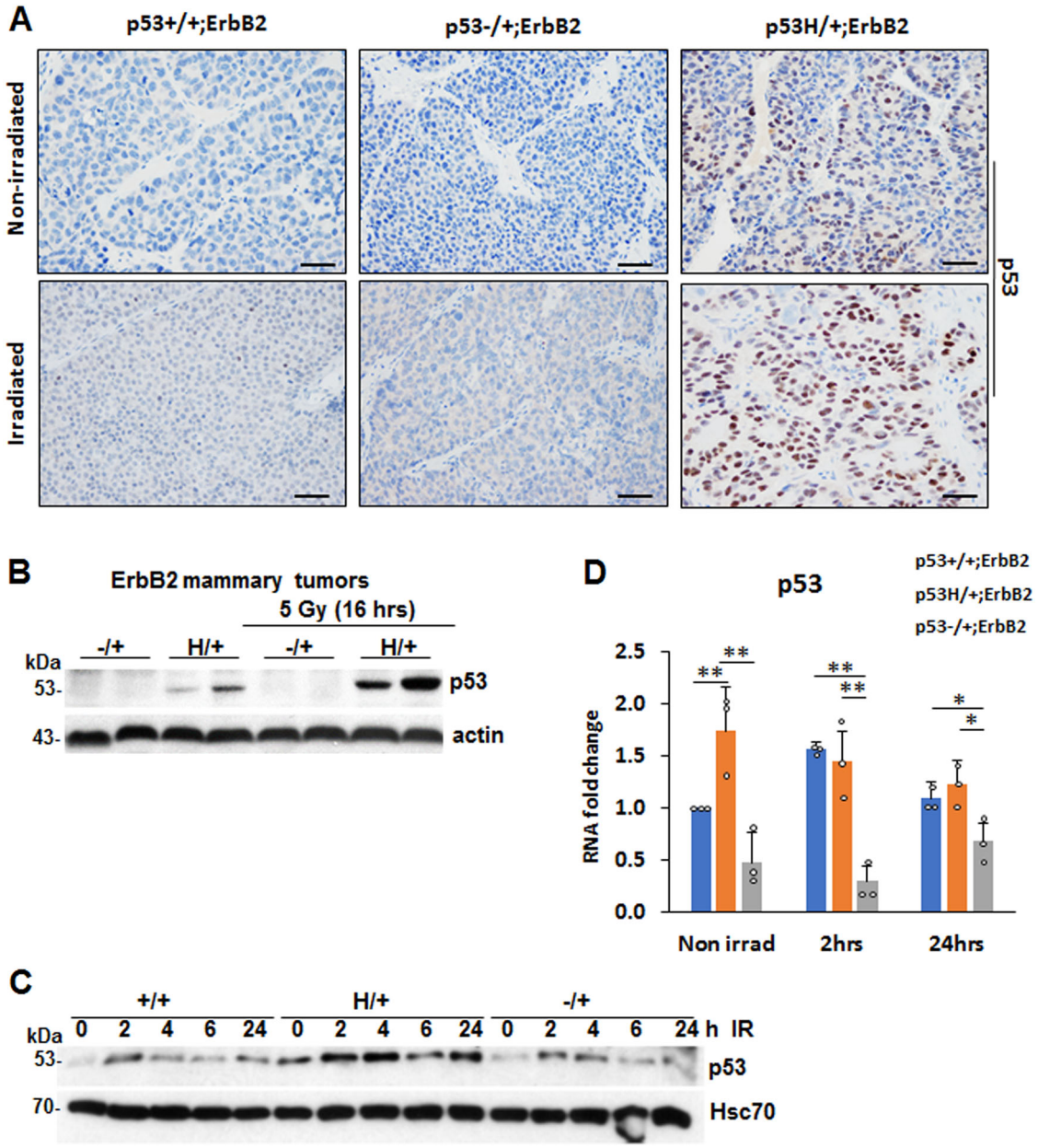

Fig. 3 Irradiation induces the accumulation of mutant p53 protein in heterozygous cancer cells. **a** The increase in p53LOH in p53H/+;ErbB2 mammary tumors are associated with the stabilization of mutp53 after irradiation of pre-malignant lesions, while irradiation does not affect wtp53 levels in p53+/+;ErbB2 and p53−/+;ErbB2 tumors. Representative images of p53 IHC of mammary tumors with indicated genotypes that were non-irradiated and irradiated. Four tumors per genotype were analyzed. The scale bar represents 50 μm. **b** Irradiation stabilizes mutp53 protein in mutp53 heterozygous tumors, but not in p53−/+;ErbB2 tumors. Western blot 16 h after irradiation in vivo. Actin is a loading control. **c** wtp53 in p53+/+;ErbB2 cells was only transiently upregulated at 2 h post-irradiation (9 Gy), mutp53 shows much higher and continuous stabilization in p53H/+;ErbB2 cells. HSC70 is a loading control. **d** Irradiation in vitro does not induce p53 mRNA in p53H/+;ErbB2 cells, 24 h post-irradiation. $n = 3$ independent experiments. $^{*}p < 0.05$; $^{**}p < 0.01$; $^{***}p < 0.001$. Error bars represent ± SD.

deletion of R248Q mutp53 allele (flQ/−;ErbB2) upon tamoxifen administration[15]. Genetic ablation of R248Qp53 in vivo significantly reduced the mutp53 expression in established ErbB2 tumors compared to vehicle-treated tumors (Fig. 4d) and was concomitant with a two-fold AB decrease (Fig. 4e). Thus, our results indicate elevated AB independently of the type of p53 mutation compared to p53−/− tumors (Fig. 4e).

Several studies have implicated centrosome abnormalities and mitotic multipolar spindle formation, as the origin of chromosome instability in a variety of human tumors[27–30]. P53 is required for proper centrosome duplication and was shown to localize to the centrosomes[31–34]. To identify centrosome aberrations (>2 or absence of centrosomes), we analyzed mitotic cells in mammary tumors for centrosome and spindle formation. Indeed, we observed acentrosomal multipolar polar spindles in p53H/−;ErbB2 tumors (Fig. 4f) only.

Collectively our data suggest that in heterozygosity wtp53 enables the maintenance of the genomic integrity in cancer cells. It is plausible that DNA damage via stabilization of mutp53 protein shifts the balance between mutant and wtp53 alleles and unveils the oncogenic power of mutp53, leading to increased genomic aberrations and p53LOH. Consequently, loss of wtp53

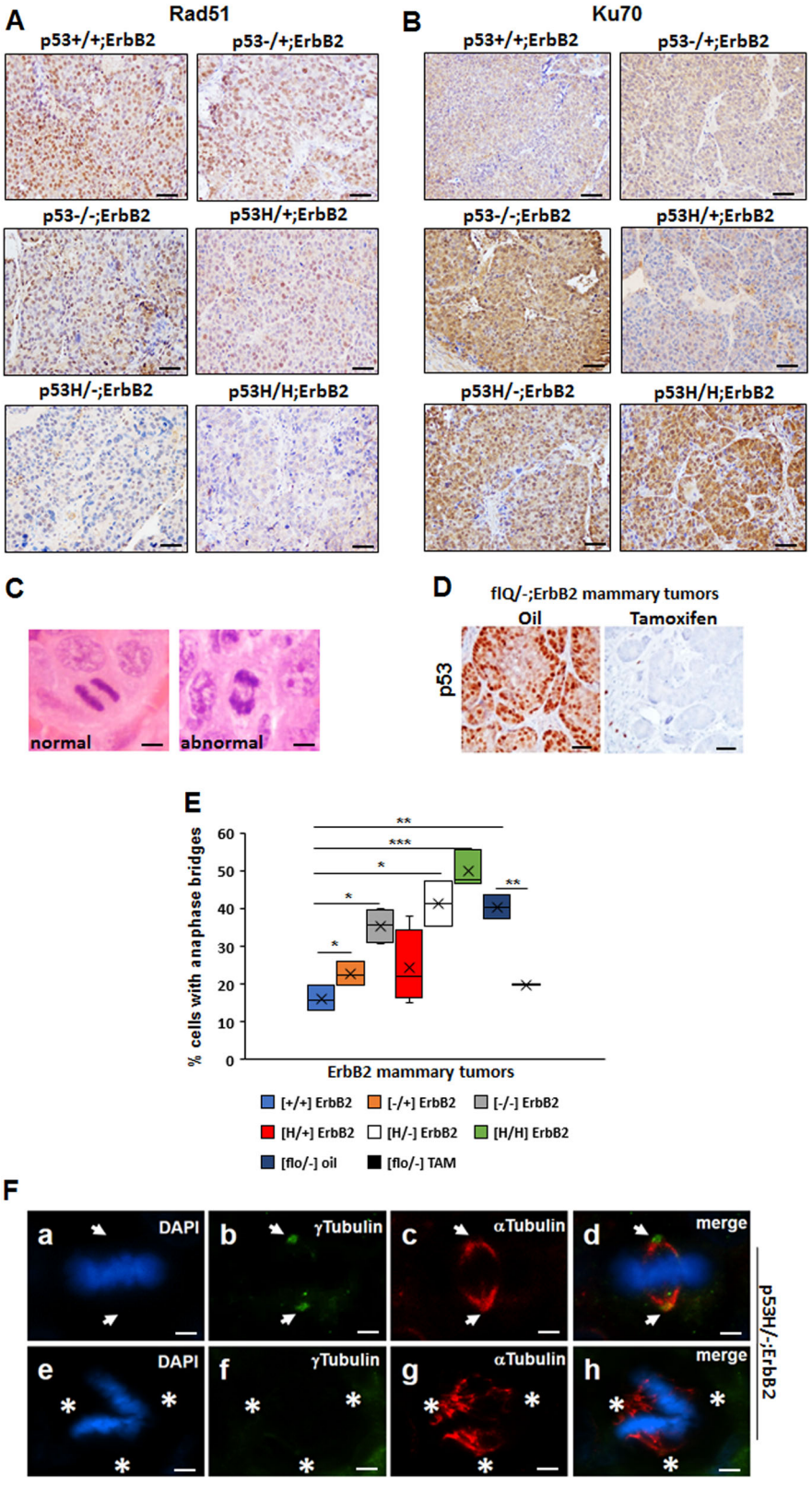

allele leads to further genome perturbations fueling tumor progression.

P53LOH is associated with the activation of the mTOR pathway. The mTOR pathway is a key downstream component of ErbB2 signaling[35]. Indeed, specific inhibitors of ErbB2 (lapatinib and trastuzumab) effectively suppressed mTOR, as indicated by downregulation of pS6, a downstream target of mTOR, (Fig. 5a and Supplementary Figs. 4a and 5a). The mTOR pathway plays an essential role in regulating many oncogenic processes – such as genomic instability in different cancer types[18,36,37], including breast cancer[36,38]. The stimulation of the mTOR pathway followed by translational deregulation and accelerated G1-S transition was implicated in inducing genomic instability and Apc LOH

Fig. 4 P53LOH is associated with the switch from homologous recombinational repair (HRR) to nonhomologous end joining (NHEJ) and genomic instability. **a** Rad51(marker for HRR) IHC in ErbB2 mammary tumors of mice with indicated p53 genotypes. **b** Ku70 (a marker for NHEJ) in ErbB2 mammary tumors of mice with indicated p53 genotypes. Four mammary tumors per genotype were stained. **c** H&E staining of normal anaphase showing the segregating masses of chromosomes and bridging (arrow) between the segregating masses of chromosomes during anaphase. **d** p53 IHC staining in the tumor from flR248Q/−;ErbB2 mouse injected with oil or following the depletion of p53 in the tumor from flR248Q/-;ErbB2 mouse after tamoxifen injection. The scale bars in A–D represent 50 μm. Images in A–D are representative stainings from 10 mice per group. **e** Quantification of anaphase bridges (AB) in ErbB2 mammary tumors of mice with indicated p53 genotypes. $n = 3$ tumors per genotype. $^{*}p < 0.05$; $^{**}p < 0.01$; $^{***}p < 0.001$. **f** Staining for mitotic spindles in a mitotic cell (metaphase) in p53H/-;ErbB2 mouse mammary tumor (**a**, **e**). Nuclear staining (DAPI), (**b**, **f**) centrosomes (γ-Tubulin), (**c**, **g**) mitotic spindles (α-Tubulin), (**d**, **h**) merge. **a**–**d** a mitotic cell with normal (2) spindle poles and 2 centrosomes. **e**–**h** a mitotic cell with no centrosomes (acentrosomal) and abnormal (>2) spindle poles. Arrows point to the position of the centrosomes in the mitotic cell. Asterisks indicate the three directions of the pull of the acentrosomal spindle poles. Data are representative of 10 images from 4 mice per genotype. The scale bar represents 145 μm.

in a colon cancer mouse model[18]. Hence, we asked whether the increased genomic instability and elevated p53LOH observed in the presence of mutp53 (Fig. 2, Table 1) is attributed to increased mTOR signaling.

Several studies showed that wtp53 inhibits the mTOR pathway via inducing Sestrin 1 and 2 expressions, that interact and activate AMPK leading to mTOR inhibition[39,40]. Our data show elevated mTOR signaling in mutp53;ErbB2 vs. wtp53;ErbB2 human cancer cells as indicated by high levels of downstream effectors of mTOR—p70S6 and pS6, whereas the level of mTOR and p-mTOR protein were comparable (Fig. 5b and Supplementary Figs. 4b and 5b). Furthermore, upregulation of wtp53 by nutlin suppressed mTOR signaling in wtp53;ErbB2 cells, but not in mutp53;ErbB2 cells (Fig. 5c and Supplementary Figs. 4c and 5c). Consistent with transcriptional activity of wtp53 (Fig. 2f), Sestrin 2 and p21 mRNA expression was upregulated 24 h post-irradiation in all mouse cell lines genotypes (Fig. 5d–e), and this upregulation was associated with downregulation of mTOR activity (Fig. 5f and Supplementary Fig. 5d). Importantly, irradiation did not alter pAKT, the upstream effector of mTOR, (Fig. 5f and Supplementary Fig. 5d), indicating that wtp53-mediated induction of Sestrins is the main regulator of mTOR activity post-irradiation.

To investigate the effect of p53LOH on mTOR activity, we tested cells 7 days post-irradiation (Fig. 2f). Compared to p53+/+;ErbB2, the loss of wtp53 allele in p53H/+;ErbB2 cells was associated with mTOR upregulation and p21 suppression (Fig. 5g and Supplementary Fig. 5e), while there were sustained mTOR inhibition and p21 upregulation in p53−/+;ErbB2 cells (Fig. 5g). Similarly, irradiation in vivo exacerbated p53LOH concomitant with significant upregulation of mTOR signaling in p53H/+;ErbB2 tumors (Fig. 5h and Supplementary Fig. 6a, b; Table 1).

Next, we asked whether mutp53 impacts the mTOR pathway through a gain-of-function (GOF) mechanism. We previously showed that mutp53 amplifies ErbB2 signaling via stimulation of HSF1 and its transcriptional target Hsp90, which, in turn, stabilizes numerous Hsp90 clients, such as ErbB2 and mutp53 itself[41]. The mTOR pathway components, which are Hsp90 clients (https://www.picard.ch/downloads/Hsp90interactors.pdf), may also be stabilized by mutp53-HSF1-Hsp90 loop. Indeed, inhibition of both Hsp90 and HSF1, efficiently suppressed mTOR signaling in mutp53;ErbB2 cell lines BT474 (Fig. 5I, j and Supplementary Fig. 6c, d) and SKBR3 (Supplementary Fig. 4a–c). Furthermore, p53LOH post-irradiation was associated with the activation of both mTOR and HSF1 (as indicated by its elevated target, Hsp70) only in p53H/+;ErbB2 cells (Fig. 5k and Supplementary Fig. 6e). Hence, in addition to the loss of wtp53 suppressive activity, p53LOH may lead to mTOR activation via stimulation of HSF1-ErbB2 axis in a mutp53-dependent manner, providing the survival advantage over p53 +/+;ErbB2 and p53−/+;ErbB2 cells. Thus, the activation of the mTOR pathway associated with p53LOH may generate selective pressure for the loss of wtp53 allele in p53H/+;ErbB2 cells.

Cells with mutant p53 have defective DNA-damage repair response and cell-cycle profile following γ-irradiation. Upon genotoxic stress, wtp53 activates the transcription of genes involved in cell-cycle arrest and DNA repair or apoptosis, to protect the genome from the accumulation of mutations, while mutp53 may perturb these genome-guarding mechanisms and promote genomic instability[19,42]. Yet, how p53 heterozygous cells respond to DNA damage is not fully understood.

Hence, we irradiated (9 Gy) cultured mouse mammary tumor cells and examined the extent of DNA damage using γH2AX as a marker of DNA double-strand breaks. Western blot analysis (Fig. 6a, b and Supplementary Fig. 7) and foci assessment (Fig. 6c) showed sustained DNA damage up to 24 h in p53H/+;ErbB2 cells. Conversely, in p53+/+;ErbB2 cells, γH2AX peaked at 2 hr post-irradiation, was efficiently resolved by 4 h, and resumed to a normal level by 24 h post-irradiation (Fig. 6a, c and Supplementary Fig. 7). These results suggest that, while p53+/+ cells exhibit a functional DNA-damage response, wtp53 haploinsufficient cells manifest persistent DNA damage due to a deficient DNA repair following γ-irradiation.

Next, we compared cell-cycle profiles of cells with various genotypes 24 h after γ-irradiation. Non-irradiated p53+/+;ErbB2 and p53−/+;ErbB2 cells exhibited comparable cell-cycle profiles, whereas p53H/+;ErbB2 cells showed cell-cycle profile with lower G1 and S and significantly higher G2/M indicating an increased rate of proliferation (Fig. 6d). Consistent with fast recovery from DNA-damage post-irradiation, p53+/+;ErbB2 cells did not significantly change G1 and S content and had a slight increase in G2/M arrest (Fig. 6d). In p53−/+;ErbB2 cells, irradiation-induced G1 and G2/M arrest, and significantly reduced S-phase (Fig. 6d). Conversely, p53H/+;ErbB2 cells continued cell cycling with sustained DNA damage (Fig. 6a, b), as indicated by the unchanged S-phase and increased G2/M (Fig. 6d).

We then evaluated the expression of cyclin D1, cyclin E, and cyclin B 24 h post-irradiation. Cyclin D1 is essential for G1-S progression[43–45], and its level varies by cell-cycle phase[43–45]. At basal level all three cell lines had similar cyclin D1 transcription (Fig. 6e), though p53H/+;ErbB2 cells tended to have a higher level (1.5-fold higher than p53+/+;ErbB2) reflecting a higher overall proliferation. Consistent with unchanged S-phase post-irradiation, cyclin D1 transcription level remained unchanged in both p53+/+;ErbB2 and p53H/+;ErbB2 cell as compared to non-irradiated controls (Fig. 6e). However, p53−/+;ErbB2 cells showed the highest increase in cyclin D1 transcription post-irradiation (Fig. 6d) consistent with G1 arrest and diminished S-phase.

Cyclin E prepares cells for DNA replication during the G1-S transition and is required for centrosome duplication in the S-phase[46]. While there was no significant difference in cyclin E2

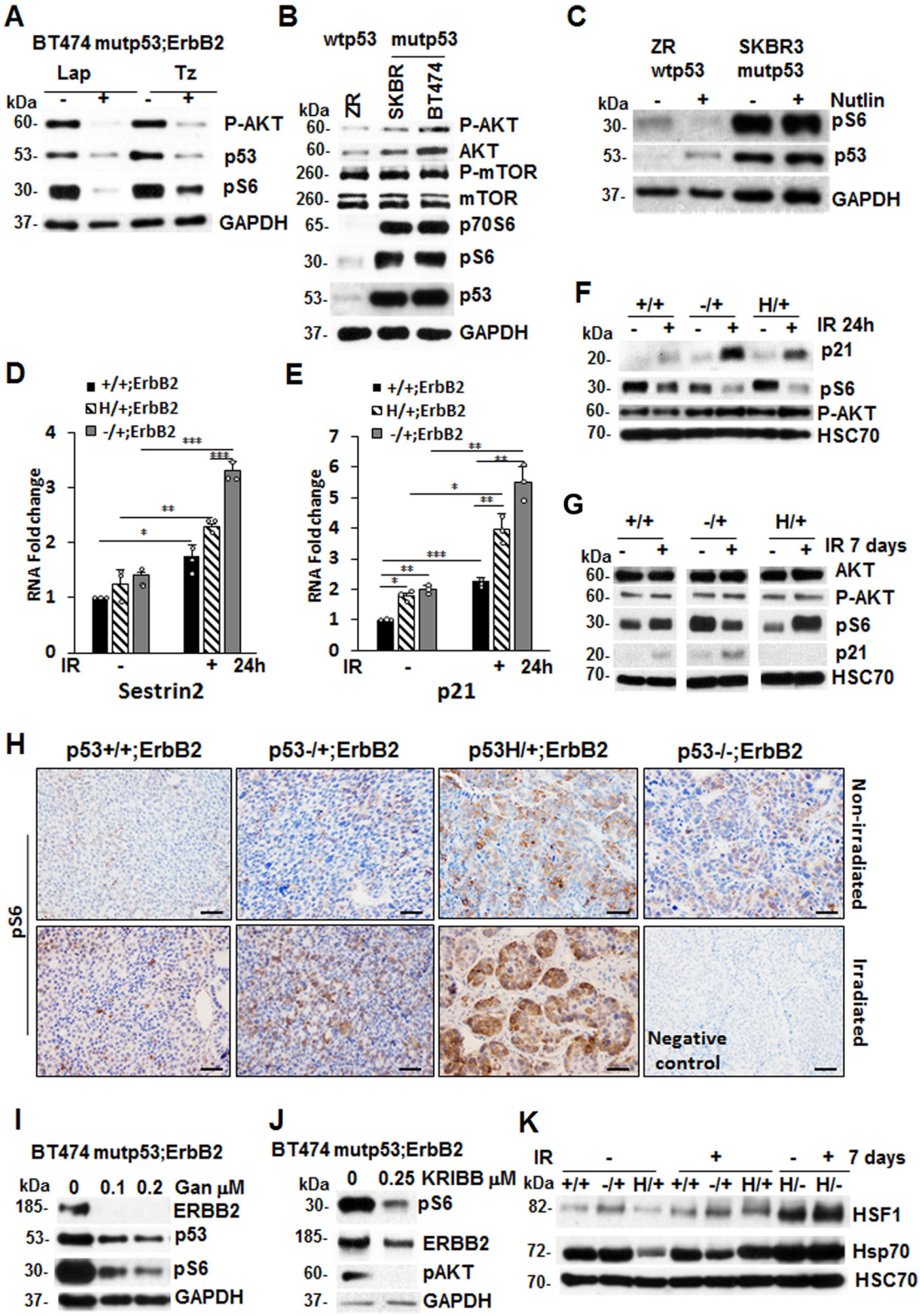

transcription level in non-irradiated cell lines, both p53H/+; ErbB2 and p53−/+;ErbB2 cells showed a significant reduction in cyclin E2 transcription post-irradiation. This result suggests that following DNA-damage wtp53 induces growth arrest in p53−/+; ErbB2 cells, while this mechanism malfunctions in p53H/+; ErbB2 cells, which enter S-phase unprepared for correct centrosome number and DNA duplication. Additionally, our results indicate that following DNA-damage cyclin E requires both wtp53 alleles, whereas p53 haploinsufficiency leads to inadequate cyclin E expression (Fig. 6f).

Cyclin B is required for mitotic spindle assembly and entry into mitosis[47]. There was no significant difference in cyclin B transcription level in non-irradiated cell lines (Fig. 6g). However, irradiation induced a significant cyclin B transcription reduction only in p53−/+;ErbB2 cells, indicating a blockage in entering mitosis. In agreement with elevated G2/M-phase post-irradiation,

Fig. 5 P53LOH is associated with the activation of the mTOR pathway. **a** ErbB2 inhibition by lapatinib and trastuzumab inhibits mTOR (pS6) in human mutp53 (BT474) cells. **b** The mTOR (pS6) pathway is more activated in mutp53;ErbB2 (BT474 and SKBR3) than in wtp53 cells (ZR75–30). **c** Upregulation of wtp53 by nutlin suppresses mTOR signaling in wtp53;ErbB2 cells ZR 75–30, but not in mutp53;ErbB2 SKBR3 cells. **d**, **e** Irradiation induces RNA expression of p53 targets Sestrin 2 (**d**) and p21 (**e**) in all genotypes p53+/+;ErbB2, p53−/+;ErbB2 and p53H/+;ErbB2 cells. QRT-PCR 24 h post-irradiation. $n = 3$ independent experiments. $^{*}p < 0.05$; $^{**}p < 0.01$; $^{***}p < 0.001$. **f** The mTOR (pS6) pathway is downregulated in the presence of wtp53 allele 24 h after irradiation that is concomitant with p21 upregulation. **g** irradiation-induced p53LOH in p53H/+;ErbB2 cells is associated with upregulation of mTOR and lack of detectable p21 in the long term. This is in contrast to p53+/+;ErbB2 and p53−/+;ErbB2 cells. Western blot 7 days post-irradiation. HSC70 as a loading control. **h** Irradiation-induced p53LOH is concomitant with the upregulation of mTOR signaling that is more profound in mutp53 heterozygous tumors. The scale bar represents 50 μm. Hsp90 inhibition by ganetespib (**i**) and HSF1 inhibition by KRIBB11 (**j**) suppresses mTOR in mutp53 human BT474 cells. Western blot after 24 h treatment with indicated concentrations. GAPDH as a loading control. **k** p53LOH after irradiation is associated with both mTOR and HSF1 activation (as indicated by elevated Hsp70) only in p53H/+;ErbB2 cells. Western blot 7 days after irradiation. HSC70 as a loading control. Error bars represent ± SD. Experiments were repeated three times with similar results.

cyclin B showed a marginal increase in p53H/+;ErbB2 cells indicating a transition to mitosis with unrepaired DNA.

Hence, in p53H/+;ErbB2 cells, the aberrant G1-S transition coupled with defective DNA repair may generate the genomic plasticity that facilitates p53LOH. In turn, p53LOH upregulates the mTOR pathway to further enhance cancer cells fitness and enable their survival after DNA damage.

Discussion

As the predictive value of mutp53 status in response to genotoxic therapies remains controversial[5], here we analyzed the oncogenic impact of mutant R172H p53 on the development and progression of mammary tumors after irradiation. Previously we showed that in heterozygosity mutant p53 R172H is a more potent activator of ErbB2-mediated mammary tumorigenesis than simple loss of p53[12].

In the current study, we demonstrated that a single dose of irradiation, at the time of onset of pre-malignant lesions, profoundly accelerated mammary tumorigenesis in heterozygous, but not in p53+/+;ErbB2 mice (Fig. 2a, b). We identified a novel oncogenic activity of mutp53 where it exacerbated p53LOH in response to irradiation, which correlated with enhanced metastasis only in the presence of mutp53 allele. To our knowledge this has not been reported before. Despite the difference in p53LOH rate, irradiation equally shortened the survival of p53H/+;ErbB2 and p53−/+;ErbB2 mice (Fig. 2a). This could be attributed to an alternative p53LOH-independent mechanism(s) in tumors in response to irradiation. In addition, mouse cancer models have limitations in recapitulating human disease, e.g. the survival analysis of mice reflects only the rate of tumor growth since mice were usually sacrificed when the tumor reaches a certain size. Conversely, 90% of deaths of breast cancer patients are a consequence of metastasis. In relation to human data, we observed in p53H/+;ErbB2 mice a strong association between enhanced p53LOH and the increased rate of metastases (Table 1). Also, we previously noted significant stabilization of mutp53 protein in metastatic lesions as opposed to heterogeneous p53 staining in primary p53H/+;ErbB2 mammary tumors[12], which is consistent with the p53LOH phenotype (Fig. 3a and Supplementary Fig. 2b)[11]. We speculate that mutp53 stabilization after p53LOH, with the subsequent induction of genomic instability (Fig. 4), may lead to the acquisition of metastatic properties in cancer cells.

In support of our in vivo findings, the analysis of METABRIC human database demonstrated stage-dependent benefit from genotoxic modalities for patients with mutp53 breast cancer: improved survival of stage 2 patients, but the shorter survival of stage 1 patients (Fig. 1a–h) that strongly correlates with p53LOH status (80 and 48% respectively) (Fig. 1i). Conversely, patients with wtp53 tumors, benefit from radiotherapy independently of the stage. In support of our hypothesis, a previous study showed that TP53/KRAS co-mutations are predictive of the deleterious effect of adjuvant chemotherapy compared to KRAS mutation alone[6]. Hence, studies are needed to determine whether negative outcomes from genotoxic therapies in the early stages of mutp53 breast cancer patients are caused by radiation-induced p53LOH.

Our data on survival of non-irradiated mice (Fig. 2a, Table 1,[12]) implies, that despite the transcriptional activity of wtp53 towards a subset of targets (Figs. 2f and 5d–e) mutp53 may exert DN function in heterozygous mammary tumors. Notably, neither straight p53H/+ knock-in mice[48,49] nor the H allele crossed into the Ras, EμMyc[50] or Wnt[10] models demonstrated shortened survival compared to their p53null counterparts, suggesting that mutp53 contributes to tumorigenesis only in cooperation with particular oncogenic drivers, such as ErbB2. This is supported by clinical data showing that TP53 mutations are associated with poor prognosis in HER2-positive breast cancer patients, but not in patients with luminal A and basal-like tumors despite the high frequency of TP53 mutations[51].

Furthermore, oncogenic activities of mutp53 in heterozygosity were manifested by the increased rate of p53LOH and metastasis post-irradiation (Table 1). These outcomes were associated with the continuous stabilization of mutp53 protein post-irradiation in vivo and in vitro, while wtp53 upregulation was quickly resolved after stress (Fig. 3b, c). It is conceivable that in heterozygosity the ratio of wtp53 to mutp53 defines the oncogenic function of mutp53, either through DN effect or GOF, and irradiation can drive mutp53 protein level over a threshold necessary to manifest its oncogenic activity. In support, heterozygous expression of mutp53 (R270H) exerted DN effect on tumor latency, multiplicity, and progression only after UV exposure but not spontaneous tumors[52]. In R246S mutp53 knock-in mouse model, the DN effect on transactivation was detectable only after acute p53 activation[53]. Also, DNA damage increased mutp53 DN activity in various tissues of p53H/+;ErbB2 mice[48,49].

Nevertheless, we were unable to clearly detect DN effect of mutp53 on the analyzed subset of wtp53 targets post-irradiation, as p21 and sestrin 2 mRNA was upregulated in heterozygous cells 24 h post-irradiation (Fig. 5d–e). These results are consistent with previous report on the MMTV-Wnt1 mouse model showing that wtp53 induces reversible p21-mediated growth arrest in p53H/+;ErbB2 tumors after doxorubicin treatment[10]. Our data on the differential expression of mTOR pathway and p21 post-irradiation (Figs. 2e, 5g–h) indicates that p53LOH may be the key oncogenic event that overrides irradiation-induced growth arrest and inhibition of metabolic activity.

Wtp53 is crucial in regulating key cellular processes such as proliferation and the maintenance of genomic integrity[19,20]. Conversely, mutp53 is an important driver of genomic instability,[19,54] which may constitute the main mechanism underlying p53LOH after irradiation. Our data show differential deployment of HRR vs. NHEJ DNA repair mechanisms

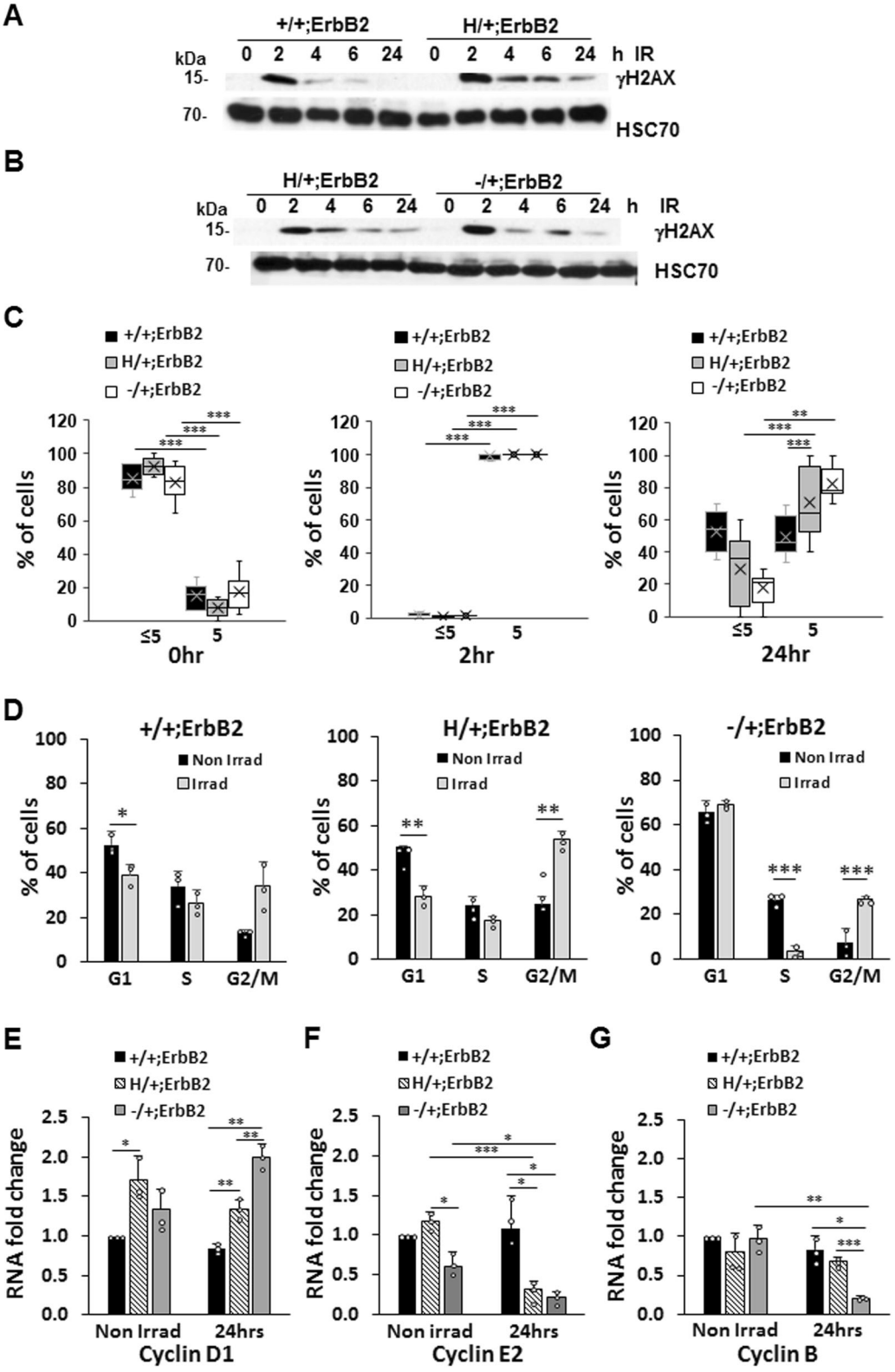

Fig. 6 Cells with mutant p53 have defect both in DNA-damage repair response and in cell-cycle profile following γ-irradiation (**a**, **b**) Western blot of γH2AX level (representing DNA damage) post-irradiation (9 Gy, single dose) showing γH2AX efficient resolution in p53+/+;ErbB2 cells (**a**) but is sustained up to 24 h in p53H/+;ErbB2 and p53−/+;ErbB2 cells (**b**). HSC70 as a loading control. **c** Quantification of cells with >5 and <5 γH2AX foci/cell in p53+/+; ErbB2, p53H/+;ErbB2, and p53−/+;ErbB2 cell lines, before and after γ-irradiation (9 Gy, 2 and 24 h post-irradiation). **d** Aberrant cell-cycle checkpoint following γ-irradiation in p53H/+;ErbB2 cells. Bar graphs showing cell-cycle analysis of p53+/+;ErbB2, p53H/+;ErbB2, and p53−/+;ErbB2 cell lines irradiated (gray bars) or not (black bars). **e**, **f** QRT-PCR 24 h post-irradiation is showing the impact of a single dose of γ-irradiation (9 Gy) on the transcription of Cyclin D1 (**e**), Cyclin E2 (**f**), Cyclin B (**g**). Level of transcripts was quantified relatively to HPRT. $n = 3$ independent experiments. $^{*}p < 0.05$; $^{**}p < 0.01$; $^{***}p < 0.001$. Error bars represent ± SD.

depending on p53 genotype where the presence of wtp53 allele correlated with HRR, while after p53LOH mutp53 may inhibit HRR and induce NHEJ (Fig. 4), thus enhancing genomic instability. This is consistent with a previous study showing that mutp53 allows the bypassing of G2/M DNA-damage checkpoint, causing inefficient HRR in a lymphoma mouse model[42]. Additionally, the frequency of AB formation correlated with the lack of wtp53 allele, whereas mutp53 exacerbated AB in the absence of wtp53 (Fig. 4c, e) and correlated with aberrant centrosome formation and multipolar spindles (Fig. 4f).

Furthermore, our data suggest that DNA-damage hinders the wtp53 genome-protective function, leading to persistent DNA damage in both p53H/+;ErbB2 and p53−/+;ErbB2 cells. Conversely, DNA damage was quickly resolved in p53+/+;ErbB2 cells (Fig. 6a–c). Importantly, persistent DNA damage-induced growth arrest in p53−/+;ErbB2 cells, whereas p53H/+;ErbB2 cells were able to overcome p21-mediated G1 arrest and enter mitosis with unrepaired DNA and defective centrosome duplication. In support, transcriptome analysis of TSGA database showed mutant TP53-associated dysregulation of cell-cycle regulatory genes in the majority of human cancer types, including breast cancer[55].

It remains unclear how mutp53 heterozygous cells escape DNA-damage-induced growth arrest. One possibility is that p53 targets, other than p21 and Mdm2, are affected by stabilized mutp53, leading to the defective checkpoint and cell-cycle progression. Indeed, the expression of ~50% of genes induced by wtp53 was significantly altered in the presence of mutp53 in KRAS lung cancer model suggesting that DN effect of mutp53 might be selective towards the specific subset of genes[56]. Alternatively, stabilized mutp53 in heterozygosity can mitigate wtp53-mediated suppression of the mTOR pathway after irradiation. As a result, the enhanced mTOR signaling may accelerate the G1-S transition in p53H/+;ErbB2 cells with erroneously repaired DNA, leading to p53LOH. In support, previous studies showed the importance of the mTOR pathway in regulating every phase of the cell-cycle progression, partly by interacting with cyclin E and cyclin B [reviewed in ref. [57]]. Also, the stimulation of the mTOR pathway, followed by G1-S acceleration was implicated in genomic instability and Apc LOH in a colon cancer mouse model[18].

How can mutp53 promote mTOR signaling? Earlier work by us and others showed that, depending on the oncogenic environment, mutp53 could drive tumorigenesis by activating a number of growth factor receptors implicated in the activation of PI3K/Akt signaling[58–61], including ErbB2[12], that are upstream of the mTOR pathway. Previously we demonstrated that mutp53 enhances ErbB2 signaling via HSF1-Hsp90 axis[12]. Additionally, components of the mTOR pathway, as a Hsp90 clients (https://www.picard.ch/downloads/Hsp90interactors.pdf), may also be stabilized by mutp53-HSF1-Hsp90 cascade. Indeed, ErbB2, HSF1, and Hsp90 inhibition suppress mTOR signaling (Fig. 5a, i–k). Thus, mutp53 may contribute to mTOR activation by stimulating HSF1-ErbB2 axis, and/or by direct interaction and suppression of AMPK signaling[62].

Collectively, our data suggest a two-phase response to irradiation-induced DNA damage where mutp53 may play a role in promoting LOH (Fig. 7): acute response to irradiation (phase 1) and the recovery phase (phase 2). In phase 1, p53+/+;ErbB2 cells activate efficient DNA-damage repair, and after its completion resume cell cycling. In p53−/+;ErbB2 cells, irradiation induces sustained cell-cycle arrest due to deficient DNA-damage repair (high p21, low cyclin E and B1, and suppressed S-phase). In p53H/+;ErbB2 cells, mutp53 interferes with the regulation of the cell-cycle checkpoint to induce cell-cycle arrest despite inefficient DNA repair (high p21, low cyclin E, high cyclin B1, and increased G1-S transition and G2/M).

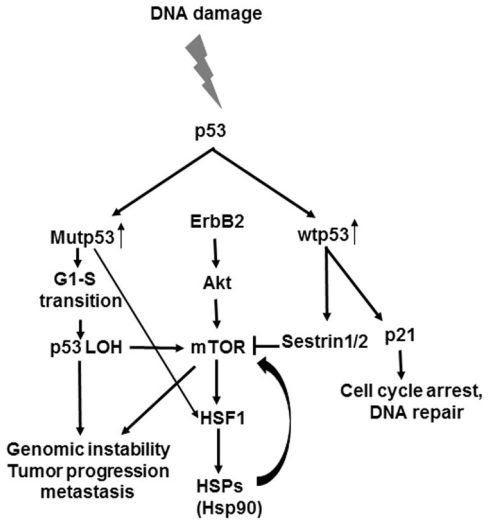

Fig. 7 Molecular mechanisms of p53 loss of heterozygosity in breast cancer in response to DNA damage. Proposed model for the role of mutp53 in promoting tumorigenesis. Following DNA damage, p53 expression is induced. Wtp53 would induce cell-cycle arrest and suppression of the mTOR pathway. On the other hand, mutp53 would promote cell-cycle progression with unrepaired DNA, LOH and cell survival via activation of the mTOR pathway through HSF1-HS90 axis, eventually leading to genomic instability, tumor progression, and metastasis.

In phase 2, p53+/+;ErbB2 cells resume normal cell cycling (low p21 and close-to-normal mTOR) after DNA-damage repair. Conversely, in p53−/+;ErbB2 cells unrepaired DNA induces persistent cell-cycle checkpoint and the suppression of cell-cycle (high p21 and low mTOR). In p53H/+;ErbB2 cells, mutp53 via enhanced mTOR signaling (and possibly other mechanisms) forces the cell to by-pass cell-cycle checkpoint (p21 lacking, high level of mTOR), despite DNA is not efficiently repaired. Consequently, aberrant cell-cycle progression with damaged DNA leads to p53LOH followed by enhancement of genomic instability (NHEJ DNA repair, centrosome abnormalities) and loss of p21-mediated checkpoints enabling unrestricted proliferation. In support, it was previously demonstrated that loss of wtp53-mediated p21 expression induces the transcription of hTERT after irradiation, confering proliferation and radio-resistance in HER2-positive breast cancer[63].

In the current work, we mainly studied R175H p53 mutation, which was identified as a hotspot in ErbB2 breast cancer[64]. Our study on mutant p53 R248Q/+;Neu mouse breast cancer model demonstrated that loss of wtp53 allele is required for mutp53 stabilization[11] and GOF activities, promoting chromosomal aberration. This suggests that our conclusions can be applied to a variety of p53 mutations. Still, it remains undetermined whether irradiation accelerates p53LOH and tumorigenesis in the presence of various types of p53 mutations, and in other types of cancers.

In sum, our study may have significant implications on the therapeutic interventions for early stages of human breast cancer and help to prevent the potentially deleterious effects of genotoxic therapies and conquer the problem of overtreatment in breast cancer.

Methods

Metabric data. Human Metabric data analysis, of the somatic mutation profiles of 2433 breast cancers, was done using data from a retrospective study(10). The data are deposited and is publicly available at http://www.cbioportal.org. The analysis

was done using the program and tools made available online at http://www.cbioportal.org.

Mice. MMTV-ErbB2 mice carrying activated ErbB2 (strain FVBN-Tg(MMTV-ErbB2)NK1Mul/J) were from Jackson Labs. p53 R172H (called p53H/H) and control p53 null (p53−/−) mice (C57Bl6J background) were a gift from G. Lozano[49]. p53H/−;ErbB2 mice were generated by crossing ErbB2 mice with p53−/− mice and then breeding the p53+/−;ErbB2 progeny with p53H/H mice. p53H/-;ErbB2 mice were then crossed to generate p53H/H;ErbB2 and p53−/−;ErbB2 females for analysis. p53+/+;ErbB2 were generated from crossing of p53H/+;ErbB2 and p53+/−;ErbB2 mice. Mice carrying the floxed p53R248Q mutation (referred to as floxQ) was generated as described before[15]. For all mice genotypes, only female littermates were used for all analyses. Animals were monitored weekly to determine their breast cancer and sarcoma onset and were promptly killed when their tumors reached 4 cm^3 in volume or when animals appeared moribund. Careful necropsies were performed, and tumors and all major organs collected, fixed in 10% formalin, embedded in paraffin and sectioned for histopathologic analysis. For survival analysis, P-values were determined by log-rank analysis. Mice were treated according to guidelines approved by the Institutional Animal Care and Use Committee at Stony Brook University.

Cell lines. Human ErbB2-positive breast cancer cell lines ZR-75–30 carrying wild-type TP53, and BT474, SKBR3, carrying E285K, R175HTP53 mutations, respectively, were purchased from ATCC. Where shown, cells were treated with indicated concentrations of HER2 inhibitors lapatinib (L-4899, LC Lab) and Trastuzumab (gift of Dr. A. Kudelka), ganetespib (HSP90 inhibitor) (STA-9090, Synta Pharmaceuticals), or KRIBB11 (HSF1 inhibitor) (385570, Calbiochem). Establishing mouse mammary tumors cell lines was described before[65]. Mouse mammary tumor cell lines: p53+/+;ErbB2, p53H/+;ErbB2 and p53+/−;ErbB2, were isolated from their corresponding mammary tumors and maintained in culture. Mouse mammary epithelial cells (MECs) p53H/H;ErbB2 and p53−/+;ErbB2 were also isolated and maintained in culture. Isolated mouse mammary tumor cell line clones 176.3 p53+/+;ErbB2, 136.12 p53+/+;ErbB2, 134.9 p53H/+;ErbB2 and 221 p53H/−;ErbB2 were selected for all cell culture experiments.

Gamma irradiation. Mice were exposed to total-body γ-irradiation with a 137Cs source, with a dose rate of 0.8 Gy/min, for a total of 5 Gy. Another group of mice (sham) were placed in the room without being exposed to irradiation. Animals were either observed for survival post-irradiation or were killed by CO_2 asphyxiation followed by cervical dislocation at set times after irradiation, and the mammary tumors were removed for further analysis. For the survival experiment, all animals (irradiated or not) were monitored weekly to determine their breast cancer and sarcoma onset and were promptly killed when their tumors reached 3 cm^3 in volume or when animals appeared moribund. Necropsy, tumor removal, and fixation and analysis were carried out as described above. For γ-irradiation of cells, a total of 9 Gy was used. Non-irradiated cells (sham) were placed in the room without being exposed to irradiation.

Immunofluorescence and immunohistochemistry. H&E staining was performed by the Research Histology Core Laboratory, Department of Pathology, Stony Brook University. For tissue immunostaining, sections were deparaffinized in xylene, rehydrated in ethanol gradient, and then treated with 10 mM Na citrate buffer, pH 6.0, at 120 °C for 10 min in a pressure cooker. The histological sections were incubated with a blocking buffer [10% normal horse serum (NHS) and 0.01% Tween 20 in 1x Tris-buffered PBS (TTBS)] for 1 h at 37 °C. Sections were then stained using rabbit anti-p53 (1:200; Santa Cruz Biotechnology), rabbit anti-pS6 (1:100; Abcam), mouse anti-γTubulin (1:100 clone D10 Santa Cruz Biotechnology), rabbit anti-αTubulin (1:500 cell signal), rabbit anti-Rad51 (1:100; Abcam), and rabbit anti-Ku70 (1:100; Abcam), at 4 °C overnight. Washes were done using TTBS, and detection of primary antibodies for immunofluorescence (IF) was carried out using appropriate Alexa Fluor-labeled secondary antibodies (Molecular Probes) at 1:500 dilutions for 30 min at 37 °C, counterstained with Hoechst 33258 (2 μg/ml), mounted with Prolong gold (Molecular Probes), and cover-slipped. For IHC, secondary unconjugated bovine anti-rabbit antibody (Jackson Immuno Research), were added at 1:300 dilution in 10% NHS in TTBS for 30 min at 37 °C. After being washed, goat anti-bovine horseradish peroxidase-conjugated tertiary antibody was used at 1:500 dilution 30 min at 37 °C. All antibody dilutions were made in 10% NHS in TTBS. The color was developed using substrate-chromogen solution, counterstained with hematoxylin, and then mounted. For IF on cells, media aspired from cells grown on chamber slides, cells were fixed with methanol at −20 °C for 10 min, and then washed 3X with PBS. Cells were incubated with blocking buffer [10% normal horse serum (NHS) and 0.01% Tween 20 in PBS], for 1 h at 37 °C. Cells were then stained with rabbit anti-γH2AX (1:200, Cell Signaling) for 1 h at 37 °C, and then washed 3X with PBS. Goat anti-rabbit Alexa fluor-labeled 568 secondary antibodies (Molecular Probes) at 1:500 dilution for 30 min at 37 °C, counterstained with Hoechst 33258 (2 μg/ml), mounted with Prolong gold (Molecular Probes), and cover-slipped. Images for H&E and IHC slides were acquired at ×400 total magnification using Olympus microscope (Olympus) equipped with Olympus DP72 camera. For IF, images were acquired at x600 total magnification using a Nikon Eclipse Ti-S microscope (Nikon Instruments) equipped with QI-Click camera (QImaging). Where applicable, quantification of IHC staining intensity was performed, using ImageJ[66], on 10 images of randomly selected fields per genotype per treatment. For γH2AX foci, cells were counted from at least five randomly selected fields.

Anaphase bridging index (ABI). The ABI was determined as described before[18]. A minimum of 50 anaphases per mouse (3–5 per group) was scored from H&E sections.

Determination of LOH of the *p53*+ locus. DNA was extracted from frozen mouse mammary tumors, using QIAmp DNA Micro Kit (Qiagen). An equal amount of DNA was used for PCR amplification of p53 locus using primers described before[49]. For loading control, we used primers for ROSA locus: [F], 5'-AAAGTCGCTCTGAGTTGTTAT-3', [R], 5'-TAAGCCTGCCCAGAAGACTC-3'. An equal volume of the amplified product was electrophoresed through a 1.5% agarose gel. Amplified DNA bands were visualized, and the image captured using FluoroChem HD2 (ProteinSimple). LOH was determined based on the presence or absence of the amplified wild-type band.

Real-time PCR. All real-time PCR was done on cultured cells using 3 biological replicas. For determining p53 wild-type and R172H allele copy number in cultured cells, DNA was extracted from cultured cells using QIAmp DNA Micro Kit (Qiagen). An equal amount of DNA was used for PCR amplification of p53 locus using the following primers: p53 wild-type [F], 5'-CACATGACGGAGGTCGTGAGTTG-3', R172H mutation [F], 5'-CACATGACGGAGGTCGTGAGTTA-3', [R], 5'-CTGTCTTCCAGATACTCGGGATAC-3'. The primers were designed to detect the nucleotide point mutation G→A that results in amino acid mutation R172H. The specificity of the primers was validated by DNA extracted from p53+/+;ErbB2, p53H/+;ErbB2, p53−/+;ErbB2, p53−/−;ErbB2 and p53H/H;ErbB2 mouse tails. Genotypes of generated cell lines were confirmed by quantitative real-time PCR (qPCR).

For determination mRNA transcript level, RNA was extracted from cultured cells using Trizol as per manufacturer instructions. For cDNA synthesis, 200 ng/sample was used in a 20 μl reaction volume prepared from QuantiTect Reverse Transcription Kit (Qiagen). After cDNA synthesis, the reaction volume was diluted to 200 μl using DEPC-treated water. For qPCR, 1 μl of the diluted cDNA was used per reaction volume. The following primers were used: allele-specific p53 wild-type [F], 5'-CACATGACGGAGGTCGTGAGTTG-3', R172H mutation [F], 5'-CACATGACGGAGGTCGTGAGTTA-3', [R], 5'-CTGTCTTCCAGATACTCGGGATAC-3'; total p53 [F], 5'-CACATGACGGAGGTCGTGAGAC-3', [R], 5'-CTGTCTTCCAGATACTCGGGATAC-3'; p21 [F], 5'-CCTGGTGATGTCCGACCTG-3', [R], CCATGAGCGCATCGCAATC-3'; sestrin2 [F], 5'-ACACCCGGACTACCTTAGCA, [R], 5'-TGGGAACCCACCAGGTAAGA-3'; cyclin D1 [F], 5'-GCGTACCCTGACACCAATCTC-3', [R], 5'-CTCCTCTTCGCACTTCTGCTC-3'; cyclin E2 [F], 5'-ATGTCAAGACGCAGCCGTTTA-3', [R], 5'-GCTGATTCCTCCAGACAGTACA-3'; cyclin B [F], 5'-AAGGTGCCTGTGTGTGAACC-3', [R], 5'-GTCAGCCCCATCATCTGCG-3'. For loading control, we used Hprt primers[67]: [F], 5'- GGCTATAAGTTCTTTGCTGACC-3', [R], 5'- CTCCACCAATAACTTTTATGTCC-3'. For all real-time PCR, amplification was done using Quantitech sybr green (Qiagen) reaction mixture, and detection was done using QuantStudio3 (Thermo Fisher Scientific).

Cell-cycle analysis. Cultured cells were harvested by trypsinization and pelleted by spinning at 1500 r.p.m. for 10 min. The cells pellet was twice with PBS, and the cells pellet fixed in 70% ethanol. The cells were pipetted gently up and down to loosen the cells in a suspension and stored in −20 °C overnight. The cells were then pelleted by spinning at 1500 r.p.m. for 10 min, washed once in PBS, then resuspended in permeabilization buffer (0.25% tritonX100 in PBS) and incubated for 15 min at RT. The cells were then pelleted and resuspended in staining solution (20 μg/ml propidium iodide and 10 μg/ml RNase A in PBS), and incubated in the dark on ice for 30 min before analysis. Cell-cycle analysis by flow cytometry was done at Stony Brook Flow-cytometry Core Facility, using Becton Dickinson FACSCAN analyzer.

Immunoblot analysis. For immunoblots, cell lysates with equal total protein content (2–20 μg) were blotted with antibodies to p53 (FL393), p21 GAPDH, Hsc70 (all from Santa Cruz Biotechnology); ErbB2, AKT, pAKT, p-mTOR, mTOR, p70S6, pS6, γH2AX (all from Cell Signaling); HSF1 Hsp70, (all from Enzo Life Sciences Inc.).

Statistics and reproducibility. All statistical analysis between groups was done using the *t*-test. Significance was determined at $p < 0.05$. All immunoblots were repeated at least two times.Cell culture experiments were repeated three times.

Reporting summary. Further information on research design is available in the Nature Research Reporting Summary linked to this article.

Data availability

The Human Metabric data set used here is available at http://www.cbioportal.org. Source data can be found in Supplementary Data 1. All other data are available from authors on reasonable request.

Received: 14 November 2018; Accepted: 16 October 2019;
Published online: 27 November 2019

References

1. Clarke, M. et al. Effects of radiotherapy and of differences in the extent of surgery for early breast cancer on local recurrence and 15-year survival: an overview of the randomised trials. *Lancet* **366**, 2087–2106 (2005).
2. Bleyer, A. & Welch, H. G. Effect of three decades of screening mammography on breast-cancer incidence. *N. Engl. J. Med.* **367**, 1998–2005 (2012).
3. Baum, M. Harms from breast cancer screening outweigh benefits if death caused by treatment is included. *BMJ* **346**, f385, https://doi.org/10.1136/bmj.f385 (2013).
4. Atlas, N. Comprehensive molecular portraits of human breast tumours. *Nature* **490**, 61–70 (2012).
5. He, C., Li, L., Guan, X., Xiong, L. & Miao, X. Mutant p53 gain of function and chemoresistance: the role of mutant p53 in response to clinical chemotherapy. *Chemotherapy* **62**, 43–53, https://doi.org/10.1159/000446361 (2017).
6. Shepherd, F. A. et al. Pooled analysis of the prognostic and predictive effects of TP53 comutation status combined with KRAS or EGFR mutation in early-stage resected non-small-cell lung cancer in four trials of adjuvant chemotherapy. *J. Clin. Oncol.* **35**, 2018–2027 (2017).
7. Bertheau, P. et al. TP53 status and response to chemotherapy in breast cancer. *Pathobiology* **75**, 132–139 (2008).
8. Levine, A. J., Momand, J. & Finlay, C. A. The p53 tumour suppressor gene. *Nature* **351**, 453–456(1991).
9. Petitjean, A. et al. Impact of mutant p53 functional properties on TP53 mutation patterns and tumor phenotype: lessons from recent developments in the IARC TP53 database. *Hum. Mutat.* **28**, 622–629 (2007).
10. Jackson, J. G. et al. p53-mediated senescence impairs the apoptotic response to chemotherapy and clinical outcome in breast cancer. *Cancer Cell* **21**, 793–806 (2012).
11. Alexandrova, E. M. et al. p53 loss-of-heterozygosity is a necessary prerequisite for mutant p53 stabilization and gain-of-function in vivo. *Cell Death Dis.* **8**, e2661 (2017).
12. Yallowitz, A. R. et al. Mutant p53 amplifies epidermal growth factor receptor family signaling to promote mammary tumorigenesis. *Mol. Cancer Res.* **13**, 743–754 (2015).
13. Vassilev, L. T. et al. In vivo activation of the p53 pathway by small-molecule antagonists of MDM2. *Science* **303**, 844–848 (2004).
14. Li, S. J. et al. Low-dose irradiation promotes proliferation of the human breast cancer MDA-MB-231 cells through accumulation of mutant P53. *Int J. Oncol.* **50**, 290–296 (2017).
15. Alexandrova, E. M. et al. Improving survival by exploiting tumour dependence on stabilized mutant p53 for treatment. *Nature* **523**, 352–356 (2015).
16. Bug, M. & Dobbelstein, M. Anthracyclines induce the accumulation of mutant p53 through E2F1-dependent and -independent mechanisms. *Oncogene* **30**, 3612–3624 (2011).
17. Rao, C. V. & Yamada, H. Y. Genomic instability and colon carcinogenesis: from the perspective of genes. *Front. Oncol.* **3**, 130 (2013).
18. Aoki, K., Tamai, Y., Horiike, S., Oshima, M. & Taketo, M. M. Colonic polyposis caused by mTOR-mediated chromosomal instability in Apc+/Delta716 Cdx2 +/− compound mutant mice. *Nat. Genet.* **35**, 323–330 (2003).
19. Hanel, W. & Moll, U. M. Links between mutant p53 and genomic instability. *J. Cell Biochem.* **113,** 433–439 (2012).
20. Lane, D. & Levine, A. p53 Research: the past thirty years and the next thirty years. *Cold Spring Harb. Perspect. Biol.* **2**, a000893 (2010).
21. Linke, S. P. et al. p53 interacts with hRAD51 and hRAD54, and directly modulates homologous recombination. *Cancer Res.* **63**, 2596–2605 (2003).
22. Menon, V. & Povirk, L. Involvement of p53 in the repair of DNA double strand breaks: multifaceted Roles of p53 in homologous recombination repair (HRR) and non-homologous end joining (NHEJ). *Subcell. Biochem* **85**, 321–336 (2014).
23. Akyuz, N. et al. DNA substrate dependence of p53-mediated regulation of double-strand break repair. *Mol. Cell Biol.* **22**, 6306–6317 (2002).
24. Lin, Y., Waldman, B. C. & Waldman, A. S. Suppression of high-fidelity double-strand break repair in mammalian chromosomes by pifithrin-alpha, a chemical inhibitor of p53. *DNA Repair (Amst.)* **2**, 1–11 (2003).
25. Rodgers, K. & McVey, M. Error-prone repair of DNA double-strand breaks. *J. Cell Physiol.* **231**, 15–24 (2016).
26. Chin, K. et al. In situ analyses of genome instability in breast cancer. *Nat. Genet.* **36**, 984–988 (2004).
27. Ghadimi, B. M. et al. Centrosome amplification and instability occurs exclusively in aneuploid, but not in diploid colorectal cancer cell lines, and correlates with numerical chromosomal aberrations. *Genes Chromosomes Cancer* **27**, 183–190 (2000).
28. Lingle, W. L. et al. Centrosome amplification drives chromosomal instability in breast tumor development. *Proc. Natl Acad. Sci. USA* **99**, 1978–1983 (2002).
29. Pihan, G. A. et al. Centrosome defects and genetic instability in malignant tumors. *Cancer Res.* **58**, 3974–3985 (1998).
30. Pihan, G. A., Wallace, J., Zhou, Y. & Doxsey, S. J. Centrosome abnormalities and chromosome instability occur together in pre-invasive carcinomas. *Cancer Res.* **63**, 1398–1404 (2003).
31. Fukasawa, K., Choi, T., Kuriyama, R., Rulong, S. & Vande Woude, G. F. Abnormal centrosome amplification in the absence of p53. *Science* **271**, 1744–1747 (1996).
32. Shinmura, K., Bennett, R. A., Tarapore, P. & Fukasawa, K. Direct evidence for the role of centrosomally localized p53 in the regulation of centrosome duplication. *Oncogene* **26**, 2939–2944 (2007).
33. Tarapore, P. & Fukasawa, K. Loss of p53 and centrosome hyperamplification. *Oncogene* **21**, 6234–6240 (2002).
34. Tarapore, P., Horn, H. F., Tokuyama, Y. & Fukasawa, K. Direct regulation of the centrosome duplication cycle by the p53-p21Waf1/Cip1 pathway. *Oncogene* **20**, 3173–3184 (2001).
35. Porta, C., Paglino, C. & Mosca, A. Targeting PI3K/Akt/mTOR signaling in cancer. *Front. Oncol.* **4**, 64, https://doi.org/10.3389/fonc.2014.00064 (2014).
36. Leonard, M. K., Hill, N. T., Bubulya, P. A. & Kadakia, M. P. The PTEN-Akt pathway impacts the integrity and composition of mitotic centrosomes. *Cell Cycle* **12**, 1406–1415, https://doi.org/10.4161/cc.24516 (2013).
37. Ghaleb, A. M., Elkarim, E. A., Bialkowska, A. B. & Yang, V. W. KLF4 suppresses tumor formation in genetic and pharmacological mouse models of colonic tumorigenesis. *Mol. Cancer Res.* **14**, 385–396(2016).
38. Wang, X. et al. Overexpression of aurora kinase A in mouse mammary epithelium induces genetic instability preceding mammary tumor formation. *Oncogene* **25**, 7148–7158 (2006).
39. Budanov, A. V. & Karin, M. p53 target genes sestrin1 and sestrin2 connect genotoxic stress and mTOR signaling. *Cell* **134**, 451–460 (2008).
40. Vadysirisack, D. D., Baenke, F., Ory, B., Lei, K. & Ellisen, L. W. Feedback control of p53 translation by REDD1 and mTORC1 limits the p53-dependent DNA damage response. *Mol. Cell Biol.* **31,** 4356–4365 (2011).
41. Workman, P., Burrows, F., Neckers, L. & Rosen, N. Drugging the cancer chaperone HSP90: combinatorial therapeutic exploitation of oncogene addiction and tumor stress. *Ann. N. Y Acad. Sci.* **1113**, 202–216 (2007).
42. Song, H., Hollstein, M. & Xu, Y. p53 gain-of-function cancer mutants induce genetic instability by inactivating ATM. *Nat. Cell Biol.* **9**, 573–580 (2007).
43. Yang, K., Hitomi, M. & Stacey, D. W. Variations in cyclin D1 levels through the cell cycle determine the proliferative fate of a cell. *Cell Div.* **1**, 32 (2006).
44. Hitomi, M. & Stacey, D. W. Cyclin D1 production in cycling cells depends on ras in a cell-cycle-specific manner. *Curr. Biol.* **9**, 1075–1084 (1999).
45. Hitomi, M. & Stacey, D. W. Cellular ras and cyclin D1 are required during different cell cycle periods in cycling NIH 3T3 cells. *Mol. Cell Biol.* **19**, 4623–4632 (1999).
46. Aleem, E., Kiyokawa, H. & Kaldis, P. Cdc2-cyclin E complexes regulate the G1/S phase transition. *Nat. Cell Biol.* **7**, 831–836 (2005).
47. Musacchio, A. & Salmon, E. D. The spindle-assembly checkpoint in space and time. *Nat. Rev. Mol. Cell Biol.* **8**, 379–393 (2007).
48. Olive, K. P. et al. Mutant p53 gain of function in two mouse models of Li-Fraumeni syndrome. *Cell* **119**, 847–860 (2004).
49. Lang, G. A. et al. Gain of function of a p53 hot spot mutation in a mouse model of Li-Fraumeni syndrome. *Cell* **119**, 861–872 (2004).
50. Suh, Y. A. et al. Multiple stress signals activate mutant p53 in vivo. *Cancer Res.* **71**, 7168–7175 (2011).
51. Silwal-Pandit, L. et al. TP53 mutation spectrum in breast cancer is subtype specific and has distinct prognostic relevance. *Clin. Cancer Res.* **20,** 3569–3580 (2014).
52. Wijnhoven, S. W. et al. Dominant-negative but not gain-of-function effects of a p53.R270H mutation in mouse epithelium tissue after DNA damage. *Cancer Res.* **67**, 4648–4656 (2007).
53. Lee, M. K. et al. Cell-type, dose, and mutation-type specificity dictate mutant p53 functions in vivo. *Cancer Cell* **22**, 751–764 (2012).
54. Hanel, W. et al. Two hot spot mutant p53 mouse models display differential gain of function in tumorigenesis. *Cell Death Differ.* **20,** 898–909 (2013).
55. Parikh, N. et al. Effects of TP53 mutational status on gene expression patterns across 10 human cancer types. *J. Pathol.* **232**, 522–533 (2014).
56. Turrell, F. K. et al. Lung tumors with distinct p53 mutations respond similarly to p53 targeted therapy but exhibit genotype-specific statin sensitivity. *Genes Dev.* **31**, 1339–1353 (2017).

57. Cuyas, E., Corominas-Faja, B., Joven, J. & Menendez, J. A. Cell cycle regulation by the nutrient-sensing mammalian target of rapamycin (mTOR) pathway. *Methods Mol. Biol.* **1170**, 113–144 (2014).
58. Adorno, M. et al. A Mutant-p53/Smad complex opposes p63 to empower TGFbeta-induced metastasis. *Cell* **137**, 87–98 (2009).
59. Acquaviva, J. et al. mTOR inhibition potentiates HSP90 inhibitor activity via cessation of HSP synthesis. *Mol. Cancer Res.* **12**, 703–713 (2014).
60. Muller, P. A. et al. Mutant p53 drives invasion by promoting integrin recycling. *Cell* **139**, 1327–1341 (2009).
61. Muller, P. A. & Vousden, K. H. p53 mutations in cancer. *Nat. Cell Biol.* **15**, 2–8 (2013).
62. Zhou, G. et al. Gain-of-function mutant p53 promotes cell growth and cancer cell metabolism via inhibition of AMPK activation. *Mol. Cell* **54**, 960–974 (2014).
63. Papanikolaou, V. et al. The involvement of HER2 and p53 status in the regulation of telomerase in irradiated breast cancer cells. *Int J. Oncol.* **35**, 1141–1149 (2009).
64. Bouaoun, L. et al. TP53 variations in human cancers: new lessons from the IARC TP53 database and genomics data. *Hum. Mutat.* **37**, 865–876 (2016).
65. Yallowitz, A., Ghaleb, A., Garcia, L., Alexandrova, E. M. & Marchenko, N. Heat shock factor 1 confers resistance to lapatinib in ERBB2-positive breast cancer cells. *Cell Death Dis.* **9**, 621 (2018).
66. Schneider, C. A., Rasband, W. S. & Eliceiri, K. W. NIH Image to ImageJ: 25 years of image analysis. *Nat. Methods* **9**, 671–675 (2012).
67. Nemajerova, A., Petrenko, O., Trumper, L., Palacios, G. & Moll, U. M. Loss of p73 promotes dissemination of Myc-induced B cell lymphomas in mice. *J. Clin. Invest.* **120**, 2070–2080 (2010).

Acknowledgements

This work was supported by the Department of Defense grant W81XWH-16-1-0448 (BC151569) and the Carol Baldwin Breast Cancer Research Fund to N.M.

Author contributions

A.G.: study design, data acquisition, analysis and interpretation, and preparation and revision of the manuscript. A.Y.: data acquisition, and revision of the manuscript. N.M.: study design, study supervision, data acquisition, analysis and interpretation, and preparation and revision of the manuscript.

Competing interests

The authors declare no competing interests.

Additional information

Supplementary information is available for this paper at https://doi.org/10.1038/s42003-019-0669-y.

Correspondence and requests for materials should be addressed to A.G. or N.M.

Reprints and permission information is available at http://www.nature.com/reprints

Publisher's note Springer Nature remains neutral with regard to jurisdictional claims in published maps and institutional affiliations.

Ghaleb et al. Breast Cancer Research (2020) 22:133
https://doi.org/10.1186/s13058-020-01370-y

Breast Cancer Research

RESEARCH ARTICLE Open Access

Mutant p53 drives the loss of heterozygosity by the upregulation of Nek2 in breast cancer cells

Amr Ghaleb[1*], Malik Padellan[2] and Natalia Marchenko[1]

Abstract

Background: Mutations in one allele of the TP53 gene in early stages are frequently followed by the loss of the remaining wild-type p53 (wtp53) allele (p53LOH) during tumor progression. Despite the strong notion of p53LOH as a critical step in tumor progression, its oncogenic outcomes that facilitate the selective pressure for p53LOH occurrence were not elucidated.

Methods: Using MMTV;ErbB2 mouse model of breast cancer carrying heterozygous R172H p53 mutation, we identified a novel gain-of-function (GOF) activity of mutant p53 (mutp53): the exacerbated loss of wtp53 allele in response to γ-irradiation.

Results: As consequences of p53LOH in mutp53 heterozygous cells, we observed profound stabilization of mutp53 protein, the loss of p21 expression, the abrogation of G2/M checkpoint, chromosomal instability, centrosome amplification, and transcriptional upregulation of mitotic kinase Nek2 (a member of Never in Mitosis (NIMA) Kinases family) involved in the regulation of centrosome function. To avoid the mitotic catastrophe in the absence of G2/M checkpoint, cells with centrosome amplification adapt Nek2-mediated centrosomes clustering as pro-survival mutp53 GOF mechanism enabling unrestricted proliferation and clonal expansion of cells with p53LOH. Thus, the clonal dominance of mutp53 cells with p53LOH may represent the mechanism of irradiation-induced p53LOH. We show that pharmacological and genetic ablation of Nek2 decreases centrosome clustering and viability of specifically mutp53 cells with p53LOH.

Conclusion: In a heterogeneous tumor population, Nek2 inhibition may alter the selective pressure for p53LOH by contraction of the mutp53 population with p53LOH, thus, preventing the outgrowth of genetically unstable, more aggressive cells.

Keywords: Mutant p53, Nek2, LOH, Centrosome clustering, Breast cancer

* Correspondence: amr.ghaleb@stonybrookmedicine.edu
[1]Department of Pathology, Stony Brook University, Stony Brook, NY 11794-8691, USA
Full list of author information is available at the end of the article

Introduction

P53 is a tumor suppressor that plays a crucial role in inducing cancer cell death and growth arrest to protect the genome from the accumulation of DNA errors in response to genotoxic stress [1]. TP53 is the most frequently mutated gene in human breast cancer and, particularly, in Her2(ErbB2)-positive breast cancer (72%), where it is associated with poor outcomes for patients [2]. Typically, mutations in the TP53 gene occur through a two-hit mechanism, where a missense mutation in one allele is followed by loss of the remaining wtp53 allele (p53LOH, loss of heterozygosity). Markedly, the frequency of p53LOH increases as cancer progress: 52% of stage 1, but only 20% of stage 2 breast cancer patients retain wild type p53 (wtp53) allele [3], that suggests the strong selective pressure for p53LOH occurrence during tumor progression. It is generally accepted that p53LOH is a crucial oncogenic event in tumorigenesis. However, understanding the precise mechanism and biological outcomes of p53LOH has been hindered by the lack of relevant experimental in vitro models. Nevertheless, it becomes an important clinical question as the targeting of p53LOH occurrence may lead to novel therapeutic strategies that delay or hinder tumor progression. Hence, we sought to elucidate the functional outcomes of p53LOH that may generate the selective pressure for the loss of wtp53 allele during tumor progression in mutant p53 (mutp53) heterozygous mammary tumors leading to the expansion of cells with p53LOH.

In our previous study, we established and characterized a novel MMTV;ErbB2 mouse model carrying both wtp53 and R172H mutp53 alleles (heterozygous mice, H/+;ErbB2 after that) that mimics early stages of Her2-positive breast cancer [3]. We identified a novel oncogenic activity of mutp53: the exacerbated loss of wtp53 allele in response to irradiation compared to p53 −/+;ErbB2 mice. We found that p53LOH is associated with the marked stabilization of mutp53 protein in vivo and in vitro, enhanced chromosomal aberrations, and increased metastases only in the presence of mutp53 allele [3]. As the elevated level of mutp53 protein has been proposed to be essential for its oncogenic activities [4, 5], p53LOH with subsequent stabilization of mutp53 protein may represent key tumor-promoting steps in vivo. Nevertheless, it remains to be elucidated how mutp53 aggravates p53LOH and metastases in response to genotoxic stress such as γ-irradiation.

The previous ectopic expression studies suggested that in heterozygous cells, mutp53 may exert its oncogenic activities via the dominant-negative (DN) mechanism by inhibiting the tumor-suppressive function of wtp53 allele or in the gain-of-function (GOF) manner [6, 7]. To evaluate the interplay between endogenous wtp53 and mutp53 in heterozygosity, we generated cell lines from mammary tumors of heterozygous mice with an identical genetic background. Surprisingly, despite a strong notion of the mutp53 DN effect, we have not observed the global suppression of "canonical" wtp53 target genes such as p21, sestrins, and Mdm2 in response to irradiation in the presence of mutp53 allele [3]. Consistent with these findings, here we demonstrate that wtp53 allele in mutp53 heterozygous cells (H/+;ErbB2) is competent partially to induce G2/M checkpoint and growth arrest in response to irradiation. Conversely, p53LOH (H/−; ErbB2 cells) completely abrogate G2/M checkpoint and sustain the S-phase after irradiation leading to cell cycle re-entry with genomic aberrations. Therefore, the competitive growth advantage of cells with p53LOH over mutp53 heterozygous cells may underlie the exacerbated p53LOH, which we observed in vivo. We hypothesized that irradiation-induced p53LOH generates the clonal pool of genetically unstable cells prone to expand after DNA damage, leading to tumor progression and metastases.

Here, we aimed to identify potential vulnerabilities of cells with p53LOH that would provide a therapeutic opportunity to prevent the expansion of cells with p53LOH. The transcriptional and functional characterization of cell lines with distinct p53 deficiencies identified Nek2 (a member of Never in Mitosis (NIMA) Related Kinases family) as a potential target for p53LOH prevention. We demonstrated that the presence of functional wtp53 allele reduces sensitivity to specific Nek2 inhibitor JH295, while p53LOH significantly sensitizes cancer cells to Nek2 inhibition and prevents p53LOH occurrence after irradiation. Hence, our data suggest targeting Nek2 as the potential strategy to avoid p53LOH onset in the context of γ-radiation.

Materials and methods

Metabric data

Human Metabric data analysis, of the somatic mutation profiles of 2433 breast cancers, was done using data from a retrospective study [8]. The data is deposited and is publicly available at http://www.cbioportal.org. The analysis was done using the program and tools made available online at http://www.cbioportal.org.

Mice

MMTV-ErbB2 mice carrying activated ErbB2 (strain FVBN-Tg(MMTV-ErbB2)NK1Mul/J) were from Jackson Labs. p53 R172H (called p53H/H) and control p53 null (p53−/−) mice (C57Bl6J background) were a gift from G. Lozano [9]. p53H/−;ErbB2 mice were generated by crossing ErbB2 mice with p53−/− mice and then breeding the p53+/−;ErbB2 progeny with p53H/H mice. p53H/−;ErbB2 mice were then crossed to generate p53H/H;ErbB2 and p53−/−;ErbB2 females for analysis. p53+/+;ErbB2 were generated from crossing of p53H/+;

ErbB2 and p53+/−;ErbB2 mice. Mice carrying the floxed p53R248Q mutation (referred to as floxQ) was generated as described before [10]. For all mice genotypes, only female littermates were used for all analyses. Animals were monitored weekly to determine their breast cancer and sarcoma onset and were promptly killed when their tumors reached 4 cm^3 in volume or when animals appeared moribund. Careful necropsies were performed, and tumors and all major organs collected, fixed in 10% formalin, embedded in paraffin, and sectioned for histopathologic analysis. For survival analysis, *P* values were determined by log-rank analysis. Mice were treated according to guidelines approved by the Institutional Animal Care and Use Committee at Stony Brook University.

Cell lines

Human ErbB2-positive breast cancer cell lines ZR-75-30 carrying wild type TP53, and BT474, SKBR3, carrying E285K, R175H *TP53* mutations respectively, were purchased from ATCC. Establishing mouse mammary tumors cell lines was described before [11]. Mouse mammary tumor cell lines: p53+/+;ErbB2, p53H/+;ErbB2, and p53−/+;ErbB2 were isolated from their corresponding mammary tumors and maintained in culture. P53H/−;ErbB2 cells were obtained from p53H/+;ErbB2 tumors with confirmed LOH and p53−/−;ErbB2 cells were obtained from p53−/+;ErbB2 tumors with confirmed LOH. Where shown, cells were treated with 1.2 μM of Nek2 specific inhibitor JH295 (Tocris Bioscience).

Gamma irradiation

For γ-irradiation of cells, a 137Cs source with a dose rate of 0.8 Gy/min was used, for a total of 0.1 Gy or 9 Gy. Non-irradiated cells (sham) were placed in the room without being exposed to irradiation.

Immunofluorescence

For IF on cells, media was aspirated from cells grown on chamber slides, cells were fixed with methanol at − 20 °C for 10 min, and then washed 3x with PBS. Cells were permeabilized with 0.2% Tween 20 in PBS at RT for 10 min, and then incubated with blocking buffer [10% normal horse serum (NHS) and 0.1% Tween 20 in PBS], for 1 h at 37 °C. Cells were then stained with rabbit anti-γtubulin (1:200, Sigma) for 1 h at 37 °C, and then washed 3x with PBS. Goat anti-rabbit Alexa fluor-labeled 568 secondary antibodies (Molecular Probes) at 1:500 dilution for 30 min at 37 °C, counterstained with Hoechst 33258 (2 μg/ml), mounted with Prolong gold (Molecular Probes), and cover-slipped. Images were acquired at × 600 total magnification using a Nikon Eclipse Ti-S microscope (Nikon Instruments) equipped with QI-Click camera (QImaging). Where applicable, quantification of centrosome number was performed on 10 images of randomly selected fields per genotype per treatment.

Determination of LOH of the *p53*+ locus

Mouse p53H/+;ErbB2 cells were irradiated (9 Gy), or not, and Nek2 inhibitor was added (1.2 μg/ml) 6 h post irradiation. Cells were maintained in culture for 10 days with or without Nek2 inhibitor and fresh media, with or without Nek2 inhibitor, was replenished every 3–4 days. DNA was then extracted using QIAmp DNA Micro Kit (Qiagen). An equal amount of DNA was used for PCR amplification of p53 locus using primers described before [9]. An equal volume of the amplified product was electrophoresed through a 1.5% agarose gel. Amplified DNA bands were visualized, and the image captured using FluoroChem HD2 (ProteinSimple). LOH was determined based on the presence or absence of the amplified wild type band. Band intensity of wtp53 and mutp53 amplicons were measured using ImageJ [12].

Real-time PCR

All real-time PCR was done on cultured cells using 3 biological replicas. For determination mRNA transcript level, RNA was extracted from cultured cells using Trizol as per manufacturer instructions. For cDNA synthesis, 200 ng/sample was used in a 20 μl reaction volume prepared from QuantiTect Reverse Transcription Kit (Qiagen). After cDNA synthesis, the reaction volume was diluted to 200 μl using DEPC-treated water. For qPCR, 1 μl of the diluted cDNA was used per reaction volume. The following primers were used: for human cell lines: NEK2 [F] 5′-AGCGAGCTCTCAAAGCAAGA-3′, [R] 5′-ACTGAGGATGGAAGATTAAGAAGT-3′; HPRT [13] [F] 5′-GCTATAAATTCTTTGCTGACCTGCTG-3′, [R] 5′-AATTACTTTTATGTCCCCTGTTGACTGG-3′; for mouse cell lines: cyclin E2 [F] 5′-ATGTCAAGACGCAG CCGTTTA-3′, [R] 5′-GCTGATTCCTCCAGACAG TACA-3′; Nek2 [F] 5′-TAACGGGATGCGTATG GCAG-3′, [R] 5′-TTAACTGGCACAGTGAGCGT-3′; Hprt [14] [F] 5′-GGCTATAAGTTCTTTGCTGACC-3′, [R] 5′-CTCCACCAATAACTTTTATGTCC-3′. For all real-time PCR, amplification was done using Quantitech sybr green (Qiagen) reaction mixture, and detection was done using QuantStudio3 (Thermo Fisher Scientific).

siRNA and CRISPR/Cas9 treatment

Human p53-specific siRNA was purchased from Santa Cruz Biotech. CRISPR/Cas9 was used to delete *p53* or *Nek2* from cultured mouse cell lines by transfecting cells with *p53* or *Nek2* double nickase plasmid (Santa Cruz Biotech), using TransIT-X2® Transfection Reagent (Mirusbio) according to manufacturer's recommendations. Selection of transfected cells was done by adding puromycin (6 μg/ml) (Fisher) to culture media 2 days post transfection. Selected cells were maintained in media with puromycin (6 μg/ml) throughout.

Cell cycle analysis

Cultured cells were harvested by trypsinization and pelleted by spinning at 1500 r.p.m. for 10 min. The cell pellet was washed twice with PBS, then fixed in 70% ethanol. The cells were pipetted gently up and down to loosen the cells in a suspension and stored in − 20 °C overnight. The cells were then pelleted by spinning at 1500 r.p.m. for 10 min, washed once in PBS, then resuspended in permeabilization buffer (0.25% tritonX100 in PBS) and incubated for 15 min at RT. The cells were then pelleted and resuspended in staining solution (20 μg/ml propidium iodide and 10 μg/ml RNase A in PBS) and incubated in the dark on ice for 30 min before analysis. Cell cycle analysis by flow cytometry was done at Stony Brook Flowcytometry Core Facility, using Becton Dickinson FACSCAN analyzer.

Immunoblot analysis

For immunoblots, cell lysates with equal total protein content (2–20 μg) were blotted with antibodies to p53 (FL393), p21 GAPDH, Hsc70, Nek2, and tubulin (all from Santa Cruz Biotechnology); γH2AX (all from Cell Signaling)). All immunoblots were repeated at least two times.

Colony formation assay and staining

Mouse cells were plated at 20×10^3 cells per well and treated, or not, with Nek2 inhibitor (1.2 μg/ml). Cells were maintained in culture for 15 days with or without Nek2 inhibitor and fresh media, with or without Nek2 inhibitor, was replenished every 3–4 days. For staining, cells were fixed by adding 4% paraformaldehyde to growth media (final concentration 1%) for 10 min at RT. The media was then aspirated, and a staining solution (0.5% crystal violet in 20% methanol) was gently added to cover wells. Cells were left to stain for 20 min at RT, and the staining solution was removed by aspiration. Excess staining was then washed by gently dipping one plate at a time into a beaker of water. The plates were then air-dried and visualized.

Purification and preparation of RNA for microarray expression analysis

RNA was processed from cells that had reached 80–90 confluency. Total RNA from cultured cells was extracted using Trizol reagent as recommended by the manufacturer (Invitrogen; Carlsbad, CA). RNA was subjected to DNase I treatment in order to remove any contaminating genomic DNA. Final purification was performed on RNAeasy columns (Qiagen; Valencia, CA), according to the manufacturer's recommendations. The integrity, quality, and quantity of total RNA were confirmed by Eukaryotic Total RNA Nano Bioanalyzer (Agilent Technologies) at the genomic core facility at Stony Brook University. RNA with OD260/OD280 > 1.8 and RNA integrity number of > 8.5 were submitted for microarray analysis.

Microarray expression analysis

After the QC procedures, mRNA from eukaryotic organisms was enriched using oligo(dT) beads. For prokaryotic samples, rRNA was removed using a specialized kit that cleaves the mRNA. The mRNA was then fragmented randomly in a fragmentation buffer, followed by cDNA synthesis using random hexamers and reverse transcriptase. After first-strand synthesis, a custom second-strand synthesis buffer (Illumina) was added with dNTPs, RNase H, and *Escherichia coli* polymerase I to generate the second strand by nick-translation. The final cDNA library was used for a round of purification, terminal repair, A-tailing, ligation of sequencing adapters, size selection, and PCR enrichment. Library concentration was first quantified using a Qubit 2.0 fluorometer (Life Technologies) and then diluted to 1 ng/μl before checking insert size on an Agilent 2100 and quantifying to greater accuracy by quantitative PCR (Q-PCR) (library activity > 2 nM).

The original raw data from Illumina HiSeqTM are transformed into Sequenced Reads by base calling. Raw reads are filtered to remove reads containing adapters or reads of low quality so that downstream analyses are based on clean reads. TopHat2 software was used for mapping sequences of animal genome. The mismatch parameter is set to two, and other parameters are set to default. Only filtered reads are used to analyze the mapping status of RNA-seq data to the reference genome.

Gene expression level was measured by transcript abundance. The gene expression level was estimated by counting the reads that map to genes or exons. Read count was proportional to the actual gene expression level and to the gene length and the sequencing depth. The FPKM (Fragments Per Kilobase of transcript sequence per Millions base pairs sequenced) was used in order for the gene expression levels estimated from different genes and experiments to be comparable. HTSeq software was used to analyze the gene expression levels using the union mode. The result files present the number of genes with different expression levels and the expression level of single genes. In general, an FPKM value of 0.1 or 1 is set as the threshold for determining whether the gene is expressed or not. The overall results of FPKM cluster analysis were done using the log10(FPKM+ 1) value.

Centrosome proteins and their genes were identified based on data from MiCroKit database [15] (http://microkit.biocuckoo.org/). FPKM values of these identified genes were used for cluster analysis using the publicly available program, Morpheus (https://software.broadinstitute.org/morpheus/).

Statistics and reproducibility

All statistical analysis between groups was done using the t test. Significance was determined at $p < 0.05$. Cell culture experiments were repeated three times.

Results

p53LOH enhances cell proliferation

Previously, we established a novel genetic mouse model of early stages of Her2 positive breast cancer by crossing MMTV-ErbB2 and R172H KI mice [16]. We characterized the following mouse genotypes: R172H/wtp53;ErbB2 (H/+;ErbB2), p53null/wtp53;ErbB2 (−/+;ErbB2), and wtp53/wtp53;ErbB2 (+/+;ErbB2). The murine R172H p53 mutation corresponds to human R175H p53 mutation, which was identified as a hotspot in ErbB2 breast cancer [17]. To evaluate the phenotypic effects of mutp53 in heterozygosity, we established stable cell lines from mouse mammary tumors of +/+;ErbB2, H/+;ErbB2, H/−;ErbB2 (R172H/p53null;ErbB2), −/+;ErbB2, and −/−;ErbB2 genotype (three biological replicas per genotype) (Fig. 1a). In contrast to the existing human breast cancer cell lines that are mutp53 homo- or hemizygous, our panel of cell lines (isogenic and non-isogenic) allows us to evaluate the pathological consequences of p53LOH in the well-controlled model.

We found that compared to p53+/+;ErbB2 and p53−/+;ErbB2 cells, the presence of mutp53 allele in heterozygous cells elevates the total p53 protein level, while p53LOH leads to further stabilization of mutp53 protein (Fig. 1a). We have previously shown that γ-irradiation leads to the profound loss of wtp53 allele in p53H/+;ErbB2, but not in p53−/+;ErbB2 cell lines [3]. Hence, we utilized the established cell line panel to elucidate the mechanism of mutp53-mediated p53LOH.

Markedly, the cell growth analysis demonstrated that p53 LOH (H/−;ErbB2 cells) increases cell proliferation over cells with wtp53 allele (+/+;ErbB2, H/+;ErbB2 and −/+;ErbB2 cells) and over cells null for p53 (p53−/−;ErbB2) (Fig. 1b). Consistent with growth curves, loss of wtp53 allele in mutp53 heterozygous cells (H/−;ErbB2) shows the highest percentage of cells in mitosis compared to other p53 genotypes (Fig. 1c). Our previous study demonstrated that in H/+;ErbB2 cells, mutp53 does not exert a global DN effect over wtp53 allele in response to DNA damage [3]. In agreement with previous data, here we show that the presence of wtp53 allele in H/+;ErbB2 cells is sufficient to induce canonical p53 target p21 at the RNA (Fig. 1d) and protein level (Figs. 1a, 2b) under normal conditions. Loss of wtp53 allele in H/−;ErbB2 and p53−/−;ErbB2 cells abrogates p21 expression (Fig. 1d), which remains undetectable even after irradiation (Fig. 2b). Consistent with the transcriptional activity of wtp53 in heterozygous cells, CRISPR/Cas9-deletion of p53 (mutp53 and wtp53) obliterates the basal p21 expression in unstressed H/+;ErbB2 cells (Fig. 1e).

This finding suggests that the loss of wtp53-mediated p21 expression may enhance proliferation and provide a competitive advantage to cells with p53LOH over cells retaining wtp53 allele. Additionally, CRISPR/Cas9 deletion of mutp53 in H/−;ErbB2 cells decreased cell proliferation significantly (Fig 1f), suggesting that mutp53 enhances cell proliferation in GOF manner.

These results led us to speculate that under normal conditions, spontaneous p53LOH in heterogeneous H/+;ErbB2 tumor population provides a competitive growth advantage to H/−;ErbB2 cells by two complementary mechanisms: the ablation of basal p21 expression via loss-of-function mechanism and stabilization of mutp53 protein enabling its GOF activities.

p53LOH abrogates the G2/M checkpoint after irradiation

An increased incidence of p53LOH in the presence of mutp53 allele after irradiation [3] set us to investigate the mechanism by which mutp53 promotes p53LOH. The cell cycle analysis demonstrated that p53LOH in mutp53 cells abrogates G2/M checkpoint, which is preserved in the presence of wtp53 allele in −/+;ErbB2 and is partially functional in H/+;ErbB2 (Fig. 2a). As p21 was shown to play a distinct role in the G2/M checkpoint [18, 19], we analyzed p21 protein level in response to irradiation. To avoid nonspecific effects of high dose irradiation, in subsequent experiments, we utilized the low dose irradiation (0.1 Gy). Consistent with the transcriptional activity of wtp53 allele in heterozygous cells (Fig. 1d), we found that irradiation induces p21 in H/+;ErbB2 cells, while the loss of wtp53 allele (H/−;ErbB2) correlates with a lack of detectable p21 protein even after irradiation (Fig. 2b). The dominance of the wtp53 allele over mutp53 in response to DNA damage and the induction of p21 has been reported previously [20].

Cyclin E is necessary for centrosome duplication in the S phase that precedes the G2/M transition [21]. Previously, we demonstrated a significant reduction of cyclin E2 transcription after irradiation in the presence of wtp53 allele (p53H/+;ErbB2 and p53−/+;ErbB2), which is indicative of G2/M arrest [3]. Contrary, irradiation does not affect cyclin E2 transcription in H/−;ErbB2 (Fig. 2c) that was associated with the deficient G2/M checkpoint after irradiation (Fig. 2a). In agreement with defective G2/M checkpoint (Fig. 2a), the lack of p21 expression (Figs. 1d and 2bb), and elevated cyclin E2 mRNA (Fig. 2c), H/−;ErbB2 cells sustain proliferation after irradiation (Fig. 2a, d). This is in the stark contrast to continuous growth arrest of −/+;ErbB2 and H/+;ErbB2 cells after irradiation (Fig. 2a, d).

Importantly, we found that mutp53 CRISPR/Cas9 deletion in H/−;ErbB2 cells restored G2/M arrest after irradiation, as indicated by increased G2/M populations (Fig. 2e). A similar cell cycle profile was observed in H/+;ErbB2 and −/+;ErbB2 cells after p53 CRISPR/Cas9 deletion (Fig. 2e). Consistently, p53−/−;ErbB2 cells maintain functional G2/M checkpoint as indicated by increased G2/M population after irradiation (Fig. 2e), with no mitotic slippage except in H/−;ErbB2 cells (Fig. 2f).

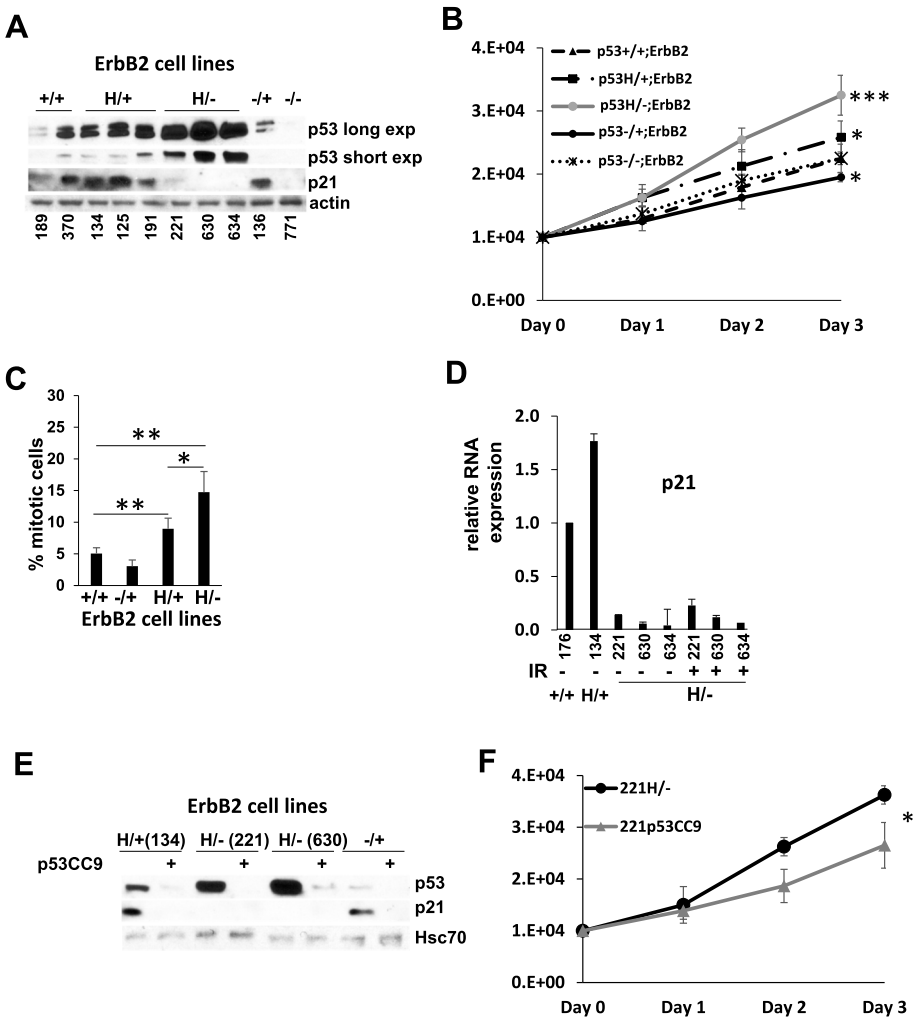

Fig. 1 Mutp53 promotes cell proliferation. **a** Western blot analysis of p53 and p21 levels in mouse ErbB2 mammary epithelial tumor cell lines with different p53 status. Actin is loading control. **b** Growth curve of mouse ErbB2 mammary epithelial tumor cell lines with different p53 status. $n = 3$ independent experiments per genotype (one cell line per genotype except for p53+/+ and p53 H/− where 2 different cell lines derived from different tumors and result per genotype was averaged). **c** Bar graph showing percent mitotic cells in mouse ErbB2 mammary epithelial tumor cell lines with different p53 status. Each bar represents the average percent of mitotic per genotype counted from at least 5 randomly selected fields at × 400 magnification (one cell line per genotype except for p53+/+ and p53 H/− where 2 different cell lines derived from different tumors and result per genotype was averaged). **d** Bar graph showing relative mRNA expression level of p21 in ErbB2 mammary epithelial tumor cell lines with different p53 status. $n = 3$ independent experiments per cell line per genotype. **e** Western blot analysis of p53 and p21 levels in mouse ErbB2 mammary epithelial tumor cell lines with different p53 status before and after CRISPR/Cas9 p53 deletion (p53CC9). Hsc70 is loading control. **f** Growth curve of mouse ErbB2 mammary epithelial tumor cell line with mutp53, before and after CRISPR/Cas9 p53 deletion (p53CC9). $n = 3$ independent experiments per cell line. Where applicable $^{*}p < 0.05$; $^{**}p < 0.01$; $^{***}p < 0.001$. Error bars represent ± SD

Of note, the cell cycle profiles of H/−;CC9 and −/−;ErbB2 cells are slightly different. The −/−;ErbB2 line was established from −/+;ErbB2 tumor that lost its wtp53 allele through LOH, while the H/−;CC9 cells had mutp53 before CRIPSR depletion. The original presence of mutp53 in the H/−;ErbB2 cells may have led to genetic alterations that are persistent after p53 deletion leading to the differences in the cell cycle profile observed in H/−;CC9 line and −/−;ErbB2 cells. Most importantly, all CC9 (including 630H/−;CC9) and −/−;ErbB2 cells exhibit functional G2/M checkpoint post-irradiation. This data indicates wtp53 independent G2/M checkpoint; however, skipping the G2/M arrest is driven by mutp53 (Fig. 2a). These results strongly suggest that p53LOH in mutp53 heterozygous cells abrogates G2/M checkpoint in the mutp53 GOF manner leading to cell cycle progression after γ-irradiation in the presence of unrepaired DNA (Fig. 2e).

Together, our data indicate that γ-irradiation enhances the clonal expansion of mutp53 cells with p53LOH by providing the competitive growth advantage over cells retaining the wtp53 allele, which induce

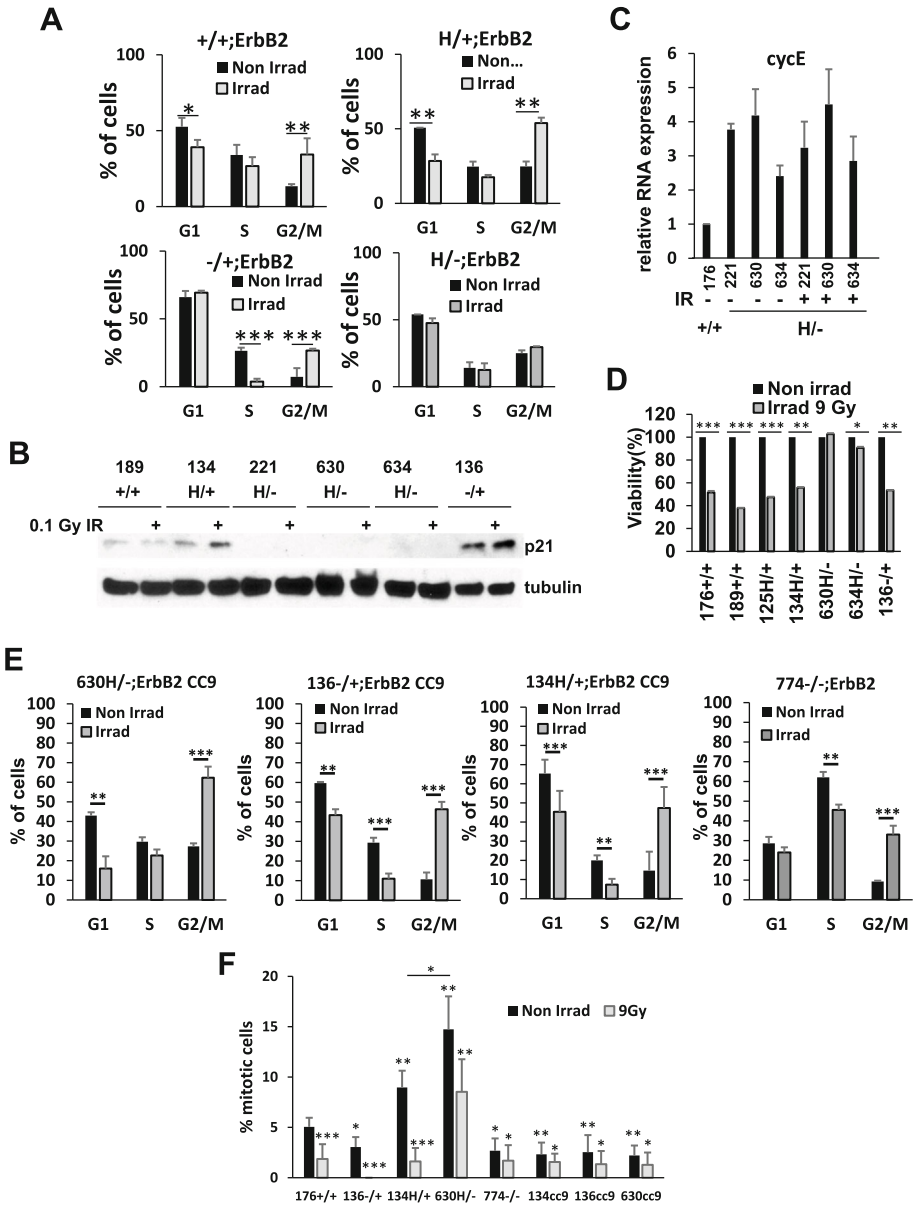

Fig. 2 Mutp53 suppresses cell cycle checkpoint following γ-irradiation. **a** Aberrant cell cycle checkpoint following γ-irradiation in p53H/−;ErbB2 cells. Bar graphs showing cell cycle analysis of p53+/+;ErbB2, p53H/+;ErbB2, p53−/+;ErbB2, and p53H/−;ErbB2 cell lines irradiated (gray bars) or not (black bars). $n = 3$ independent experiments per genotype (one cell line per genotype except for p53+/+ and p53 H/− where 2 different cell lines derived from different tumors and result per genotype was averaged). **b** Western blot analysis of p21 level before and 24 h after γ-irradiation (0.1 Gy) in mouse ErbB2 mammary epithelial tumor cell lines with different p53 status. α-Tubulin is loading control. **c** Bar graph showing relative mRNA expression level of CycE before and 24 h after γ-irradiation in ErbB2 mammary epithelial tumor cell lines with different p53 status. $n = 3$ independent experiments per cell line per genotype. **d** Bar graph showing percent viability before and 24 h after γ-irradiation in ErbB2 mammary epithelial tumor cell lines with different p53 status. $n = 3$ independent experiments per cell line per genotype. **e** Restoration of cell cycle checkpoint 24 h post γ-irradiation p53-null cells. Bar graphs showing cell cycle analysis of p53H/−;ErbB2, p53H/+;ErbB2, p53−/+;ErbB2 following CRISPR/Cas9 p53 deletion (p53CC9) and in p53 −/−;ErbB2 cell lines irradiated (gray bars) or not (black bars). $n = 3$ independent experiments per genotype. **f** Bar graphs showing mitotic index in different cell lines irradiated (gray bars) or not (black bars) (result for each irradiated genotype was compared to its own control). $n = 3$ independent experiments per genotype. Where applicable $^{*}p < 0.05$; $^{**}p < 0.01$; $^{***}p < 0.001$. Error bars represent ± SD

p21 and undergo G2/M arrest in response to irradiation. Therefore, the clonal dominance of cells with p53LOH may represent the mechanism of irradiation-induced p53LOH.

p53LOH drives chromosomal instability in mutant p53 cancer cells

While mutp53 was implicated as an essential driver of various forms of chromosomal instability—aneuploidy,

translocation, and amplification [22, 23]—the underpinning mechanism of how mutp53 induces chromosomal aberrations remains vague. Previously, we demonstrated that p53LOH in the presence of mutp53 allele is associated with increased chromosomal instability in vivo indicated by the higher incidence of anaphase bridges in mammary tumors [3]. In addition, errors in chromosome segregation (chromosomal instability) during mitosis might be monitored by the formation of micronuclei [24, 25]. Consistent with our previous finding [3], we found that irradiation more profoundly drives chromosomal instability in the presence of a mutp53 allele that is further augmented by p53LOH, as indicated by micronuclei formation (Fig. 3a).

As chromosomal instability may arise from abnormal chromosome segregation in mitosis, we investigated centrosome aberration with respect to p53 status. During mitosis, two centrosomes form spindle poles and direct the formation of bipolar mitotic spindles, which is an essential event for accurate segregation of chromosomes. The presence of more than two centrosomes (centrosome amplification) severely disturbs cytokinesis during mitosis via the formation of more than two spindle poles (Fig. 3b), resulting in an increased frequency of chromosome segregation errors, such as aneuploidy, amplifications, and deletions. These genetic events may further facilitate tumor progression and the acquisition of metastatic phenotype. Significantly, the presence of mutp53 allele in heterozygous cells significantly increases centrosome amplification compared to −/+;ErbB2 cells (Fig. 3b, c) in an apparent DN fashion. Therefore, the elevated centrosome amplification in H/+;ErbB2 cells may increase the incidence of spontaneous p53LOH under normal conditions as compared to −/+;ErbB2 cells. Subsequently, p53LOH (H/−;ErbB2 and −/−;ErbB2 cells) slightly increases the abnormal centrosome number (Fig. 3b, c). On the other hand, the excessive centrosome amplification within tumor cells can be deleterious as it may lead to multipolar mitosis and generate sufficiently high levels of aneuploidy to pose a challenge for cell viability [26]. As a pro-survival mechanism, cancer cells adapt to avoid multipolar mitosis by clustering their extra centrosomes at the two poles of the spindle during mitosis, thus ensuring bipolar chromosome segregation [27]. However, pseudo-bipolar spindle formation through centrosome clustering causes slower mitosis. The latter leads to increased frequency of lagging chromosomes during anaphase and thus to chromosomal instability, thereby explaining the link between supernumerary centrosomes and chromosomal instability [28]. Although centrosome clustering occurs both in vivo [29, 30] and in vitro [31], its underpinning mechanism is not well understood. Thus, we set to determine whether the mutp53 cells ensure cell survival by evasion of multipolar mitosis via centrosome clustering at the expense of chromosomal instability. We observed mitotic cells with centrosome clustering in all mouse mammary tumor cell lines; however, the percent of mitotic cells with centrosome clustering was significantly higher in cells with mutp53 as compared to mitotic +/+;ErbB2, −/+;ErbB2 and −/−;ErbB2 cells (Fig. 3d). Furthermore, p53LOH (H/−;ErbB2 cells) significantly increased mitotic centrosome clustering compared to H/+;ErbB2 cells (Fig. 3d). Notably, the loss of protective wtp53 allele (−/−;ErbB2 and H/−;ErbB2) significantly elevated multipolar mitosis (Fig. 3e), but only H/−;ErbB2 cells adapt centrosome clustering as a pro-survival mechanism to avoid cell death due to mitotic catastrophe (Fig. 3d). In support of GOF mechanism of centrosome clustering, deletion of mutp53 by CRISPR/Cas9 significantly reduced centrosome clustering but does not affect centrosome amplification or multipolar spindle formation Fig. 3f–h.

Together, our data identify centrosome clustering a novel pro-survival GOF mechanism that underlies an increased fitness of mutp53 cancer cells with p53LOH at the expense of chromosomal instability.

Mutant p53 allele is associated with the elevated Nek2 function

Understanding of how p53LOH enables the proliferation of mutp53 cells (Fig. 1b) and disrupts the mitotic checkpoint (Fig. 2a) in the presence of centrosomal and chromosomal aberrations (Fig. 3) would provide an essential insight into how to prevent the outgrowth of mutp53 cells with p53LOH.

To identify the putative mechanism, we performed RNAseq of mouse mammary tumor cell lines with various p53 genotypes, irradiated, or not (Fig. 4a). The expression analysis of genes involved in the regulation of mitosis identified Nek2 among the top 10 differentially up-regulated genes in the presence of mutp53. Neks (Never in Mitosis (NIMA) Kinases) are a family of serine/threonine kinases involved in the regulation of centrosome function and bipolar division during mitosis. Nek2 is overexpressed in various cancers, including Her2 positive breast cancer, where it predicts poor overall survival [32, 33]. RNAseq analysis showed upregulation of Nek2 at basal level in H/+;ErbB2 as compared to +/+;ErbB2 cells (Fig. 4b).

We focused on studying of Nek2 for the following reasons: (*i*) Nek2 plays an indispensable role for the entry into mitosis and G2/M progression, as it is required for centrosome assembly/maintenance, spindle formation, and chromosome segregation [34–37]. (*ii*) Nek2 overexpression promotes centrosome amplification and aneuploidy by disrupting the mitotic checkpoint, leading to malignant transformation [38, 39]. (*iii*) Silencing Nek2 with siRNA inhibited proliferation, induced cell death (due to mitotic errors), and dramatically increased the

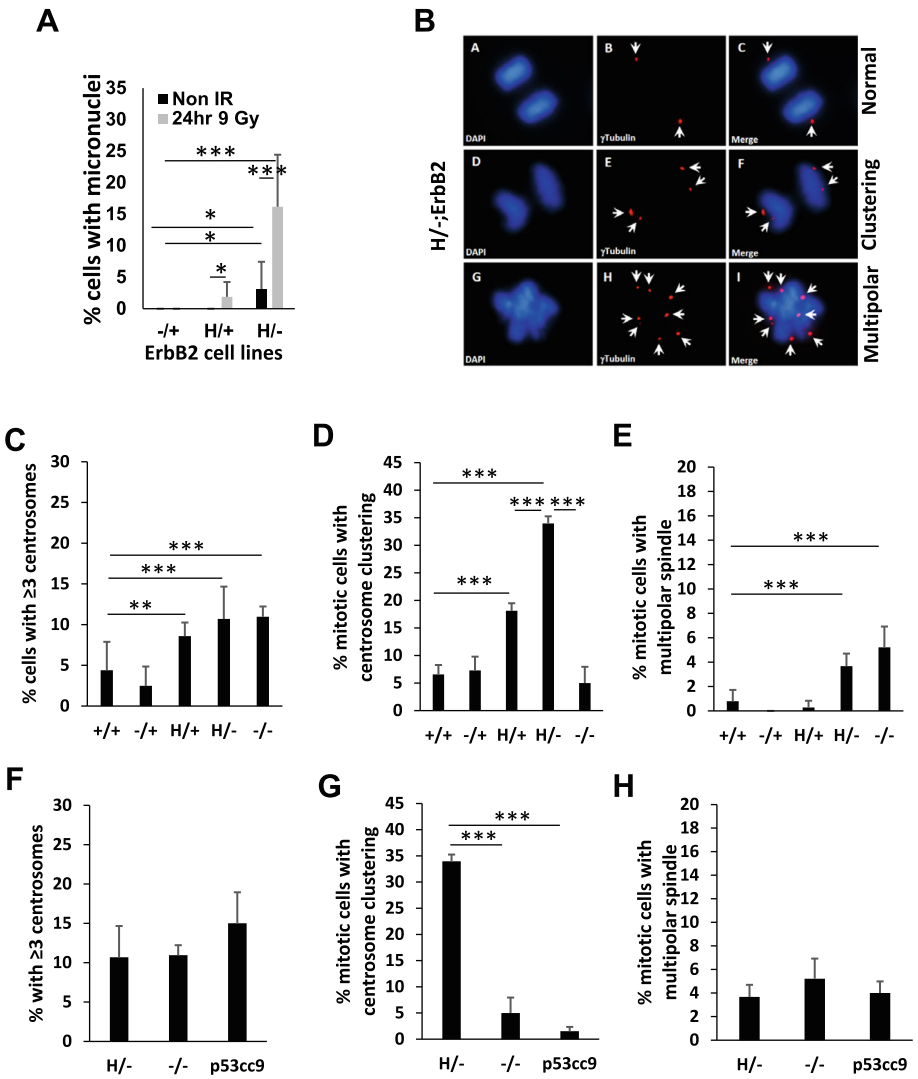

Fig. 3 Mutp53 increases centrosomal aberrations and clustering. **a** Bar graph showing percent of cells with micronuclei before and 24 h after γ-irradiation in ErbB2 mammary epithelial tumor cell lines with different p53 status. $n = 3$ independent experiments per cell line per genotype (one cell line per genotype except for p53+/+ and p53 H/− where 2 different cell lines derived from different tumors and p53CC9 3 different cell lines, and result per genotype was averaged). **b** Immunofluorescence staining showing centrosome clustering in mitotic p53H/−;ErbB2-mouse mammary epithelium tumor cell line. Centrosomes identified by γ-tubulin staining (red) and DNA by DAPI (blue). **b** (A–C) Normal bipolar mitosis with one centrosome at each side. **b** (D–F) Bipolar mitosis showing supernumerary centrosome (≥ 3) clustering, 2 centrosomes on each side. **b** (G–I) Multipolar mitosis showing failure of supernumerary centrosomes to cluster. **c**–**e** Bar graphs showing percent of cells with ≥ 3 centrosomes, with centrosome clustering and with multipolar spindle, respectively, in ErbB2 mammary epithelial tumor cell lines with different p53 status. $n = 3$ independent experiments per genotype. **f**–**h** Bar graphs showing percent of cells with ≥ 3 centrosomes, with centrosome clustering and with multipolar spindle, respectively, in p53H/−;ErbB2 cell line before and after CRISPR/Cas9 p53 deletion (p53CC9) and in p53−/−;ErbB2 cell line. $n = 3$ independent experiments per genotype (for **c**–**h**, one cell line per genotype except for p53+/+ and p53 H/− where 2 different cell lines derived from different tumors and p53CC9 3 different cell lines, and result per genotype was averaged). Where applicable $^{*}p < 0.05$; $^{**}p < 0.01$; $^{***}p < 0.001$. Error bars represent ± SD

susceptibility of breast cancer cells to DNA-damaging modalities [38, 39]. (*iv*) Wtp53–Nek2 autoregulatory feedback loop has previously been described [40–42], while no mutp53-Nek2 functional interaction has been investigated. (*v*) Nek2 can be targeted by highly specific small-molecular inhibitor JH29525 that opens the opportunity for therapeutic intervention.

We validated the RNAseq data by Western (Fig. 4c). Consistent with wtp53 as a negative regulator of Nek2 expression [41], we observed the lowest level of Nek2 in +/+;ErbB2 and −/+;ErbB2 cells (Fig. 4c). Furthermore, irradiation downregulates Nek2 in cells carrying at least one p53 allele (Fig. 4c), while the loss of wtp53 allele (H/−;ErbB2) leads to Nek2 upregulation that is insensitive

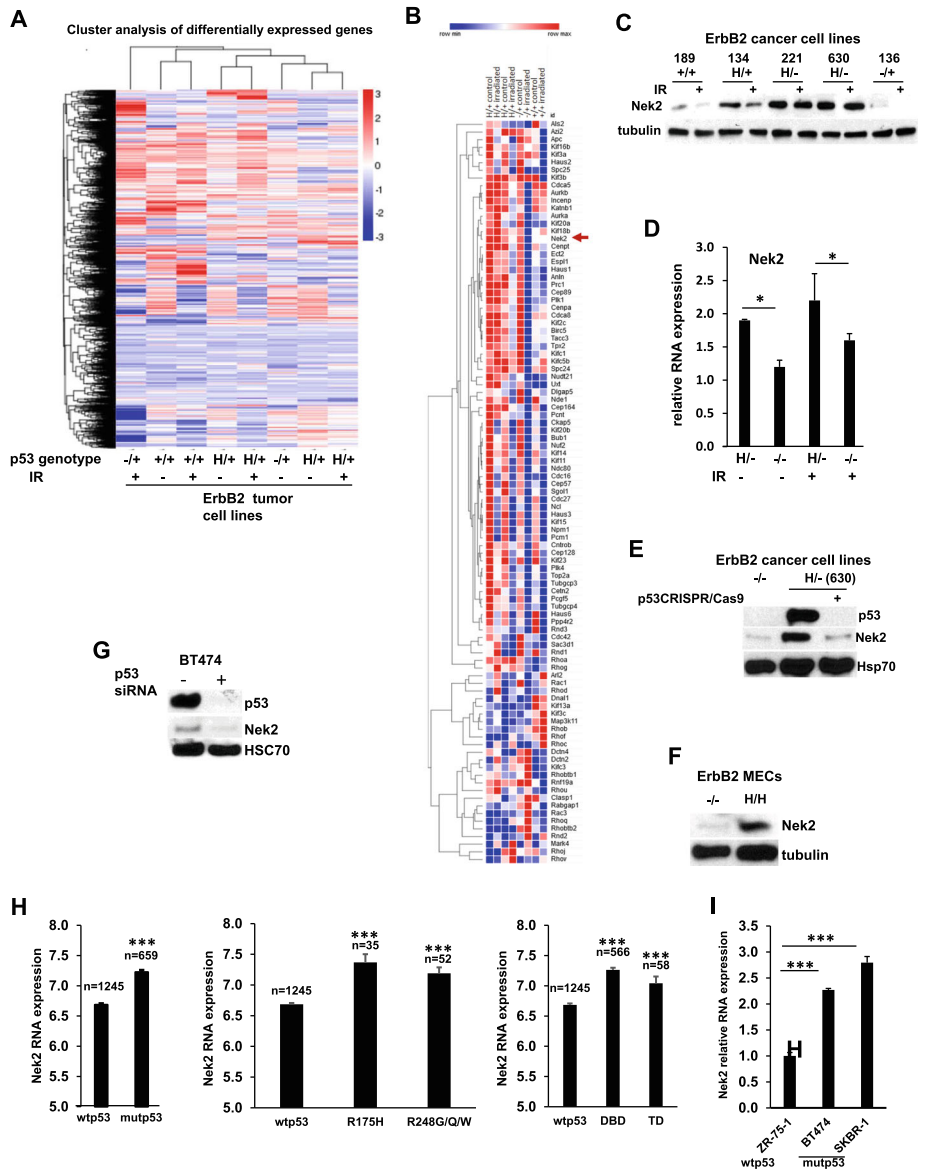

Fig. 4 Mutp53 is associated with elevated mRNA and protein levels of NEK2. **a** Heat map showing cluster analysis of differentially expressed genes in p53+/+;ErbB2, p53H/+;ErbB2 and p53−/+;ErbB2 before and after γ-irradiation (9 Gy, 24 h). **b** Heat map of RNAseq analysis showing differentially regulated centrosome proteins in p53+/+;ErbB2, p53H/+;ErbB2 and p53−/+;ErbB2 before and after γ-irradiation (9 Gy, 24 h). Arrowhead indicates Nek2. **c** Western blot analysis of Nek2 level before and 24 h after γ-irradiation in mouse ErbB2 mammary epithelial tumor cell lines with different p53 status. α-tubulin is loading control. **d** Bar graph showing relative mRNA expression level of Nek2 in p53H/−;ErbB2 and p53 −/−;ErbB2 cell lines before and after irradiation. $n = 3$ independent experiments per genotype (one cell line per genotype except for p53 H/− where 2 different cell lines derived from different tumors and result was averaged). **e** Western blot analysis of p53 and Nek2 levels in p53 −/−;ErbB2 cells and in p53H/−;ErbB2 cells before and after CRISPR/Cas9 p53 deletion. Hsp70 is loading control. **f** Western blot analysis of Nek2 level in p53−/− MECs and p53H/H MECs. α-Tubulin is loading control. **g** Western blot analysis of p53 and Nek2 levels in BT474 cells before and after p53 suppression with siRNA. HSC70 is loading control. **h** Bar graphs showing NEK2 relative mRNA expression in patients with wtp53 ($n = 1245$) compared to with mutp53 ($n = 659$) (all mutations combined vs different types of mutations) (DBD = DNA binding domain; TD = tetramerization domain). **i** Bar graph showing Nek2 relative mRNA expression in human breast cancer cell lines with different p53 status. $n = 3$ independent experiments per genotype. Where applicable $*p < 0.05$; $**p < 0.01$; $***p < 0.001$. Error bars represent ± SD

to irradiation on both protein (Fig. 4c) and RNA levels (Fig. 4d). In addition to the loss of wtp53 function, mutp53 in H/−;ErbB2 cells upregulates Nek2 expression in apparent GOF manner as stabilized mutp53 protein in H/−;ErbB2 cancer cells was associated with a higher level of Nek2 mRNA and protein levels compared to −/−;ErbB2 cancer cells (Fig. 4d) or following mutp53 ablation by CRISPR/Cas9 (Fig. 4e). Similarly, mammary

epithelial cells (MECs) established from mammary of −/−;ErbB2 mice [17] express significantly lower levels of Nek2 protein compared to H/H;ErbB2 MECs (Fig 4f). Importantly, mutp53 promotes Nek2 expression independently of host and the type of p53 mutation. Mutp53 depletion by siRNA decreases the Nek2 level in human cancer cell line BT474 (E285K) (Fig. 4g).

In further support of the mutp53-Nek2 association in human cancer, a retrospective analysis of the Metabric cohort of breast cancer patients (www.cbioportal.org) demonstrated a significantly higher median of Nek2 mRNA expression in mutp53 patients, regardless of the mutation type, as compared to patients with wtp53 (Fig. 4h). Furthermore, human mutp53 HER2-positive human breast cancer lines (BT474 (E285K), SKBR3 (R175H)) showed significantly higher expression of NEK2 mRNA as compared to ZR-75-1(wtp53) (Fig. 4i).

Together, these experiments indicate that mutp53 can affect Nek2 expression by two complementary mechanisms: the loss of wtp53 inhibitory function and mutp53 GOF upregulation of Nek2. Hence, mutp53-mediated Nek2 expression may reinforce G2/M transition, override G2/M checkpoints, and protect cancer cells from multipolar mitosis at the expense of chromosomal instability.

Nek2 inhibition prevents p53LOH in mutant p53 heterozygous cells

We hypothesized that deficient checkpoints and the increased proliferation of H/−;ErbB2 cells confer a positive selection for p53LOH during tumor progression. Therefore, the identification of specific vulnerabilities of mutp53 cancer cells with p53LOH would provide the therapeutic opportunity to prevent p53LOH and, thus, the expansion of genetically unstable, more aggressive cancer cells population. As a mutp53-mediated upregulation of Nek2 (Fig. 4) may facilitate G2/M transition by reinforcing centrosome clustering, mutp53 cells with p53LOH may specifically be dependent on Nek2 expression for their survival to avoid multipolar mitosis and mitotic catastrophe.

To test this hypothesis, we investigated the effect of Nek2 inhibitors on mitotic spindle formation and centrosome clustering with respect to p53 genotypes. Several Nek2-specific inhibitors were described in the literature (JH 295, TOCRIS, or TAI-95, Probechem) [43]. In our study, we utilized JH295 (oxindole propynamide, IC50 = 770 nM), which is a highly specific and irreversible Nek2 inhibitor that blocks Nek2 activity via alkylation of residue Cys22, and does not affect the activities of other mitotic kinases (CDK1, PLK1, Aurora B, or Mps1) [43]. Moreover, JH295 does not perturb bipolar spindle assembly or the spindle assembly checkpoint [43]. Given this selective profile, we thought that JH295 is as useful for identifying the biological roles of Nek2 as RNAi interference approach.

Strikingly, we observed a genotype-specific inhibitory effect of JH295 in mutp53 cells with p53LOH (H/−;ErbB2) as compared to cells with wtp53 allele (+/+;ErbB2, −/+;ErbB2, H/+ErbB2) as indicated by the colony formation assay (Fig. 5a, b). JH295 had an intermediate inhibitory effect on H/+ErbB2 cells (Fig. 5b). The specificity of JH295 was validated on cells where Nek2 was deleted using CRISPR/Cas9. Consistent with the requirement of Nek2 for the survival of mutp53 cancer cells, we were able to generate H/+;ErbB2/Nek2−/−, but not H/−;ErbB2/Nek2−/− cell lines by CRISPR/Cas9 technology. However, the genetic depletion of Nek2 significantly reduced the proliferation rate of H/+;ErbB2 cells in short-term assay (Fig. 5c). The analysis of mitotic H/+;ErbB2/Nek2−/− cells revealed that the genetic ablation of Nek2 did not increase the proportion of cells with centrosome amplification (Fig. 5d), but dramatically reduced centrosome clustering (Fig. 5e) with a concomitant increase in cells carrying multipolar mitotic spindle (Fig. 5f). Consistent with the genetic depletion of Nek2, the sensitivity to JH295 correlates with the complete abrogation of centrosome clustering in H/+;ErbB2 and H/−;ErbB2 cells (Fig. 5h), while the proportion of mitotic cells carrying supernumerary centrosomes did not change (Fig. 5g). Importantly, JH295 most robustly affected H/−;ErbB2 cells, but not +/+;ErbB2 cells in any tested assays (Fig. 5a, g, h), suggesting an alternative Nek2-independent mechanism of centrosome regulation in wtp53 cells. In sum, our data identified the requisite function of Nek2 for centrosome clustering and, thus, survival of H/−;ErbB2 cells.

The increased sensitivity of H/−;ErbB2 cells to Nek2 inhibition set us to test whether JH295 prevents outgrowth mutp53 cells with p53LOH, thus preventing loss of wtp53 allele after irradiation. Hence, H/+;ErbB2 cells were irradiated (9 Gy), or not, and then treated them with JH295, or not, for 10 days. DNA from surviving cells was analyzed for p53LOH by PCR. As shown in Fig. 5i, j, we observed p53LOH only in irradiated cells (lanes 7–9), but not in non-irradiated (lanes 1–3) or JH295-treated cells (lanes 4–6). Remarkably, Nek2 inhibition protects cells from irradiation-induced p53LOH (lanes 10–12).

In sum, our results suggest that Nek2 inhibition may alter the selective pressure for p53LOH in heterogeneous tumor population by contraction of specifically mutp53 population with p53LOH, thus, preventing the outgrowth of genetically unstable and metastatic cells.

Discussion

Monoallelic mutations in the TP53 gene are widespread at the early stages of Her2-positive breast cancer (DCIS

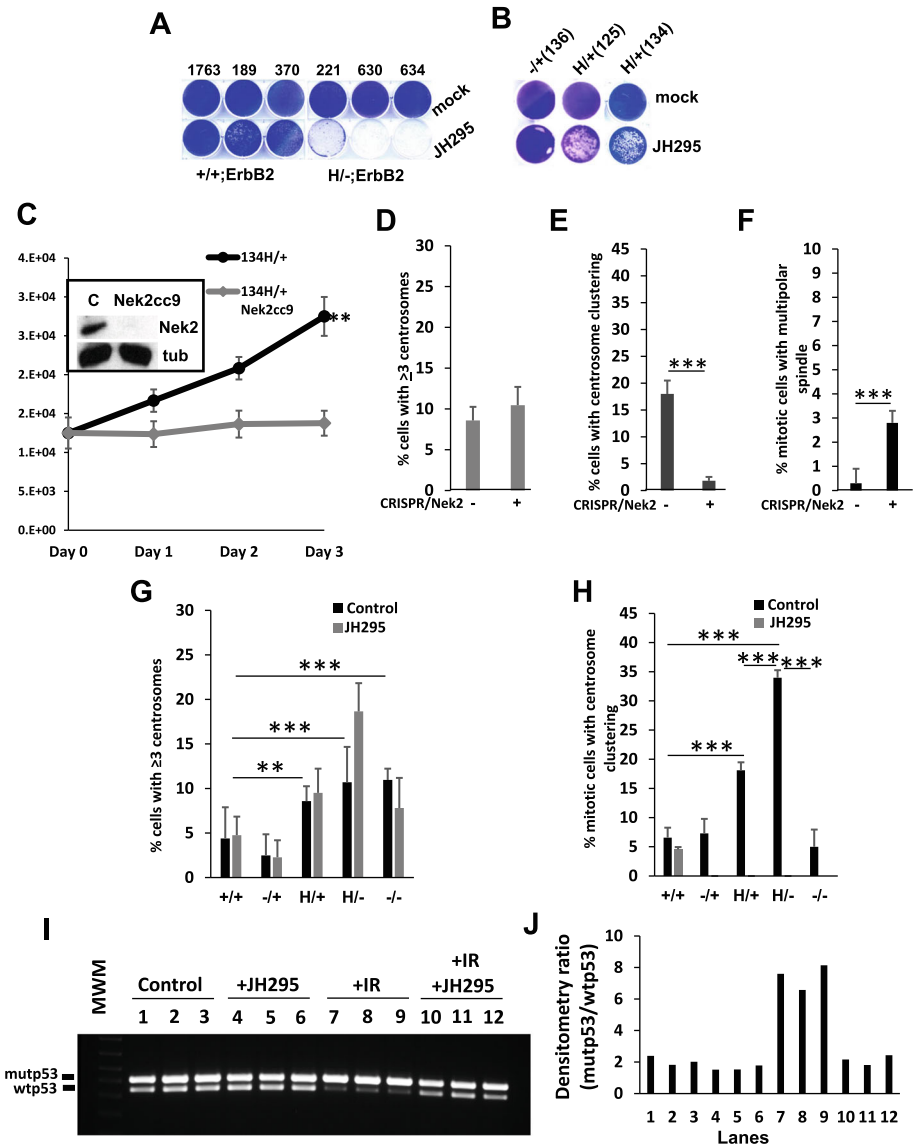

Fig. 5 Nek2 ablation suppresses centrosome clustering and p53LOH. **a** Colony formation assay showing suppressed proliferation of H/−;ErbB2 cells, as compared to +/+;ErbB2 cells, following treatment with Nek2 inhibitor JH295. **b** Colony formation assay showing partial suppression of proliferation of H/+;ErbB2 cells, as compared to −/+;ErbB2 cells, following treatment with Nek2 inhibitor JH295. **c** Growth curve showing suppressed proliferation in H/+;ErbB2 cells following CRISPR/Cas9 Nek2 deletion (Nek2cc9). Inset shows western blot for Nek2 before and after CRISPR/Cas9 Nek2 deletion. α-Tubulin is loading control. **d**–**f** Bar graphs showing percent of cells with ≥ 3 centrosomes, with centrosome clustering and with multipolar spindle, respectively, in H/+;ErbB2 cells before and following CRISPR/Cas9 Nek2 deletion. $n = 3$ independent experiments per genotype. **g**, **h** Bar graphs showing percent of cells with ≥ 3 centrosomes and with centrosome clustering, respectively, in ErbB2 mammary epithelial tumor cell lines with different p53 status with and without treatment with Nek2 inhibitor JH295. $n = 3$ independent experiments per genotype (one cell line per genotype except for p53+/+ and p53 H/− where 2 different cell lines derived from different tumors and result per genotype was averaged). **i** Analysis of LOH in H/+;ErbB2 cell line. $n = 3$ independent experiments per treatment. Non-irradiated cells (lanes 1–3) and cells treated with JH295 (lanes 4–6) are showing no LOH. Irradiated cells showing LOH (lanes 7–9). Cells irradiated and treated with JH295 are showing no LOH (lanes 10–12). **j** Densitometric analysis of band intensity ratio of PCR amplification product shown in **i**

and stage 1) and usually followed by loss of the remaining wtp53 allele during tumor progression. Although previous studies suggested that mutp53 inactivates wtp53 protein in heterozygous tumors in the dominant-negative fashion [44], integrated large scale human data analysis (TCGA) argues for the strong selection for the loss wtp53 allele in tumors with monoallelic p53 mutations [45]. However, the underlying selective force for p53LOH, its mechanism, and oncogenic outcomes remain elusive.

Using MMTV;ErbB2 model carrying a heterozygous R172H p53 mutation previously, we demonstrated a novel oncogenic activity of mutp53: the exacerbation of

p53LOH after γ-irradiation. We found that wtp53 partially retains the transcriptional activity allele and enables the maintenance of the genomic integrity under normal conditions in mutp53 heterozygous cells. Consistent with our mouse data, human cancer TCGA database analysis revealed that mutp53 tumors displayed a 2.5-fold higher rate of deletions at the frequent deletion sites of their wtp53 tumors counterparts [46]. Although in our previous study, we demonstrated that irradiation in the early stages of breast cancer facilitates the selective pressure for p53LOH, the underpinning mechanism remained unclear. These findings may have a significant clinical impact, as in the early stages of breast cancer patients with mutp53 heterozygous tumors [2], radiotherapy may potentially have adverse effects.

By using the unique panel of isogenic and non-isogenic breast cancer cell lines with the distinct p53 deficiencies, we identified functional outcomes of p53LOH in mutp53 heterozygous cells that may underlie the selective pressure for p53LOH. First, we found that p53LOH in mutp53 heterozygous cells is the crucial event in promoting mutp53 protein stabilization (Fig. 1a), which was shown to be critical for oncogenic GOF activities of mutp53 [45]. Second, p53LOH increases cell proliferation in both loss-of-function (Fig. 1d, e) and mutp53 gain-of-function (Fig. 1c, f) manner that may cause the clonal expansion cells with p53LOH. The p53LOH-enhanced proliferation can be a consequence of the loss of wtp53-induced p21 expression (Fig. 1d, e), and mutp53-mediated upregulation of mTOR pathway [3], that together increase cancer cell fitness and provide the growth advantage over heterozygous cells retaining wtp53 allele (Fig. 5l). Third, we observed a robust increase in genomic and chromosomal instability in mutp53 cells after p53LOH that may provide the genomic plasticity to acquire secondary mutations, thus, contributing to clonal expansion of cells with p53LOH. Consistent with our results, the examination of human cancer TCGA data revealed significantly enhanced chromosomal instability in mutp53 tumors that mainly lost wtp53 allele relative to their wtp53 counterparts [46]. The enhanced chromosomal instability after p53LOH can arise from increased centrosome amplification (Fig. 3b, c) and multipolar mitotic spindle formation (Fig. 3e, h) that we observed in H/−;ErbB2 cells. However, excessive centrosome amplification can be detrimental to cell viability. As a novel mutp53 GOF pro-survival mechanism, we demonstrate that H/−;ErbB2 cells adapt to avoid mitotic catastrophe or replicative senescence by bipolar clustering centrosome, allowing pseudo-bipolar division (Fig. 3b, d) at the expense of genomic instability. Fourth, p53LOH completely abrogates G2/M checkpoint in response to irradiation in the mutp53 GOF manner (Fig. 2a, e) suggesting that γ-irradiation may further facilitate the clonal expansion of mutp53 cells with p53LOH (Fig. 2a). Together, our study provides mechanistic insights into how p53LOH provides the growth advantage to mutp53 cancer cells and outcompete heterozygous cells retaining wtp53 allele and how γ-irradiation may exacerbate the clonal expansion of genomically unstable mutp53 cells with p53LOH leading to tumor progression (Fig. 6). Therefore, the targeting of pro-survival pathways activated in cancer cells after p53LOH may impede their clonal dominance and prevent tumor progression.

In an attempt to delineate the pro-survival pathways upregulated in H/−;ErbB2 cells, we identified Nek2 as a potential GOF target of mutp53. Nek2 kinase is a crucial regulator of mitotic processes such as centrosome duplication and spindle assembly. The aberrant activity of Nek2 compromises mitotic checkpoint and centrosome duplication (reviewed in [32]). Nek2 overexpression induced centrosome amplification, while Nek2 silencing decreased cell proliferation in vitro and in vivo (reviewed in [32]). Nek2 is overexpressed in various human cancers, including Her2-positive breast cancer [47], and several mutations in breast and stomach cancers have been identified (https://cancer.sanger.ac.uk) [48]. The relapse-free survival of patients with Nek2-overexpressing tumors was significantly worse than that of patients exhibiting low expression, regardless of breast cancer subtype. In support of mutp53-Nek2 link in human breast cancer, we found a strong correlation between mutp53 (all mutations, Metabric) and Nek2 mRNA expression compared to patients with wtp53 (Fig. 4f). Together, these data support Nek2 as an attractive therapeutic target in mutp53 breast cancer.

As previous studies demonstrated the inhibitory effect of wtp53 on Nek2 RNA expression [41], the loss of the wtp53 allele in heterozygous cells may induce Nek2 in a loss-of-function manner. Here, we demonstrated that in addition to loss-of-function, p53LOH in mutp53 heterozygous cells might upregulate Nek2 expression in mutp53 GOF fashion (Fig. 4e–g). Of note, median expression of NEK2 was significantly upregulated in patients with mutp53, regardless of the mutation type (Fig. 4h), not just in missense mutations. This may suggest that GOF might not be limited to a particular type of TP53 mutation, e.g., missense [49], and that all TP53 mutations might be equal at a certain level. This notion of equal TP53 mutations has been previously shown in the context of different p53 mutations exerting a dominant-negative effect [50].

While we utilized MMTV/ErbB2 mice as a model for breast cancer, a similar mechanism may take place in other subtypes of breast cancer. In support, clinical data demonstrated significant overexpression Nek2 in human triple-negative breast cancer (> 80% harbor p53 mutations) [51]. Furthermore, our retrospective analysis of Metabric data shows that Nek2 is significantly overexpressed in patients with mutp53, regardless of BC type

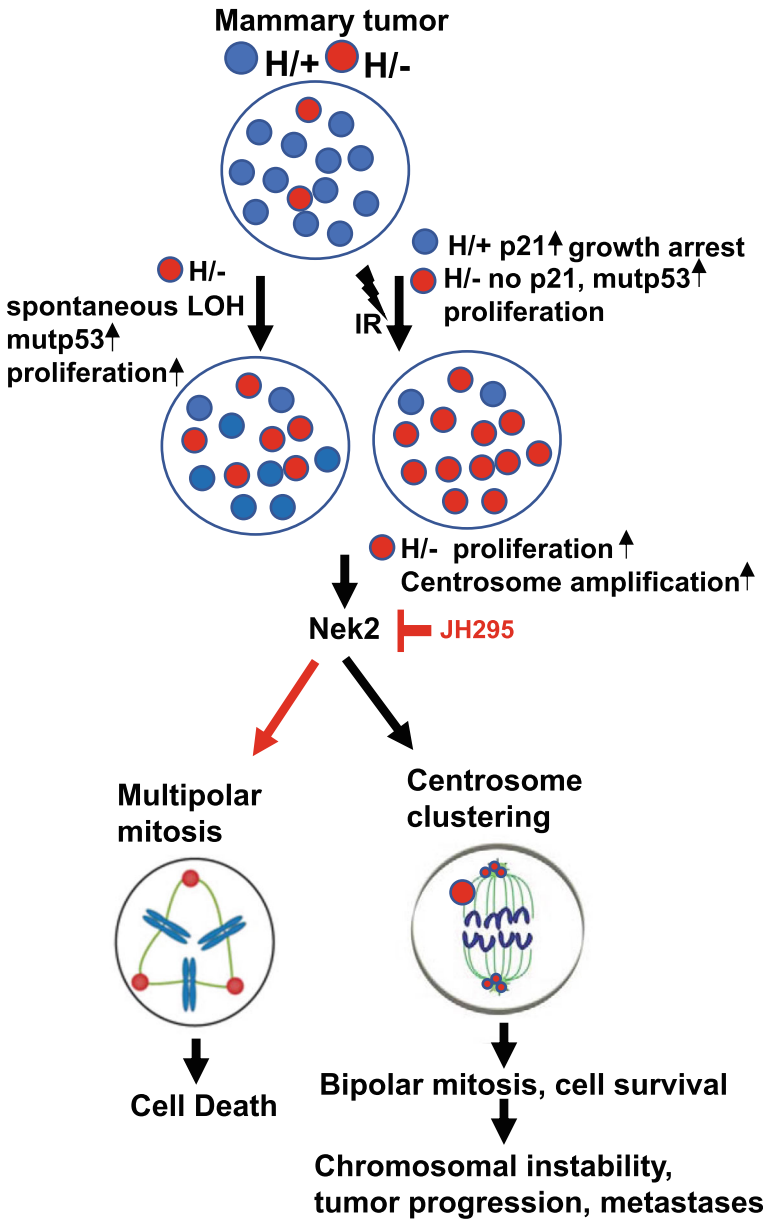

Fig. 6 Proposed model for the role of mutp53 and Nek2 in promoting tumorigenesis. In tumors heterozygous for mutp53 there is a mixed population of heterozygous cells (H/+) and cells that underwent spontaneous LOH (H/−). Genotoxic stress, such as γ-irradiation, leads to slow proliferation and expansion of H/+ population due to the presence of wtp53 that can induce cell cycle checkpoint and arrest. On the other hand, H/− cells continue unrestricted proliferation, taking over the H/+ population. In both cases, absence of wtp53 in H/− leads to increased cell proliferation and to centrosome amplification. To avoid multipolar mitosis and cell death of H/− cells with centrosome amplification, mutp53 utilizes Nek2 to induce centrosome clustering to promote bipolar mitosis and cell survival. Centrosome clustering process lengthens mitosis which then leads to increased chromosomal instability and thus enhancing tumor progression and metastasis. Our model proposes Nek2 as an Achilles heel, for tumor cells with mutp53, that can be used as a therapeutic target to prevent p53 LOH and cells that have lost the wtp53 alleles

and HER2 status (Fig. 4h). These results strengthen our notion that Nek2 overexpression is linked primarily to mutp53 presence. The mechanism by which mutp53 upregulates Nek2 is still unclear. Emerging evidence implies that mutp53 promotes malignant transformation by the physical recruitment of other transcription factors (TF) to the chromatin, thus rewiring the transcriptome towards oncogenic pathways [52]. As previously shown, Nek2 expression is downregulated by E2F4 transcription factor [53]. On the other hand, mutp53 and E2F4 proteins were shown to form a protein complex in tumor cells [54]. Thus, it is feasible that mutp53 can promote Nek2 expression by suppressing E2F4 transcriptional function. Alternatively, the overexpression of Nek2 in

human breast cancer is commonly attributed to the amplification of region 1q32, the locus of the human Nek2 gene. Here, we demonstrated that p53LOH results in the significant increase of chromosomal aberrations (Fig. 3) that can lead to amplification of 1q32 locus. Alternatively, mutp53 may upregulate Nek2 expression through the forkhead transcription factor FoxM1, which was shown to positively regulate Nek2 [55, 56]. Mutp53 GOF was shown to occur in p53-AMPK-FOXO3a-FOXM1 signaling cascade to promote tumor survival and progression in head and neck squamous cell carcinoma [57]. On the other hand, while we believe that mutp53 upregulates the transcription of Nek2, there may be other direct effects of mutp53-Nek2 axis (e.g., protein-protein interactions) as well as indirect effects (e.g., phosphorylation of mutp53 by Nek2) that may contribute to aberrant mitosis. Whether mutp53 regulates Nek2 expression directly by regulating its transcription or indirectly is under current investigation in the lab.

Furthermore, the present study identified the novel requisite function of Nek2 in centrosome clustering. We demonstrated that the genetic depletion (Fig. 5e) and the specific pharmacological inhibition of Nek2 (Fig. 5h) alleviate centrosome clustering and increase the formation of multipolar spindles in mitotic cells (Fig. 5f). Therefore, mutp53-mediated upregulation of Nek2 can cause mitotic progression, thus offering the selective survival advantage to genomically unstable H/−;ErbB2 cells (Fig. 6). Not surprising that elevated centrosome clustering was associated with the increased sensitivity to pharmacological and genetic inactivation of Nek2 in H/−;ErbB2 cells. In stark contrast, Nek2 inhibitor does not affect the viability of p53+/+;ErbB2 cells (Fig. 5a). Most importantly, the selective sensitivity of H/−;ErbB2 cells to Nek2 inhibition opens the therapeutic opportunity to alter the clonal competition and prevent the outgrowth of mutp53 cells with p53LOH. In support of our hypothesis, we found that Nek2 inhibitor prevents p53LOH induced by irradiation (Fig. 5i, j).

It is worth mentioning that the clinical studies on the prognostic and predictive significance of TP53 mutations in breast cancers have been controversial [58–61]. For example, it was shown that chemo/radiotherapy-treated breast cancer patients (all stages combined, no hormone therapy), with mutp53 tumors have a greater probability of complete pathological response than wtp53 patients, whereas addition of hormone therapy improved the survival of wtp53 patients but not mutp53 patients [62]. However, the stratification by stage within the large dataset revealed that, in contrast to wtp53 patients, the survival benefits from radiotherapy for patients with mutp53 breast cancer is stage-dependent, where radiotherapy improved the survival of stage 2 patients but was detrimental to stage 1 patients [3]. Therefore, the response of mutp53 cancers can be extremely variable according to tumor type, stage, type of treatment, tumor environment and heterogeneity, and the presence or absence of other mutations [58, 59]. This indicates that for patients with mutp53 cancers, certain factors have to be considered for optimal therapeutic outcomes. Our data imply that some non-genotoxic therapies, e.g., drugs targeting cell cycle regulatory proteins in combination with radiotherapy can be used for the tumors with mutp53 depending on the stage and p53 heterozygosity.

In sum, our data suggest that Nek2 inhibition via selective toxicity prevents outgrowth of H/−;ErbB2 cells, hindering the expansion of cells with p53LOH (Fig. 6). We speculate that in heterogeneous tumor populations, p53LOH generates the clonal pool of genetically unstable cells prone to expand after γ-irradiation due to the loss of G2/M checkpoint and p21 expression leading to the selection mutp53/LOH cells. Following p53LOH, mutp53-mediated upregulation of Nek2 provides the competitive survival advantage to mutp53/LOH (H/−;ErbB2) over mutp53 heterozygous cells (H/+;ErbB2). As a pro-survival mechanism of escape from mitotic catastrophe after irradiation in the presence of centrosome amplification, mutp53/LOH cells adapt Nek2-mediated pseudo-bipolar mitosis and evasion of G2/M checkpoint by centrosome clustering.

Conclusions

To our knowledge, this is the first evidence that p53LOH can be prevented pharmacologically, which can have a significant clinical impact. As several Nek2 inhibiting compounds were described in the literature (reviewed in [32]), their clinical development is in an early stage, and no clinical trials have been reported. Some Nek2 inhibitors have shown low nanomolar activity in vitro and significant antitumor activity in xenografts (reviewed in [32]). Finally, our data suggest that wtp53 cancers and normal tissues retaining wtp53 may be unresponsive to Nek2 inhibition. In support of this conclusion, the initial characterization of Nek2 knockout mice demonstrated no significant defects under normal conditions (International Mouse Phenotyping Consortium), suggesting potentially low toxicity of Nek2 inhibitors in normal tissues. Prospective studies in vivo will determine whether genetic and pharmacological inhibition of Nek2 prevents p53LOH and alleviates tumor progression.

Acknowledgements

Not applicable.

Authors' contributions

MP—performing experiments, data collection and analysis, and reviewing manuscript; NM—concept development, performing experiments, data collection and analysis, and writing and reviewing manuscript; AG—concept development, performing experiments, data collection and analysis, and

writing and reviewing manuscript. The authors read and approved the final manuscript.

Funding
This work was supported by the Department of Defense grant W81XWH-16-1-0448 (BC151569) and the Carol Baldwin Breast Cancer Research Fund to N.Marchenko.

Availability of data and materials
Human Metabric data analysis, of the somatic mutation profiles of 2,433 breast cancers, was done using data from a retrospective study [8]. The data is deposited and is publicly available at http://www.cbioportal.org. The analysis was done using the program and tools made available online at http://www.cbioportal.org. Other datasets used and/or analyzed during the current study are available from the corresponding author on reasonable request.

Ethics approval and consent to participate
Not applicable.

Consent for publication
Not applicable.

Competing interests
The authors declare no competing interests.

Author details
[1]Department of Pathology, Stony Brook University, Stony Brook, NY 11794-8691, USA. [2]Biologics Process Research & Development, Merck & Co., Inc., Kenilworth, NJ 07033, USA.

Received: 6 July 2020 Accepted: 12 November 2020
Published online: 02 December 2020

References

1. Clarke M, Collins R, Darby S, Davies C, Elphinstone P, Evans V, et al. Effects of radiotherapy and of differences in the extent of surgery for early breast cancer on local recurrence and 15-year survival: an overview of the randomised trials. Lancet. 2005;366(9503):2087–106.
2. Cancer Genome Atlas N. Comprehensive molecular portraits of human breast tumours. Nature. 2012;490(7418):61–70.
3. Ghaleb A, Yallowitz A, Marchenko N. Irradiation induces p53 loss of heterozygosity in breast cancer expressing mutant p53. Commun Biol. 2019; 2:436.
4. Li D, Marchenko ND, Schulz R, Fischer V, Velasco-Hernandez T, Talos F, et al. Functional inactivation of endogenous MDM2 and CHIP by HSP90 causes aberrant stabilization of mutant p53 in human cancer cells. Mol Cancer Res. 2011;9(5):577–88.
5. Terzian T, Suh YA, Iwakuma T, Post SM, Neumann M, Lang GA, et al. The inherent instability of mutant p53 is alleviated by Mdm2 or p16INK4a loss. Genes Dev. 2008;22(10):1337–44.
6. Hitomi M, Stacey DW. Cyclin D1 production in cycling cells depends on ras in a cell-cycle-specific manner. Curr Biol. 1999;9(19):1075–84.
7. Silwal-Pandit L, Vollan HK, Chin SF, Rueda OM, McKinney S, Osako T, et al. TP53 mutation spectrum in breast cancer is subtype specific and has distinct prognostic relevance. Clin Cancer Res. 2014;20(13):3569–80.
8. Pereira B, Chin SF, Rueda OM, Vollan HK, Provenzano E, Bardwell HA, et al. The somatic mutation profiles of 2,433 breast cancers refines their genomic and transcriptomic landscapes. Nat Commun. 2016;7:11479.
9. Lang GA, Iwakuma T, Suh YA, Liu G, Rao VA, Parant JM, et al. Gain of function of a p53 hot spot mutation in a mouse model of Li-Fraumeni syndrome. Cell. 2004;119(6):861–72.
10. Alexandrova EM, Yallowitz AR, Li D, Xu S, Schulz R, Proia DA, et al. Improving survival by exploiting tumour dependence on stabilized mutant p53 for treatment. Nature. 2015;523(7560):352–6.
11. Yallowitz A, Ghaleb A, Garcia L, Alexandrova EM, Marchenko N. Heat shock factor 1 confers resistance to lapatinib in ERBB2-positive breast cancer cells. Cell Death Dis. 2018;9(6):621.
12. Schneider CA, Rasband WS, Eliceiri KW. NIH Image to ImageJ: 25 years of image analysis. Nat Methods. 2012;9(7):671–5.
13. Larson Gedman A, Chen Q, Kugel Desmoulin S, Ge Y, LaFiura K, Haska CL, et al. The impact of NOTCH1, FBW7 and PTEN mutations on prognosis and downstream signaling in pediatric T-cell acute lymphoblastic leukemia: a report from the Children's Oncology Group. Leukemia. 2009;23(8):1417-25.
14. Nemajerova A, Petrenko O, Trumper L, Palacios G, Moll UM. Loss of p73 promotes dissemination of Myc-induced B cell lymphomas in mice. J Clin Invest. 2010;120(6):2070–80.
15. Ren J, Liu Z, Gao X, Jin C, Ye M, Zou H, et al. MiCroKit 3.0: an integrated database of midbody, centrosome and kinetochore. Nucleic Acids Res. 2010; 38(Database issue):D155–60.
16. Olive KP, Tuveson DA, Ruhe ZC, Yin B, Willis NA, Bronson RT, et al. Mutant p53 gain of function in two mouse models of Li-Fraumeni syndrome. Cell. 2004;119(6):847–60.
17. Yallowitz AR, Li D, Lobko A, Mott D, Nemajerova A, Marchenko N. Mutant p53 amplifies epidermal growth factor receptor family signaling to promote mammary tumorigenesis. Mol Cancer Res. 2015;13(4):743–54.
18. Maeda T, Chong MT, Espino RA, Chua PP, Cao JQ, Chomey EG, et al. Role of p21(Waf-1) in regulating the G1 and G2/M checkpoints in ultraviolet-irradiated keratinocytes. J Invest Dermatol. 2002;119(2):513–21.
19. Koyano T, Namba M, Kobayashi T, Nakakuni K, Nakano D, Fukushima M, et al. The p21 dependent G2 arrest of the cell cycle in epithelial tubular cells links to the early stage of renal fibrosis. Sci Rep. 2019;9(1):12059.
20. Jackson JG, Pant V, Li Q, Chang LL, Quintas-Cardama A, Garza D, et al. p53-mediated senescence impairs the apoptotic response to chemotherapy and clinical outcome in breast cancer. Cancer Cell. 2012;21(6):793–806.
21. Aleem E, Kiyokawa H, Kaldis P. Cdc2-cyclin E complexes regulate the G1/S phase transition. Nat Cell Biol. 2005;7(8):831–6.
22. Budanov AV, Karin M. p53 target genes sestrin1 and sestrin2 connect genotoxic stress and mTOR signaling. Cell. 2008;134(3):451–60.
23. Porta C, Paglino C, Mosca A. Targeting PI3K/Akt/mTOR signaling in cancer. Front Oncol. 2014;4:64.
24. Fenech M. Chromosomal biomarkers of genomic instability relevant to cancer. Drug Discov Today. 2002;7(22):1128–37.
25. Iarmarcovai G, Bonassi S, Botta A, Baan RA, Orsiere T. Genetic polymorphisms and micronucleus formation: a review of the literature. Mutat Res. 2008;658(3):215–33.
26. Kramer A, Maier B, Bartek J. Centrosome clustering and chromosomal (in)stability: a matter of life and death. Mol Oncol. 2011;5(4):324–35.
27. Saunders W. Centrosomal amplification and spindle multipolarity in cancer cells. Semin Cancer Biol. 2005;15(1):25–32.
28. Ganem NJ, Godinho SA, Pellman D. A mechanism linking extra centrosomes to chromosomal instability. Nature. 2009;460(7252):278–82.
29. Basto R, Brunk K, Vinadogrova T, Peel N, Franz A, Khodjakov A, et al. Centrosome amplification can initiate tumorigenesis in flies. Cell. 2008; 133(6):1032–42.
30. Murphy TD. Drosophila skpA, a component of SCF ubiquitin ligases, regulates centrosome duplication independently of cyclin E accumulation. J Cell Sci. 2003;116(Pt 11):2321–32.
31. Quintyne NJ, Reing JE, Hoffelder DR, Gollin SM, Saunders WS. Spindle multipolarity is prevented by centrosomal clustering. Science. 2005; 307(5706):127–9.
32. Fang Y, Zhang X. Targeting NEK2 as a promising therapeutic approach for cancer treatment. Cell Cycle. 2016;15(7):895–907.
33. Hayward DG, Fry AM. Nek2 kinase in chromosome instability and cancer. Cancer Lett. 2006;237(2):155–66.
34. Bahe S, Stierhof YD, Wilkinson CJ, Leiss F, Nigg EA. Rootletin forms centriole-associated filaments and functions in centrosome cohesion. J Cell Biol. 2005;171(1):27–33.
35. Fry AM, Mayor T, Meraldi P, Stierhof YD, Tanaka K, Nigg EA. C-Nap1, a novel centrosomal coiled-coil protein and candidate substrate of the cell cycle-regulated protein kinase Nek2. J Cell Biol. 1998;141(7):1563–74.
36. Man X, Megraw TL, Lim YP. Cep68 can be regulated by Nek2 and SCF complex. Eur J Cell Biol. 2015;94(3–4):162–72.
37. Rapley J, Baxter JE, Blot J, Wattam SL, Casenghi M, Meraldi P, et al. Coordinate regulation of the mother centriole component nlp by nek2 and plk1 protein kinases. Mol Cell Biol. 2005;25(4):1309–24.
38. Muller PA, Vousden KH. p53 mutations in cancer. Nat Cell Biol. 2013; 15(1):2–8.
39. Musacchio A, Salmon ED. The spindle-assembly checkpoint in space and time. Nat Rev Mol Cell Biol. 2007;8(5):379–93.

40. Fischer M, Steiner L, Engeland K. The transcription factor p53: not a repressor, solely an activator. Cell Cycle. 2014;13(19):3037–58.
41. Nabilsi NH, Ryder DJ, Peraza-Penton AC, Poudyal R, Loose DS, Kladde MP. Local depletion of DNA methylation identifies a repressive p53 regulatory region in the NEK2 promoter. J Biol Chem. 2013;288(50):35940–51.
42. Tabach Y, Milyavsky M, Shats I, Brosh R, Zuk O, Yitzhaky A, et al. The promoters of human cell cycle genes integrate signals from two tumor suppressive pathways during cellular transformation. Mol Syst Biol 2005;1: 2005 0022.
43. Henise JC, Taunton J. Irreversible Nek2 kinase inhibitors with cellular activity. J Med Chem. 2011;54(12):4133–46.
44. Willis A, Jung EJ, Wakefield T, Chen X. Mutant p53 exerts a dominant negative effect by preventing wild-type p53 from binding to the promoter of its target genes. Oncogene. 2004;23(13):2330–8.
45. Alexandrova EM, Mirza SA, Xu S, Schulz-Heddergott R, Marchenko ND, Moll UM. p53 loss-of-heterozygosity is a necessary prerequisite for mutant p53 stabilization and gain-of-function in vivo. Cell Death Dis. 2017;8(3):e2661.
46. Donehower LA, Soussi T, Korkut A, Liu Y, Schultz A, Cardenas M, et al. Integrated analysis of TP53 gene and pathway alterations in the Cancer Genome Atlas. Cell Rep. 2019;28(11):3010.
47. Marina M, Saavedra HI. Nek2 and Plk4: prognostic markers, drivers of breast tumorigenesis and drug resistance. Front Biosci (Landmark Ed). 2014;19:352–65.
48. Moniz L, Dutt P, Haider N, Stambolic V. Nek family of kinases in cell cycle, checkpoint control and cancer. Cell Div. 2011;6:18.
49. Bargonetti J, Prives C. Gain-of-function mutant p53: history and speculation. J Mol Cell Biol. 2019;11(7):605–9.
50. Shahbandi A, Jackson JG. Analysis across multiple tumor types provides no evidence that mutant p53 exerts dominant negative activity. NPJ Precis Oncol. 2019;3:1.
51. Komatsu M, Yoshimaru T, Matsuo T, Kiyotani K, Miyoshi Y, Tanahashi T, et al. Molecular features of triple negative breast cancer cells by genome-wide gene expression profiling analysis. Int J Oncol. 2013;42(2):478–506.
52. Freed-Pastor WA, Prives C. Mutant p53: one name, many proteins. Genes Dev. 2012;26(12):1268–86.
53. Ren B, Cam H, Takahashi Y, Volkert T, Terragni J, Young RA, et al. E2F integrates cell cycle progression with DNA repair, replication, and G(2)/M checkpoints. Genes Dev. 2002;16(2):245–56.
54. Valenti F, Ganci F, Fontemaggi G, Sacconi A, Strano S, Blandino G, et al. Gain of function mutant p53 proteins cooperate with E2F4 to transcriptionally downregulate RAD17 and BRCA1 gene expression. Oncotarget. 2015;6(8): 5547–66.
55. Laoukili J, Kooistra MR, Bras A, Kauw J, Kerkhoven RM, Morrison A, et al. FoxM1 is required for execution of the mitotic programme and chromosome stability. Nat Cell Biol. 2005;7(2):126–36.
56. Wonsey DR, Follettie MT. Loss of the forkhead transcription factor FoxM1 causes centrosome amplification and mitotic catastrophe. Cancer Res. 2005; 65(12):5181–9.
57. Tanaka N, Zhao M, Tang L, Patel AA, Xi Q, Van HT, et al. Gain-of-function mutant p53 promotes the oncogenic potential of head and neck squamous cell carcinoma cells by targeting the transcription factors FOXO3a and FOXM1. Oncogene. 2018;37(10):1279–92.
58. Bertheau P, Espie M, Turpin E, Lehmann J, Plassa LF, Varna M, et al. TP53 status and response to chemotherapy in breast cancer. Pathobiology. 2008; 75(2):132–9.
59. Olivier M, Hollstein M, Hainaut P. TP53 mutations in human cancers: origins, consequences, and clinical use. Cold Spring Harb Perspect Biol. 2010;2(1): a001008.
60. Robles AI, Jen J, Harris CC. Clinical outcomes of TP53 mutations in cancers. Cold Spring Harb Perspect Med. 2016;6(9):a026294.
61. Zhou X, Hao Q, Lu H. Mutant p53 in cancer therapy-the barrier or the path. J Mol Cell Biol. 2019;11(4):293–305.
62. Ungerleider NA, Rao SG, Shahbandi A, Yee D, Niu T, Frey WD, et al. Breast cancer survival predicted by TP53 mutation status differs markedly depending on treatment. Breast Cancer Res. 2018;20(1):115.

Publisher's Note

OPEN

Citation: Cell Death and Disease (2017) 8, e2661; doi:10.1038/cddis.2017.80
Official journal of the Cell Death Differentiation Association

www.nature.com/cddis

p53 loss-of-heterozygosity is a necessary prerequisite for mutant p53 stabilization and gain-of-function *in vivo*

Evguenia M Alexandrova[1], Safia A Mirza[1], Sulan Xu[1], Ramona Schulz-Heddergott[2], Natalia D Marchenko[1] and Ute M Moll*[,1,2]

Missense mutations in *TP53* comprise >75% of all p53 alterations in cancer, resulting in highly stabilized mutant p53 proteins that not only lose their tumor-suppressor activity, but often acquire oncogenic gain-of-functions (GOFs). GOF manifests itself in accelerated tumor onset, increased metastasis, increased drug resistance and shortened survival in patients and mice. A known prerequisite for GOF is mutant p53 protein stabilization, which itself is linked to aberrant protein conformation. However, additional determinants for mutant p53 stabilization likely exist. Here we show that in initially heterozygous mouse tumors carrying the hotspot GOF allele R248Q (p53Q/+), another necessary prerequisite for mutant p53 stabilization and GOF *in vivo* is loss of the remaining wild-type p53 allele, termed loss-of-heterozygosity (LOH). Thus, in mouse tumors with high frequency of p53 LOH (osteosarcomas and fibrosarcomas), we find that mutant p53 protein is stabilized (16/17 cases, 94%) and tumor onset is significantly accelerated compared with p53+/− tumors (GOF). In contrast, in mouse tumors with low frequency of p53 LOH (MMTV-Neu breast carcinomas), mutant p53 protein is not stabilized (16/20 cases, 80%) and GOF is not observed. Of note, human genomic databases (TCGA, METABRIC etc.) show a high degree of p53 LOH in all examined tumor types that carry missense p53 mutations, including sarcomas and breast carcinomas (with and without HER2 amplification). These data – while cautioning that not all genetic mouse models faithfully represent the human situation – demonstrate for the first time that p53 LOH is a critical prerequisite for missense mutant p53 stabilization and GOF *in vivo*.

Cell Death and Disease (2017) **8,** e2661; doi:10.1038/cddis.2017.80; published online 9 March 2017

Missense mutations in *TP53* (mutp53) comprise >75% of all p53 alterations in cancer, resulting in highly stabilized mutant p53 proteins that not only lose their tumor-suppressor activity, but often acquire oncogenic gain-of-functions (GOFs).[1–5] GOF activities promote cancer metabolism, stemness, and malignant progression and invasion. This results in accelerated tumor onset, increased metastasis, increased drug resistance and shortened survival in patients and mice.[5–7] Accordingly, mutp53 knockin mice carrying the human hotspot missense R248Q mutation have significantly earlier tumor onset and shorter survival than p53-null mice.[5] In agreement, in human patients with sporadic cancers across six major tumor entities, cancers with GOF mutp53 R282 and R248 alleles show a twofold higher hazard ratio (i.e., increased mortality) compared with cancers with loss-of-function (LOF) mutp53 alleles (nonsense, frameshift and deletion mutations).[8] Similarly, germline Li–Fraumeni syndrome (LFS) patients carrying R248Q mutp53 exhibit markedly faster tumor onset by 10.5 years and higher tumor numbers per person than LFS patients carrying LOF mutp53.[5]

Conversely, mutp53 elimination significantly suppresses tumor growth and metastasis and markedly extends survival in various mouse models.[7,9,10] For example, mutp53 depletion by RNAi has strong cytotoxic effects in human cancer cell lines *in vitro* and in xenografts.[7] In allografts, knockdown of mutp53 in K*ras*^{G12D} pancreatic cancer cells strongly reduces their metastatic ability.[9] Finally, in a conditional inactivatable ('floxable') autochthonous mouse model, ablation of the R248Q knockin allele extends survival by 37%, induces regression or stagnation of advanced tumors and strongly suppresses metastasis.[10]

A known prerequisite for mutp53 GOF is its massive constitutive protein stabilization specifically in tumors – but not in normal cells – of knockin mice.[6,11,12] Currently about 11 million patients worldwide live with cancers expressing highly stabilized mutp53, raising the question: what factors determine mutp53 stabilization leading to oncogenic GOF? One established determinant are the aberrant protein conformations of both the structural and DNA-contact classes of missense mutant p53 proteins, requiring constitutive chaperone complexing (with, e.g., Hsp90 and Hsp40) to protect them from their E3 ubiquitin ligases Mdm2 and CHIP and proteasomal degradation.[10,13–18] Indeed, pharmacological inhibition of the HSP90 chaperone machinery destabilizes mutp53, leading to 48% and 59% prolonged survival in R175H and R248Q knockin mice, respectively.[10] We hypothesized that besides aberrant conformation additional determinants of mutp53 stabilization likely exist. Here we show that loss of the remaining wild-type p53 (wtp53) allele, termed loss-of-heterozygosity (LOH), is also critical for missense mutp53 stabilization and GOF *in vivo*.

Results

TCGA, METABRIC and other databases of sporadic human cancer show wtp53 allele loss (LOH) in the majority of

[1]Department of Pathology, Stony Brook University, Stony Brook, NY, USA and [2]Institute of Molecular Oncology, University of Göttingen, Göttingen, Germany
*Corresponding author: UM Moll, Department of Pathology, Stony Brook University, Stony Brook, NY 11794, USA. Tel: +1 631 444 6816; Fax: +1 631 444 2434.
E-mail: Ute.Moll@stonybrookmedicine.edu
Received 01.2.17; accepted 02.2.17; Edited by G Melino

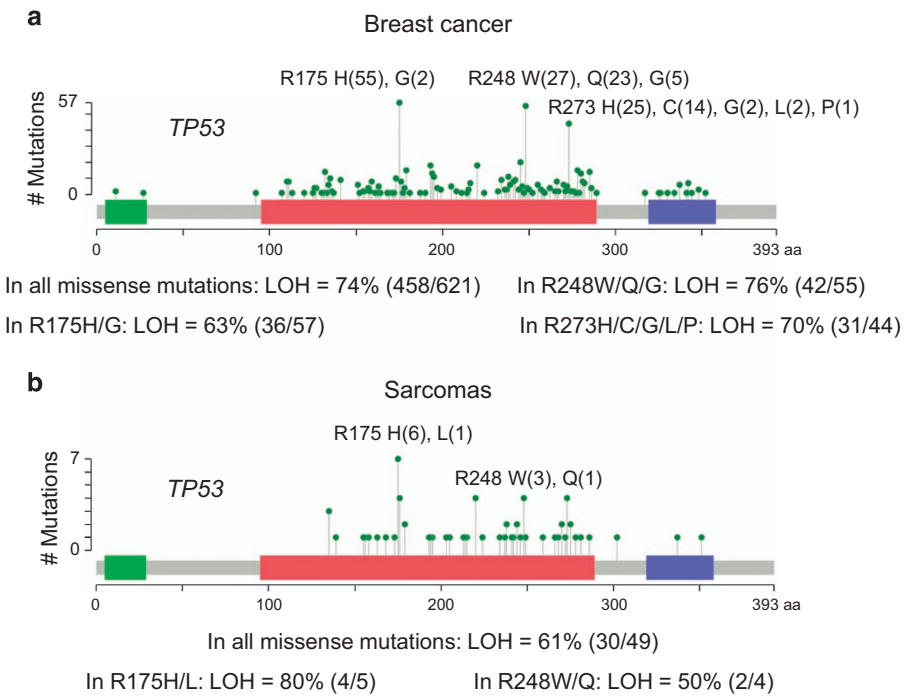

Figure 1 Analysis of the databases of sporadic human breast cancer (**a**) and sarcomas (**b**) (METABRIC, provisional TCGA and others, see Materials and Methods section) show a high frequency of wtp53 allele loss (LOH) in missense mutp53 tumors

Table 1 Frequency of p53 LOH in human HER2-positive breast cancer carrying concomitant missense mutp53

Database	Cases with p53 LOH	Total number of cases	LOH frequency
METABRIC	97	124	78.2%
TCGA provisional	38	40	95.0%
Total	135	164	82.3%

Table 2 Frequency of p53 LOH in human high-grade serous ovarian adenocarcinoma carrying concomitant missense mutp53

Database	Cases with p53 LOH	Total number of cases	LOH frequency
TCGA provisional	206	274	75.2%

missense mutp53 tumors, including ovarian cancer, breast cancer and sarcomas (Figure 1, Tables 1 and 2). Specifically, in human HER2 breast cancer with concomitant missense mutp53, wtp53 LOH occurs in 82.3% of patients (Table 1). Thus, we hypothesized that LOH is a second determinant of mutp53 stabilization and GOF *in vivo*.

To test this, we combined the heterozygous hotspot GOF allele R248Q ('p53Q/+')[5,10] with the MMTV-Neu ('Neu') oncogene[19] expressing additional wild-type HER2 copies selectively in the mammary gland, as mutp53 has a strong prognostic value in HER2-positive breast cancer, that is, significantly increased mortality.[20] Although p53Q/+;Neu mice developed breast cancer faster than p53+/+;Neu mice, surprisingly breast cancer latency between p53Q/+;Neu and p53 – /+;Neu siblings was similar (Figure 2b), suggesting that mutp53 R248Q did not exert a dominant-negative (DN) effect over wtp53 but simply behaved as a LOF allele in Neu-driven breast tumorigenesis *in vivo*, hence the curves overlap.

However, about half of p53Q/+;Neu and p53 – /+;Neu mice did not develop breast cancer but instead developed osteosarcomas and fibrosarcomas, which originate from mesenchymal tissues where MMTV-Neu is not expressed (Figure 2a). Notably, sarcoma onset was faster in p53Q/+;Neu compared with p53 – /+;Neu mice, indicating either a DN effect of mutp53 over wtp53 or, alternatively, wtp53 LOH resulting in mutp53 GOF specifically in sarcoma. Importantly, this survival difference between sarcoma and breast cancer correlated with mutp53 stabilization in nearly all examined sarcomas (94%, 16/17), but only in rare breast carcinomas (20%, 4/20), even within the same animal (Figure 3a, e.g., animal #1248).

Thus, we asked whether sarcomas are more prone to p53 LOH than breast tumors. Indeed, qPCR of genomic DNA showed that p53 LOH occurs in all sarcomas, but rarely in breast cancer (Figure 3b). Moreover, the few breast tumors that did stabilize mutp53 also underwent p53 LOH. Together, this strongly suggests that LOH is a critical prerequisite for mutp53 stabilization and GOF (Figure 3c). To corroborate our LOH data, we analyzed p53 target genes as another readout for the remaining wtp53 allele activity (Figure 4). Indeed, all tumors with stabilized mutp53, including the single 'outlier' breast cancer tested, had reduced or undetectable *Mdm2* and *p21* levels, respectively, and sarcomas also had reduced *Bax* and *Puma* expression correlating with their LOH.

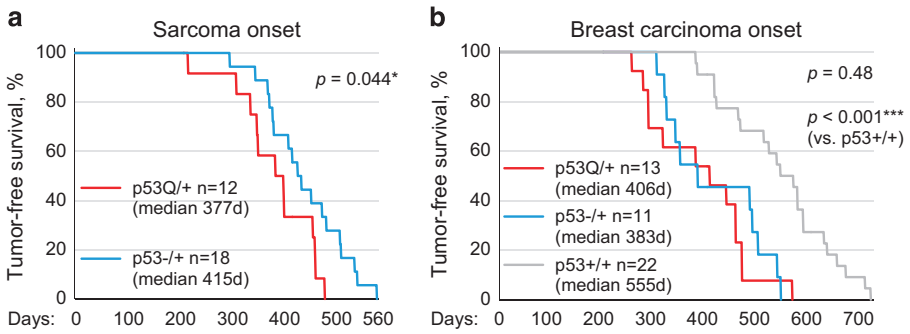

Figure 2 Survival curves analyzing tumor onset of sarcomas and breast carcinomas in p53Q/+;Neu, p53 – /+;Neu and p53+/+;Neu mouse cohorts. (**a**) Sarcoma onset is faster in p53Q/+;Neu compared with p53 – /+;Neu mice. This indicates either a DN effect over wtp53 or, alternatively, p53 LOH resulting in mutp53 GOF specifically in sarcoma. (**b**) Breast cancer latency in p53Q/+;Neu and p53 – /+;Neu siblings is similar, reflecting that the majority of p53Q/+ breast tumors did not undergo LOH (see Figure 3b) in contrast to human breast cancer, and also did not exert a DN effect over wtp53 but simply behaved as a LOF allele. Kaplan–Meier analysis; *n*, number of mice; *P*, log rank statistics

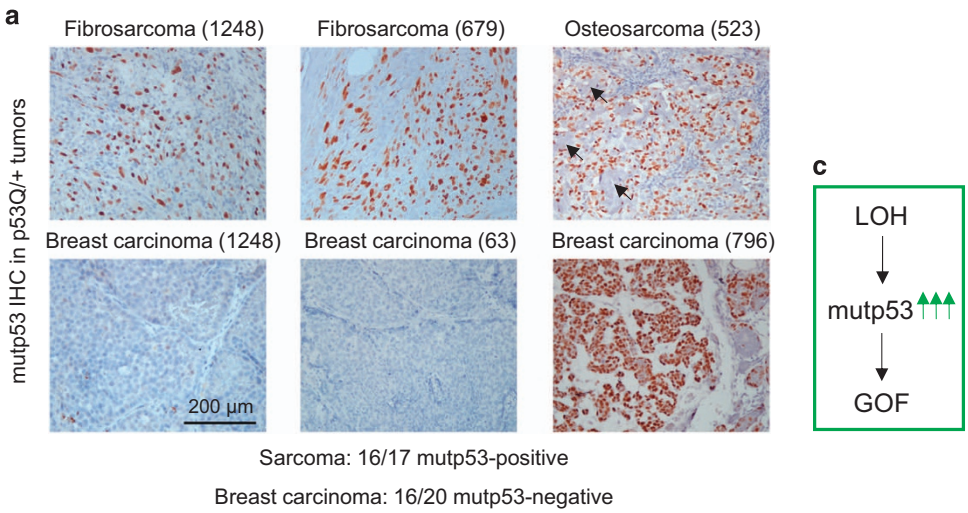

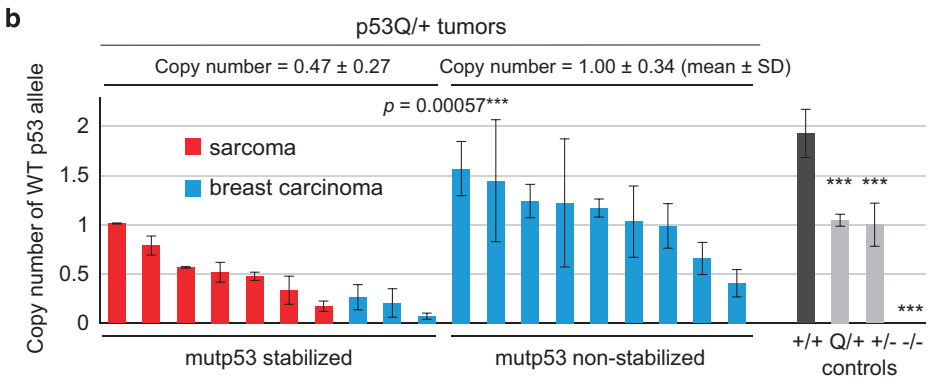

Figure 3 Loss of wtp53 allele is required for missense mutant p53 stabilization and GOF. (**a**) The vast majority of sarcomas (16/17 cases, 94%) have stabilized mutp53. In contrast, the majority of breast carcinomas (16/20 cases, 80%) do not. Immunohistochemistry for mutp53. Mouse identity in parentheses. Arrows indicate the osteoid in osteosarcoma. (**b**) Analysis of wtp53 copy number in sarcomas and breast carcinomas of p53Q/+;Neu mice by quantitative genotyping. Tumors with mutp53 stabilization (all sarcomas and three breast cancers tested) have significantly higher LOH than tumors without mutp53 stabilization (majority of breast cancers). Note, as sarcomas have high normal stroma contamination (top, blue mutp53-negative stromal cells, which do not have LOH), the actual LOH in sarcomas is most likely even higher because of dilution of the tumor genotype, causing LOH underestimation. For the same reason, copy numbers of the two highest sarcoma cases (two left red bars) are likely inflated. The wtp53 signal was normalized to the Rosa26 signal. Tail biopsies from p53+/+ (two wt alleles), p53Q/+, p53 – /+ (one wt allele) and p53 – / – mice (no wt alleles) were used as normal control tissues without LOH. Bars represent mean ± S.D. of two technical replicas of individual cases. ***$P < 0.001$. (**c**) Schematic diagram of the proposed mechanism for mutp53 stabilization and GOF in heterozygous tumors. Loss of the wtp53 allele (LOH) causes accumulation of highly stabilized mutp53 protein, which triggers tumor development and is the principle mechanism and prerequisite of GOF

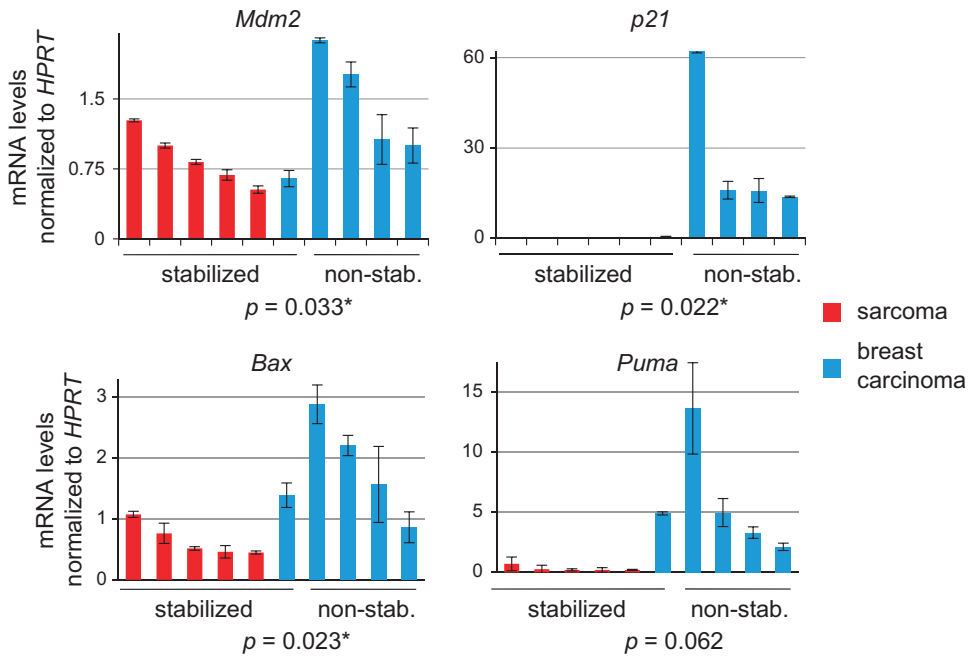

Figure 4 Real-time qPCR analysis of wtp53 target genes *Mdm2, p21, Bax* and *Puma* shows that their expression is largely decreased in samples with mutp53 stabilization compared with samples without mutp53 stabilization

Discussion

In sum, we propose that p53 LOH is a necessary prerequisite for mutp53 stabilization and GOF activity *in vivo* (Figure 3c). Indeed, we find that *TP53* LOH is a frequent event in human cancers with missense mutp53, including sarcomas (61%), breast cancer with or without HER2 amplification (up to 82%) and ovarian cancer (75%) (Figure 1, Tables 1 and 2). This high LOH frequency coincides with mutp53 protein stabilization[21,22] and GOF in human cancers.[5,8] Our *TP53* LOH data are in agreement with earlier reports finding 60% *TP53* LOH in LFS patients,[23] 81% in sporadic breast cancer patients (all molecular subtypes pooled)[20] and 93% across 10 sporadic human cancer types,[24] all expressing missense mutp53. Note that the latter study with the highest frequency includes 'copy neutral' *TP53* LOH (defined as reduced wtp53 mRNA expression but genomic copy present) and also corrects for dilutional effects from stromal contamination.[24] This suggests that conventional and even quantitative real-time PCR – which we used in our analysis – likely underestimate true functional p53 LOH.

In full agreement with the human data, sarcomas in our mouse model also exhibit GOF because they undergo LOH, which enables mutp53 stabilization. Similarly, Shetzer *et al.*[25] found that isolated mesenchymal stem cells from heterozygous R175H/+ mice form subcutaneous tumors only after they undergo wtp53 LOH. How mechanistically p53 LOH induces mutp53 stabilization awaits further investigation. A possible contributor could be reduced expression of the wtp53 target gene *Mdm2* (Figure 4), the main ubiquitin ligase for both wtp53 and mutp53.[11,16]

Although a few murine breast cancer cases in our MMTV-Neu model (4/20) did undergo LOH and exhibited mutp53 stabilization, for unknown reasons the majority (16/20) lacked LOH and therefore lacked mutp53 stabilization. We speculate that the pressure for p53 LOH is eliminated because of the Neu oncogene. This gives us pause that not all mouse models faithfully mimic the human genetic constellation for every tissue type, as the MMTV-Neu model contrasts with human breast cancer, which exhibit prominent LOH despite the presence of other oncogenic drivers (Figure 1a, Table 1).[20]

Materials and Methods

***TP53* LOH analysis in sporadic human cancers.** *TP53* LOH in sporadic human cancers was analyzed using the cBioPortal tool (www.cbioportal.org). The breast cancer data set included METABRIC and provisional TCGA databases, with 3014 samples with known mutant p53 status in total. The sarcoma data set included provisional TCGA, MSKCC/Broad Institute, Institut Curie and other databases, with 710 samples with known mutp53 status in total.

Animals. Hotspot knockin mice harboring human exons 4–9 and the p53 R248Q missense mutation ('Q' allele) and p53 – / – mice, both on pure C57Bl6 background, were previously described.[5,10] MMTV-Neu ('Neu') transgenic mice on pure FVBN background were from Jackson Laboratories (Bar Harbor, ME, USA) (FVB/N-Tg(MMTVneu)202Mul/J).[19] To obtain p53Q/+;Neu/+ and control p53+/ – ; Neu/+ mice, parental p53 R248Q/+ and p53 – /+ strains were first crossed to obtain p53 R248Q/- mice, followed by cross with Neu/Neu mice. Only female mice were used for all experiments. Animals were monitored weekly to determine their breast cancer and sarcoma onset and were promptly killed when their tumors reached 2 cm^3 in volume or when animals appeared moribund. All animals were treated humanely and according to the guidelines issued by the Institutional Animal Care and Use Committee (IACUC) at Stony Brook University.

Immunohistochemistry and histology. For immunohistochemical analysis, freshly dissected tissues were formalin fixed, paraffin embedded and sectioned (5 μm). Slides were deparaffinized and boiled in citrate buffer (10 mM, pH 6.0, 35 min) for antigen retrieval, blocked in 10% goat serum and incubated with the primary antibody (mutp53, Santa Cruz, Dallas, TX, USA, FL393, sc-6243, dilution 1:500) for 2 h at room temperature. After PBS washing, slides were incubated with

biotinylated secondary antibody and HRP-streptavidin using the Histostain SP Broad Spectrum kit (Invitrogen, Carlsbad, CA, USA, 959943B), stained with DAB substrate with hematoxylin counterstain and coverslipped. In addition, cancer type (breast cancer *versus* osteosarcoma or fibrosarcoma) was determined by H&E staining (data not shown).

Quantitative LOH analysis. Genomic DNA was isolated from sarcomas, breast carcinomas and control tails using DNeasy Blood and Tissue kit (Qiagen, 69506) and quantified by spectrophotometer. Quantitative real-time PCR was performed in duplicates with QuantiTect SYBR Green Mix (Qiagen, Germantown, MD, USA, 204143) on the MJ Research DNA Engine Opticon 2 machine, using 8 ng genomic DNA and the following mouse wtp53 allele-specific primer pairs: 5′-ACAGCGTGGTGGTACCTTAT-3′ (forward) and 5′-TATACTCAGAGCCGGCCT-3′ (reverse). These wtp53 primers anneal to mouse exons 5 and 6 and do not recognize the humanized mutp53 allele. For all samples, the wtp53 signal was normalized to the Rosa26 signal measured by the following primers: 5′-AAAGTCGCTCTGAGTTGTTAT-3′ (forward) and 5′-GGAGCGGGAGAAATGGA TATG-3′ (reverse).

Statistical analysis. Kaplan–Meier analysis and log rank statistics was used to analyze tumor onset. Unpaired two-tailed Student's *t*-test was used to analyze p53 LOH and expression of p53 target genes. $^{*}P<0.05$, $^{***}P<0.001$.

Conflict of Interest

The authors declare no conflict of interest.

Acknowledgements. This work was supported by NCI grant R01CA176647, TRO grant Walk for Beauty (Stony Brook Foundation) and Wilhelm Sander Stiftung grant 2011.029.1 to UMM, NCI grant K22CA190653-01A1 to EMA, and DOD grant W81XWH-16-1-0448 (BC151569) to NDM.

1. Lang GA, Iwakuma T, Suh YA, Liu G, Rao VA, Parant JM *et al.* Gain of function of a p53 hot spot mutation in a mouse model of Li-Fraumeni syndrome. *Cell* 2004; **119**: 861–872.
2. Olive KP, Tuveson DA, Ruhe ZC, Yin B, Willis NA, Bronson RT *et al.* Mutant p53 gain of function in two mouse models of Li-Fraumeni syndrome. *Cell* 2004; **119**: 847–860.
3. Morton JP, Timpson P, Karim SA, Ridgway RA, Athineos D, Doyle B *et al.* Mutant p53 drives metastasis and overcomes growth arrest/senescence in pancreatic cancer. *Proc Natl Acad Sci USA* 2010; **107**: 246–251.
4. Doyle B, Morton JP, Delaney DW, Ridgway RA, Wilkins JA, Sansom OJ. p53 mutation and loss have different effects on tumourigenesis in a novel mouse model of pleomorphic rhabdomyosarcoma. *J Pathol* 2010; **222**: 129–137.
5. Hanel W, Marchenko N, Xu S, Yu SX, Weng W, Moll U. Two hot spot mutant p53 mouse models display differential gain of function in tumorigenesis. *Cell Death Differ* 2013; **20**: 898–909.
6. Brosh R, Rotter V. When mutants gain new powers: news from the mutant p53 field. *Nat Rev Cancer* 2009; **9**: 701–713.
7. Muller PA, Vousden KH. Mutant p53 in cancer: new functions and therapeutic opportunities. *Cancer Cell* 2014; **25**: 304–317.
8. Xu J, Wang J, Hu Y, Qian J, Xu B, Chen H *et al.* Unequal prognostic potentials of p53 gain-of-function mutations in human cancers associate with drug-metabolizing activity. *Cell Death Dis* 2014; **5**: e1108.
9. Weissmueller S, Manchado E, Saborowski M, Morris JP 4th, Wagenblast E, Davis CA *et al.* Mutant p53 drives pancreatic cancer metastasis through cell-autonomous PDGF receptor beta signaling. *Cell* 2014; **157**: 382–394.
10. Alexandrova EM, Yallowitz AR, Li D, Xu S, Schulz R, Proia DA *et al.* Improving survival by exploiting tumour dependence on stabilized mutant p53 for treatment. *Nature* 2015; **523**: 352–356.
11. Terzian T, Suh Y-A, Iwakuma T, Post SM, Neumann M, Lang GA *et al.* The inherent instability of mutant p53 is alleviated by Mdm2 or p16INK4a loss. *Genes Dev* 2008; **22**: 1337–1344.
12. Suh YA, Post SM, Elizondo-Fraire AC, Maccio DR, Jackson JG, El-Naggar AK *et al.* Multiple stress signals activate mutant p53 *in vivo*. *Cancer Res* 2011; **71**: 7168–7175.
13. Blagosklonny MV, Toretsky J, Bohen S, Neckers L. Mutant conformation of p53 translated *in vitro* or *in vivo* requires functional HSP90. *Proc Natl Acad Sci USA* 1996; **93**: 8379–8383.
14. Whitesell L, Sutphin PD, Pulcini EJ, Martinez JD, Cook PH. The physical association of multiple molecular chaperone proteins with mutant p53 is altered by geldanamycin, an hsp90-binding agent. *Mol Cell Biol* 1998; **18**: 1517–1524.
15. Li D, Marchenko ND, Moll UM. SAHA shows preferential cytotoxicity in mutant p53 cancer cells by destabilizing mutant p53 through inhibition of the HDAC6-Hsp90 chaperone axis. *Cell Death Differ* 2011; **18**: 1904–1913.
16. Li D, Marchenko ND, Schulz R, Fischer V, Velasco-Hernandez T, Talos F *et al.* Functional inactivation of endogenous MDM2 and CHIP by HSP90 causes aberrant stabilization of mutant p53 in human cancer cells. *Mol Cancer Res* 2011; **9**: 577–588.
17. Parrales A, Ranjan A, Iyer SV, Padhye S, Weir SJ, Roy A, Iwakuma T. DNAJA1 controls the fate of misfolded mutant p53 through the mevalonate pathway. *Nat Cell Biol* 2016; **18**: 1233–1243.
18. Alexandrova EM, Moll UM. Depleting stabilized GOF mutant p53 proteins by inhibiting molecular folding chaperones: a new promise in cancer therapy. *Cell Death Differ* 2017; **24**: 3–5.
19. Guy CT, Webster MA, Schaller M, Parsons TJ, Cardiff RD, Muller WJ. Expression of the neu protooncogene in the mammary epithelium of transgenic mice induces metastatic disease. *Proc Natl Acad Sci USA* 1992; **89**: 10578–10582.
20. Silwal-Pandit L, Vollan HK, Chin SF, Rueda OM, McKinney S, Osako T *et al.* TP53 mutation spectrum in breast cancer is subtype specific and has distinct prognostic relevance. *Clin Cancer Res* 2014; **20**: 3569–3580.
21. Yemelyanova A, Vang R, Kshirsagar M, Lu D, Marks MA, Shih IM *et al.* Immunohistochemical staining patterns of p53 can serve as a surrogate marker for *TP53* mutations in ovarian carcinoma: an immunohistochemical and nucleotide sequencing analysis. *Mod Pathol* 2011; **24**: 1248–1253.
22. Köbel M, Piskorz AM, Lee S, Lui S, LePage C, Marass F *et al.* Optimized p53 immunohistochemistry is an accurate predictor of *TP53* mutation in ovarian carcinoma. *J Pathol Clin Res* 2016; **2**: 247–258.
23. Varley JM, Evans DG, Birch JM. Li-Fraumeni syndrome—a molecular and clinical review. *Br J Cancer* 1997; **76**: 1–14.
24. Parikh N, Hilsenbeck S, Creighton CJ, Dayaram T, Shuck R, Shinbrot E *et al.* Effects of TP53 mutational status on gene expression patterns across 10 human cancer types. *J Pathol* 2014; **232**: 522–533.
25. Shetzer Y, Kagan S, Koifman G, Sarig R, Kogan-Sakin I, Charni M *et al.* The onset of p53 loss of heterozygosity is differentially induced in various stem cell types and may involve the loss of either allele. *Cell Death Differ* 2014; **21**: 1419–1431.

www.impactjournals.com/oncotarget/ Oncotarget, 2017, Vol. 8, (No. 4), pp: 5823-5833

Research Paper

ErbB2 inhibition by lapatinib promotes degradation of mutant p53 protein in cancer cells

Dun Li[1,2], **Natalia D. Marchenko**[1]

[1]Department of Pathology, Stony Brook University, Stony Brook, NY, 11794, USA

[2]Department of Pharmacology, Boston University School of Medicine, Boston, MA, 02118, USA

Correspondence to: Natalia D. Marchenko, **email:** natalia.marchenko@stonybrook.edu

Keywords: *lapatinib, mutant p53, ErbB2, Hsp90, MDM2*

Received: *July 28, 2016* ***Accepted:*** *October 13, 2016* ***Published:*** *October 25, 2016*

ABSTRACT

Mutations in the p53 tumor suppressor gene are the most prevalent genetic events in human Her2-positive breast cancer and are associated with poor prognosis and survival. Human clinical data and our *in vitro* and *in vivo* studies strongly suggest potent oncogenic cooperation between mutant p53 and Her2 (ErbB2). Yet, the translational significance of mutant p53 in Her2 positive breast cancer, especially with respect to Her2-targeted therapies, has not been evaluated. Our previous work identified novel oncogenic activity of mutant p53 whereby mutp53 amplifies ErbB2 signaling via the mutp53-HSF1-ErbB2 feed-forward loop. Here we report that pharmacological interception of this circuit by ErbB2 inhibitor lapatinib downregulates mutant p53 *in vitro* and *in vivo*. We found that ErbB2 inhibition by lapatinib inhibits transcription factor HSF1, and its target Hsp90, followed by mutant p53 degradation in MDM2 dependent manner. Thus, our data suggest that mutant p53 sensitizes cancer cells to lapatinib via two complementary mechanisms: mutant p53 mediated amplification of ErbB2 signaling, and simultaneous annihilation of both potent oncogenic drivers, ErbB2 and mutant p53. Hence, our study could provide valuable information for the optimization of therapeutic protocols to achieve superior clinical effects in the treatment of Her2 positive breast cancer.

INTRODUCTION

Recent evidence suggests that although mutations in the p53 tumor suppressor gene are recognized as "driver" mutations in cancer [1], additional tumor-promoting events, such as cooperation with other oncogenic pathways, are emerging as essential mechanisms of cancer progression [2].

The human epidermal growth factor receptor-2 (Her2, ErbB2) is frequently overexpressed in human breast cancer, which is associated with poor survival [3]. Contrary to Luminal A and B subtypes, sporadic Her2 breast cancer has a high prevalence of p53 mutations (72%) [1] that predict poor prognosis due to a more aggressive disease and increased susceptibility to metastatic recurrence [4]. Furthermore, female patients with germline p53 mutations (Li-Fraumeni syndrome [LFS]) are especially prone to the Her2 subtype of breast cancer (up to 83% of all breast cancer in LFS women [5, 6] compared to 20% in sporadic breast cancer [1]), suggesting cooperative co-selection of these potent oncogenes during Her2 breast cancer progression. This strongly suggests a causative connection between p53 mutations and Her2 breast cancer development. Yet, no systematic studies have been done to assess mutant p53 (mutp53)'s significance in Her2 breast cancer development and therapy.

The main tumor suppressor function of p53 is to respond to cellular stress by activating transcriptional programs that induce apoptosis, growth arrest or senescence. It is widely recognized that when mutated, p53 not only loses its wild-type tumor suppressor functions, but often also actively promotes tumor development by inhibiting wtp53 in a dominant-negative manner or gains novel oncogenic activities, known as gain-of-function (reviewed in [2]). In contrast to the majority of tumor suppressors that are usually inactivated by deletion (i.e. PTEN, Brca1/2, NF1, APC), p53 is typically missense mutated, which suggests a selective advantage of p53 missense mutations over p53 loss. Compared to normal cells, the tight control of mutp53 by MDM2 is diminished in mutp53 tumors, leading to

tumor -specific stabilization of mutp53, which is thought to be critical for the manifestation of its oncogenic activities (reviewed in [2], [7]). This is strongly supported by *in vivo* studies, e.g. homozygous deletion of Mdm2 in mutp53 knock-in mice leads to further stabilization of mutp53 in tumors and in some normal tissues, shortened tumor latency and enhanced metastases [8]. In support of the oncogenic power of highly stabilized mutp53, we and others have shown that downregulation of mutp53 by RNA interference (RNAi) inhibits the malignant phenotype [9–11]. Knockdown of endogenous mutp53 in human breast (MDA231) and colon cancer (SW480) cells by shp53 suppresses cancer cell growth and invasion *in vitro* and in xenografts [9, 10]. Furthermore, mutp53 downregulation by RNAi decreases cell viability *in vitro* and in xenografts [12], invasion [11, 13] , restores normal mammary architecture in 3D culture in breast cancer cell lines [14], inhibits metastases *in vivo* [15, 16] and suppresses mammary stem cells [17]. Genetic ablation of mutp53 in allotransplanted and autochthonous mouse T/B-lymphoma model curbs tumor growth and extends survival of mutp53 knock-in mice [18]. Together, these proof-of-principle experiments suggest strong addiction to high levels of mutp53 protein in tumors cells. Therefore, depletion of mutp53 in mammary tumors could be therapeutically beneficial. However, pharmacological targeting of mutp53 is a challenging task. Mutp53 is not a surface molecule and does not have enzymatic activity. Hence, identifying the mechanisms of tumor-specific stabilization of mutp53 would open up new therapeutic approaches in the treatment of mutp53 harboring cancer.

Previously we found that compared to p53null counterparts, the mutp53 R172H allele ('H' thereafter) aggravates mammary tumorigenesis in the MMTV/ErbB2 mouse breast cancer model, which correlates with amplification of ErbB2 signaling [17]. When dissecting the mechanism of cooperation between ErbB2 and mutp53, we established a novel oncogenic role of mutp53 in the amplification of the ErbB2 pathway *in vivo* and *in vitro* [17, 19]. We found that mutp53 physically interacts with and enhances the transcriptional activity of HSF1 (Heat Shock Transcription Factor 1), the master transcriptional regulator of heat shock proteins (HSP) including Hsp90. In turn, Hsp90 stabilizes its clients ErbB2 and mutp53 itself [19], thereby promoting mammary tumorigenesis [17].

Following this observation, in the present study we demonstrate that the pharmacological interception of the ErbB2-HSF1-mutp53 feed-forward loop by the FDA-approved dual ErbB2/EGFR inhibitor lapatinib destabilizes mutp53 protein in cancer cells. Our data could provide valuable information for the optimization of therapeutic protocols and development predictive biomarkers to achieve superior clinical effects in the treatment of Her2 positive cancer.

RESULTS

Lapatinib induces downregulation of mutp53 in ErbB2-expressing mammary cells

Our discovery of the novel oncogenic role of mutp53 in modulation of heat shock response and ErbB2 signaling [17, 19] led us to hypothesize that pharmacological intervention of ErbB2-mutp53-HSF1 loop should diminish HSF1 activity and reduce the levels of its transcriptional target, Hsp90, ultimately leading to destabilization of mutp53, a well-established Hsp90 client [20].

To test this hypothesis we utilized several *in vitro* models: primary cultures of mammary epithelial cells (MECs) and mammary tumors derived from previously described p53−/−;ErbB2 and H/H;ErbB2 mice [17]. To determine whether the observed effects are dependent on the type of p53 mutation, we also established MECs from mutp53 R248Q/-;ErbB2 mice. According to clinical data, codon 248 of the p53 gene is the most frequently mutated in Her2-enriched breast cancer [21]. Thus, we generated a novel breast cancer mouse model by introducing humanized R248Q mutp53 allele [18, 22] ('Q' thereafter) into MMTV-ErbB2 transgenic mice. MECs derived from p53 −/−;ErbB2 littermates served as a control. These cell lines, which derived from mice with identical genetic background, provide the unique platform to delineate mutp53-mediated effects in ErbB2 positive cancer. To validate our results in human breast cancer cells we utilized ErbB2 positive human breast cancer cell line BT474 (E285K p53 mutation).

In support of our hypothesis, we found that inhibition of ErbB2 by lapatinib destabilizes mutp53, independently of type p53 mutation, in both H/H;ErbB2 and Q/-ErbB2 cultured mouse MECs (Figure 1A, 1B, 1D) and Her2 positive human breast cancer cell line BT474 (E285K) (Figure 1C, 1E). In murine and human cells mutp53 protein decrease is detectable in 24h after lapatinib treatment (Figure 1B, 1C). Importantly, the decline in pErbB2(Y1221/1222) and pErk levels (a hallmark of ErbB2 inhibition) was detectable as early as 4 h after lapatinib treatment and preceded mutp53 protein drop (Figure 1C). Furthermore, mutp53 downregulation coincides with both HSF1 (Figure 1C) and Hsp90 (Figure 1D) drop. The dose elevation experiment indicated that as low as 40nM of lapatinib is sufficient to block ErbB2 signaling, Erk phosphorylation and downregulate mutp53 (Figure 1E). *In vivo*, lapatinib suppresses tumor growth in allografted H/H;ErbB2 MECs, which was correlated with downregulation of mutp53 in tumors (Figure 1F). Together, our results imply that in addition to ErbB2/EGFR inhibition, lapatinib efficiently downregulates mutp53: *i) in vitro* and *in vivo*; *ii)* does not depend on type of p53 mutation (R172H vs R248Q mutation in murine cells with identical genetic background)*; iii)* does not depend on the cell host origin (human vs mouse).

Lapatinib promotes degradation of mup53 protein

To address the mechanism of lapatinib induced downregulation of mutp53, we tested whether lapatinib affects the transcription of mutp53 by quantitative RT-PCR analysis. We found RNA levels were unchanged in both Q/-;ErbB2 and H/H;MECs before/after lapatinib treatment (Figure 2A), suggesting that lapatinib downregulates mutp53 at post-transcriptional level.

Previously we [9] and others [20] have shown that in tumor cells aberrantly folded mutp53 proteins form stable complexes with Hsp90, which protects mutp53 from MDM2-mediated degradation. To test whether lapatinib induces degradation of mutp53 protein we treated mutp53 cells with proteasome inhibitor MG132. Indeed, proteasome inhibition by MG132 rescued lapatinib-mediated downregulation of mutp53 in both H/H;ErbB2 MECs and human BT474 cells (Figure 2B), confirming our notion that lapatinib promotes degradation of mutp53 protein. Previously, we and others have shown that E3 ligases Mdm2 as well as CHIP are inherently capable of degrading mutant p53 [8, 9]. Thus, specific MDM2 inhibitor nutlin blocks the interaction between MDM2 and mutp53 and stabilizes the latter (Figure 2C). Furthermore, both nutlin [23] (Figure 2C) and siRNA-mediated knockdown of MDM2 (Figure 2D) restore mutp53 levels after lapatinib treatment. Hence, our data implies that lapatinib induces degradation of mutp53 protein by re-activation of MDM2 E3 ligase activity. Previously, we have extensively studied the kinetics and activity of MDM2 in response to Hsp90 inhibition [9]. We found, in contrast to wtp53 harboring cells, MDM2 E3 ligase activity is selectively impaired in mutp53 expressing cells, while the physical interaction between endogenous mutp53 and MDM2 remains fully preserved [9].

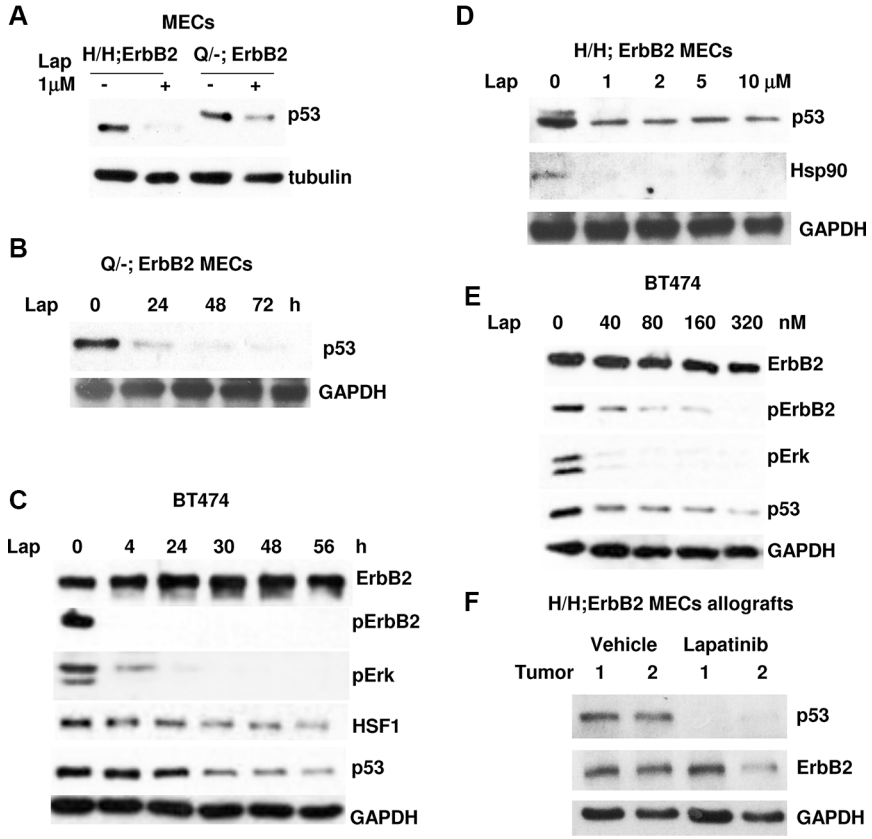

Figure 1: Lapatinib induces downregulation of mutp53 in ErbB2-expressing mammary cells. (**A**) Lapatinib induces degradation of mup53 protein in H/H;ErbB2 and R248Q/-;ErbB2 MECs. Cells were treated with 1 μM of lapatinib for 24 h. (**B**) Mutp53 protein decline is detectable in 24 h after lapatinib treatment in murine Q/-;ErbB2 MECs. Cells were treated with 1 μM of lapatinib for indicated periods of times. (**C**) Mutp53 protein decrease is detectable in 24 h after lapatinib treatment in human BT474 cells. Cells were treated with 300 nM of lapatinib for indicated periods of times. (**D**) R172H mutp53 downregulation coincides with Hsp90 decline after lapatinib treatment. Cells were treated increasing concentrations of lapatinib for 48 h. (**E**) 40 nM of lapatinib is sufficient to block ErbB2 signaling, Erk phosphorylation and downregulate mutp53 in BT474 cells. Cells were treated increasing concentrations of lapatinib for 48 h. (**F**) 6–7 wks old Nu/Nu females (Harlan, strain Hsd:Athymic Nude-Foxn1nu) were subcutaneously injected into two dorsal sites with 2×10^6 cells of cultured H/H;ErbB2 MECs per site. Mice were monitored twice weekly and upon appearance of palpable tumors were mock or lapatinib treated (100 mg/kg by oral gavage 3 times a week). At endpoint (tumor size ~3.5 cm^3) in mock treated mice, animals were sacrificed. Tumors analyzed by Western blotting.

Importantly, Hsp90 inhibition notably reduced the half-life of MDM2 and its bona fide substrates [9]. Thus, this study strongly supports the idea of enzymatic re-activation, self-ubiquitination and degradation of MDM2 in response to Hsp90 inhibition. As our model is based on the idea that ErbB2 signaling is upstream of Hsp90, we believe that a similar mechanism of MDM2 destabilization takes place upon ErbB2 inhibition. In Figure 2D we show that lapatinib decreases MDM2 level, which can be explained by enhanced MDM2 E3 ligase activity, its autoubiquitination and degradation (Figure 2D, compare lanes 1 and 3). Together, our data indicates that lapatinib restores MDM2 activity, followed by both mutp53 protein degradation, MDM2 autoubiquitynation and self-degradation.

Lapatinib destabilizes mutp53 via modulation of HSF1 activity

Our previous studies identified HSF1 and its transcriptional target Hsp90 as important determinants of mutp53 stability [19]. Furthermore, we found that ErbB2 and/or EGFR signaling via phosphorylation HSF1 at Ser326 induces transcriptional activation of HSF1 [19], which also protects HSF1 from polyubiquitination and proteasomal degradation [24]. Importantly, lapatinib blocks phosphorylation of downstream effectors of ErbB2 - AKT and Erk, which has been shown to play an important role in transcriptional activation of HSF1 by Ser326 phosphorylation [24, 25] (Figure 3A). Consistent with these data, we found that lapatinib blocks AKT, Erk and Ser326 HSF1 phosphorylation induced by heat shock (42°C, 30 min) in BT474 cells (Figure 3A). Furthermore, lapatinib downregulates HSF1 levels concomitant with the Hsp90 drop, but does not affect constitutive HSP- Hsc70 (Figure 3A). Also, transcriptional activation of HSF1 by heat shock alleviates lapatinib induced mutp53 degradation in p53Q/-;ErbB2 MECs (Figure 3B). Seemingly, lapatinib affects HSF1 signaling in mutp53-dependent, since HSF1 drop after lapatinib treatment occurs only in mutp53 expressing (Q/-;ErbB2), but not in p53 −/−;ErbB2 MECs (Figure 3C). To further prove that lapatinib destabilizes mutp53 via modulation of HSF1 activity, we examined the effect of HSF1 silencing. As expected, we found that siRNA mediated HSF1 ablation downregulates mutp53 (Figure 3D, compare lanes 1 and 3). Nevertheless, lapatinib does not induce further destabilization of mutp53 in the absence of HSF1 (Figure 3D, compare lanes 2 and 4). Consistent with mutp53 as a Hsp90 client, Hsp90 downregulation after HSF1 ablation was concomitant with mutp53 decline (Figure 3D). To further prove that

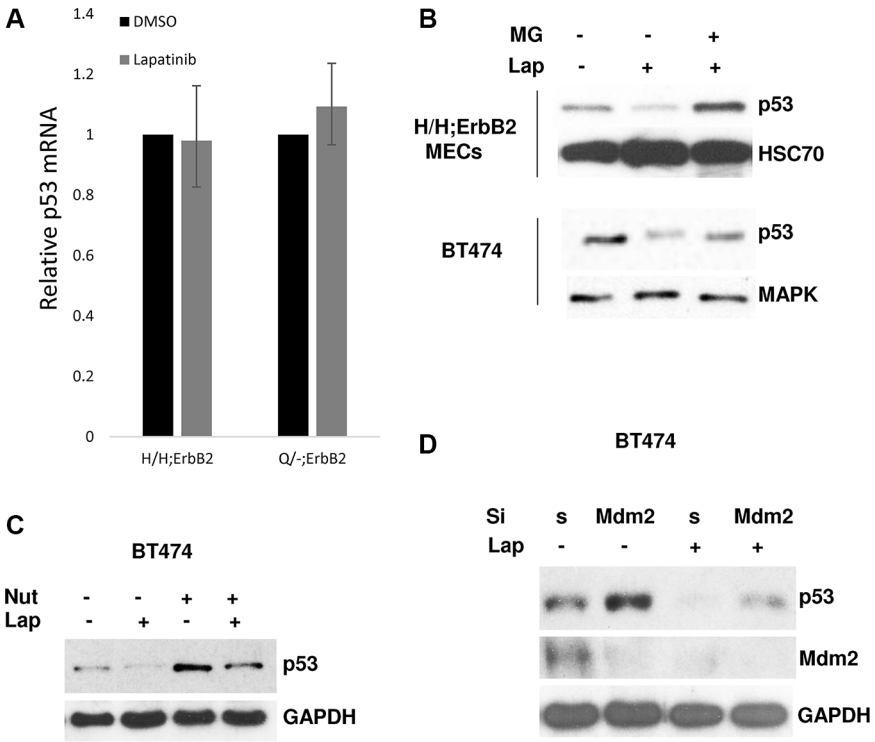

Figure 2: Lapatinib promotes degradation of mup53 protein. (**A**) RNA levels were unchanged in both Q/-;ErbB2 and H/H;MECs before/after lapatinib treatment (1 μM for 48 h) p53 mRNA levels measured by qRT-PCR. Two independent experiments were performed in triplicate. (**B**) Proteasome inhibition by MG132 rescues lapatinib-mediated downregulation of mutp53 in H/H;ErbB2 MECs (top) and BT474 (bottom). Cells were simultaneously treated with lapatinib (300 nM) and MG132 (5 μM) for 24 h. (**C**) MDM2 inhibition by nutlin rescues lapatinib-mediated destabilization of mutp53. BT474 cells were simultaneously treated with lapatininb (300 nM) and nutlin (5 μM) for 24 h. (**D**) siRNA-mediated knockdown of MDM2 restores mutp53 levels after lapatinib treatment. BT474 cells were transfected with scrambled or siMDM2, followed by lapatinib treatment (300 nM) for 24 h. GAPDH as loading control.

lapatinib destabilizes mutp53 via HSF1 transcriptional target Hsp90, we pre-treated BT474 with Hsp90 inhibitor ganetespib [18] for 6h followed by lapatinib treatment for 24 h. We found that lapatinib, even at high concentrations, does not further decrease mutp53 and MDM2 levels in cells pre-treated with ganetespib (Figure 3E). These results suggest that lapatinib could target mutp53 for degradation only in the presence of functional Hsp90.

In sum, these experiments support our hypothesis that inhibition of ErbB2 by lapatinib suppresses HSF1 transcriptional activation (Figure 3A) and protein levels (Figure 1C) with subsequent decline of its target Hsp90, releasing mutp53 from the Hsp90 inhibitory complex followed by MDM2 reactivation and mutp53 degradation.

Mutant p53 sensitizes cells to lapatinib

The therapeutic benefit of targeting mutp53 was established by Alexandrova et al. in recent proof-of-principle experiments. They have shown that the genetic deletion of mutp53 from T/B cell lymphoma tumors inhibits their growth and extends survival of mutp53 knock-in mice [18]. Thus, in addition to ErbB2 inhibition, lapatinib-induced destabilization of mutp53 protein could

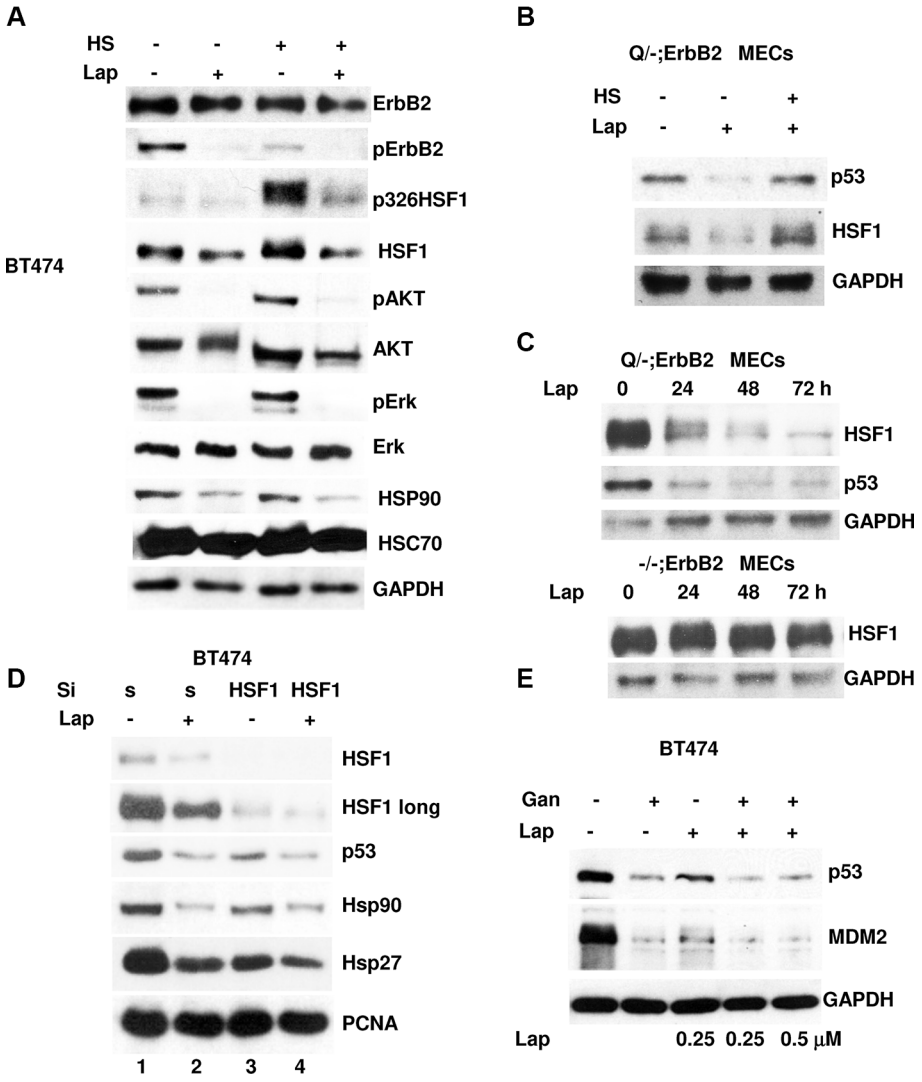

Figure 3: Lapatinib destabilizes mutp53 via modulation of HSF1 activity. (**A**) Lapatinib inhibits HSF1Ser326 phosphorylation induced by heat shock in BT474 cells. Cells were pre-treated with 300nM of lapatinib for 24 h. After heat shock (42°C, 30 min) cells were immediately analyzed by immunoblot. (**B**) Heat shock (42°C, 30 min) alleviates mutp53 destabilization by lapatinib in p53Q/-;ErbB2 MECs. Cells were pre-treated with lapatinib (300 nM, 24 h). After heat shock (42°C, 30 min) cells were immediately analyzed by immunoblot. (**C**) Lapatinib (300 nM) mediated mutp53 destabilization coincides with reduction of HSF1 levels in Q/-;ErbB2, but not in p53−/−;ErbB2 MECs. (**D**) In HSF1-ablated BT474 cells, lapatinib (300 nM) does not induce further destabilization of mutp53. Cells were transfected with siHSF1 or scrambled siRNA control. After 24 h, cells were treated with 300 nM of lapatinib for an additional 24 h followed by immunoblot. (**E**) Lapatinib destabilizes mutp53 only in the presence of functional Hsp90. BT474cells were pre-treated with ganetespib (250 nM) for 6 h followed by lapatinib (250 nM and 500 nM) treatment for 24 h. Lapatinib even at high concentrations does not further decrease mutp53 and MDM2 levels in cells pre-treated with Hsp90 inhibitor.

potentiate its therapeutic effect specifically in mutp53 harboring tumors. Hence, we hypothesized that mutp53 allele may sensitize ErbB2 expressing cells to lapatinib by two complementary mechanisms: 1) mutp53 mediated amplification of ErbB2 signaling [17] that creates superior dependency of cancer cells on ErbB2 signaling, and 2) lapatinib induced mutp53 degradation (Figures 1, 2). Therefore, mutp53 harboring cells could be more responsive to ErbB2 inhibition than p53null counterparts and, possibly, wtp53 cells.

Indeed, we found that H/H;ErbB2 MECs are more sensitive to lapatinib than their p53−/−;ErbB2 counterparts in both a colony formation assay (Figure 4A) and a cell viability assay (Figure 4B). In agreement with our model (Figure 5), mutp53 sensitizes MECs to lapatinib only in the presence of ErbB2 but not in MECs established from H/H knock-in mice (Figure 4B).

Although this data strongly supports the notion of the oncogenic cooperation of mutp53 and ErbB2, it has limited clinical application. Contrary to p53 mutations, wtp53 deletions are rather rare in breast cancer. Hence, the comparison of wtp53;ErbB2 and mutp53;ErbB2 cancer cells more faithfully recapitulates human ErbB2 positive breast cancer. Even though our previous studies identified novel oncogenic activity of mutp53 in amplification of ErbB2 signaling [17], it is not clear how wtp53 status impacts ErbB2 signaling and the response to ErbB2 targeted therapies. Contrary to mutp53, we did not observe wtp53 protein decline in response to Hsp90 inhibition in our previous study [9]. Consistently, lapatinib even at high doses does not affect wtp53 level in human MCF7 breast cancer cell line. Although MCF7 cell line is derived from ER-positive human breast cancer, MCF7 cells show detectable levels of ErbB2 (Figure 4C). Since only limited amount of wtp53;ErbB2 human cell lines are available for analysis, we established cell lines from mammary tumors of littermates p53 +/+;ErbB2 vs H/+;ErbB2 mice. In contrast to human cell lines, the identical genetic background of these mice helps to delineate mutp53-specific effects in ErbB2 context and the response to ErbB2 targeted therapies in a well-controlled experimental setting.

Consistent with our previous findings [17], we detected both elevated ErbB2 and pErbB2 levels in the presence of the mutp53 allele compared with p53 +/+;ErbB2 mammary tumor cell lines (Figure 4D). In further support of ErbB2 as an upstream effector of HSF1 activation, heat shock (42°C, 30 min) more potently induces Ser326HSF1 activation in the presence of mutp53 allele compared with p53+/+;ErbB2 tumor cell lines (Figure 4E). As a result of mutp53-mediated enhancement of ErbB2 signaling, lapatinib shows stronger inhibition of EGFR and ErbB2 signaling in the presence of mutp53 allele (compare ratio of pErbB2 and pEGFR in mock and lapatinib treated cells) (Figure 4F). Consequently, the inhibition of downstream Erk signaling is more pronounced in H/+;ErbB2 compared with p53+/+;ErbB2 cancer cells. In accord with our earlier findings (Figure 3), higher efficiency of ErbB2/EGFR inhibition in mutp53 harboring cells coincides with more robust decline of HSF1 levels (Figure 4F). Hence, compared to wtp53 cells, enhanced ErbB2 signaling in mutp53 harboring cells could generate higher addiction to ErbB2 pathway. Indeed, we found better response to lapatinib in H/+;ErbB2 tumor cell lines in H/+;ErbB2 compared to p53+/+;ErbB2 cancer cells measured by cell viability assay (Figure 4G). These results are strongly supported by meta-analysis of the COSMIC drug sensitivity database of 226 human cancer cell lines (representing breast cancer as well as other cancer types) (http://www.cancerrxgene.org/translation/Drug/119). Specifically, we found that mutp53 human cell lines are more sensitive to lapatinib than wtp53 cells ($p = 0.0408$).

Together, our data implies that in comparison to wtp53 and p53 null cancer, mutp53–mediated amplification of ErbB2 function could generate superior addiction of cancer cells to ErbB2 signaling. Thus, mutational status of p53 could serve as a potential predictive biomarker for better clinical response to ErbB2 targeted therapies in breast cancer cells.

DISCUSSION

ErbB2/Her2, a member of the human epidermal growth factor receptor family, is highly overexpressed in 20–30% of all breast cancer cases [3]. High levels of ErbB2 in cancer cells induce ligand-independent constitutive dimerization of ErbB2 and/or dimerization with other epidermal growth factor receptor family members, triggering downstream signaling through the phosphoinositide-3-kinase (PI3K)–AKT and Ras–Raf–MEK–ERK1/2 cascades [3]. Activation of these signaling pathways promotes cell proliferation and invasion, thus, enabling cancer progression and metastases. And while development of Her2-targeted therapies significantly improves patient outcomes, the primary and acquired resistance to these modalities remain a major clinical concern. Therefore, our understanding of how ErbB2 cooperates with other oncogenic pathways in context of ErbB2 targeted therapies is critical for improvement of therapeutic outcomes in these high risk breast cancer patients.

Our previous *in vivo* studies found strong evidence of oncogenic cooperation of mutp53 and ErbB2. By crossing mutp53 R172 knock-in mice with ErbB2/Neu transgenic mice we discovered that the mutp53 R172H allele is a more potent activator of ErbB2 mammary tumorigenesis than simple loss of p53, reflected by more aggressive disease, earlier tumor onset, increased tumor multiplicity and shorter survival [17]. These findings are in agreement with clinical data that mutations in the p53 gene are the most frequent oncogenic events in Her2 positive breast cancer [1], which are highly predictive of poor disease outcome [4]. Despite of evident negative impact of mutp53 on ErbB2 breast cancer development, p53 mutational status is not routinely used as a guide

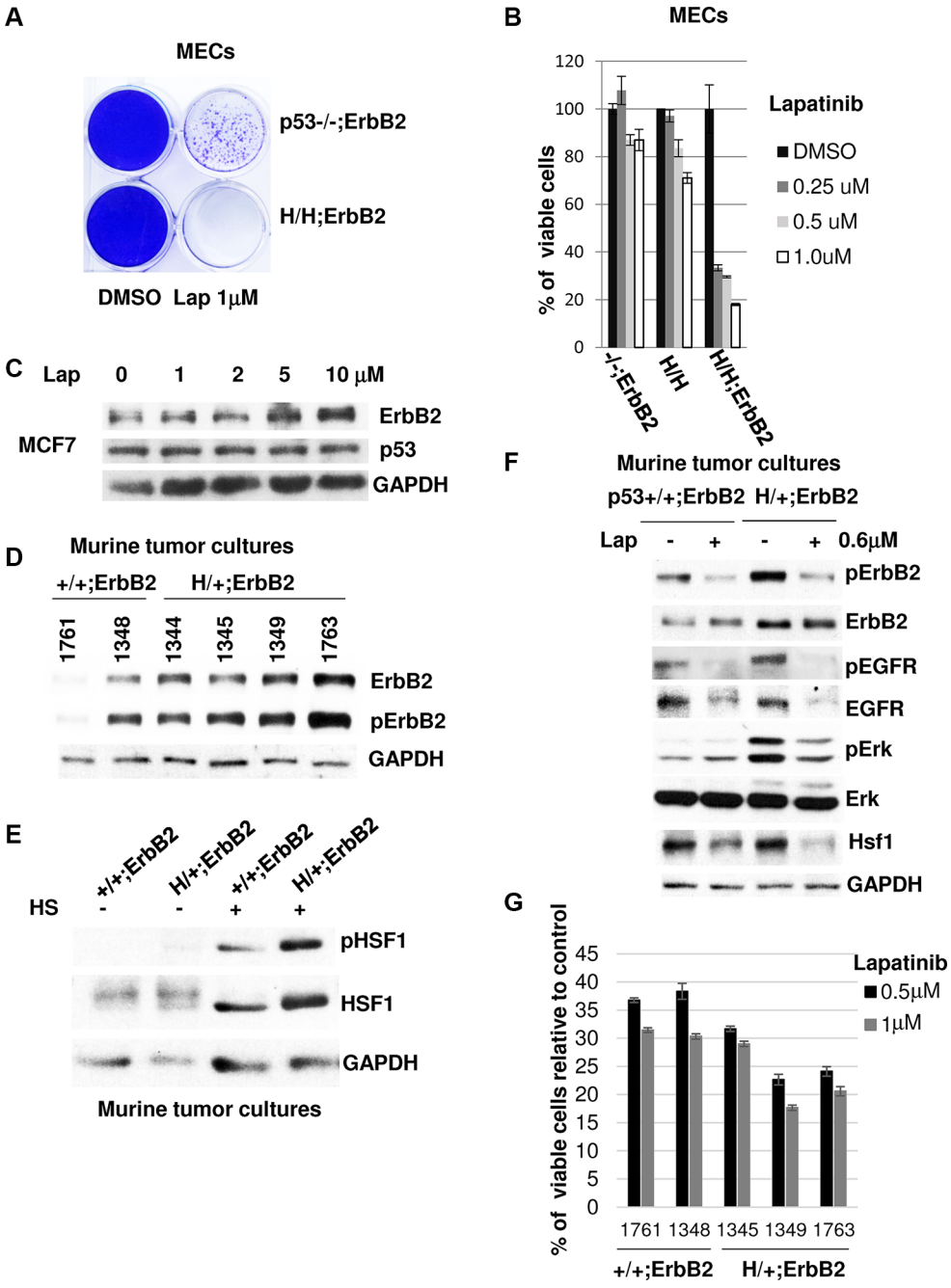

Figure 4: Mutant p53 sensitizes cells to lapatinib. (**A**) Lapatinib shows preferential cytotoxicity in mutp53;ErbB2 mammary cells. H/H;ErbB2 MECs show higher sensitivity to lapatinib, compared to p53−/−;ErbB2 counterparts in colony formation assay (crystal violet staining). H/H;ErbB2 and −/−;ErbB2 MECs were treated with 1 μM of lapatinib for 5 weeks. (**B**) H/H;ErbB2 MECs show higher viability loss in response to lapatinib compered to −/−;ErbB2 and H/H MECs. Cells were treated with indicated concentrations of lapatinib for 48h. Viability loss is shown relative to DMSO treated controls. (**C**) Lapatinib destabilizes mutp53 but not wtp53. Lapatinib does not affect wild-type p53 protein even at high concentrations. MCF7 cells were treated with indicated concentrations of lapatinib for 24 h. (**D**) Mammary tumor cell lines show both elevated ErbB2 and pErbB2 levels (Y1221/1222) in the presence of the mutp53 allele compared with p53 +/+;ErbB2. Cells were established from primary mammary tumors of mice with indicated genotypes. (**E**) Heat shock (42°C, 30 min) more potently induces Ser326HSF1 activation in the presence of mutp53 allele compared with p53+/+;ErbB2 tumor cell lines. After heat shock p53+/+;ErbB2 (#1761) and H/+;ErbB2 (#1349) cells were immediately analyzed by immunoblot. (**F**) Lapatinib more profoundly inhibits of ErbB2 downstream signaling (pErk, pErbB2, HSF1) in H/+;ErbB2 compared with p53+/+;ErbB2 cancer cells. Cells were treated with lapatinib (0.6 μM, 24 h) and analyzed by immunoblot. (**G**) Tumor cell lines harboring mutp53 allele respond better to lapatinib measured by cell viability assay. Mammary tumor cell lines with indicated genotypes were treated with 0.5 and 1 μM of lapatinib for 48 h. Viability loss is shown relative to DMSO treated controls (calculated as 100% viability).

for therapy planning in breast cancer. In this study we evaluated potential predictive value of mutational p53 status in response to Her2 targeted therapies.

We and others have previously shown that high mutp53 protein levels in cancer cells depend on heat shock protein Hsp90 [9, 18, 20]. Although basal Hsp90 protein level is highly abundant in cancer cells, it is further transcriptionally induced in response to environmental stress. It has been shown that eukaryotic cells express both constitutive Hsp90β and stress-inducible cytosolic Hsp90α. It is well established that stress-induced transcription of Hsp90α is controlled by the transcription factor HSF1 [26].

As a transcription factor, HSF1 controls a broad spectrum of events essential for protecting cells from proteotoxic stress, which is associated with the accumulation of misfolded proteins, e.g. in cancer cells. Thus, HSF1 activates transcription of genes that regulate protein homeostasis, including the molecular chaperones Hsp27, Hsp70, Hsp90 [26]. Unlike normal cells, tumor cells are characterized by a permanently high rate of protein misfolding due to abundance of mutated oncoproteins, making HSF1 ubiquitously and constitutively overexpressed [26]. Hence, HSF1 protein levels are elevated in 80% of breast cancer, leading to enhanced expression of its targets, including Hsp90 [27]. Most importantly, HSF1 transcriptional targets Hsp90 [28, 29], Hsp70 [28] and Hsp27 [26] are responsible for ErbB2 protein stability. The critical significance of HSF1-regulated heat chock response in ErbB2 mediated mammary tumorigenesis was proven by *in vivo* genetic model. Genetic knockout of HSF1 suppresses mammary hyperplasia and reduces tumorigenesis in ErbB2 transgenic mice *in vivo* [30]. Meanwhile, oncogenicity of mutp53 also critically depends on HSF1 function. In the absence of HSF1, mutp53 H/+ KI mice show a 70% reduction in tumor formation [31].

To explore potential mutp53-HSF1-ErbB2 link, we recently performed a series of mechanistic studies and described a novel mutp53-initiated oncogenic feed-forward loop, which governs resistance of cancer cells to proteotoxic stress that enables cancer cells superior survival [17]. We propose the model whereby mutp53 through enhanced recycling (similar to EGFR [13]) and/or stability of ErbB2 [17], augments MAPK and AKT signaling leading to transcriptional phospho-activation of HSF1 at Ser326 [24, 25]. Furthermore, we established that mutp53 directly interacts with phospho-activated HSF1 and facilitates its binding to DNA response elements, thereby stimulating transcription of HSPs. In turn, HSPs more potently stabilize their clients ErbB2, EGFR, mutp53, HSF1 (and possibly other oncogenes), thus, reinforcing tumor development (Figure 5) [17]. Consistently, we found that ErbB2 inhibition by lapatinib not only strongly suppressed tumor progression in ErbB2 mice, but does so, at least in part, via *inactivation of HSF1* [32]. In agreement, in present study we found that targeting of ErbB2 by lapatinib inhibits phospho-activation of HSF1 at Ser326 and destabilizes HSF1 protein (Figure 3A). Together with previous findings that ErbB2-driven mammary tumorigenesis is suppressed in

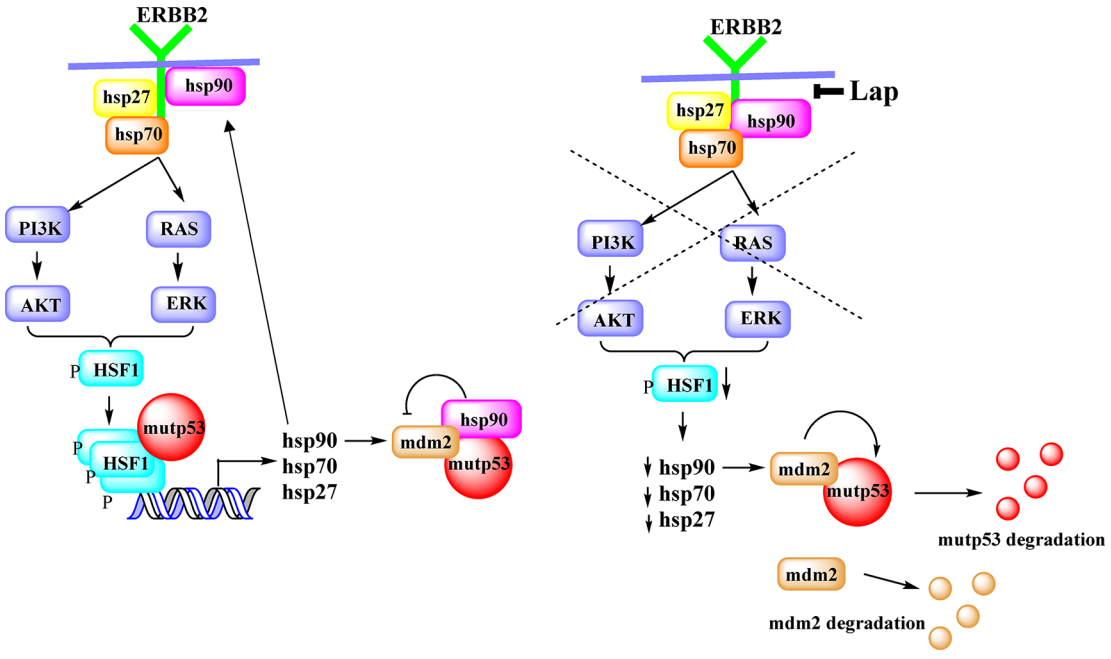

Figure 5: Proposed model. ErbB2 signaling mediates HSF1 activation in a mutp53-dependent manner. Mutp53, by enhancing ErbB2 signaling, potentiates HSF1 activity via a feed-forward loop and thereby upregulates Hsp90 clients, including mutp53. Inhibition of ErbB2 by lapatinib, leads to inhibition of HSF1 transcriptional function, decline in Hsp90 level, release MDM2 from inhibitory complex and subsequent degradation of mutp53 and MDM2.

HSF1 knockout mice [30], our results strongly support the proposed model (Figure 5). Furthermore, relevant to human disease, we found a strong correlation between mutp53 and nuclear p-Ser326 HSF1 in 150 human breast cancer biopsies (by immunochemistry) *only in Her2-positive tumors*. No correlation between mutp53 and pSer326-HSF1 staining was found in Her2-negative;ER/PR-positive breast cancer samples [19]. Altogether, this data provides a mechanistic explanation of how mutp53 potentiates ErbB2 signaling and modulates the response to ErbB2 targeting compounds (Figure 5).

Importantly, discovery of oncogenic function of mutp53 in the upregulation of heat shock response and ErbB2 signaling, opens up novel therapeutic opportunities. We found that *higher dependency* on the ErbB2-HSF1-mutp53 loop sensitizes mutp53;ErbB2 cancer cells to the interception of any of its components. The interference of proposed feed-forward loop by lapatinib inhibits HSF1 function (Figure 3), followed by Hsp90 decline and MDM2-mediated mutp53 degradation (Figure 2). Therapeutic benefit of targeting mutp53 was previously established in various cancer models [11, 18]. Hence, mutp53 status in ErbB2 positive cancer cells predicts higher sensitivity to lapatinib via two complementary mechanisms: mutp53-mediated amplification of ErbB2, and simultaneous targeting of potent oncogenic drivers, ErbB2, mutp53 and HSF1 by ErbB2 inhibition. Indeed, our *in vitro* and *in silico* analysis confirms this hypothesis and shows superior response to lapatinib in mutp53 harboring cells compared with p53 null and wtp53 cancer cells (Figure 4).

Many Her2-targeted drugs are currently on the market (trastuzumab, pertuzumab, lapatinib, TDM-1) or have recently entered clinical trials, e.g. CI-1033 (Pfizer), NVP-AEW541 (Novartis) and Perifosine (Keryx) [33]. In this study, we primarily focused on the small molecule inhibitor lapatinib, since human Her2-specific monoclonal antibodies trastuzumab and pertuzumab cannot be studied in mouse models. However, our data strongly suggest that mutp53 harboring breast cancer cells also could be sensitized to Her2-antibody based therapies via similar mechanism. This important clinical question should be addressed in further retrospective human clinical studies.

Overall, our data provides important information that can help to improve treatment options for ErbB2-positive breast cancer patients. We showed that pharmacological targeting of ErbB2 leads to destabilization of mutp53 protein via modulation of heat shock response, and therefore, could be more therapeutically beneficial specifically for mutp53 harboring patients.

MATERIALS AND METHODS

Human cancer cells

Human Her2 positive breast cancer cell line BT474 (E285K p53 mutation) and human breast cancer cell line MCF7 (contain functional wtp53) were obtained from ATCC. Where indicated, cells were treated with indicated concentrations of lapatinib (LC lab, # L-4899). Concentrations of lapatinib were optimized for every experimental setting, depending on cell types. Where indicated cells were treated with 5 μM MG132 (Sigma) and 5 μM nutlin (Sigma) added to the medium. All cell viability assays were done using standard clonogenicity assays and CellTiter-Blue Cell Viability Assay (Promega, 96-well format with 5,000 cells/well seeded 24 hrs prior). Cells were treated for 48 hours in various concentrations of drug used. Florescence was detected by SPECTRAmax M2 (Molecular Devices).

RNA interference

Pools of 4 different siRNA duplexes specific for human HSF1 (Dharmacon), MDM2 (Ambion) or scrambled control duplexes were transfected with Lipofectamine 2000 (Invitrogen). Cells were harvested 48 h later for analysis.

Immunoblots

For immunoblots, equal total protein of cell lysates (2.5–20 μg) were detected with antibodies to mouse p53 (FL393), human p53 (PAb1801), MDM2, GAPDH, HSC 70 (all Santa Cruz Biotechnology), Erk, pErk (T202/Y204), EGFR, EGRF-Tyr845P, ErbB2, pErbB2 (Y1221/1222) (all Cell Signaling), HSF1, pSer326 HSF1, Hsp90 (Enzo Life Sciences, Inc., Farmingdale, NY).

Quantitative PCR

Total RNA from cells was isolated using Trizol (Invitrogen) according to manufacturer's guidelines. Equal amounts of RNA were reverse-transcribed and real-time PCR analysis was performed using qPCR Master-Mix (75 mM Tris-HCl, pH 8.8, 20 mM (NH4)2SO4, 0.01% Tween-20, 3 mM MgCl2, SYBR Green 1:80,000, 0.2 mM dNTPs, 20 U/ml Taq-polymerase, 0.25% TritonX-100, 0.3M Trehalose and 0.3 mM primers).

Mice

MMTV-ErbB2 mice harboring activated ErbB2 (strain FVBN-Tg(MMTV-ErbB2)NK1Mul/J) were from Jackson Labs. p53 R172H (called p53H/H) and control p53 null (p53−/−) mice (C57Bl6J background) were a gift from G. Lozano [34]. Humanized R248Q knock-in mice were a gift from Dr. Moll [18], knock-in p53 mice were interbred to generate H/- and Q/- mice. Compound p53H/-;ErbB2 and Q/-;ErbB2 mice were generated by crossing ErbB2 into the p53−/− background and then breeding the p53+/−;ErbB2 progeny with p53H/H and p53 Q/Q animals. H/-;ErbB2 mice were then crossed to generate p53H/H;ErbB2 and p53−/−;ErbB2 females for analysis.

These F2 mice were of mixed background. Littermates were used for all analyses. Mice were regularly monitored and euthanized when they became moribund. Careful necropsies were performed and tumors and all major organs collected. Mice were treated according to guidelines approved by the Institutional Animal Care and Use Committee.

Allografts

6–7 wks old Nu/Nu females (Harlan, strain Hsd:Athymic Nude-Foxn1^{nu}) were subcutaneously injected into two dorsal sites with 2×10^6 cells of cultured H/H;ErbB2 MECs per site suspended in 3:1 PBS/Matrigel (BD Biosciences). Mice were monitored twice weekly and upon appearance of palpable tumors were mock (18% Cremophor/3.6% dextrose) or lapatinib treated (100 mg/kg by oral gavage 3 times a week). At endpoint (tumor size ~3.5 cm^3) in mock treated mice, mice were sacrificed. Tumors were analyzed by Western blotting.

Mammary cells cultures

Mammary glands were dissected from 8 wk-old virgin female mice and sequentially digested at 37°C for 2 h in collagenase/hyaluronidase, 0.05% Trypsin, DNAse I and Dispase (Stem Cell Technology). The ensuing cell suspension was treated with red blood cell lysis buffer, rinsed with PBS, and passed through a 40 µm mesh after resuspension in Opti-Mem medium (Gibco). Cells were plated on gelatin-coated plates and grown in CnT-BM1 medium (Cell-N-Tec). For the establishing mammary tumors culture, mammary tumors were dissected, rinsed three times in PBS, minced and processed as described above.

ACKNOWLEDGMENTS

We thank Lynden Lee (Boston University Pharmacology Department) for the proofreading of the manuscript.

CONFLICTS OF INTEREST

None of the authors have conflicts of interest to disclose. There was no sponsor involved in the study design; the collection, analysis, and interpretation of data; the writing of the report; or the decision to submit the paper for publication.

GRANT SUPPORT

This work was funded by grants from the American Cancer Society (RSG-11-188-01 to NM) and the Carol Baldwin Breast Cancer Research Fund (to NM).

REFERENCES

1. Cancer Genome Atlas N. Comprehensive molecular portraits of human breast tumours. Nature. 2012; 490:61–70.
2. Brosh R, Rotter V. When mutants gain new powers: news from the mutant p53 field. Nature reviews Cancer. 2009; 9:701–713.
3. Eccles SA. The epidermal growth factor receptor/Erb-B/HER family in normal and malignant breast biology. The International journal of developmental biology. 2011; 55:685–696.
4. Yamashita H, Nishio M, Toyama T, Sugiura H, Zhang Z, Kobayashi S, Iwase H. Coexistence of HER2 over-expression and p53 protein accumulation is a strong prognostic molecular marker in breast cancer. Breast cancer res. 2004; 6:R24–30.
5. Masciari S, Dillon DA, Rath M, Robson M, Weitzel JN, Balmana J, Gruber SB, Ford JM, Euhus D, Lebensohn A, Telli M, Pochebit SM, Lypas G, et al. Breast cancer phenotype in women with TP53 germline mutations: a Li-Fraumeni syndrome consortium effort. Breast cancer res and treatment. 2012; 133:1125–1130.
6. Melhem-Bertrandt A, Bojadzieva J, Ready KJ, Obeid E, Liu DD, Gutierrez-Barrera AM, Litton JK, Olopade OI, Hortobagyi GN, Strong LC, Arun BK. Early onset HER2-positive breast cancer is associated with germline TP53 mutations. Cancer. 2012; 118:908–913.
7. Freed-Pastor WA, Prives C. Mutant p53: one name, many proteins. Genes dev. 2012; 26:1268–1286.
8. Terzian T, Suh YA, Iwakuma T, Post SM, Neumann M, Lang GA, Van Pelt CS, Lozano G. The inherent instability of mutant p53 is alleviated by Mdm2 or p16INK4a loss. Genes dev. 2008; 22:1337–1344.
9. Li D, Marchenko ND, Schulz R, Fischer V, Velasco-Hernandez T, Talos F, Moll UM. Functional inactivation of endogenous MDM2 and CHIP by HSP90 causes aberrant stabilization of mutant p53 in human cancer cells. Mol cancer res. 2011; 9:577–588.
10. Yan W, Liu G, Scoumanne A, Chen X. Suppression of inhibitor of differentiation 2, a target of mutant p53, is required for gain-of-function mutations. Cancer res. 2008; 68:6789–6796.
11. Adorno M, Cordenonsi M, Montagner M, Dupont S, Wong C, Hann B, Solari A, Bobisse S, Rondina MB, Guzzardo V, Parenti AR, Rosato A, Bicciato S, et al. A Mutant-p53/Smad complex opposes p63 to empower TGFbeta-induced metastasis. Cell. 2009; 137:87–98.
12. Bossi G, Lapi E, Strano S, Rinaldo C, Blandino G, Sacchi A. Mutant p53 gain of function: reduction of tumor malignancy of human cancer cell lines through abrogation of mutant p53 expression. Oncogene. 2006; 25:304–309.
13. Muller PA, Caswell PT, Doyle B, Iwanicki MP, Tan EH, Karim S, Lukashchuk N, Gillespie DA, Ludwig RL,

Gosselin P, Cromer A, Brugge JS, Sansom OJ, et al. Mutant p53 drives invasion by promoting integrin recycling. Cell. 2009; 139:1327–1341.

14. Freed-Pastor WA, Mizuno H, Zhao X, Langerod A, Moon SH, Rodriguez-Barrueco R, Barsotti A, Chicas A, Li W, Polotskaia A, Bissell MJ, Osborne TF, Tian B, et al. Mutant p53 disrupts mammary tissue architecture via the mevalonate pathway. Cell. 2012; 148:244–258.
15. Morton JP, Timpson P, Karim SA, Ridgway RA, Athineos D, Doyle B, Jamieson NB, Oien KA, Lowy AM, Brunton VG, Frame MC, Evans TR, Sansom OJ. Mutant p53 drives metastasis and overcomes growth arrest/senescence in pancreatic cancer. PNAS. 2010; 107:246–251.
16. Weissmueller S, Manchado E, Saborowski M, Morris JPt, Wagenblast E, Davis CA, Moon SH, Pfister NT, Tschaharganeh DF, Kitzing T, Aust D, Markert EK, Wu J, et al. Mutant p53 drives pancreatic cancer metastasis through cell-autonomous PDGF receptor beta signaling. Cell. 2014; 157:382–394.
17. Yallowitz AR, Li D, Lobko A, Mott D, Nemajerova A, Marchenko N. Mutant p53 Amplifies Epidermal Growth Factor Receptor Family Signaling to Promote Mammary Tumorigenesis. Mol cancer res. 2015.
18. Alexandrova EM, Yallowitz AR, Li D, Xu S, Schulz R, Proia DA, Lozano G, Dobbelstein M, Moll UM. Improving survival by exploiting tumour dependence on stabilized mutant p53 for treatment. Nature. 2015.
19. Li D, Yallowitz A, Ozog L, Marchenko N. A gain-of-function mutant p53-HSF1 feed forward circuit governs adaptation of cancer cells to proteotoxic stress. Cell death dis. 2014; 5:e1194.
20. Blagosklonny MV, Toretsky J, Neckers L. Geldanamycin selectively destabilizes and conformationally alters mutated p53. Oncogene. 1995; 11:933–939.
21. Silwal-Pandit L, Vollan HK, Chin SF, Rueda OM, McKinney S, Osako T, Quigley DA, Kristensen VN, Aparicio S, Borresen-Dale AL, Caldas C, Langerod A. TP53 mutation spectrum in breast cancer is subtype specific and has distinct prognostic relevance. Clin cancer res. 2014; 20:3569–3580.
22. Hanel W, Marchenko N, Xu S, Yu SX, Weng W, Moll U. Two hot spot mutant p53 mouse models display differential gain of function in tumorigenesis. Cell death and differentiation. 2013; 20:898–909.
23. Vassilev LT, Vu BT, Graves B, Carvajal D, Podlaski F, Filipovic Z, Kong N, Kammlott U, Lukacs C, Klein C, Fotouhi N, Liu EA. *In vivo* activation of the p53 pathway by small-molecule antagonists of MDM2. Science. 2004; 303:844–848.
24. Dai C, Santagata S, Tang Z, Shi J, Cao J, Kwon H, Bronson RT, Whitesell L, Lindquist S. Loss of tumor suppressor NF1 activates HSF1 to promote carcinogenesis. J Clin Invest. 2012; 122:3742–3754.
25. Carpenter RL, Paw I, Dewhirst MW, Lo HW. Akt phosphorylates and activates HSF-1 independent of heat shock, leading to Slug overexpression and epithelial-mesenchymal transition (EMT) of HER2-overexpressing breast cancer cells. Oncogene. 2015; 34:546–557.
26. Ciocca DR, Arrigo AP, Calderwood SK. Heat shock proteins and heat shock factor 1 in carcinogenesis and tumor development: an update. Arch Toxicol. 2013; 87:19–48.
27. Santagata S, Hu R, Lin NU, Mendillo ML, Collins LC, Hankinson SE, Schnitt SJ, Whitesell L, Tamimi RM, Lindquist S, Ince TA. High levels of nuclear heat-shock factor 1 (HSF1) are associated with poor prognosis in breast cancer. PNAS. 2011; 108:18378–18383.
28. Powers MV, Clarke PA, Workman P. Dual targeting of HSC70 and HSP72 inhibits HSP90 function and induces tumor-specific apoptosis. Cancer cell. 2008; 14:250–262.
29. Powers MV, Workman P. Targeting of multiple signalling pathways by heat shock protein 90 molecular chaperone inhibitors. Endocrine-related cancer. 2006; 13:S125–135.
30. Xi C, Hu Y, Buckhaults P, Moskophidis D, Mivechi NF. Heat shock factor Hsf1 cooperates with ErbB2 (Her2/Neu) protein to promote mammary tumorigenesis and metastasis. J Biol Chem. 2012; 287:35646–35657.
31. Dai C, Whitesell L, Rogers AB, Lindquist S. Heat shock factor 1 is a powerful multifaceted modifier of carcinogenesis. Cell. 2007; 130:1005–1018.
32. Schulz R, Streller F, Scheel AH, Ruschoff J, Reinert MC, Dobbelstein M, Marchenko ND, Moll UM. HER2/ErbB2 activates HSF1 and thereby controls HSP90 clients including MIF in HER2-overexpressing breast cancer. Cell death dis. 2014; 5:e980.
33. Moasser MM, Krop IE. The Evolving Landscape of HER2 Targeting in Breast Cancer. JAMA Oncol. 2015; 1:1154–1161.
34. Lang GA, Iwakuma T, Suh YA, Liu G, Rao VA, Parant JM, Valentin-Vega YA, Terzian T, Caldwell LC, Strong LC, El-Naggar AK, Lozano G. Gain of function of a p53 hot spot mutation in a mouse model of Li-Fraumeni syndrome. Cell. 2004; 119:861–872.

Yallowitz et al. *Cell Death and Disease* (2018)9:621
DOI 10.1038/s41419-018-0691-x

Cell Death & Disease

ARTICLE Open Access

Heat shock factor 1 confers resistance to lapatinib in ERBB2-positive breast cancer cells

Alisha Yallowitz[1,2], Amr Ghaleb[1], Lucas Garcia[1], Evguenia M. Alexandrova[1] and Natalia Marchenko[1]

Abstract

Despite success of ERBB2-targeted therapies such as lapatinib, resistance remains a major clinical concern. Multiple compensatory receptor tyrosine kinase (RTK) pathways are known to contribute to lapatinib resistance. The heterogeneity of these adaptive responses is a significant hurdle for finding most effective combinatorial treatments. The goal of this study was to identify a unifying molecular mechanism whose targeting could help prevent and/or overcome lapatinib resistance. Using the MMTV-ERBB2;mutant p53 (R175H) in vivo mouse model of ERBB2-positive breast cancer, together with mouse and human cell lines, we compared lapatinib-resistant vs. lapatinib-sensitive tumor cells biochemically and by kinome arrays and evaluated their viability in response to a variety of compounds affecting heat shock response. We found that multiple adaptive RTKs are activated in lapatinib-resistant cells in vivo, some of which have been previously described (Axl, MET) and some were novel (PDGFRα, PDGFRβ, VEGFR1, MUSK, NFGR). Strikingly, all lapatinib-resistant cells show chronically activated HSF1 and its transcriptional targets, heat shock proteins (HSPs), and, as a result, superior tolerance to proteotoxic stress. Importantly, lapatinib-resistant tumors and cells retained sensitivity to Hsp90 and HSF1 inhibitors, both in vitro and in vivo, thus providing a unifying and actionable therapeutic node. Indeed, HSF1 inhibition simultaneously downregulated ERBB2, adaptive RTKs and mutant p53, and its combination with lapatinib prevented development of lapatinib resistance in vitro. Thus, the kinome adaptation in lapatinib-resistant ERBB2-positive breast cancer cells is governed, at least in part, by HSF1-mediated heat shock pathway, providing a novel potential intervention strategy to combat resistance.

Introduction

Human epidermal growth factor receptor 2 (Her2, ERBB2) is overexpressed in about 25% of sporadic human breast cancer cases, which correlates with poor prognosis[1]. Several ERBB2-targeted therapies are currently available that improve patients' outcomes, including a dual ERBB2/EGFR kinase inhibitor lapatinib[2]. However, acquired resistance to lapatinib remains a major concern for its clinical utilization.

Multiple mechanisms of lapatinib resistance are described in the literature. They primarily involve compensatory activation of receptor tyrosine kinases (RTKs), such as ERBB3, IGF1R, MET, FGFR2, FAK, Axl, as well as other mechanisms[2]. Importantly, not a single, but multiple RTKs have been shown to be activated in response to lapatinib[3]. Also, the substantial heterogeneity among adaptive RTKs exists in different cell lines in response to lapatinib[3]. This represents a major hurdle for the development of successful combinatorial strategies to reverse and/or prevent lapatinib resistance. Hence, identification and targeting of an upstream effector governing the kinome adaption in response to ERBB2 inhibition would help to overcome this clinical dilemma.

Correspondence: Natalia Marchenko (natalia.marchenko@stonybrook.edu)
[1]Department of Pathology, Stony Brook University, Stony Brook, NY 11794-8691, USA
[2]Weill Cornell Medicine, 1300 York Avenue, LC-902, New York, NY 10065, USA
Edited by R. Aqeilan

SPRINGER NATURE CDDpress

Our previous studies identified heat shock factor 1 (HSF1) as a key effector of ERBB2 signaling[4–6]. HSF1 is a transcription factor that controls a broad spectrum of pro-survival events essential for protecting cells from proteotoxic stress, which is caused by the accumulation of misfolded proteins in cancer cells. HSF1 activates transcription of genes that regulate protein homeostasis, including heat shock proteins (HSPs), Hsp27, Hsp70, and Hsp90[7], as well as supports other oncogenic processes such as cell cycle regulation, metabolism, adhesion, and protein translation[8, 9]. The impact of HSF1 on ERBB2-driven mammary tumorigenesis was unequivocally proven by in vivo studies. The genetic ablation of HSF1 suppresses mammary hyperplasia and reduces tumorigenesis in ERBB2 transgenic mice[10]. Consistently, the stability of ERBB2 protein is shown to be maintained by transcriptional targets of HSF1: Hsp70, Hsp90[11], and Hsp27[7].

Mutations in the *TP53* gene (mutp53) are the most frequent genetic events in ERBB2-positive breast cancer (72%)[12] and correlate with poor patient outcomes[13]. To recapitulate human ERBB2-positive breast cancer in mice, we previously generated a novel mouse model that combines activated ERBB2 (MMTV-ERBB2 allele[14]) with the mutp53 allele R172H corresponding to human hotspot mutp53 allele R175H[12]. We found that mutp53 accelerates ERBB2-driven mammary tumorigenesis[15]. The underlying molecular mechanism is a mutp53-driven oncogenic feed-forward loop governing a superior survival of cancer cells. We found that mutp53, through enhanced recycling and/or stability of ERBB2/EGFR, augments MAPK and PI3K signaling, leading to transcriptional phospho-activation of HSF1 at Ser326. Furthermore, mutp53 directly interacts with phospho-activated HSF1 and facilitates its binding to DNA-response elements, thereby stimulating transcription of HSPs[5]. In turn, HSPs more potently stabilize their oncogenic clients ERBB2, EGFR, mutp53, HSF1, thus reinforcing tumor development[5]. Consistently, we found that lapatinib not only suppresses tumor progression, but does so, at least in part, via inactivation of HSF1[15]. Furthermore, the interception of the ERBB2-HSF1-mutp53 feed-forward loop by lapatinib destabilizes mutp53 protein in Hsp90-dependent and Mdm2-dependent manner[4]. Since mutp53 ablation has been shown to have therapeutic effects in vivo[16], it is possible that mutp53 destabilization by lapatinib contributes to its anti-cancer activity.

In the present study, we identified HSF1 as an important upstream node responsible for the kinome adaptation of lapatinib-resistant cells. We found that lapatinib-resistant cancer cells have enhanced HSF1 activity, a superior resistance to proteotoxic stress, and lose their ability to degrade mutp53 in response to lapatinib. In contrast, HSF1 inhibition blocks lapatinib-induced kinome adaption and prevents the development of lapatinib resistance. Our data suggest a mechanism-based rationale for the clinical utilization of HSF1 inhibitors for the treatment of lapatinib-resistant ERBB2-positive breast cancer and/or—in combination with lapatinib—to prevent development of lapatinib resistance.

Results

Generation and characterization of human and mouse lapatinib-resistant ERBB2-positive breast cancer cell lines

To gain the mechanistic insight into lapatinib resistance we utilized two complementary approaches: in vitro and in vivo. For in vitro studies, we continuously cultivated human ERBB2-positive BT474 breast cancer cells in the presence of increasing concentrations (100–300 nM) of lapatinib for 6 months. All selected lapatinib-resistant clones were combined and maintained as a pool, as previously described[3]. Lapatinib-resistant cells approximately doubled their viability compared to lapatinib-sensitive cells (Fig. 1a), which was associated with decreased apoptosis in the presence of lapatinib (Fig. 1b).

To investigate lapatinib resistance acquired in vivo, we utilized the previously described MMTV-ERBB2;R172H mouse model of ERBB2-positive breast cancer ("R172H/+;ERBB2" hereafter)[15]. At the age of mammary microlesions (8-weeks old), R172H/+;ERBB2 females were given lapatinib (75 mg/kg three times a week) or vehicle by oral gavage, lifelong. Consistent with human data, lapatinib shows a tendency to delay tumor onset (from 256 to 319 days, median onset, $p = 0.091$) and significantly extended overall survival (from 321 to 362 days, median survival, $p = 0.014$) compared to vehicle-treated mice (Fig. 1c). However, after initial response (Fig. 1c) mammary tumors acquired lapatinib resistance and started to exhibit growth kinetics similar to vehicle-treated tumors (Fig. 4a).

We established cell lines from both vehicle-treated (lapatinib-sensitive; 1349, 1347, 1251, 1252, 1253) and lapatinib-treated (lapatinib-resistant; 125R) mouse mammary tumors. In contrast to previous studies using human ERBB2-positive breast cancer cell lines[3], our murine cell lines were derived from littermates, have an identical genetic background, the same mutation and acquired lapatinib resistance in vivo (with normal gland architecture, tumor microenvironment, immune system status), and therefore should better reflect the resistance mechanisms encountered in patients in the clinic. The short-term cell viability assay and the long-term colony formation assays both confirmed that the established cell lines continued to maintain their lapatinib resistance acquired in vivo (Fig. 1d, e).

To test for possible compensatory mechanisms induced in vivo, we performed the kinome profiling of 39 activated

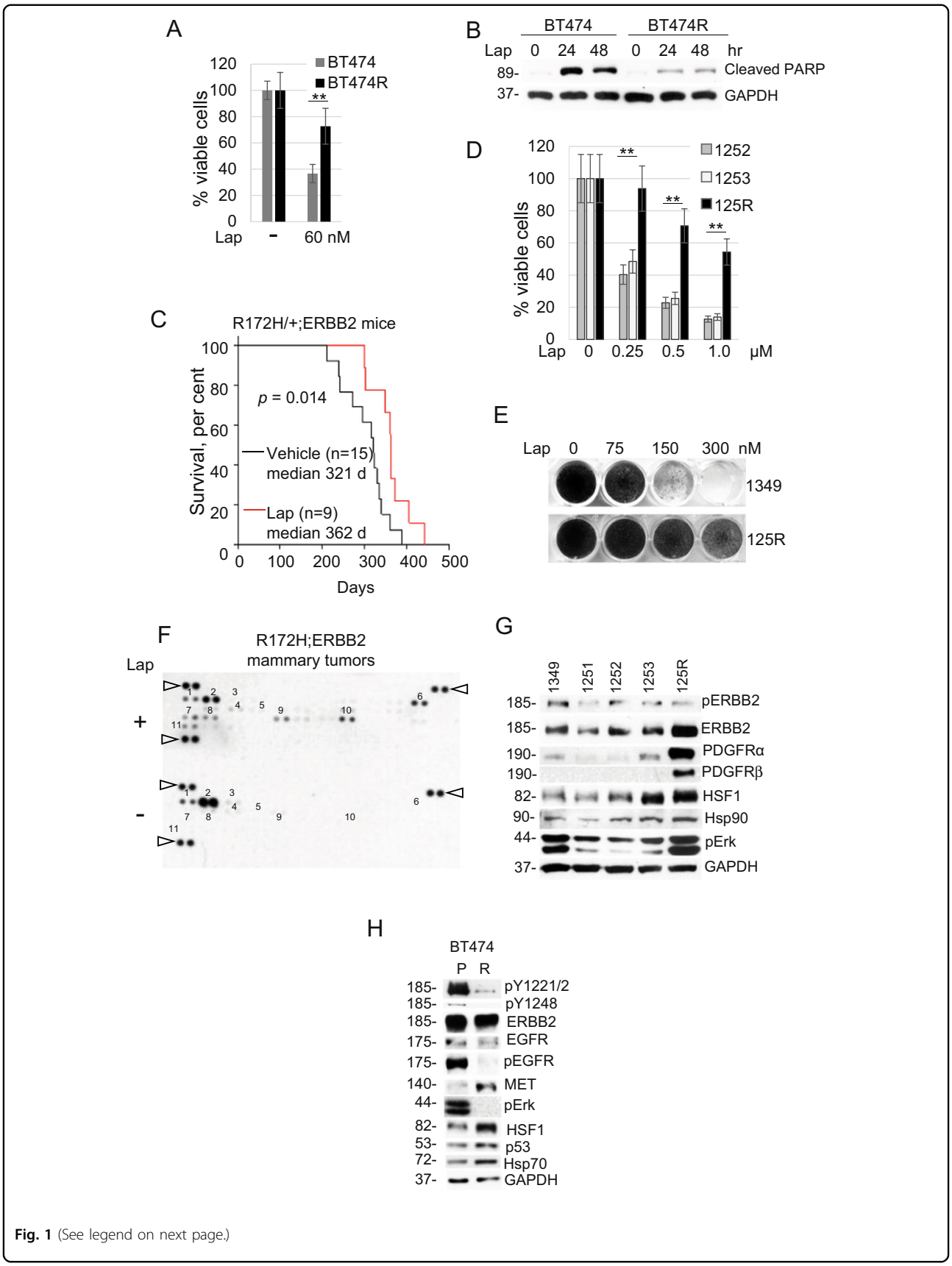

Fig. 1 (See legend on next page.)

(see figure on previous page)
Fig. 1 Generation and characterization of lapatinib-resistant human and mouse Her2-positive cancer cell lines. a, **b** Lapatinib-resistant human BT474R cells exhibit a two-fold increased viability after 48 h treatment with lapatinib (**a**) and a significantly decreased apoptosis after treatment with 300 nM lapatinib for indicated times (measured by cleaved PARP, **b**) compared to lapatinib-sensitive parental BT474 cells. **b** Western blot analysis, GAPDH is a loading control. One representative experiment out of two independent experiments (each performed in triplicate) is shown; $^{**}p < 0.01$ for three technical replicas, Student's *t*-test (**a**). **c** Tumor onset is significantly delayed in R172H/+;ERBB2 females treated with 75 mg/kg lapatinib three times a week starting at 8 weeks of age lifelong (red line) compared to vehicle-treated siblings (black line). Kaplan–Meier analysis, log rank statistics. **d**, **e** Murine primary cell lines established from lapatinib-sensitive mammary tumors (1252, 1253, 1349) and from a lapatinib-resistant mammary tumor (125R) maintain lapatinib sensitivity and lapatinib resistance in vitro, respectively. **d** Short-term cell viability assay (48 h). One representative experiment out of two independent experiments (each performed in triplicate) is shown; $^{**}p < 0.01$ for three technical replicas, Student's *t*-test. **e** Long-term colony formation assay (4 weeks). **f** Lapatinib induces activation of multiple adaptive RTKs in vivo. Representative images of the mouse Phospho-RTK array kit comparing lapatinib-treated (i.e., lapatinib-resistant, top) with vehicle-treated (i.e., lapatinib-sensitive, bottom) tumors. 1. EGFR*, 2. ERBB2*, 3. ERBB3, 4. PDGFRα*, 5. PDGFRβ*, 6. Axl*, 7. NGFR, 8. VEGFR1*, 9. MUSK*, 10. EPHA2*, 11. EPHB2. Known Hsp90 clients are marked with an asterisk. Triangles mark reference spots. **g**, **h** Murine lapatinib-resistant 125R cells show upregulated PDGFRα and PDGFRβ compared to murine lapatinib-sensitive cells 1349, 1251, 1252, 1253 (**g**), while human lapatinib-resistant BT474R cells have upregulated MET and downregulated ErbB2 and EGFR signaling (measured by phospho-ERBB2 pY1221/2 and pY1248, two top panels, phospho-EGFR and their effector phospho-Erk), compared to parental BT474 cells (**h**). Note that both human and mouse lapatinib-resistant cells have upregulated HSF1 and its transcriptional targets Hsp90 (**g**) and Hsp70 (**h**). Western blot analysis, constitutive heat shock protein 70 (Hsc70) and GAPDH served as a loading control

RTKs in lapatinib-treated vs. vehicle-treated tumors, respectively. In lapatinib-treated tumors we found expected downregulation of phospho-activated ERBB2 and EGFR and upregulation of multiple compensatory RTKs (Fig. 1f), including previously described Axl[2] and novel RTKs, such as NFGR, MUSK, VEGFR1, PDGFRα, PDGFβ, EPHA2, and EPHB2 (Fig. 1f). These results suggest a robust kinome reprogramming and a switch to multiple alternative RTKs in lapatinib-resistant cells. Consistently, we observed enhanced phospho-Erk, a common downstream RTK effector, in lapatinib-resistant 125R murine cell line (Fig. 1g). We validated the arrays data by Western blot analysis of the cell lines established from murine mammary tumors. Consistent with the array, PDGFRα and PDGFRβ were upregulated in lapatinib-resistant 125R cells compared to lapatinib-sensitive cells (Fig. 1g). Interestingly, in human lapatinib-resistant BT474 PDGFRα and PDGFRβ were not upregulated, and, instead, MET was elevated (Fig. 1h). This difference likely reflects the heterogeneity in adaptive responses noted previously[3].

Despite the distinct adaptive RTK response in mouse vs. human lapatinib-resistant cancer cells, notably, they share an important common feature, i.e., stabilized PDGFRα, PDGFRβ, and MET that are maintained by Hsp90 (https://www.picard.ch/downloads/Hsp90interactors.pdf). Therefore, we hypothesized that HSF1-mediated heat shock response is causative to the observed adaptive RTKs upregulation in lapatinib-resistant cells. Indeed, this link is supported by the fact that six out of eight RTKs upregulated in lapatinib-resistant mammary tumors—Axl, VEGFR1, MUSK, PDGFRβ, PDGFRα, EPHA2—are known Hsp90 clients (www.picard.ch/downloads/Hsp90interactors.pdf).

Lapatinib-resistant breast cancer cells are resistant to proteotoxic stress

To test whether HSF1-induced heat shock response is involved in the kinome adaptation of lapatinib-resistant cells, we compared their viability under the proteotoxic stress condition with lapatinib-sensitive cells. We found both the cells that acquired lapatinib resistance in vitro (Fig. 2a) and in vivo (Fig. 2b) to be more resistant to the proteotoxic stress induced by the proteasome inhibitor MG132 (Fig. 2c) and heat shock (Fig. 2d), which correlated with reduced apoptosis measured by PARP cleavage (Fig. 2c, d).

HSF1 reveals its protective role under proteotoxic stress via transcriptional activation of HSPs by transcriptionally active pSer326-HSF1. Indeed, upon proteotoxic stress induced by heat shock (Fig. 2e) and proteasome inhibition (Fig. 2f) lapatinib-resistant BT474 cells show a higher level of pSer326-HSF1. Since pSer326-HSF1 antibodies are human specific, we tested activity of pHSF1 in murine lapatinib-resistant 125R cells by the level of HSF1 transcriptional targets Hsp70 and Hsp90, and again found their significant upregulation upon proteotoxic stress induced by heat shock (Fig. 2g) and proteasome inhibition (Fig. 2h). These data indicate that lapatinib resistance correlates with augmented HSF1 function, and, as a result, with a superior tolerance to proteotoxic stress.

Lapatinib fails to modulate the ERBB2–HSF1–mutp53 axis in lapatinib-resistant breast cancer cells

Previously we showed that lapatinib destabilizes mutp53 via inhibition of HSF1 activity[4]. We now tested the effect of lapatinib on mutp53 levels in lapatinib-resistant BT474 cells (Fig. 3a) and found that lapatinib lost its ability to destabilize mutp53 even at higher doses (Fig. 3a), likely as a result of chronic HSF1 activity. Indeed, lapatinib did not

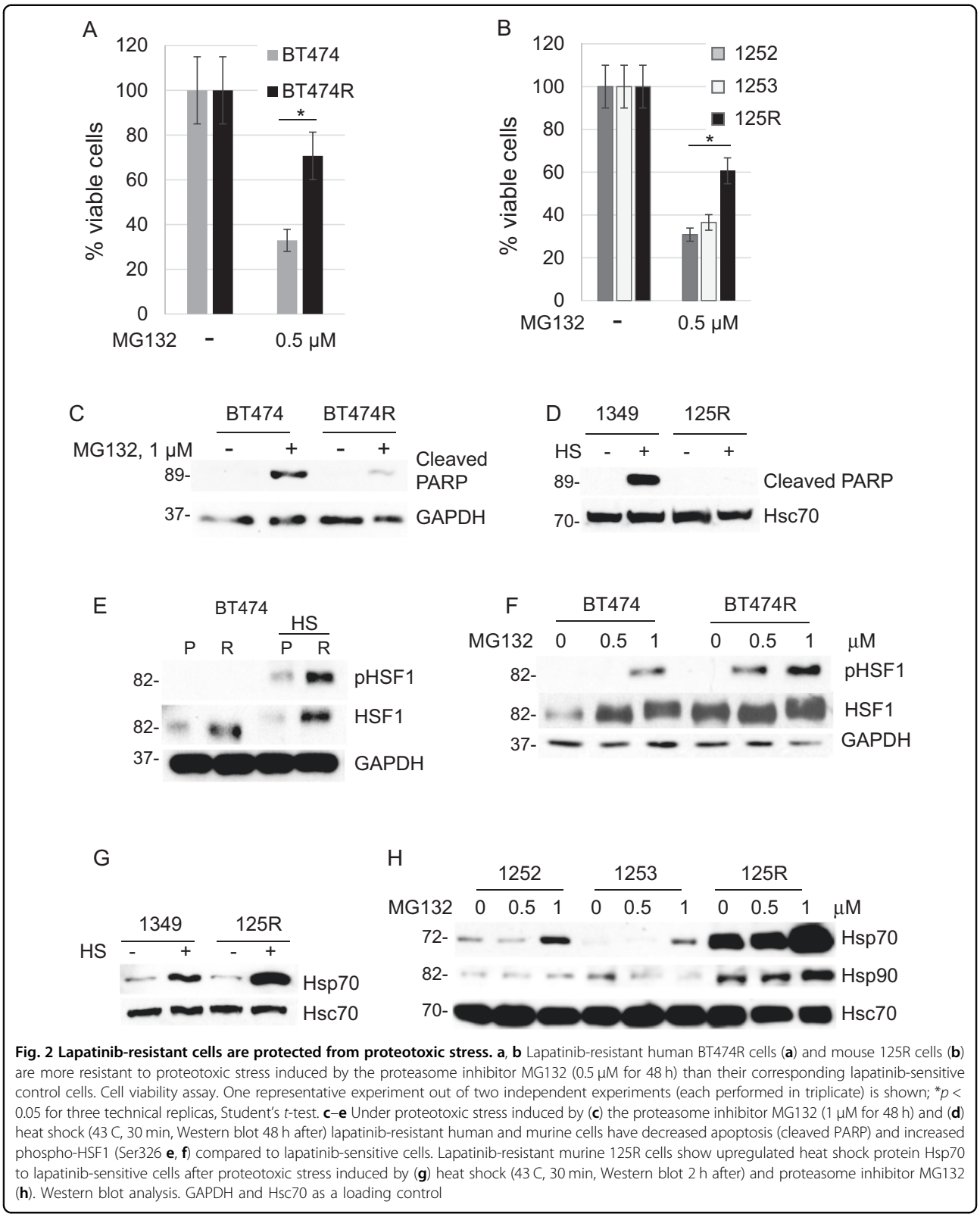

Fig. 2 Lapatinib-resistant cells are protected from proteotoxic stress. a, **b** Lapatinib-resistant human BT474R cells (**a**) and mouse 125R cells (**b**) are more resistant to proteotoxic stress induced by the proteasome inhibitor MG132 (0.5 μM for 48 h) than their corresponding lapatinib-sensitive control cells. Cell viability assay. One representative experiment out of two independent experiments (each performed in triplicate) is shown; *$p <$ 0.05 for three technical replicas, Student's *t*-test. **c**–**e** Under proteotoxic stress induced by (**c**) the proteasome inhibitor MG132 (1 μM for 48 h) and (**d**) heat shock (43 C, 30 min, Western blot 48 h after) lapatinib-resistant human and murine cells have decreased apoptosis (cleaved PARP) and increased phospho-HSF1 (Ser326 **e**, **f**) compared to lapatinib-sensitive cells. Lapatinib-resistant murine 125R cells show upregulated heat shock protein Hsp70 to lapatinib-sensitive cells after proteotoxic stress induced by (**g**) heat shock (43 C, 30 min, Western blot 2 h after) and proteasome inhibitor MG132 (**h**). Western blot analysis. GAPDH and Hsc70 as a loading control

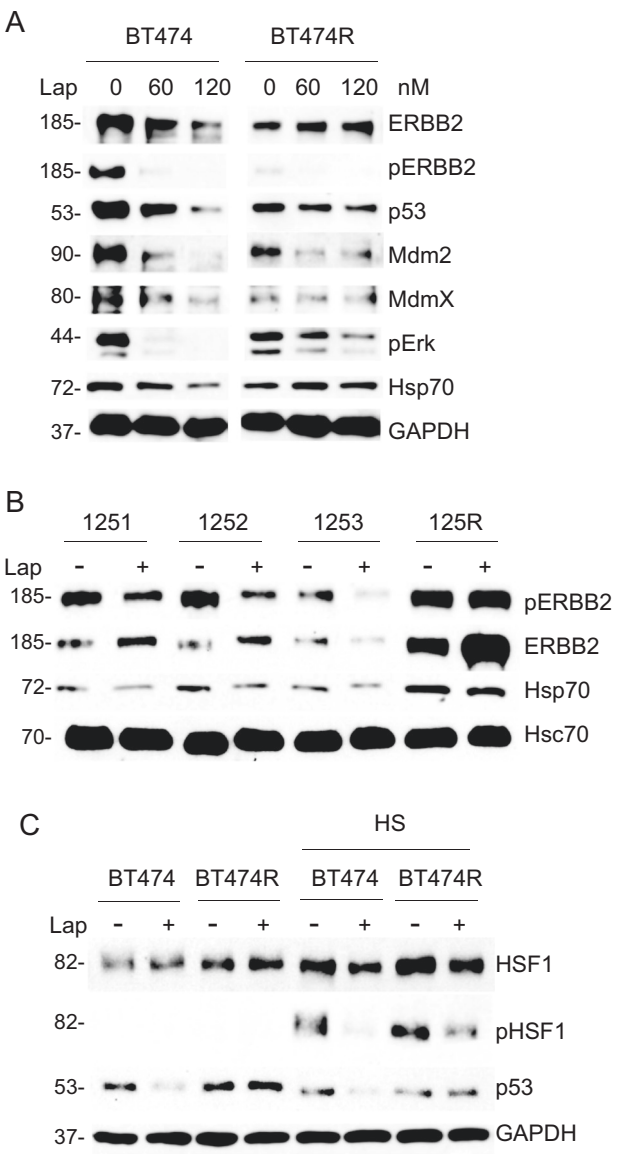

Fig. 3 Lapatinib fails to modulate the ErbB2–HSF1–mutp53 axis in lapatinib-resistant cells. a Downregulation of HSF1, mutp53, and Mdm2 in lapatinib-sensitive parental BT474, but not in lapatinib-resistant BT474R cells, treated with indicated lapatinib concentrations for 24 h (**a**). **b** Lapatinib (300 nM, 48 h) blocks ERBB2 activation (measured by phospho-ERBB2) and its downstream effector Hsp70 in murine lapatinib-sensitive (1251, 1252, 1253), but not in lapatinib-resistant 125R cells. Hsc70 served as a loading control. **c** Lapatinib (300 nM, 24 h) blocks HSF1 activation (measured by phospho-Ser326) in human lapatinib-sensitive BT474, but not in lapatinib-resistant BT474R cells after heat shock (42°C, 30 min). Cells were pre-treated with lapatinib followed by heat shock. Western blot analyses. GAPDH as a loading control

suppress HSF1 transcriptional target Hsp70, compared to lapatinib-sensitive cells, and failed to induce auto-degradation of Mdm2 and its bona fide substrates MdmX and mutp53 (Fig. 3a). Since previous studies identified highly stabilized mutp53 protein as an essential pro-survival factor in cancer cells[17], mutp53 depletion by lapatinib in lapatinib-sensitive cells could further enhance lapatinib's efficiency, while unresponsive high levels of mutp53 in lapatinib-resistant cells might contribute to the resistance mechanism. Similarly, lapatinib inhibited ERBB2 signaling (measured by phospho-ERBB2) and Hsp70 levels in sensitive murine lines, but failed to do so in the lapatinib-resistant murine 125R cells (Fig. 3b).

Proteotoxic stress induced by heat shock leads to transcriptional activation of HSF1 by Ser326 phosphorylation in both lapatinib-sensitive and resistant BT474 cells. However, lapatinib prevents phospho-activation of HSF1 after heat shock only in lapatinib-sensitive cells (Fig. 3c, compare lanes 5 and 6), but not in lapatinib-resistant BT474 cells (Fig. 3c, compare lanes 7 and 8). Most likely, HSF1 lost its dependency on the ERBB2 signaling in lapatinib-resistant cells due to the switch to alternative RTKs and their downstream effectors like Erk and Akt[17, 18], which reconstitutes HSF1 function and supports cells survival after ERBB2 inhibition[19].

Altogether, these data reinforce that despite of the heterogeneity of adaptive responses, tumors acquire lapatinib resistance, at least in part, via unified HSF1-guided mechanism that feeds into stabilization of mutp53.

Lapatinib-resistant breast cancer cells are sensitive to Hsp90 inhibition

Since the majority of adaptive RTKs that we identified in vivo (Fig. 1f) are known Hsp90 clients, we hypothesized that lapatinib-resistant cells retain their sensitivity to Hsp90 inhibitors. To test this hypothesis, we used ganetespib, a new generation Hsp90 inhibitor, which is currently in several clinical trials[20]. First, we tested the effect of ganetespib in vivo, using R172H/+;ERBB2 mice with mammary tumors that have been previously treated with lapatinib until they acquired resistance, i.e., lapatinib no longer suppressed their growth. Starting with the same average tumor size in each group, we designated three groups of animals (Fig. 4a): (i) animals previously treated with vehicle were continued on vehicle (Veh/Veh); (ii) animals previously treated with lapatinib (i.e., lapatinib-resistant) were continued on lapatinib alone (75 mg/kg three times a week lifelong) (Lap/Lap); (iii) some animals previously treated with lapatinib (i.e., lapatinib-resistant) were continued on lapatinib (75 mg/kg three times a week lifelong) together with ganetespib (50 mg/kg once a week lifelong) (Lap/Lap + Gan).

Consistently with their lapatinib resistance, the tumors on lapatinib alone continued to grow fast, with the rate very similar to vehicle-treated tumors (Fig. 4a, solid vs. small-dash lines). In contrast, addition of ganetespib significantly suppressed growth of lapatinib-resistant tumors

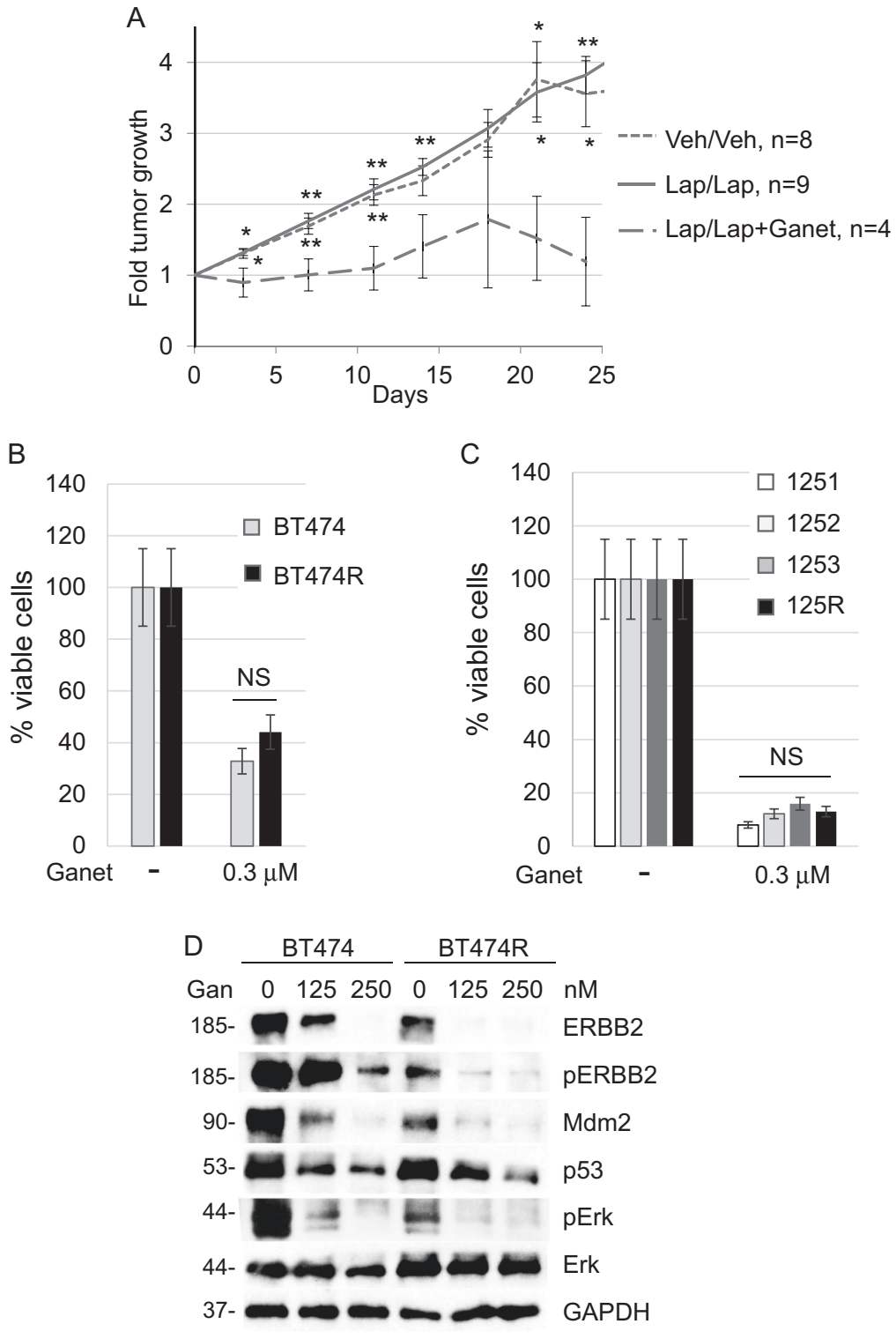

Fig. 4 (See legend on next page.)

(see figure on previous page)

Fig. 4 Lapatinib-resistant breast cancer cells are sensitive to Hsp90 inhibition. a R172H/+;ERBB2 female mice were treated either with vehicle or 50 mg/kg lapatinib (three times a week starting at 8 weeks of age) until tumors acquired lapatinib resistance, i.e., lapatinib no longer suppressed tumor growth. At this point, previously vehicle-treated mice were continued on vehicle (Veh/Veh), while previously lapatinib-treated mice continued to be treated with either lapatinib alone (Lap/Lap) or with lapatinib together with 50 mg/kg ganetespib once a week (Lap/Lap + Ganet), as described in Results. Note that the initial tumor size in all three groups was on average comparable. Tumor size was measured and plotted every 5 days. The treatment has been ended and mice were sacrificed when tumors in Veh/Veh and Lap/Lap arms reached the size of 3.5 cm^3. Note that while lapatinib-resistant tumors grew similarly to untreated tumors (did not respond to lapatinib), addition of ganetespib significantly suppressed tumor growth (wide-dash line). *$p < 0.05$, **$p < 0.01$, Student's *t*-test. Top asterisks compare the Lap/Lap + Ganet group with Lap/Lap, bottom asterisks compare the Lap/Lap + Ganet group with the Veh/Veh group. n number of independent tumors. **b**, **c** Lapatinib-sensitive human BT474 (**b**) and murine 125R (**c**) cells have similar sensitivity to ganetespib as their corresponding lapatinib-sensitive cells (BT474 and 1251, 1252, 1253, respectively). Cells were treated with DMSO or 0.3 μM ganetespib for 48 h, followed by the cell viability assay. One representative experiment out of two independent experiments (each performed in triplicate) is shown; NS non-significant. **d** Ganetespib (indicated concentrations, 24 h) inhibits ERBB2 signaling (measured by phospho-ERBB2 and phospho-Erk) and destabilizes mutp53 and Mdm2 in both, lapatinib-sensitive BT474 and lapatinib-resistant BT474R cells. Western blot analysis, GAPDH is a loading control

(Fig. 4a, wide-dash vs. small-dash lines). These data demonstrate that, despite lapatinib and ganetespib having overlapping targets (ERBB2, EGFR, mutp53), ganetespib overcomes lapatinib-resistant adaptive responses and efficiently curbs growth of lapatinib-resistant tumors in vivo. Consistently with these in vivo data, both human and mouse lapatinib-resistant cell lines were highly sensitive to ganetespib in vitro (Fig. 4b, c). As expected, ganetespib effectively inhibited ERBB2 signaling (measured by phospho-ERBB2) and—contrary to lapatinib—depleted mutp53 and Mdm2 in both lapatinib-sensitive and lapatinib-resistant cells (Fig. 4d). We speculate that ganetespib suppresses growth of lapatinib-resistant tumors via two complementary mechanisms: targeting of compensatory RTKs and release Mdm2 from the Hsp90 inhibitory complex, leading to mutp53 degradation.

HSF1 inhibition targets mutp53 and ERBB2 for degradation and suppresses growth of lapatinib-resistant breast cancer cells

Although Hsp90 inhibition seems to be an effective strategy to overcome lapatinib resistance, it has significant limitations. Hsp90 inhibitors have been shown to activate HSF1-mediated heat shock response, which in the long run protects cancer cells from apoptosis[7].

Therefore, the efficacy of Hsp90 inhibitors is limited by HSF1 function. Thus, we set to test the effect of specific HSF1 inhibitor KRIBB11 (N2-(1H-indazole-5-yl)-N6-methyl-3-nitropyridine-2,6-diamine)[21] on lapatinib-resistant vs. lapatinib-sensitive cells. Consistently with a previous report[22], KRIBB11 inhibits HSF1 phosphorylation with or without proteotoxic stress (MG132) (Fig. 5a). As a readout of HSP suppression, KRIBB11 also dose-dependently suppressed Hsp90 clients ERBB2, mutp53 and Mdm2 in both lapatinib-sensitive and lapatinib-resistant human BT474 and mouse 125R cancer cells (Fig. 5b, c). Similarly, to Hsp90 inhibition by ganetespib (Fig. 4d), KRIBB11 reactivated Mdm2 E3 ligase activity as manifested by downregulation of Mdm2 ubiquitination substrates MdmX, mutp53, and Mdm2 itself (Fig. 5b), which was rescued by the proteasome inhibitor MG132 (Fig. 5a, lanes 3, 4, Fig. 5d). These data indicate that HSF1 inhibition by KRIBB11 simultaneously targets both key oncogenic drivers, ERBB2 and mutp53, in lapatinib-sensitive and lapatinib-resistant ERBB2-overexpressing breast cancer cells. As a result, KRIBB11 dose-dependently kills lapatinib-sensitive and lapatinib-resistant human (Fig. 5e) and mouse (Fig. 5f) breast cancer cells with comparable efficiency.

HSF1 inhibition suppresses adaptive RTK activation and overcome lapatinib resistance in ERBB2-positive breast cancer cells

Consistent with previous studies[3], we noted a substantial heterogeneity of adaptive responses in lapatinib-resistant cancer cells, including RTKs such as MET[3] and PDGFRα in human and mouse cells, respectively (Fig. 1). Interestingly, activation in response to lapatinib of both MET (Fig. 6a, b) and PDGFRα (Fig. 6c) occurred as quickly as 48 h after lapatinib treatment in lapatinib-resistant, as well as lapatinib-sensitive cells. It appears that it takes place at posttranscriptional level. RNAseg analysis of BT474 cells treated with lapatinib did not reveal induction of MET RNA transcript, while MET signaling was shown to be activated[3]. Since MET[22] and PDGFRα[23] are both Hsp90 clients, we asked if HSF1 inhibition by KRIBB11 would reverse MET and PDGFRα lapatinib-induced compensatory upregulation. Indeed, even the low KRIBB11 dose (1 μM, compare to Fig. 5b, e) alleviated lapatinib-induced MET upregulation in both lapatinib-sensitive and lapatinib-resistant BT474 cells (Fig. 6a, b). Moreover, KRIBB11 synergized with lapatinib in degrading mutp53 and EGFR in lapatinib-sensitive BT474 cells (Fig. 6a) and restored mutp53 responsiveness to lapatinib in lapatinib-resistant BT474R cells (Fig. 6b).

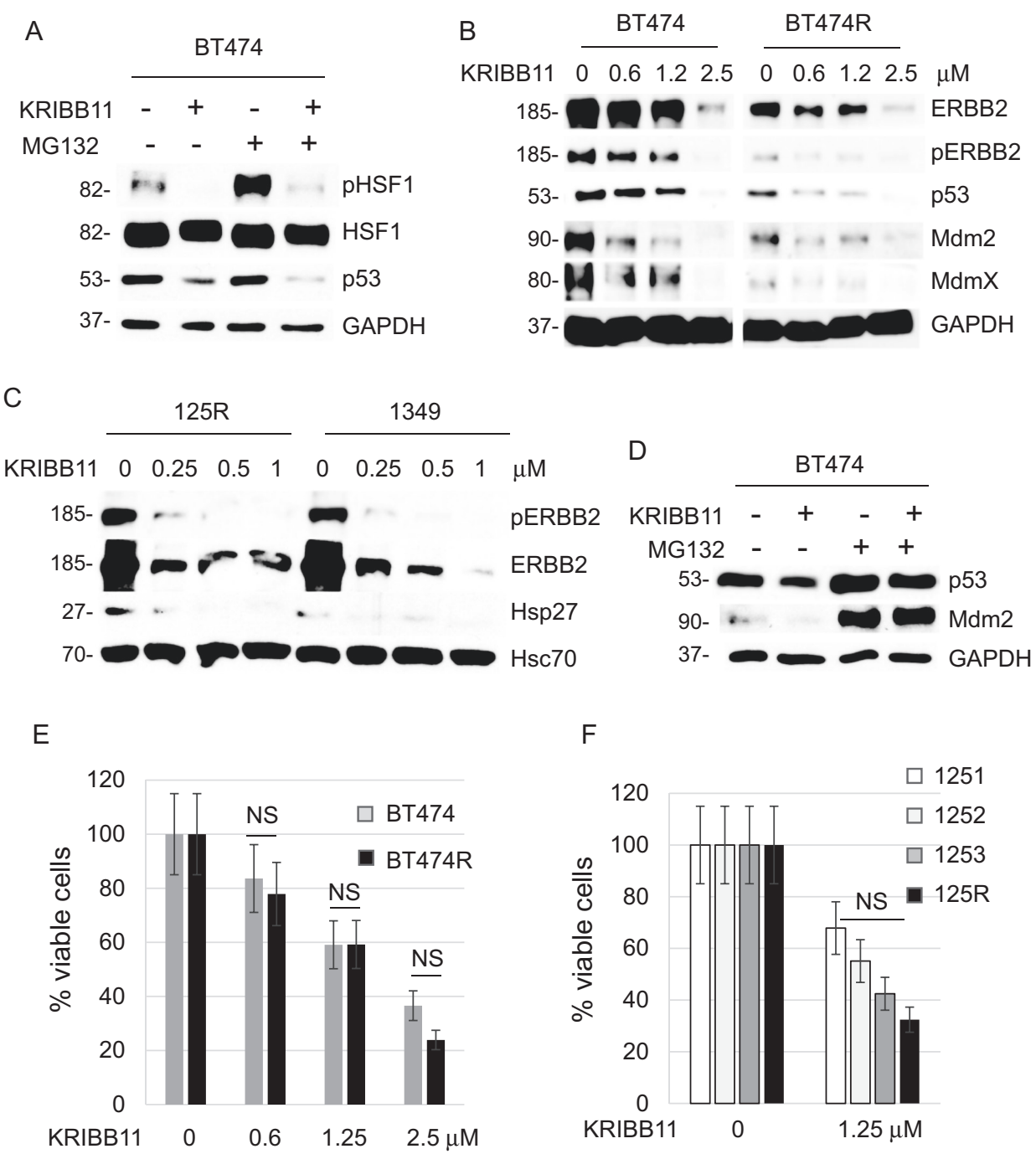

Fig. 5 HSF1 inhibition causes degradation of mutp53 and ErbB2, and suppresses growth of both lapatinib-sensitive and lapatinib-resistant cancer cells. a–**d** The HSF1 inhibitor KRIBB11 suppresses activation of HSF1 (measured by phospho-Ser326) after MG132-induced proteotoxic stress (1 μM, 2.5 h) in lapatinib-sensitive BT474 cells (**a**), suppresses ERBB2 signaling and destabilizes mutp53 in both lapatinib-sensitive BT474 and lapatinib-resistant BT474R cells (**b**), suppresses ERBB2 signaling and HSF1 target Hsp27 in both lapatinib-sensitive 1349 and lapatinib-resistant 125R murine cells (**c**); and induces degradation of mutp53 and Mdm2 in lapatinib-sensitive BT474 cells, which is rescued by the proteasome inhibitor MG132 (**d**). Cells were pre-treated with KRIBB11 (2.5 μM, 24 h) followed by MG132 treatment (1 μM, 2.5 h) (**a**) or simultaneously treated with KRIBB11 (2.5 μM) and MG132 (2.5 μM) for 24 h (**d**). Western blot analyses, GAPDH and Hsc70 served as a loading control. **e**, **f** The HSF1 inhibitor KRIBB11 suppresses growth of human BT474R (**e**) and mouse 125R (**f**) lapatinib-resistant cells as efficiently as their corresponding lapatinib-sensitive controls, BT474 and 1251, 1252, 1349 cells, respectively. Cells were treated with indicated concentrations of KRIBB11 for 48 h, followed by cell viability assays, which are shown relative to DMSO-treated cells. One representative experiment out of two independent experiments (each performed in triplicate) is shown; NS non-significant

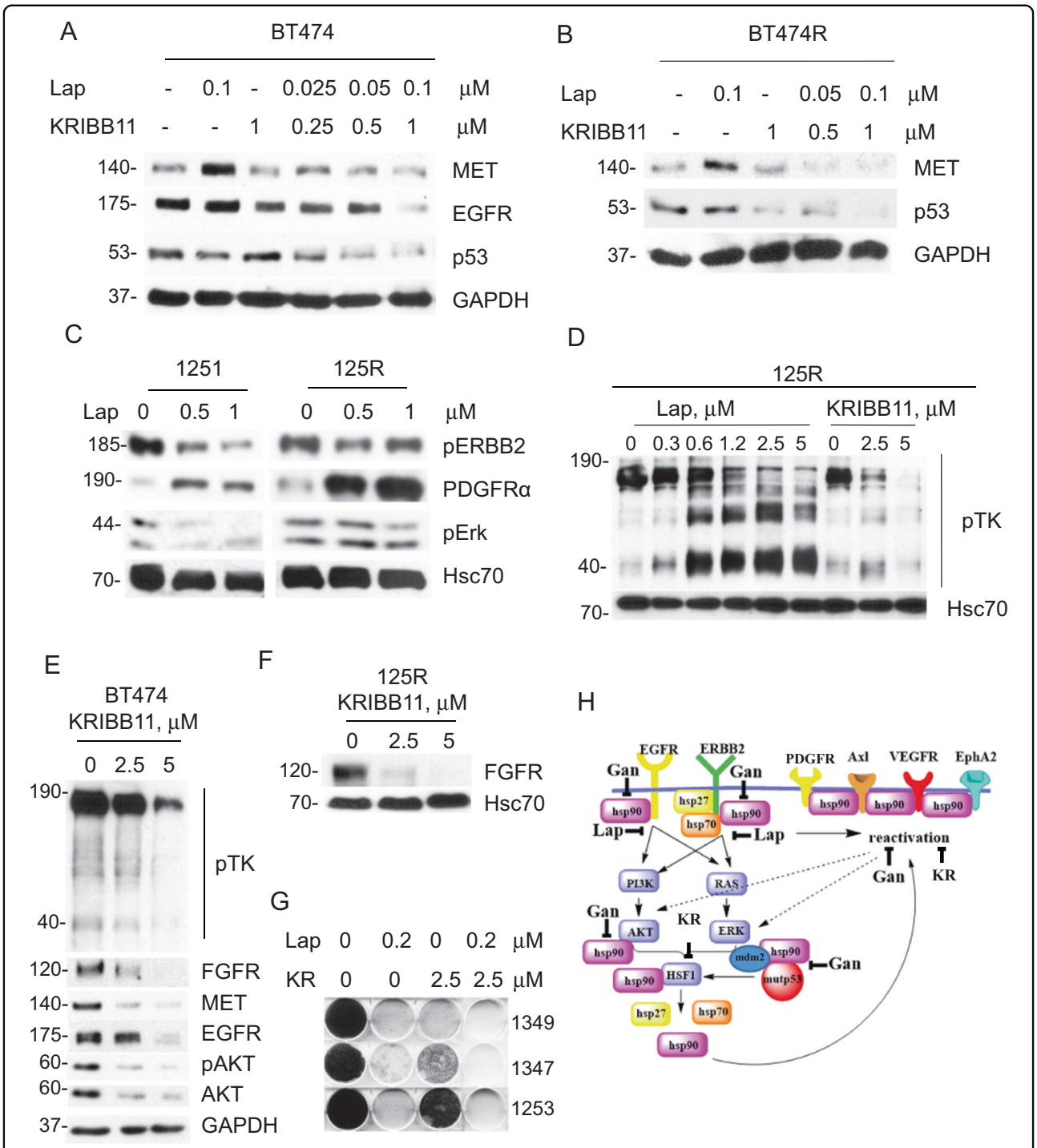

Fig. 6 HSF1 inhibition bypasses lapatinib-induced adaptive signaling and prevents the onset of lapatinib resistance. a, **b** While lapatinib (0.1 μM, 48 h) upregulates MET in both lapatinib-sensitive BT474 (**a**) and lapatinib-resistant BT474R (**b**) cells, HSF1 inhibitor KRIBB11 reverses this effect. Moreover, KRIBB11 synergizes with lapatinib in degradation of EGFR and mutp53 (**a**) and restores responsiveness of mutp53 to lapatinib (**b**). Western blot analyses, GAPDH is a loading control. **c**–**f** Lapatinib (at indicated concentrations, 48 h) induces PDGFRα in both lapatinib-sensitive 1251 and lapatinib-resistant 125R murine cells (**c**) and induces global kinome activation (measured by phospho-Tyr antibody, pTK) in lapatinib-resistant 125R cells (**d**), KRIBB11 inhibits the global pTK activity and individual kinases in 125R cells (**d**, **e**), and BT474 cells (**f**). Western blot analysis, Hsc70 and GAPDH are loading controls. **g** KRIBB11 cooperates with lapatinib (at indicated concentrations, for 4 weeks) in suppressing emergence of lapatinib-resistant colonies. Colony formation assay. Representative images out of two technical replicas. **h** The proposed model. ERBB2 signaling mediates HSF1 activation[4,16], which is potentiated by mutp53 via a feed-forward loop[5,15], thereby upregulating Hsp90 clients including compensatory RTKs and mutp53 itself. Inhibition of ERBB2 by lapatinib leads to inhibition of HSF1 transcriptional activity and therefore decreased Hsp90 and release of Mdm2 from its inhibitory complex with Hsp90[4,5] and subsequent degradation of mutp53 and Mdm2. KRIBB11 simultaneously inhibits diverse adaptive RTKs, as well as destabilizes potent oncogenic drivers—ERBB2, EGFR, and mutp53

In addition, global assessment of Tyr-phosphorylated proteins—as an indirect readout of overall levels of kinases—revealed an extensive and dose-dependent kinome activation in response to lapatinib in murine 125R cells (Fig. 6d, left), while HSF1 inhibition by KRIBB11 suppressed global kinome activation (Fig. 6d, right) and individual Hsp90 kinase clients, e.g., ERBB2/pERBB2 (Fig. 5c), FGFR (Fig. 6e). To ensure that these effects are specific only to cancer cells, we tested the effect of lapatinib on normal mammary epithelial cells (MECs) isolated from H/H;ERBB2 mice. We found that lapatinib increases total pTK activity only in cancer, but not in MECs (Suppl. Fig. 1), suggesting cancer-specific mechanism of lapatinib-induced kinome reprogramming. This result is consistent with previous study showing high level and activity of HSF1 specifically in human tumor biopsies, but not in normal mammary tissues[24]. Also, global pTK signal and individual Hsp90 client kinases, e.g., ERBB2, pERBB2 (Fig. 5b), FGFR, MET, EGFR, AKT, and pAKT (Figs. 5b, 6f), were downregulated in human BT474 cells in response to HSF1 inhibition in a dose-dependent manner.

Finally, a colony formation assay showed that while lapatinib-sensitive murine 1349, 1347, and 1253 cells treated with lapatinib or KRIBB11 alone did develop resistant clones, the combinatorial lapatinib/KRIBB11 treatment completely blocked the emergence of resistance (Fig. 6g). Taken together, these results indicate that HSF1 inhibition suppresses global activation of compensatory RTK pathways in response to lapatinib, and therefore can prevent the onset of lapatinib resistance.

Discussion

Although ERBB2-targeted therapies, such as lapatinib, revolutionized management of ERBB2-overexpressing breast cancer, primary and acquired resistance remains a major obstacle for the cure of this deadly disease. Therefore, understanding the mechanisms of lapatinib resistance will greatly facilitate development of successful combinatorial treatments with a durable therapeutic effect. In this study, we utilized an preclinical MMTV-ERBB2;mutp53 mouse model to investigate the mechanism of lapatinib resistance acquired in vivo in ERBB2-positive mammary tumors and to compare them to the resistance mechanisms acquired in vitro.

In both in vivo and in vitro scenarios, we found a robust kinome re-organization in response to ERBB2 inhibition by lapatinib. In agreement with previous studies[3], a substantial heterogeneity of adaptive responses was observed in lapatinib-resistant cancer cells, including previously described (Axl, MET)[2] and novel upregulated pathways, such as NFGR, MUSK, VEGFR1, PDGFRα, PDGFRβ, EPHA2, and EPHB2 (Fig. 1f). This multifaceted nature of compensatory responses underscores the difficulty of choosing the most effective drug combination to prevent or overcome lapatinib resistance. In this study we uncovered a common pro-survival mechanism of lapatinib resistance acquired in vivo and in vitro, i.e., an augmented HSF1-mediated heat shock response.

The oncogenic cooperation between ERBB2 and HSF1 was noted previously. Several in vivo studies demonstrated a crucial role of HSF1 in the development of ERBB2-driven breast cancer[10]. Not surprisingly, HSF1 protein levels are elevated in 80% of breast cancer cases that are associated with poor prognosis[25]. Although no clinical studies have directly analyzed the levels of HSF1 or HSPs in lapatinib-resistant tumors, emerging clinical evidence strongly supports our main conclusion. Thus, Phase II clinical trial with an Hsp90 inhibitor tanespimycin (17-AAG) plus trastuzumab (ERBB2-targeted therapy) showed a significant anticancer activity in patients with ERBB2-positive trastuzumab-resistant metastatic breast cancer[25]. Another a Phase I trial of ganetespib in combination with paclitaxel and trastuzumab in trastuzumab-refractory patients with human ERBB2-positive metastatic breast cancer showed significant clinical benefit of Hsp90 inhibition in triplet therapy[26]. Altogether, these clinical data strongly support the idea that inhibition of HSF1 and its downstream effectors (e.g., Hsp90) is effective strategy to overcome the resistance to ERBB2-targeted therapies.

Furthermore, we previously demonstrated that HSF1 is an important downstream effector of ERBB2 signaling and that lapatinib inhibits transcriptional activation of HSF1, by suppressing its Ser326 phosphorylation[5]. Most likely, lapatinib affects HSF1 function by inhibiting MAPK and AKT activation, both of which can induce transcriptional phospho-activation of HSF1 at Ser326[18, 19]. On the other hand, upregulation of compensatory RTKs in lapatinib-resistant cells can induce sustained MAPK and AKT signaling leading to enhanced S326-HSF1 phosphorylation and HSF1 protein stability. In support of this hypothesis we observed higher HSF1 protein and S326-HSF1 level after heat shock in lapatinib-resistant cells (Figs. 1g, h, 2e, f). Our previous study has shown that ERBB2 inhibition in lapatinib-sensitive cells impedes HSF1 activation, leading to the release of Mdm2 from its inhibitory complex with Hsp90 and to mutp53 destabilization[4] (Figs. 3a, 6h). Strikingly, we now found that in lapatinib-resistant cells, lapatinib fails to modulate the ERBB2–HSF1–mutp53 axis (Fig. 3). Instead, HSF1 is constitutively activated and does not depend on the ERBB2 signaling (Fig. 3c), resulting in a superior tolerance of lapatinib-resistant cells to proteotoxic stress (Fig. 2).

We speculate that in lapatinib-resistant cells, the HSF1 function is restored by activation of adaptive RTKs and their downstream signaling components (Fig. 6h). In turn,

sustained expression of HSPs promotes stability of their clients, adaptive RTKs, thus maintaining continuous HSF1 function (Fig. 6h). Although some elements of this model await further investigation, here we identified HSF1 as an upstream node of the lapatinib resistance mechanisms and demonstrated that its inhibition (i) suppresses global tyrosine-phosphorylation (Fig. 6d, f), (ii) alleviates lapatinib-induced upregulation of specific adaptive RTKs (Fig. 6a, b, c), (iii) synergizes with lapatinib in degradation of mutp53 (Fig. 6a, b), and (iv) prevents development of lapatinib resistance, as measured by appearance of lapatinib-resistant colonies (Fig. 6g).

Importantly, HSF1 inhibition in lapatinib-resistant cells restores mutp53 destabilization in response to lapatinib (Fig. 6b). Highly stabilized mutp53 levels are required for mutp53 oncogenic gain-off-function[17], and mutp53 genetic and pharmacological ablation significantly suppresses malignant phenotypes in mutp53-carrying cancers[17]. Therefore, identification of compounds targeting mutp53 for degradation has a major translational impact for ERBB2-positive breast cancer therapy, given the high frequency of p53 mutations in this breast cancer subtype.

In sum, we showed that pharmacological inhibition of HSF1 simultaneously inhibits diverse adaptive responses endowing lapatinib resistance, as well as destabilizes potent oncogenic drivers of ERBB2-positive breast cancer, such as ERBB2, EGFR, and mutp53. Thus, targeting HSF1 and opens up a new therapeutic possibility for the clinical application of HSF1 inhibitors to prevent and/or delay onset of lapatinib resistance with a potential of the instant clinical translation.

Materials and methods

Human cancer cells

Human ERBB2-positive breast cancer cell line BT474 carrying E285K *TP53* mutation was purchased from ATCC in 2013. ATCC verifies cell's identity with short tandem repeat analysis. To generate lapatinib-resistant BT474R cell line, parental BT474 cells were cultivated in the presence of increasing concentrations (100–300 nM) of lapatinib for 6 months, as previously described[3]. No further cell's identity verification was performed. Unless indicated otherwise, lapatinib-resistant BT474R cells were routinely maintained in the presence of 300 nM lapatinib. Where shown, cells were treated with indicated concentrations of lapatinib (L-4899, LC Lab), MG132 (M7449, Sigma), ganetespib (STA-9090, Synta Pharmaceuticals, Lexington, MA, USA), KRIBB11 (385570, Calbiochem, Billerica, MA, USA). All cell viability assays were done using standard clonogenicity assays and CellTiter-Blue Cell Viability Assay (Promega, 96-well format with 5000 cells/well seeded 24 h prior). Prior to the CTB assay (Fig. 1a), cells were maintained in lapatinib-free media for 3 days. Cells were treated with drugs for 48 h, unless indicated otherwise, with drug concentrations as shown. Florescence was detected by SPECTRAmax M2 (Molecular Devices).

Animals

MMTV-ERBB2 mice harboring activated ERBB2 were from Jackson Labs (strain FVBN-Tg(MMTV-ERBB2) NK1Mul/J). mutp53 R172H mice were a gift from G. Lozano[27]. Generation of R172H/+;ERBB2 compound mice was described previously[15]. Eight weeks old R172H/+;ERBB2 littermate females, all on C57Bl6/J:FVB/N 50:50 background, were treated with vehicle (18% Cremophor/3.6% dextrose) or lapatinib (75 mg/kg three times a week) by oral gavage lifelong. When lapatinib-treated tumors acquired lapatinib resistance, animals were treated with either vehicle, lapatinib alone, or lapatinib with ganetespib, as described in the text. Ganetespib was prepared as previously described[17] and injected into the tail vein at 50 mg/kg once a week. At endpoint (tumor size ~3.5 cm^3) mice were sacrificed and some of lapatinib only treated tumors were used to establish cell cultures. Mice were treated according to the guidelines approved by the Stony Brook University Institutional Animal Care and Use Committee.

Establishing primary mammary tumor cell cultures

Mammary tumors were dissected from mice, rinsed three times in PBS, and sequentially digested with collagenase/hyaluronidase (37°C, 2 h), 0.05% Trypsin, DNAse I, and Dispase (Stem Cell Technology). The ensuing cell suspensions were treated with red blood cell lysis buffer, rinsed with PBS, resuspended in Opti-MEM medium (Gibco) and passed through a 40 μm mesh to remove cell chunks. Cells were plated on gelatin-coated plates and grown in CnT-BM1 medium (Cell-N-Tec). Unless indicated otherwise, lapatinib-resistant 125R cells derived from a lapatinib-resistant mammary tumor were routinely maintained in the presence of 300 nM of lapatinib. Heterozygous mutant p53 R172H/+ status was verified and confirmed by using genotyping primers[27] in all established mouse cell lines.

Immunoblot analysis and kinome arrays

For immunoblots, cell lysates with equal total protein content (2–20 μg) were blotted with antibodies to p53 (FL393), Mdm2, GAPDH, Hsc70 (all from Santa Cruz Biotechnology); Erk1, pErk1/2 (T202/Y204), EGFR, pEGFR (Y845), ERBB2, pERBB2 (Y1221/1222 and pY1248), MET, cleaved PARP, PDGFRα, PDGFRβ, FGFR, AKT, pAKT MdmX, pTK (all from Cell Signaling); HSF1, pHSF1 (S326), Hsp90, Hsp70, Hsp27 (all from Enzo Life Sciences Inc., Farmingdale, NY). All Western blots were repeated at least two times. The phospho-RTK array on primary mammary tumor cells was performed according

to the manufacturer's protocol (Mouse Phospho-RTK Array Kit, R&D Systems).

Statistical analysis

Unpaired two-tailed Student's *t*-test was used to calculate statistical significance (*p*-value). Kaplan–Meier analysis and log rank statistics were used to compare animal survival. All experiments were repeated in at least two biological replicas with three technical replicas each, unless indicated otherwise.

Acknowledgements
This work was supported by the Department of Defense grant W81XWH-16-1-0448 (BC151569) and the Carol Baldwin Breast Cancer Research Fund to N.M. and NIH/NCI grant K22CA190653-01A1 to E.M.A.

Conflict of interest
The authors declare that they have no conflict of interest.

Supplementary Information accompanies this paper at (https://doi.org/10.1038/s41419-018-0691-x).

Received: 29 January 2018 Revised: 6 May 2018 Accepted: 7 May 2018
Published online: 24 May 2018

References

1. Yarden, Y. & Pines, G. The ERBB network: at last, cancer therapy meets systems biology. *Nat. Rev. Cancer* **12**, 553–563 (2012).
2. D'Amato, V. et al. Mechanisms of lapatinib resistance in HER2-driven breast cancer. *Cancer Treat. Rev.* **41**, 877–883 (2015).
3. Stuhlmiller, T. J. et al. Inhibition of lapatinib-induced kinome reprogramming in ERBB2-positive breast cancer by targeting BET family bromodomains. *Cell Rep.* **11**, 390–404 (2015).
4. Li, D. & Marchenko, N. D. ErbB2 inhibition by lapatinib promotes degradation of mutant p53 protein in cancer cells. *Oncotarget* **8**, 5823–5833 (2017).
5. Li, D., Yallowitz, A., Ozog, L. & Marchenko, N. A gain-of-function mutant p53-HSF1 feed forward circuit governs adaptation of cancer cells to proteotoxic stress. *Cell Death Dis.* **5**, e1194 (2014).
6. Alexandrova, E. M. & Marchenko, N. D. Mutant p53-heat shock response oncogenic cooperation: a new mechanism of cancer cell survival. *Front. Endocrinol.* **6**, 53 (2015).
7. Ciocca, D. R., Arrigo, A. P. & Calderwood, S. K. Heat shock proteins and heat shock factor 1 in carcinogenesis and tumor development: an update. *Arch. Toxicol.* **87**, 19–48 (2013).
8. Dai, C., Whitesell, L., Rogers, A. B. & Lindquist, S. Heat shock factor 1 is a powerful multifaceted modifier of carcinogenesis. *Cell* **130**, 1005–1018 (2007).
9. Mendillo, M. L. et al. HSF1 drives a transcriptional program distinct from heat shock to support highly malignant human cancers. *Cell* **150**, 549–562 (2012).
10. Xi, C., Hu, Y., Buckhaults, P., Moskophidis, D. & Mivechi, N. F. Heat shock factor Hsf1 cooperates with ErbB2 (Her2/Neu) protein to promote mammary tumorigenesis and metastasis. *J. Biol. Chem.* **287**, 35646–35657 (2012).
11. Powers, M. V., Clarke, P. A. & Workman, P. Dual targeting of HSC70 and HSP72 inhibits HSP90 function and induces tumor-specific apoptosis. *Cancer Cell.* **14**, 250–262 (2008).
12. Cancer Genome Atlas N. Comprehensive molecular portraits of human breast tumours. *Nature* **490**, 61–70 (2012).
13. Rahko, E., Blanco, G., Soini, Y., Bloigu, R. & Jukkola, A. A mutant TP53 gene status is associated with a poor prognosis and anthracycline-resistance in breast cancer patients. *Eur. J. Cancer* **39**, 447–453 (2003).
14. Yallowitz, A. R. et al. Mutant p53 amplifies epidermal growth factor receptor family signaling to promote mammary tumorigenesis. *Mol. Cancer Res.* **13**, 743–754 (2015).
15. Schulz, R. et al. HER2/ErbB2 activates HSF1 and thereby controls HSP90 clients including MIF in HER2-overexpressing breast cancer. *Cell Death Dis.* **5**, e980 (2014).
16. Alexandrova, E. M. et al. Improving survival by exploiting tumour dependence on stabilized mutant p53 for treatment. *Nature* **523**, 352–356 (2015).
17. Dai, C. et al. Loss of tumor suppressor NF1 activates HSF1 to promote carcinogenesis. *J. Clin. Invest.* **122**, 3742–3754 (2012).
18. Carpenter, R. L., Paw, I., Dewhirst, M. W. & Lo, H. W. Akt phosphorylates and activates HSF-1 independent of heat shock, leading to Slug overexpression and epithelial-mesenchymal transition (EMT) of HER2-overexpressing breast cancer cells. *Oncogene* **34**, 546–557 (2015).
19. Powers, M. V. & Workman, P. Targeting of multiple signalling pathways by heat shock protein 90 molecular chaperone inhibitors. *Endocr. Relat. Cancer* **13**, S125–S135 (2006).
20. Friedland, J. C. et al. Targeted inhibition of Hsp90 by ganetespib is effective across a broad spectrum of breast cancer subtypes. *Invest. New Drugs* **32**, 14–24 (2014).
21. Yoon, Y. J. et al. KRIBB11 inhibits HSP70 synthesis through inhibition of heat shock factor 1 function by impairing the recruitment of positive transcription elongation factor b to the hsp70 promoter. *J. Biol. Chem.* **286**, 1737–1747 (2011).
22. Choi, Y. J. et al. AUY922 effectively overcomes MET- and AXL-mediated resistance to EGFR-TKI in lung cancer cells. *PLoS ONE* **10**, e0119832 (2015).
23. Matei, D. et al. The platelet-derived growth factor receptor alpha is destabilized by geldanamycins in cancer cells. *J. Biol. Chem.* **282**, 445–453 (2007).
24. Santagata, S. et al. High levels of nuclear heat-shock factor 1 (HSF1) are associated with poor prognosis in breast cancer. *Proc. Natl Acad. Sci. USA* **108**, 18378–18383 (2011).
25. Modi, S. et al. HSP90 inhibition is effective in breast cancer: a phase II trial of tanespimycin (17-AAG) plus trastuzumab in patients with HER2-positive metastatic breast cancer progressing on trastuzumab. *Clin. Cancer Res.* **17**, 5132–5139 (2011).
26. Jhaveri, K. et al. A phase I trial of ganetespib in combination with paclitaxel and trastuzumab in patients with human epidermal growth factor receptor-2 (HER2)-positive metastatic breast cancer. *Breast Cancer Res.* **19**, 89 (2017).
27. Lang, G. A. et al. Gain of function of a p53 hot spot mutation in a mouse model of Li-Fraumeni syndrome. *Cell* **119**, 861–872 (2004).

Low-dose but not high-dose γ-irradiation elicits dominant negative effect of mutant p53 *in vivo.*

Amr Ghaleb[1*], Lucia Roa[1] and Natalia Marchenko[1*]

1 Department of Pathology, Stony Brook University, Stony Brook, NY 11794-8691, USA.

*** Corresponding author:** Amr Ghaleb amr.ghaleb@stonybrookmedicine.edu

Natalia Marchenko natalia.marchenko@stonybrookmedicine.edu

Abstract:

Contrary to high doses irradiation (HDR), the biological consequences of dose irradiation (LDR) in breast cancer remain unclear due to the complexity of human epidemiological studies. LDR induces DNA damage that activates p53-mediated tumor-suppressing pathways promoting DNA repair, cell death, and growth arrest. Monoallelic p53 mutations are one of the earliest and the most frequent genetic events in many subtypes of cancer. Using MMTV/ErbB2 mutant p53 (R172H) heterozygous mouse model we found differential p53 genotype-specific effect of LDR vs. HDR on mammary tumorigenesis. In mutant p53 tumors, LDR, but not HDR, causes p53 loss-of-heterozygosity. Following LDR, mutant p53 tumor cells exhibit aberrant ATM/DNA-PK signaling with defects in sensing of double-strand DNA brakes, leading to deficient DNA repair. In contrast, HDR-induced genotoxic stress is sufficient to reach the threshold of DNA damage that is necessary for wtp53 induced DNA repair and cell cycle arrest. As a result, LDR promotes genomic instability in mutant p53 cells leading to the selection of a proliferative death-resistant population, with negligible mutagenic effect on tumors carrying wtp53.

Keywords: mutant p53, low-dose γ-radiation, DNA damage, ATM, DNA-PK.

1. Introduction:

The tumor suppressor, p53 plays a pivotal role in promoting DNA repair, cell death, and growth arrest in response to DNA damage induced by conventional genotoxic modalities [1]. TP53 is the most frequently mutated gene in human breast cancer and, particularly, in Her2(ErbB2)-positive breast cancer (72%) and triple-negative breast cancer (TNBC, 80%), where it is associated with resistance to therapies and poor outcomes for patients [2-4]. Initially, p53 point mutations occur only in one allele at the very early stages of mammary tumorigenesis (DCIS, Stage 1) that is followed by loss of the wild-type allele (loss of heterozygosity (LOH)) during tumor progression [5]. In heterozygous tumors, mutant p53 (mutp53) proteins are thought to exert oncogenic functions via dominant-negative effect (DNE) [by suppressing wild-type p53 (wtp53) function] and gain-of-function mechanism (GOF) [6]. Some *in vivo* studies support the concept of mutp53 DNE in heterozygous cells [7, 8]. However, recently published data contradict this hypothesis. The high frequency of p53LOH at the advanced stages (52% of stage 1 and only 20% of stage 2 breast cancer patients retain wtp53 allele [9]) suggests that the loss of wtp53 allele is required for tumor progression. In further support, recent *in vivo* studies demonstrated partially preserved wtp53 tumor-suppressive functions in mutp53 heterozygous tumors [9-11]. This conflicting data may be explained by differential genetic and cellular context, type of treatment, and the phenotypes that are being assessed for defining DNE [8, 12-20].

As a result of this controversy, mutp53 is not taken into consideration in a clinic for the therapy or screening modality choice. Therefore, a deeper understanding of the regulation of mutp53 oncogenic and wtp53 tumor-suppressive functions in the context of heterozygous tumors is needed for the development of optimal therapeutic options tailored for the early stages of mutp53 cancers that retain wtp53 allele.

Recently LDR has gained attention because of the increasing use of screening modalities in a clinic. LDR was shown to have hormesis [21, 22] and adaptive effect [23], which is quite different from HDR. Many investigations have indicated that LDR stimulates the proliferation of normal cells, such as rat mesenchymal stem cells, mouse bone marrow hematopoietic progenitor cells, and several human normal cell lines [24, 25], but LDR does not induce proliferation of tumor cells [26]. However, the lack of a deep understanding of the molecular mechanisms of LDR, and biomarkers, which may identify the most vulnerable population; the complexity, and the length of human epidemiological studies rise the growing concern about potential health risks of exposure to LDR.

Our previous study in MMTV/ErbB2 mouse model demonstrated that in R172H mutp53 heterozygous tumors, wtp53 preserves its ability to transactivate a number of its transcriptional targets leading to growth arrest after high dose irradiation generating a strong selective pressure for p53LOH [9]. Our previous data on the lack of DNE was confirmed by a follow-up study in AOM/DSS chemically-induced colorectal cancer mouse model carrying p53R248Q heterozygous tumors [27], indicating that observed effects are not limited to the type of p53 mutation or the tumor origin. As a continuance of exploring this paradigm, here we show that mutp53 exerts its DNE in response to DNA damage in a dose-dependent manner. We found striking differential p53 genotype-specific oncogenic effect of LDR vs. HDR on mammary tumorigenesis. We show that aberrant ATM/DNA-PK signaling causes defective sensing of double-strand DNA brakes, deficient DNA repair, and cell cycle progression of genomically unstable cells after LDR. In contrast, HDR-induced genotoxic stress is sufficient to reach the DNA damage threshold that is necessary for wtp53-mediated DNA repair program and cell cycle arrest in mutp53 heterozygous cells. In contrast, the HDR is sufficient to reach the threshold of DNA damage that is necessary for wtp53-mediated DNA repair program in mutp53 heterozygous cells. Consequently, LDR in the context of mutp53 heterozygous tumors elicits tumor progression, with negligent effect on wtp53 tumors. Collectively, results from our study suggest that early stages breast cancer patients carrying monoallelic p53 mutations are a potentially high-risk group for LDR exposure.

2. Materials and methods:

2.1. Mice

MMTV-ErbB2 mice carrying activated ErbB2 (strain FVBN-Tg(MMTV-ErbB2)NK1Mul/J) were from Jackson Labs. p53 R172H (called p53H/H) and control p53 null (p53-/-) mice (C57Bl6J background) were a gift from G. Lozano [17]. p53H/-;ErbB2 mice were generated by crossing ErbB2 mice with p53-/- mice and then breeding the p53+/-;ErbB2 progeny with p53H/H mice. p53H/-;ErbB2 mice were then crossed to generate p53H/H;ErbB2 and p53-/-;ErbB2 females for analysis. p53+/+;ErbB2 were generated from crossing of p53H/+;ErbB2 and p53+/-;ErbB2 mice. For all mice genotypes, only female littermates were used for all analyses. Animals were monitored weekly to determine their breast cancer and sarcoma onset and were promptly killed when their tumors reached 4 cm^3 in volume or when animals appeared moribund. Careful necropsies were performed, and tumors and all major organs were collected, fixed in 10% formalin, embedded in paraffin, and sectioned for histopathologic analysis. Mice were treated according to guidelines approved by the Institutional Animal Care and Use Committee at Stony Brook University.

2.2. Cell lines

Mouse mammary tumor cell lines: p53+/+;ErbB2, p53H/+;ErbB2 and p53-/+;ErbB2 were isolated from their corresponding mammary tumors and maintained in culture. P53H/-;ErbB2 cells were obtained from p53H/+;ErbB2 tumors with confirmed LOH and p53-/-;ErbB2 cells were obtained from p53-/+;ErbB2 tumors with confirmed LOH.

2.3. Gamma irradiation

Mice were exposed to total-body γ-irradiation with a 137Cs source, with a dose rate of 0.8 Gy/min, for a total of 0.1 Gy or 5 Gy when the tumor reached 1 mm^3. Another group of mice (sham) were placed in the room without being exposed to irradiation. Animals were either observed for survival post-irradiation or were killed by CO_2 asphyxiation followed by cervical dislocation at set times after irradiation, and the mammary tumors were removed for further analysis. All animals (irradiated or not) were monitored weekly to determine their breast cancer and sarcoma onset and were promptly killed when their tumors reached 3 cm^3 in volume, or ulcerated, or when animals appeared moribund. Necropsy, tumor removal, and fixation and analysis were carried out as described above. For γ-irradiation of cells, a 137Cs source with a dose rate of 0.8 Gy/min was used, for a total of 0.1 Gy or 9 Gy. Non-irradiated cells (sham) were placed in the room without being exposed to irradiation.

2.4. Immunofluorescence

For IF on cells, at the indicated times post-irradiation, media was aspirated from cells grown on chamber slides and washed once with PBS. For IF staining, cells were fixed in 4% buffered paraformaldehyde for 15 min at RT, which was then aspirated, and pre-chilled methanol was added, cells incubated at -20°C for 10 min, and then washed 3x with PBS. Cells were permeabilized with 0.2% Tween 20 in PBS at RT for 10 min. Cells were then incubated with blocking buffer [10% normal horse serum (NHS) and 0.1% Tween 20 in PBS], for 1 h at 37°C. Primary antibodies, diluted in blocking buffer, were added for 1 h at 37°C. The following primary antibodies were used: rabbit anti-γH2AX (Phospho-Histone H2A.X (Ser139)) (1:200, cell signal), mouse anti-phospho ATM (Ser1981) (1:200, cell signal), and mouse anti-γH2AX (1:200, Abcam). Following incubation, the cells were washed 3x with PBS. Respective Alexa fluor-labeled goat anti-rabbit or goat anti-mouse secondary antibodies (Molecular Probes) were then added at 1:500 dilution for 30 min at 37°C. The cells were then washed, counterstained with Hoechst 33258 (2 μg/ml), mounted with Prolong gold (Molecular Probes), and cover-slipped. Images were acquired at x600 total magnification using a Nikon Eclipse Ti-S microscope (Nikon Instruments) equipped with QI-Click camera (QImaging). Where applicable, quantification of staining foci number was performed on 10 images of randomly selected fields per genotype per treatment.

2.5. Cell cycle analysis

Cultured cells were harvested by trypsinization and pelleted by spinning at 1500 r.p.m. for 10 min. The cell pellet was washed twice with PBS, then fixed in 70% ethanol. The cells were pipetted gently up and down to loosen the cells in a suspension and stored at -20°C overnight. The cells were then pelleted by spinning at 1500 r.p.m. for 10 min, washed once in PBS, then resuspended in permeabilization buffer (0.25% tritonX100 in PBS) and incubated for 15 min at RT. The cells were then pelleted and resuspended in staining solution (20 μg/ml propidium iodide and 10 μg/ml RNase A in PBS), and incubated in the dark on ice for 30 min before analysis. Cell cycle analysis by flow cytometry was done at Stony Brook Flowcytometry Core Facility, using Becton Dickinson FACSCAN analyzer.

2.6. Immunoblot analysis

For immunoblots, cell lysates with equal total protein content (2–20 μg) were blotted with antibodies to p21, Gadd45, and Hsc70 (all from Santa Cruz Biotechnology); γH2AX (all from Cell

Signaling)). All immunoblots were repeated at least two times.

Determination of LOH of the *p53*+ locus

DNA was extracted from frozen mouse mammary tumors, using QIAmp DNA Micro Kit (Qiagen). An equal amount of DNA was used for PCR amplification of p53 locus using primers described before [17]. For loading control, we used primers for ROSA locus: [F], 5'-AAAGTCGCTCTGAGTTGTTAT-3', [R], 5'-TAAGCCTGCCCAGAAGACTC-3'. An equal volume of the amplified product was electrophoresed through a 1.5% agarose gel. Amplified DNA bands were visualized, and the image was captured using FluoroChem HD2 (ProteinSimple). LOH was determined based on the presence or absence of the amplified wild-type band.

2.7. Histological analysis

Mammary tumors were collected from mice at terminal point. Tumors were fixed and embedded for H&E staining and histological analysis. At least 4 tumors per group were analyzed blindly by an independent histopathologist. For mitotic figures, per tumor, 10 random fields were scanned at 200x and the total number of mitotic figures was recorded. Percent of necrotic/apoptotic areas and of cystic areas per field at 100x per tumor (10 random fields per tumor) was estimated and averaged, by the histopathologist.

2.8. Statistics and Reproducibility

All statistical analysis between groups was done using the t-test. Significance was determined at $p<0.05$. Cell culture experiments were repeated three times.

3. Results.

3.1. Low dose γ-radiation increases the growth rate of mutp53 heterozygous mammary tumors in MMTV-ErbB2 mouse model.

The understanding of the effects of environmental irradiation on tumorigenesis has profound clinical importance but is hampered by the difficulty of human epidemiological studies. Our previous study has identified a previously unknown oncogenic activity of mutant p53 (mutp53): the exacerbation of tumor progression after HDR irradiation of early mutp53 heterozygous premalignant mammary lesions [9]. Therefore, we set to investigate the effect of single-dose of HDR vs low dose radiation (LDR) of established mammary tumors (1 cm^3). For this study, we used the MMTV-ErbB2 mouse model harboring murine R172H (H thereafter) p53 mutation, which we previously described [9]. This mutation corresponds to human hotspot R175H mutation in ErbB2 breast cancer [29] and (http://www.cbioportal.org). The following p53 genotypes were used in this study p53+/+;ErbB2 (+/+ thereafter), p5-/+;ErbB2 (-/+ thereafter), p53H/+;ErbB2(H/+ thereafter), p53H/-;ErbB2 (H/- thereafter) and p53-/- (-/- thereafter). For this study, we selected 0.1 Gy irradiation, the dose equivalent to 6-8 computed tomography scans [30]. Consistent with our previous study using HDR, [9], wtp53 haploinsufficiency accelerates mammary tumorigenesis after LDR compared to +/+ mice. Median survival of +/+ mice after tumor onset was 66 days compared to 42 and 44 days respectively for H/+ and -/+ mice (figures 1A, 2A). Both, H/+ and -/+ mice had significantly faster tumor growth rate as compared to +/+ mice (figures 1D, 2A). HDR accelerates the growth of both H/+ and -/+ heterozygous tumors (compare figure 1D and 1E), suggesting that wtp53 haploinsufficiency augments tumorigenesis after high impact DNA damage. This data is consistent with our previous report on enhanced p53 heterozygous mammary tumor growth after HDR of mammary gland before tumor onset [9]. Interestingly, LDR demonstrates the profound negative impact on H/+ mammary tumor growth as indicated by significantly shorter survival (median survival 11.5 days compared to 60 for +/+ and 26 days for -/+) (figure 1C) and significantly faster tumor growth rate (figure 1F). Histological analysis of the tumors showed a differential effect of HDR vs LDR on H/+ tumors. In -/+ tumors there appeared to be a positive correlation between number of mitotic cells (proliferation) and necrosis/apoptosis, regardless of the treatment. In contrast, untreated and HDR H/+ tumors had significantly higher number of mitotic cells (proliferation) which correlated with high necrosis/apoptosis, while LDR H/+ tumors though having significantly high number of mitotic cells (proliferation), yet they had significantly low necrosis/apoptosis. In sum, our in vivo data

indicates that p53 haploinsufficiency determines the kinetics of tumor growth after high impact DNA damage, while mutp53 endows DNE promoting mammary tumorigenesis after low-impact DNA damage.

3.2. Low dose radiation drives dominant-negative effect in mutp53 heterozygous mammary tumors in MMTV-ErbB2 mouse model.

We have previously shown that in H/+ cancer cells wtp53, at least in part, preserves its transcriptional activity and enables partial G2/M arrest in response to HDR *in vitro* [9]. Therefore, we assessed the kinetics of tumor growth response of individual tumors after HDR vs. LDR (suppl. figure 1). The average volume of every individual tumor with a distinct p53 genotype was calculated (figures 2A-C). Consistent with our previous in vitro data [9], we found that HDR transiently suppresses H/+ and -/+ tumors growth (figure 2D), which resume growing after 8 weeks after irradiation. Strikingly, LDR demonstrates p53 genotype-specific effect promoting the growth of only H/+ tumors one week post-irradiation.

Our previous study identified a novel oncogenic function of mutp53. We found that the presence of the mutp53 allele promotes p53LOH as a readout of genomic instability when mice were 5Gy irradiated before tumor onset [9]. Therefore, to assess whether the acceleration of H/+ mammary tumorigenesis after LDR is due to the early onset of p53LOH, we genotyped mammary tumors from mice subjected to HDR vs LDR after tumor onset. Consistent with our previous observation in premalignant lesions [9], mutp53 augments p53LOH (86%) in H/+ established tumors while no p53LOH (0/6) was detected in -/+ tumors (figure 2E). Following LDR, 63% of H/+ tumors and 25% of -/+ tumors lost wtp53 allele (figure 2F). These results suggest that LDR may induce genomic instability and, thus, facilitates p53LOH leading to tumor progression. However, the fast kinetic of H/+ tumors growth and lower incidence of p53LOH after LDR (figure 2D&F) suggests that other than p53LOH mechanisms may contribute to tumor progression. As LDR was shown to modulate the immune response [21-23], we evaluated immune cells tumor infiltration with regard to p53 genotype and treatment. We did not observe a significant difference in the number of immune cells or spatial distribution at any experimental condition (data not shown). Collectively, our data suggest that LDR-induced genomic instability may provide the genomic plasticity for the selection of more aggressive, death-resistant cancer cells thus promoting tumor progression.

3.3. Differential cell cycle checkpoint to high dose γ-radiation as compared to low dose γ-radiation.

Upon genotoxic stress, wtp53 activates the transcription of genes involved in cell-cycle arrest and DNA repair or apoptosis, to protect the genome from the accumulation of mutations, while mutp53 may perturb these genome-guarding mechanisms and promote genomic instability [19,42]. Our previous study on cultured tumor cells originated from MMTV/ErbB2 mice with different p53 genotypes has demonstrated the lack of DNE of mutant p53 after HDR, as wtp53 retains its ability to induce G2/M checkpoint in H/+ cells [9]. Since our in vivo data suggests that LDR elicits DNE in H/+ cells, we compared cell-cycle profiles of cells with various genotypes 24 h after HDR vs. LDR. Non-irradiated +/+ and −/+ cells exhibited comparable cell-cycle profiles, whereas H/+ cells showed cell-cycle profile with lower G1 and S and significantly higher G2/M indicating an increased rate of proliferation (Figure 3A-F). This data is in agreement with our in vivo assessment of the mitotic index of untreated H/+ tumors (figure 1G).

Consistent with fast recovery from DNA-damage post HDR, +/+ cells did not significantly change G1 and S content and had a slight increase in G2/M arrest (Figure 3A). In −/+ cells, HDR induced G1 and G2/M arrest, and significantly reduced S-phase (Figure 3C). However, following, LDR, none of the cell genotypes showed any significant change in their cell cycle profile as compared to their non-irradiated controls (Figures 3B, D & F). In line with this data, LDR is insufficient to induce neither p21 (as an indicator of active cell cycle checkpoint or γH2AX (as a sensor of DNA double-strand breaks) (figure 3G). These results suggest the existence of the threshold of the DNA damage severity that is necessary to induce DNA repair and checkpoint arrest. We hypothesized that both p53 genotype and the extend of DNA damage are key factors determining the tumor progression.

3.4. In response to low dose γ-radiation mutant p53 abolishes DNA-damage repair response in a dominant-negative manner.

Next, we investigated the mechanisms by which LDR affects DDR in the context of p53 status. We stained the cells for the formation of γH2AX foci in response to HDR vs LDR. We analyzed the dynamics of γH2AX foci formation and resolve at different time points, at 0, 2, 4, 6, and 24 hrs, in response to HDR vs LDR in +/+, H/+ and -/+ cells (Figures 4 & 5).

We counted the percent of cells with ≥5 foci post-irradiation. Examples of γH2AX staining in untreated, HDR and LDR are shown in, respectively. At the basal level, approximately 10% or less of untreated cells of the 3 genotypes had ≥5 γH2AX foci with no significant difference between them (Figure 4A&D and Figure 5A&D). The percent of cells with ≥5 γH2AX foci was

significantly increased to approximately 100% at 2 and 4 hrs post-HDR in all 3 genotypes and then returned to the basal level by 24 hrs post-HDR in +/+ and H/+ (Figure 4A-D). However, +/+ cells show much faster kinetics of recovery from HDR than heterozygous cells (figure 4D) suggesting that p53 haploinsufficiency interferes with the efficient DNA repair, leading to lingering DNA damage. Consistent with the low levels of DNA damage, LDR leads to significantly lower γH2AX foci staining across all genotypes. Importantly, however, LDR leads to increase γH2AX foci staining twofold in +/+ and -/+ cells, but not in H/+ cells (figure 5A-D). Hence, after LDR mutp53 hinders the sensing of DNA double-strand brakes, and thus mitigates DNA repair in a DNE manner. In support of this notion, we observed stabilization of mutp53 after LDR, as no wtp53 stabilization was detected in +/+ and -/+ cells (figure 5E). Furthermore, LDR fails to induce Gadd45 in H/+ cells in a DN manner, as LDR is sufficient to induce Gadd45 in both +/+ and -/+ cells (figure 5E). Well known as p53 target, Gadd45 acts as a sensor of genotoxic stress-inducing the DNA damage response and growth arrest [31]. Consistent with delayed recovery from DNA damage -/+ cells show lingering activation of Gadd45 (figure 5E). In sum, our results indicate that LDR stabilizes mutp53 over the threshold that is necessary to endow DNE over wtp53 leading to deficient sensing of DNA double-strand brakes and DNA damage response. As LDR is insufficient to alter the cell cycle (figure 3), H/+ cells continue to cycle in the presence of unrepaired DNA, thus, accumulating genomic aberration.

3.5 Mutant p53 suppresses ATM phosphorylation in response to low dose but not high dose γ-radiation.

In mammalian cells, the ATM (ataxia-telangiectasia mutated), ATR (ATM- and Rad3-Related), and DNA-PKcs (DNA-dependent protein kinase) kinases are the most upstream DNA-damage repair kinases. In response to DNA damage, many proteins are phosphorylated in an ATM- or ATR-dependent manner, whereas DNA-PKcs mainly regulate a smaller number of targets and play a role primarily in nonhomologous end joining (NHEJ) [32-36]. In vivo and in vitro studies suggest that the DNA-damage specificities and functions of ATM and ATR are distinct. ATM is primarily activated by double-stranded DNA breaks (DSBs) such as that induced by radiation [37], whereas ATR responds to a broad spectrum of DNA damage [38]. One of the first steps of sensing DSBs is the autophosphorylation of ATM (pATM) rendering it active [39-41]. pATM is required for the phosphorylation of H2AX converting it to γH2AX which then marks the DNA DSBs [42]. Additionally, pATM phosphorylates other substrates such as Chk2 [43-45]

and p53 [46, 47]. Since we observed a defect in γH2AX foci in H/+ cells following LDR, we hypothesized that mutant p53 might hamper the pATM- γH2AX axis in response to LDR-induced DSBs. To test this hypothesis, we stained for pATM and γH2AX in +/+, -/+ and in H/+ cells (Figure 6). We also included H/- and -/- cells as controls (Figure 6). Since the phosphorylation is of ATM is an early event in response to DSBs, we analyzed the cells for pATM foci at 4 hrs post HDR or LDR by counting the percent of cells with pATM foci that co-stained in cells with ≥5 γH2AX foci post-irradiation. Examples of pATM and γH2AX co-staining in untreated, HDR and LDR are shown in Figure 6. At basal level, approximately 2% or less of untreated cells of all genotypes had pATM- γH2AX co-staining with no significant difference between them (Figure 6A-F). The percent of cells with pATM- γH2AX co-staining was significantly increased to approximately 80% at 4 hrs post-HDR in +/+, -/+, H/+ and -/- (Figure 6A-C, E&F). However, though H/- had a significant increase in pATM- γH2AX co-staining, yet it was significantly lower than the other 4 genotypes, at approximately 50% (Figure 6D&F). Following LDR, the percent of cells with pATM- γH2AX co-staining was significantly increased to approximately 13%, 24% and 18% post-LDR in +/+, -/+ and -/-, respectively (Figure 6A, C, E&F). In contrast, both H/+ and H/- cells showed no increase in the percent of cells with pATM- γH2AX co-staining following LDR, as compared to their untreated controls and to the other genotypes (Figure 6B, D&F). Western blot for γH2AX in H/+, -/- and H/- cells confirmed that in -/- has higher γH2AX levels post LDR as compared to H/+ and H/- cells (Figure 6G). These results suggest that LDR is sufficient to activate DNA damage response in wtp53 cells, by inducing ATM and subsequent H2AX phosphorylation in both, p53-dependent and independent manners. Furthermore, mutant p53 may suppress ATM activation and consequently H2AX phosphorylation by both, DNE and GOF mechanisms.

3.6 DNA-PK DDR pathway is suppressed in p53 haploinsufficiency-manner in response to low dose but not high dose γ-radiation.

We have previously shown that wtp53 promotes HR DNA damage repair mechanism in response to γ-irradiation and that mutp53 diverts the DNA damage repair (DDR) mechanism to the more error prone NHEJ pathway, leading to more aggressive tumors [9]. Thus, we examined whether mutp53 would have any differential effect on HR vs NHEJ DNA damage repair in response to HDR vs LDR. We analyzed the cells for pDNA-PK foci at 4 hrs post HDR or LDR by counting the percent of cells with pDNA-PK foci that co-stained in cells with ≥5 γH2AX foci post-

irradiation. Examples of pDNA-PK and γH2AX co-staining in untreated, HDR and LDR are shown in Figure 7. Indeed, our data show that DNA-PK (NHEJ DDR) is activated in all genotypes following HDR. (Figure 7A-F). However, following LDR, DNA-PK pathway was activated only in p53++ cells, but not in the other genotypes (Figure 7A-F). Importantly, following HDR, H/+ and H/- cells showed the highest DNA-PK activation as compared to +/+, -/+ and -/- cells, indicating more active NHEJ DDR in cells with mutp53. This is in support of our previous finding [9] that mutp53 promotes NHEJ following HDR.

4. Discussion.

p53 function as a tumor suppressor is frequently impaired at the early stages (stage 1 and DCIS) of ErbB2 cancers by monoallelic p53 mutations. As a guardian of the genome p53 orchestrates a variety of DNA-damage-response (DDR) mechanisms. The loss of p53 function missense mutation and newly acquired gain-of-function activity of mutp53 drive tumorigenesis is a major driver of cancer development as cells are no longer protected from genomic aberrations. Although tumor suppressor functions of wtp53 in maintaining genomic were extensively studied in past, limited data is available on how mutant p53 functions in the presence of wtp53 allele in heterozygosity, especially in the context of genotoxic modalities.

The activation of ErbB2 signaling has been shown to induce the aberrant proliferation of mammary cells ensuing DNA replication stress and activation of ATM-mediated DDR that acts as the main barrier for tumor progression. Previously, Reddy et. al demonstrated, that ATM–induced DDR is required for p53-mediated tumor suppression in the somatic ErbB2 mouse model. Therefore, the preservation of the ATM-mediated DDR- signaling may be crucial in the prevention of cancer progression by complementary mechanisms: maintaining genomic fidelity and promoting p53 tumor suppressor functions. However, it has not been investigated how the DDR signaling functions in the context of p53 heterozygosity. This question has high clinical importance since the deregulation of DDR pathways is thought to contribute to cancer initiation and progression.

We have previously shown in H/+ and -/+ mice that premalignant HDR leads to accelerated tumor formation and LOH [9]. Additionally, we have shown that DDR in H/+ mice following HDR is skewed towards the more error-prone non-homologous end-joining repair [9]. In the current study we observed that LOH occurred following both HDR and LDR, with tumor growth rate being significantly higher in H/+ tumors following LDR, as compared to HDR and as compared to +/+ and -/+ tumors. This indicates that there is another player involved in accelerating tumor growth in post LDR.

Here, we demonstrate that mutp53 heterozygous cells (H/+) preserve the ability to induce activation of ATM in response to a HDR, while it is severely impaired only in response to LDR. ATM acts upstream of several signal transduction pathways initiated by ionizing radiation, such as p53, and Chk2 (cell cycle arrest), and DNA repair by phosphorylation of H2AX and sensing DNA double-strand breaks. However, only H/+ cells failed to sense the DNA damage following LDR (suppressed pATM and γH2AX), while it was active following HDR. Additionally, following

LDR, DNA-PK pathway was activated only in p53++ cells, but not in -/+, H/+, H/- or -/- cells. This indicates that there is a threshold for activation of DNA-PK that is dependent on the radiation dose and that requires homozygous wtp53 after LDR. Combining the results in LDR for ATM and DNA-PK, we observe that the loss of wtp53 and in absence of mutp53, this causes the wtp53 haploinsufficiency-inactivation of DNA-PK and that this is compensated by the activation of ATM. However, in presence of mutp53, ATM is suppressed. Suppression of both ATM and DNA-PK pathways following LDR led to a more aggressive tumor formation in tumors with mutp53, as compared to tumors with mutp53 following HDR. Our results can be interpreted by the presence of a radiation dose threshold below which mutp53 shows a GOF or DNE by suppressing the DNA repair mechanism.

While LOH occurred in H/+ tumors, following both HDR and LDR, but only in response to LDR that the growth of H/+ tumors was accelerated, we argue that since DNA damage went undetected in H/+ cells following LDR, it possible that this led to early occurrence of LOH on H/+ tumors following LDR which consequently led to accelerated tumor growth in response to LDR. However, in response to HDR, DDR is still active in H/+ cells and we have shown that DDR in H/+ mice following HDR is skewed towards the more error-prone non-homologous end-joining repair [9]. This active DDR following HDR would lead to a delay in the occurrence of LOH in H/+ tumors and thus a relatively slower H/+ tumor growth as compared to LDR. Figure 7G is a schematic representation of our findings and of the proposed mechanism of mutp53 in suppressing DDR following HDR vs LDR.

Although in the current study we focused on deficient DDR in mutp53 heterozygous cells, we acknowledge that LDR may accelerate tumor progression by other mechanisms and have a different biological function compared with HDR. LDR was shown to accelerate entry into the S phase in a TNBC cell line [48]. Also, it was shown to have an impact on reactive oxygen species (ROS) in an apparent context-dependent manner [49-51] LDR was shown to promote the accumulation of mutp53 (Figure 5E and [48]). As a pro-survival GOF mechanism, mutp53 protein interacts with and regulates the function of the transcription factor NRF2, a key regulator of antioxidative response, thus, accelerating the turnover of tumor suppressors such as pro-apoptotic proteins and CDK inhibitors [52].

While the high-dose radiation was shown to suppress immune responses, LDR enhances the immune response by augmenting the interaction of innate and adaptive immune cells [21-23]. On the other hand, mutp53 was shown to suppress immune response via various

mechanisms such as, by increasing pro-inflammatory cytokine release [53, 54], the physical interaction with the transcriptional regulator NF-κB amplifying its transcriptional activity [55], and reprogramming macrophages to support tumor growth [56]. On the other hand, pro-inflammatory cytokines may promote mutant p53 stability [57]. Understanding how mutp53 DNE may potentially modulate redox homeostasis and immune response after LDR deserves further studies for their high clinical impact.

Currently, ionizing radiation is widely used for therapy and imaging screening in breast cancer management. Various genetic, pathophysiological factors, and radiobiological parameters may determine the responses of cancer cells to radiation. Regardless of these factors, radiation induces DNA damage, which potentially may have detrimental effects on tumor progression. Despite the effects of HDR are being extensively studied, the biological consequences of LDR in humans remain less clear. Several reports have shown an association between diagnostic imaging and the increased risk of cancer incidence [58-62]. The single digital mammography is associated with the risk of inducing fatal breast cancer due to radiation in 25 per 100,000 average-risk women. A single examination by gamma imaging and positron emission mammography increases the risk of fatal breast cancer 20-30 times compared to digital mammography. Although imaging modalities are crucial for the early detection of relapse, they may be associated with higher risks, specifically in the cancer-risk population including patients with Li-Fraumeni syndrome. Therefore, the biomarkers that identify high-risk individuals can decrease avoidable mortalities and improve public health.

Collectively, our data show an important role for mutp53 in modulating DDR in cells in response to LDR and that its mode of action is by quenching the ability of the cells to sense DNA damage imposed by LDR and thus resulting in a more aggressive tumor.

5. Author contribution:

Amr Ghaleb: Conceptualization; Data curation; Formal analysis; Investigation; Methodology; Project administration; Supervision; Validation; Visualization; Writing - original draft, review & editing. **Natalia Marchenko:** Conceptualization; Data curation; Formal analysis; Funding acquisition; Investigation; Methodology; Project administration; Resources; Supervision; Validation; Visualization; Writing - original draft, review & editing. **Lucia Roa:** Formal analysis; Methodology.

6. Funding sources:

This work was supported by the DOD # BC151569 (Marchenko (PI).

Figure legend:

Figure 1. Increased growth rate of mutp53 heterozygous mammary tumors following low dose γ-radiation. A-C. Box plots of average survival days of +/+, H/+ and -/+ mice, untreated, or following HDR or LDR respectively. **D-F.** Box plots of average tumor growth rate of +/+, H/+ and -/+ mice, untreated, or following HDR or LDR respectively. **G.** Quantification of the number of mitotic cells in +/+, H/+ and -/+ tumors, untreated, or following HDR or LDR. **H.** Quantification of percent necrotic/apoptotic area in +/+, H/+ and -/+ tumors, untreated, or following HDR or LDR. **K&L.** H&E representative images of tumor with low necrosis/apoptosis area (K) and a tumor with high necrosis/apoptosis. Scale bar 200μm. Error bars represent ± SD. *=p<0.05; **=p<0.01; ***=p<0.001.

Figure 2. Low dose radiation drives dominant-negative effect in mutp53 heterozygous mammary tumors. **A-C.** Line graphs representations of average tumor volume measured per week in untreated, or following HDR or LDR respectively. **D.** Accelerated kinetics of growth in H/+ tumors following LDR but not HDR. Line graphs representations of average tumor volume measured per week in each genotype untreated or following HDR or LDR. **E & F.** PCR gel electrophoresis analysis of LOH in H/+ and -/+ tumors showing LOH in H/+ tumors following HDR (**E**) and lDR (**F**). Error bars represent ± SD.

Figure 3. Differential cell cycle checkpoint in response to high dose γ-radiation as compared to low dose γ-radiation. **A-F.** Bar graphs showing cell cycle analysis of +/+, H/+, and -/+ cell lines irradiated (gray bars) or not (black bars). Aberrant cell cycle checkpoint following γ-irradiation in H/+ cells following HDR, while LDR does not show any significant change in the cell cycle profile of the 3 genotypes. **G.** Western blot of p21 and γH2AX level (representing cell cycle check point and DNA damage, respectively) post-irradiation, showing p21 response and γH2AX elevation and resolution in H/+ in response to HDR, while no change in p21 and γH2AX in response to LDR. HSC70 as a loading control. Error bars represent ± SD.

Figure 4. DNA-damage repair response is activated response to high dose γ-radiation in all genotypes. A-C. Staining of cells for γH2AX in +/+, H/+, and -/+ cell lines, before and after HDR (2, 4, 6 and 24h post-irradiation). Scale bar 50μm. **D)** Quantification of cells with >5 and

<5 γH2AX foci/cell in +/+, H/+, and -/+ cell lines, before and after HDR (4 and 24h post-irradiation). Error bars represent ± SD. *=p<0.05; **=p<0.01; ***=p<0.001.

Figure 5. Mutant p53 abolishes DNA-damage repair response in a dominant-negative manner in response to low dose γ-radiation. A-C. Staining of cells for γH2AX in +/+, H/+, and -/+ cell lines, before and after LDR (2, 4, 6 and 24h post-irradiation), showing suppressed γH2AX staining in H/+. Scale bar 50μm. **D)** Quantification of cells with >5 and <5 γH2AX foci/cell in +/+, H/+, and -/+ cell lines, before and after LDR (4 and 24h post-irradiation). **E.** Western blot of Gadd45 (a downstream target of wtp53) and p53 level (representing cell cycle check point and DNA damage) post-irradiation, showing Gadd45 elevation in +/+ and -/+ in response to LDR, while no change in H/+ concomitant with elevation and stabilization of mutp53 in response to LDR. HSC70 as a loading control. Error bars represent ± SD. *=p<0.05; **=p<0.01; ***=p<0.001.

Figure 6. Mutant p53 suppresses ATM phosphorylation in response to low dose but not high dose γ-radiation. A-E. Co-staining of cells for pATM and γH2AX in +/+, H/+, -/+, H/- and -/- cell lines, before and after HDR or LDR (4h post-irradiation), showing suppressed pATM and γH2AX staining in H/+ and H/-, but not in +/+, -/+ or -/- cells. Scale bar 20μm. **F.** Quantification of cells with pATM and γH2AX co-staining foci/cell in +/+, H/+, -/+, H/- and -/- cell lines, before and after HDR or LDR (4h post-irradiation). **G.** Western blot of γH2AX level (representing DNA damage) post-LDR, showing γH2AX elevation and resolution in -/- cells in response to LDR, while suppressed change in γH2AX in response to LDR in H/+ and H/-. HSC70 as a loading control. Error bars represent ± SD. All statistical significance is made to p53+/+ cells, unless otherwise indicated by cross bars, or indicated by ### and &&& on LDR -/- where comparison was made to LDR H/+ and LDR H/-, respectively. *=p<0.05; **=p<0.01; ***=p<0.001.

Figure 7. p53 haploinsufficiency suppresses DNA-PK mediated DNA damage repair in response to low dose but not high dose γ-radiation. A-E. Co-staining of cells for pDNA-PK and γH2AX in +/+, H/+, -/+, H/- and -/- cell lines, before and after HDR or LDR (4h post-irradiation), showing suppressed pDNA-PK and γH2AX staining in all genotypes except +/+ cells. Scale bar 20μm. **F.** Quantification of cells with pDNA-PK and γH2AX co-staining foci/cell in +/+,

H/+, -/+, H/- and -/- cell lines, before and after HDR or LDR (4h post-irradiation). **G.** Model comparing DNA damage repair (DDR) in response to HDR vs LDR in presence of mutp53. Following HDR, mutp53 suppresses ATM pathway (homologous recombination (HR) DDR), allowing DNA-PK pathway (non-homologous end joining (NHEJ) DDR) to take place. Following LDR, DNA-PK pathway is suppressed in wtp53 haploinsufficiency while mutp53 suppresses ATM pathway, with a net result ablation of DDR in cells with mutp53. Error bars represent ± SD. All statistical significance is made to p53+/+ cells, unless otherwise indicated by cross bars. *=p<0.05; **=p<0.01; ***=p<0.001.

Supplementary figure 1. Line graphs showing individual tumor volume growth kinetics in untreated (A-C) and in HDR (D-F) and LDR (G-I) +/+, -/+ and H/+ mice.

Conflict of interest:

None of the authors have any conflict of interest to declare

References cited

1. Brosh R, Rotter V. When mutants gain new powers: news from the mutant p53 field. Nat Rev Cancer. 2009;9(10):701-13. doi: 10.1038/nrc2693. PubMed PMID: 19693097.
2. Cancer Genome Atlas N. Comprehensive molecular portraits of human breast tumours. Nature. 2012;490(7418):61-70. doi: 10.1038/nature11412. PubMed PMID: 23000897; PMCID: PMC3465532.
3. Stiewe T, Haran TE. How mutations shape p53 interactions with the genome to promote tumorigenesis and drug resistance. Drug Resist Updat. 2018;38:27-43. doi: 10.1016/j.drup.2018.05.001. PubMed PMID: 29857816.
4. Andersson J, Larsson L, Klaar S, Holmberg L, Nilsson J, Inganas M, Carlsson G, Ohd J, Rudenstam CM, Gustavsson B, Bergh J. Worse survival for TP53 (p53)-mutated breast cancer patients receiving adjuvant CMF. Ann Oncol. 2005;16(5):743-8. doi: 10.1093/annonc/mdi150. PubMed PMID: 15802278.
5. Rivlin N, Brosh R, Oren M, Rotter V. Mutations in the p53 Tumor Suppressor Gene: Important Milestones at the Various Steps of Tumorigenesis. Genes Cancer. 2011;2(4):466-74. doi: 10.1177/1947601911408889. PubMed PMID: 21779514; PMCID: PMC3135636.
6. Willis A, Jung EJ, Wakefield T, Chen X. Mutant p53 exerts a dominant negative effect by preventing wild-type p53 from binding to the promoter of its target genes. Oncogene. 2004;23(13):2330-8. doi: 10.1038/sj.onc.1207396. PubMed PMID: 14743206.
7. Lozano G. The oncogenic roles of p53 mutants in mouse models. Curr Opin Genet Dev. 2007;17(1):66-70. doi: 10.1016/j.gde.2006.12.003. PubMed PMID: 17208429.
8. Gencel-Augusto J, Lozano G. p53 tetramerization: at the center of the dominant-negative effect of mutant p53. Genes Dev. 2020;34(17-18):1128-46. doi: 10.1101/gad.340976.120. PubMed PMID: 32873579; PMCID: PMC7462067.
9. Ghaleb A, Yallowitz A, Marchenko N. Irradiation induces p53 loss of heterozygosity in breast cancer expressing mutant p53. Commun Biol. 2019;2:436. doi: 10.1038/s42003-019-0669-y. PubMed PMID: 31799437; PMCID: PMC6881331.
10. Isermann T, Sener OC, Stender A, Klemke L, Winkler N, Neesse A, Li J, Wegwitz F, Moll UM, Schulz-Heddergott R. Suppression of HSF1 activity by wildtype p53 creates a driving force for p53 loss-of-heterozygosity. Nat Commun. 2021;12(1):4019. doi: 10.1038/s41467-021-24064-1. PubMed PMID: 34188043; PMCID: PMC8242083.
11. Jackson EL, Olive KP, Tuveson DA, Bronson R, Crowley D, Brown M, Jacks T. The differential effects of mutant p53 alleles on advanced murine lung cancer. Cancer Res. 2005;65(22):10280-8. doi: 10.1158/0008-5472.CAN-05-2193. PubMed PMID: 16288016.
12. Aurelio ON, Kong XT, Gupta S, Stanbridge EJ. p53 mutants have selective dominant-negative effects on apoptosis but not growth arrest in human cancer cell lines. Mol Cell Biol. 2000;20(3):770-8. doi: 10.1128/MCB.20.3.770-778.2000. PubMed PMID: 10629033; PMCID: PMC85193.
13. Dearth LR, Qian H, Wang T, Baroni TE, Zeng J, Chen SW, Yi SY, Brachmann RK. Inactive full-length p53 mutants lacking dominant wild-type p53 inhibition highlight loss of heterozygosity as an important aspect of p53 status in human cancers. Carcinogenesis. 2007;28(2):289-98. doi: 10.1093/carcin/bgl132. PubMed PMID: 16861262.
14. Stein Y, Aloni-Grinstein R, Rotter V. Mutant p53 oncogenicity: dominant-negative or gain-of-function? Carcinogenesis. 2020;41(12):1635-47. doi: 10.1093/carcin/bgaa117. PubMed PMID: 33159515.
15. Goh AM, Coffill CR, Lane DP. The role of mutant p53 in human cancer. J Pathol. 2011;223(2):116-26. doi: 10.1002/path.2784. PubMed PMID: 21125670.

16. Hanel W, Marchenko N, Xu S, Yu SX, Weng W, Moll U. Two hot spot mutant p53 mouse models display differential gain of function in tumorigenesis. Cell Death Differ. 2013;20(7):898-909. doi: 10.1038/cdd.2013.17. PubMed PMID: 23538418; PMCID: PMC3679454.
17. Lang GA, Iwakuma T, Suh YA, Liu G, Rao VA, Parant JM, Valentin-Vega YA, Terzian T, Caldwell LC, Strong LC, El-Naggar AK, Lozano G. Gain of function of a p53 hot spot mutation in a mouse model of Li-Fraumeni syndrome. Cell. 2004;119(6):861-72. doi: 10.1016/j.cell.2004.11.006. PubMed PMID: 15607981.
18. Olive KP, Tuveson DA, Ruhe ZC, Yin B, Willis NA, Bronson RT, Crowley D, Jacks T. Mutant p53 gain of function in two mouse models of Li-Fraumeni syndrome. Cell. 2004;119(6):847-60. doi: 10.1016/j.cell.2004.11.004. PubMed PMID: 15607980.
19. Petitjean A, Achatz MI, Borresen-Dale AL, Hainaut P, Olivier M. TP53 mutations in human cancers: functional selection and impact on cancer prognosis and outcomes. Oncogene. 2007;26(15):2157-65. doi: 10.1038/sj.onc.1210302. PubMed PMID: 17401424.
20. Terzian T, Suh YA, Iwakuma T, Post SM, Neumann M, Lang GA, Van Pelt CS, Lozano G. The inherent instability of mutant p53 is alleviated by Mdm2 or p16INK4a loss. Genes Dev. 2008;22(10):1337-44. doi: 10.1101/gad.1662908. PubMed PMID: 18483220; PMCID: PMC2377188.
21. Feinendegen LE. Evidence for beneficial low level radiation effects and radiation hormesis. Br J Radiol. 2005;78(925):3-7. doi: 10.1259/bjr/63353075. PubMed PMID: 15673519.
22. Luckey TD. Physiological benefits from low levels of ionizing radiation. Health Phys. 1982;43(6):771-89. doi: 10.1097/00004032-198212000-00001. PubMed PMID: 6759465.
23. Olivieri G, Bodycote J, Wolff S. Adaptive response of human lymphocytes to low concentrations of radioactive thymidine. Science. 1984;223(4636):594-7. doi: 10.1126/science.6695170. PubMed PMID: 6695170.
24. Li W, Wang G, Cui J, Xue L, Cai L. Low-dose radiation (LDR) induces hematopoietic hormesis: LDR-induced mobilization of hematopoietic progenitor cells into peripheral blood circulation. Exp Hematol. 2004;32(11):1088-96. doi: 10.1016/j.exphem.2004.07.015. PubMed PMID: 15539087.
25. Liang X, So YH, Cui J, Ma K, Xu X, Zhao Y, Cai L, Li W. The low-dose ionizing radiation stimulates cell proliferation via activation of the MAPK/ERK pathway in rat cultured mesenchymal stem cells. J Radiat Res. 2011;52(3):380-6. doi: 10.1269/jrr.10121. PubMed PMID: 21436606.
26. Jiang H, Xu Y, Li W, Ma K, Cai L, Wang G. Low-dose radiation does not induce proliferation in tumor cells in vitro and in vivo. Radiat Res. 2008;170(4):477-87. doi: 10.1667/rr1132.1. PubMed PMID: 19024655.
27. Schulz-Heddergott R, Stark N, Edmunds SJ, Li J, Conradi LC, Bohnenberger H, Ceteci F, Greten FR, Dobbelstein M, Moll UM. Therapeutic Ablation of Gain-of-Function Mutant p53 in Colorectal Cancer Inhibits Stat3-Mediated Tumor Growth and Invasion. Cancer Cell. 2018;34(2):298-314 e7. doi: 10.1016/j.ccell.2018.07.004. PubMed PMID: 30107178; PMCID: PMC6582949.
28. Song H, Hollstein M, Xu Y. p53 gain-of-function cancer mutants induce genetic instability by inactivating ATM. Nat Cell Biol. 2007;9(5):573-80. doi: 10.1038/ncb1571. PubMed PMID: 17417627.
29. Yallowitz AR, Li D, Lobko A, Mott D, Nemajerova A, Marchenko N. Mutant p53 Amplifies Epidermal Growth Factor Receptor Family Signaling to Promote Mammary Tumorigenesis. Mol Cancer Res. 2015;13(4):743-54. doi: 10.1158/1541-7786.MCR-14-0360. PubMed PMID: 25573952; PMCID: PMC4824060.

30. Demb J, Chu P, Nelson T, Hall D, Seibert A, Lamba R, Boone J, Krishnam M, Cagnon C, Bostani M, Gould R, Miglioretti D, Smith-Bindman R. Optimizing Radiation Doses for Computed Tomography Across Institutions: Dose Auditing and Best Practices. JAMA Intern Med. 2017;177(6):810-7. doi: 10.1001/jamainternmed.2017.0445. PubMed PMID: 28395000; PMCID: PMC5818828.
31. Kastan MB, Zhan Q, el-Deiry WS, Carrier F, Jacks T, Walsh WV, Plunkett BS, Vogelstein B, Fornace AJ, Jr. A mammalian cell cycle checkpoint pathway utilizing p53 and GADD45 is defective in ataxia-telangiectasia. Cell. 1992;71(4):587-97. doi: 10.1016/0092-8674(92)90593-2. PubMed PMID: 1423616.
32. Bensimon A, Schmidt A, Ziv Y, Elkon R, Wang SY, Chen DJ, Aebersold R, Shiloh Y. ATM-dependent and -independent dynamics of the nuclear phosphoproteome after DNA damage. Sci Signal. 2010;3(151):rs3. doi: 10.1126/scisignal.2001034. PubMed PMID: 21139141.
33. Matsuoka S, Ballif BA, Smogorzewska A, McDonald ER, 3rd, Hurov KE, Luo J, Bakalarski CE, Zhao Z, Solimini N, Lerenthal Y, Shiloh Y, Gygi SP, Elledge SJ. ATM and ATR substrate analysis reveals extensive protein networks responsive to DNA damage. Science. 2007;316(5828):1160-6. doi: 10.1126/science.1140321. PubMed PMID: 17525332.
34. Smolka MB, Albuquerque CP, Chen SH, Zhou H. Proteome-wide identification of in vivo targets of DNA damage checkpoint kinases. Proc Natl Acad Sci U S A. 2007;104(25):10364-9. doi: 10.1073/pnas.0701622104. PubMed PMID: 17563356; PMCID: PMC1965519.
35. Stokes MP, Rush J, Macneill J, Ren JM, Sprott K, Nardone J, Yang V, Beausoleil SA, Gygi SP, Livingstone M, Zhang H, Polakiewicz RD, Comb MJ. Profiling of UV-induced ATM/ATR signaling pathways. Proc Natl Acad Sci U S A. 2007;104(50):19855-60. doi: 10.1073/pnas.0707579104. PubMed PMID: 18077418; PMCID: PMC2148387.
36. Beli P, Lukashchuk N, Wagner SA, Weinert BT, Olsen JV, Baskcomb L, Mann M, Jackson SP, Choudhary C. Proteomic investigations reveal a role for RNA processing factor THRAP3 in the DNA damage response. Mol Cell. 2012;46(2):212-25. doi: 10.1016/j.molcel.2012.01.026. PubMed PMID: 22424773; PMCID: PMC3565437.
37. Sordet O, Nakamura AJ, Redon CE, Pommier Y. DNA double-strand breaks and ATM activation by transcription-blocking DNA lesions. Cell Cycle. 2010;9(2):274-8. doi: 10.4161/cc.9.2.10506. PubMed PMID: 20023421; PMCID: PMC7289056.
38. Flynn RL, Zou L. ATR: a master conductor of cellular responses to DNA replication stress. Trends Biochem Sci. 2011;36(3):133-40. doi: 10.1016/j.tibs.2010.09.005. PubMed PMID: 20947357; PMCID: PMC3024454.
39. Bakkenist CJ, Kastan MB. DNA damage activates ATM through intermolecular autophosphorylation and dimer dissociation. Nature. 2003;421(6922):499-506. doi: 10.1038/nature01368. PubMed PMID: 12556884.
40. Kozlov SV, Graham ME, Peng C, Chen P, Robinson PJ, Lavin MF. Involvement of novel autophosphorylation sites in ATM activation. EMBO J. 2006;25(15):3504-14. doi: 10.1038/sj.emboj.7601231. PubMed PMID: 16858402; PMCID: PMC1538573.
41. So S, Davis AJ, Chen DJ. Autophosphorylation at serine 1981 stabilizes ATM at DNA damage sites. J Cell Biol. 2009;187(7):977-90. doi: 10.1083/jcb.200906064. PubMed PMID: 20026654; PMCID: PMC2806275.
42. Burma S, Chen BP, Murphy M, Kurimasa A, Chen DJ. ATM phosphorylates histone H2AX in response to DNA double-strand breaks. J Biol Chem. 2001;276(45):42462-7. doi: 10.1074/jbc.C100466200. PubMed PMID: 11571274.

43. Blasina A, de Weyer IV, Laus MC, Luyten WH, Parker AE, McGowan CH. A human homologue of the checkpoint kinase Cds1 directly inhibits Cdc25 phosphatase. Curr Biol. 1999;9(1):1-10. doi: 10.1016/s0960-9822(99)80041-4. PubMed PMID: 9889122.
44. Brown AL, Lee CH, Schwarz JK, Mitiku N, Piwnica-Worms H, Chung JH. A human Cds1-related kinase that functions downstream of ATM protein in the cellular response to DNA damage. Proc Natl Acad Sci U S A. 1999;96(7):3745-50. doi: 10.1073/pnas.96.7.3745. PubMed PMID: 10097108; PMCID: PMC22365.
45. Matsuoka S, Huang M, Elledge SJ. Linkage of ATM to cell cycle regulation by the Chk2 protein kinase. Science. 1998;282(5395):1893-7. doi: 10.1126/science.282.5395.1893. PubMed PMID: 9836640.
46. Banin S, Moyal L, Shieh S, Taya Y, Anderson CW, Chessa L, Smorodinsky NI, Prives C, Reiss Y, Shiloh Y, Ziv Y. Enhanced phosphorylation of p53 by ATM in response to DNA damage. Science. 1998;281(5383):1674-7. doi: 10.1126/science.281.5383.1674. PubMed PMID: 9733514.
47. Canman CE, Lim DS, Cimprich KA, Taya Y, Tamai K, Sakaguchi K, Appella E, Kastan MB, Siliciano JD. Activation of the ATM kinase by ionizing radiation and phosphorylation of p53. Science. 1998;281(5383):1677-9. doi: 10.1126/science.281.5383.1677. PubMed PMID: 9733515.
48. Li SJ, Liang XY, Li HJ, Li W, Zhou L, Chen HQ, Ye SG, Yu DH, Cui JW. Low-dose irradiation promotes proliferation of the human breast cancer MDA-MB-231 cells through accumulation of mutant P53. Int J Oncol. 2017;50(1):290-6. doi: 10.3892/ijo.2016.3795. PubMed PMID: 27959407.
49. Kawamura K, Qi F, Kobayashi J. Potential relationship between the biological effects of low-dose irradiation and mitochondrial ROS production. J Radiat Res. 2018;59(suppl_2):ii91-ii7. doi: 10.1093/jrr/rrx091. PubMed PMID: 29415254; PMCID: PMC5941154.
50. Shimura T. ATM-Mediated Mitochondrial Radiation Responses of Human Fibroblasts. Genes (Basel). 2021;12(7). doi: 10.3390/genes12071015. PubMed PMID: 34208940; PMCID: PMC8305810.
51. Shin E, Lee S, Kang H, Kim J, Kim K, Youn H, Jin YW, Seo S, Youn B. Organ-Specific Effects of Low Dose Radiation Exposure: A Comprehensive Review. Front Genet. 2020;11:566244. doi: 10.3389/fgene.2020.566244. PubMed PMID: 33133150; PMCID: PMC7565684.
52. Lisek K, Campaner E, Ciani Y, Walerych D, Del Sal G. Mutant p53 tunes the NRF2-dependent antioxidant response to support survival of cancer cells. Oncotarget. 2018;9(29):20508-23. doi: 10.18632/oncotarget.24974. PubMed PMID: 29755668; PMCID: PMC5945496.
53. Capaci V, Mantovani F, Del Sal G. Amplifying Tumor-Stroma Communication: An Emerging Oncogenic Function of Mutant p53. Front Oncol. 2020;10:614230. doi: 10.3389/fonc.2020.614230. PubMed PMID: 33505920; PMCID: PMC7831039.
54. Ubertini V, Norelli G, D'Arcangelo D, Gurtner A, Cesareo E, Baldari S, Gentileschi MP, Piaggio G, Nistico P, Soddu S, Facchiano A, Bossi G. Mutant p53 gains new function in promoting inflammatory signals by repression of the secreted interleukin-1 receptor antagonist. Oncogene. 2015;34(19):2493-504. doi: 10.1038/onc.2014.191. PubMed PMID: 24998848.
55. Cooks T, Pateras IS, Tarcic O, Solomon H, Schetter AJ, Wilder S, Lozano G, Pikarsky E, Forshew T, Rosenfeld N, Harpaz N, Itzkowitz S, Harris CC, Rotter V, Gorgoulis VG, Oren M. Mutant p53 prolongs NF-kappaB activation and promotes chronic inflammation and

inflammation-associated colorectal cancer. Cancer Cell. 2013;23(5):634-46. doi: 10.1016/j.ccr.2013.03.022. PubMed PMID: 23680148; PMCID: PMC3657134.
56. Cooks T, Pateras IS, Jenkins LM, Patel KM, Robles AI, Morris J, Forshew T, Appella E, Gorgoulis VG, Harris CC. Mutant p53 cancers reprogram macrophages to tumor supporting macrophages via exosomal miR-1246. Nat Commun. 2018;9(1):771. doi: 10.1038/s41467-018-03224-w. PubMed PMID: 29472616; PMCID: PMC5823939.
57. D'Orazi G, Cordani M, Cirone M. Oncogenic pathways activated by pro-inflammatory cytokines promote mutant p53 stability: clue for novel anticancer therapies. Cell Mol Life Sci. 2021;78(5):1853-60. doi: 10.1007/s00018-020-03677-7. PubMed PMID: 33070220.
58. Castells X, Domingo L, Corominas JM, Tora-Rocamora I, Quintana MJ, Bare M, Vidal C, Natal C, Sanchez M, Saladie F, Ferrer J, Vernet M, Servitja S, Rodriguez-Arana A, Roman M, Espinas JA, Sala M. Breast cancer risk after diagnosis by screening mammography of nonproliferative or proliferative benign breast disease: a study from a population-based screening program. Breast Cancer Res Treat. 2015;149(1):237-44. doi: 10.1007/s10549-014-3208-z. PubMed PMID: 25503778; PMCID: PMC4298666.
59. Doody MM, Freedman DM, Alexander BH, Hauptmann M, Miller JS, Rao RS, Mabuchi K, Ron E, Sigurdson AJ, Linet MS. Breast cancer incidence in U.S. radiologic technologists. Cancer. 2006;106(12):2707-15. doi: 10.1002/cncr.21876. PubMed PMID: 16639729.
60. Lee CI, Haims AH, Monico EP, Brink JA, Forman HP. Diagnostic CT scans: assessment of patient, physician, and radiologist awareness of radiation dose and possible risks. Radiology. 2004;231(2):393-8. doi: 10.1148/radiol.2312030767. PubMed PMID: 15031431.
61. Lin EC. Radiation risk from medical imaging. Mayo Clin Proc. 2010;85(12):1142-6; quiz 6. doi: 10.4065/mcp.2010.0260. PubMed PMID: 21123642; PMCID: PMC2996147.
62. Linet MS, Slovis TL, Miller DL, Kleinerman R, Lee C, Rajaraman P, Berrington de Gonzalez A. Cancer risks associated with external radiation from diagnostic imaging procedures. CA Cancer J Clin. 2012;62(2):75-100. doi: 10.3322/caac.21132. PubMed PMID: 22307864; PMCID: PMC3548988.

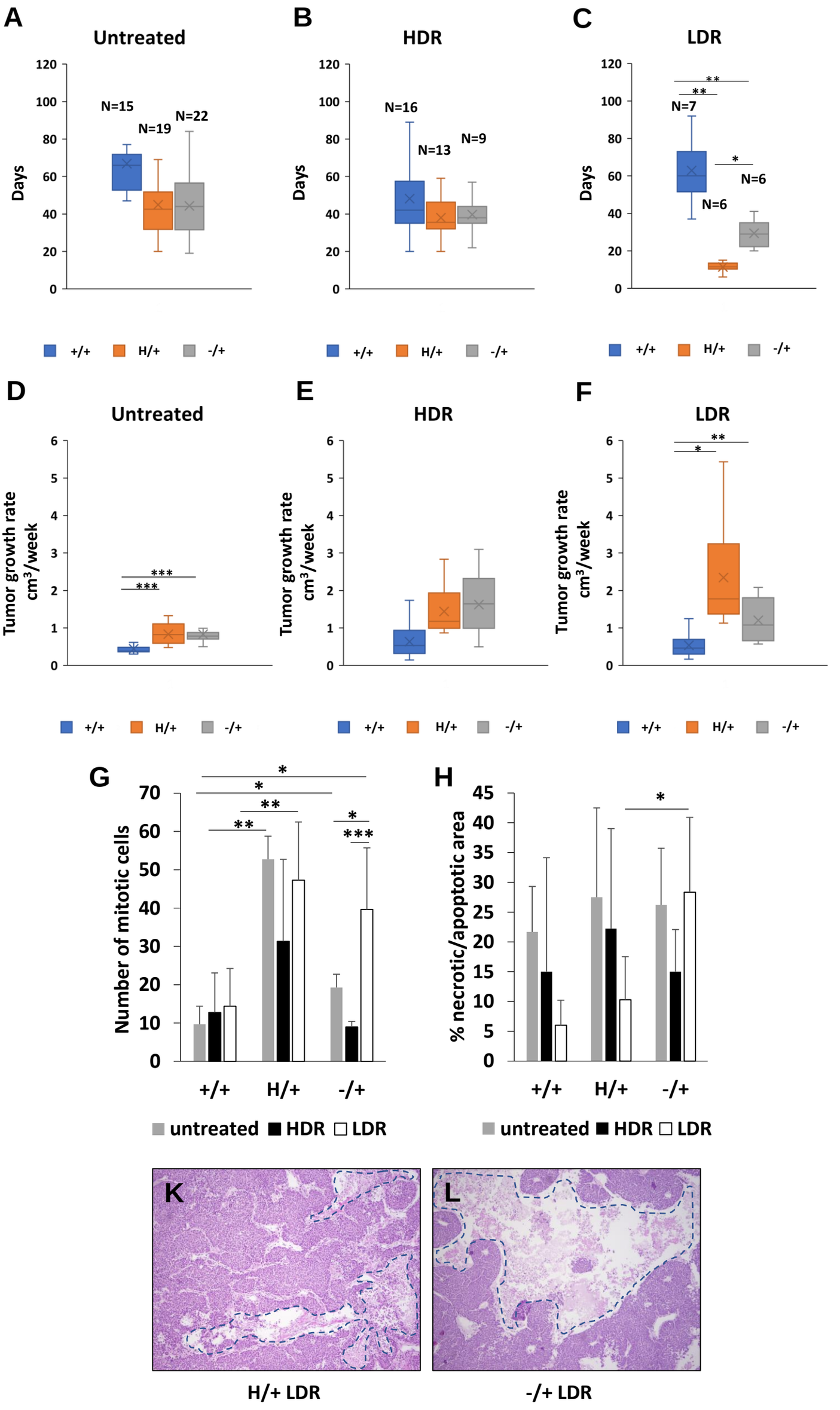
A
Untreated
Days
N=15
N=19
N=22
B
HDR
N=16
N=13
N=9
C
LDR
N=7
N=6
N=6
+/+
H/+
-/+
D
Untreated
E
HDR
F
LDR
Tumor growth rate cm³/week
G
Number of mitotic cells
H
% necrotic/apoptotic area
untreated
HDR
LDR
K
L
H/+ LDR
-/+ LDR

Figure 1

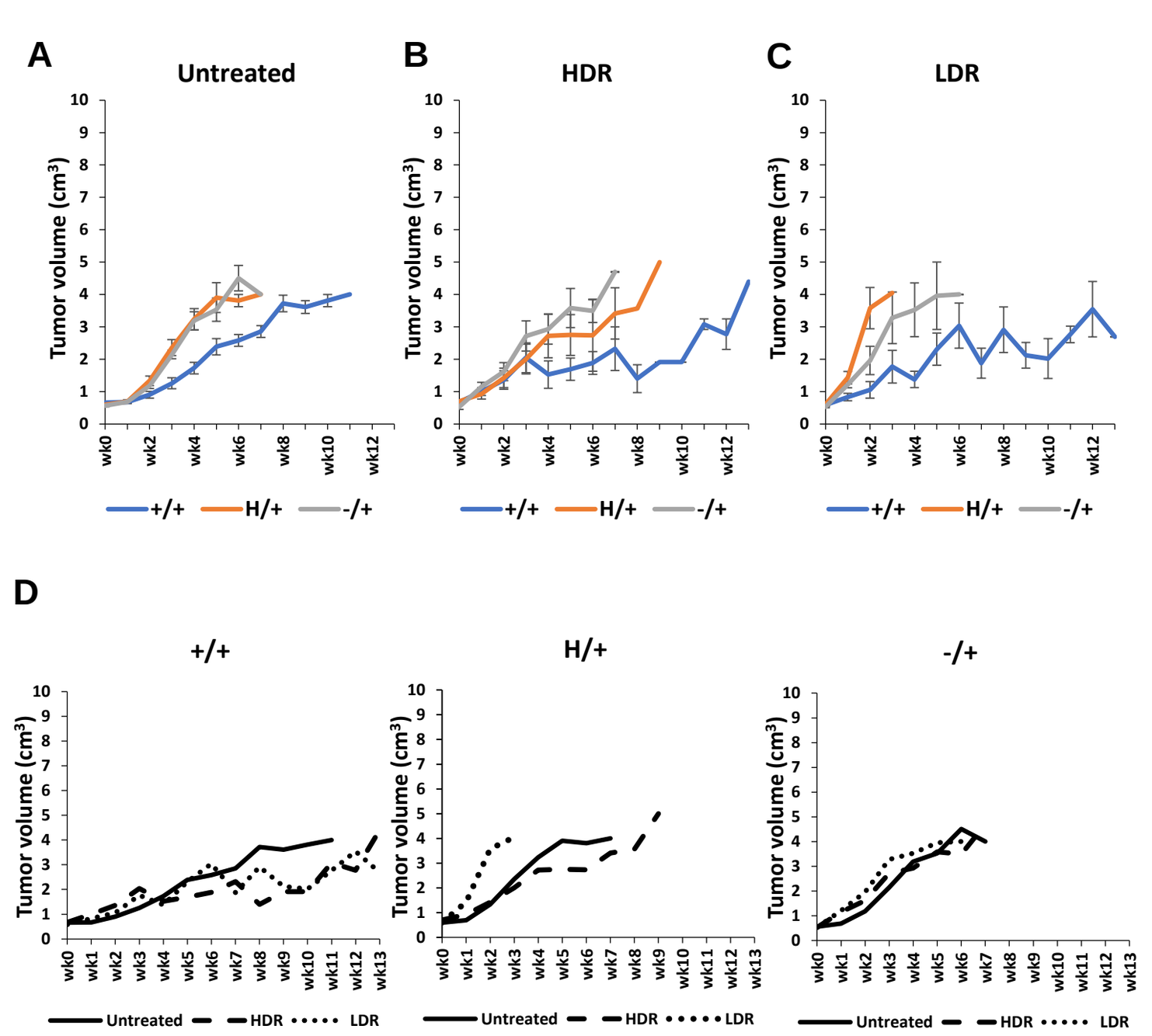

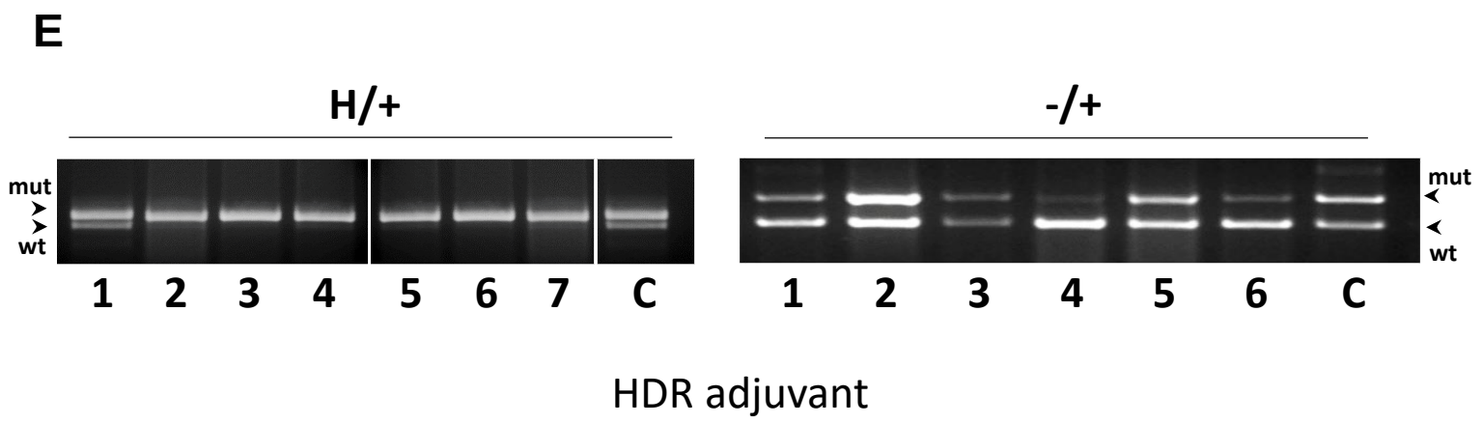

HDR adjuvant

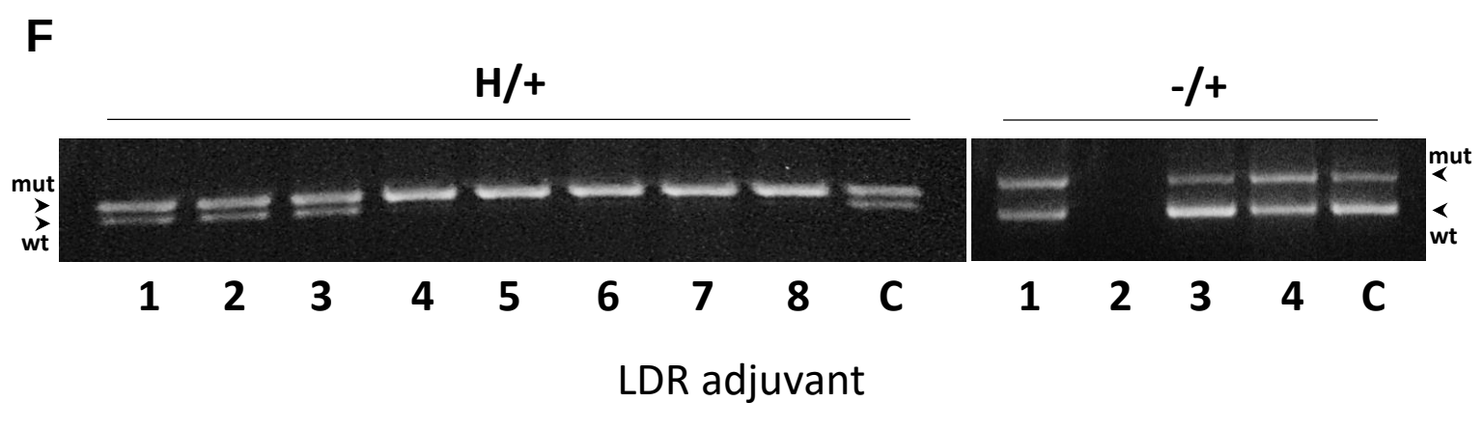

LDR adjuvant

Figure 2

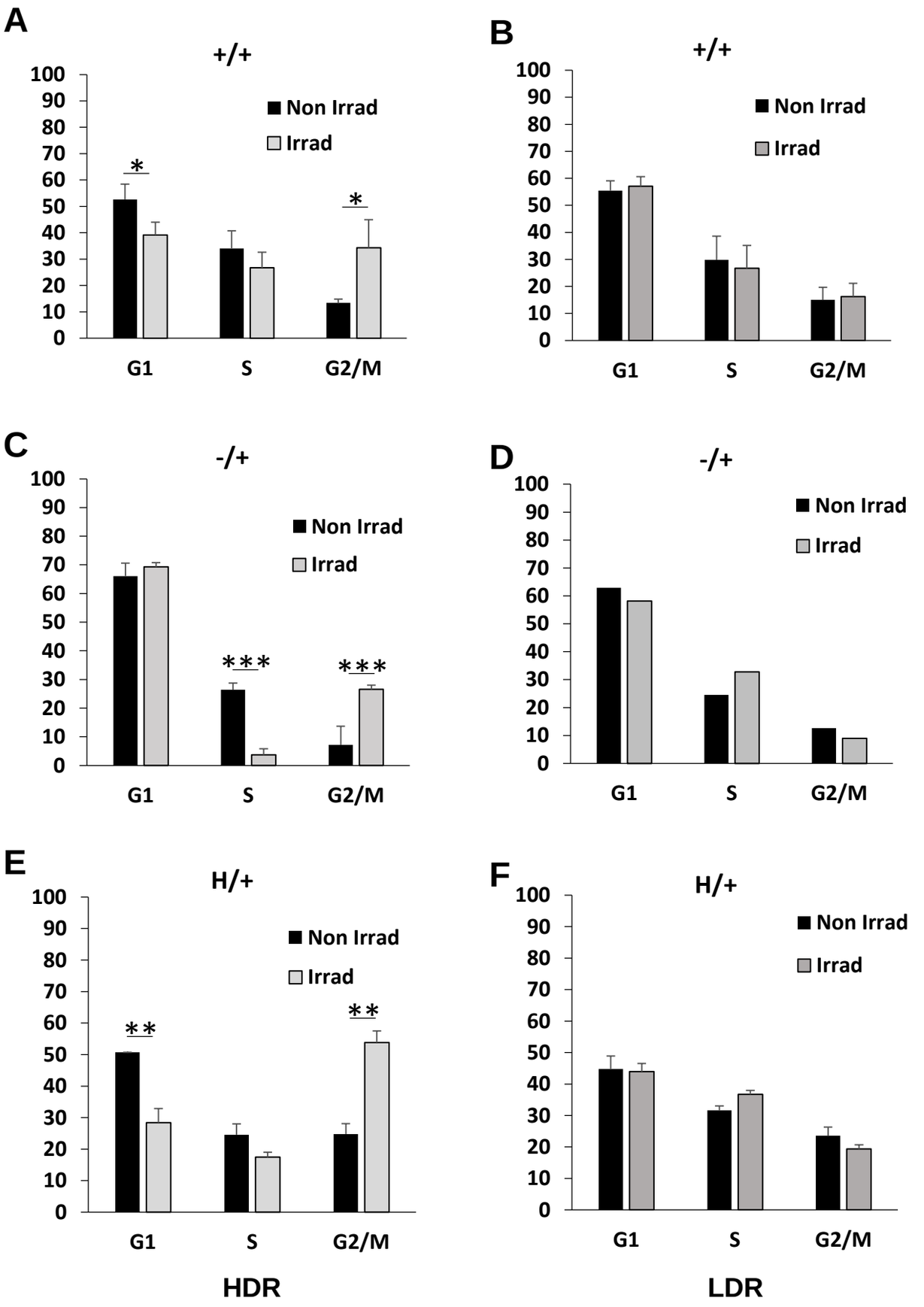
A
+/+
Non Irrad
Irrad
100
90
80
70
60
50
40
30
20
10
0
*
*
G1
S
G2/M
B
+/+
Non Irrad
Irrad
G1
S
G2/M
C
-/+
Non Irrad
Irrad
***
***
G1
S
G2/M
D
-/+
Non Irrad
Irrad
G1
S
G2/M
E
H/+
Non Irrad
Irrad
**
**
G1
S
G2/M
HDR
F
H/+
Non Irrad
Irrad
G1
S
G2/M
LDR

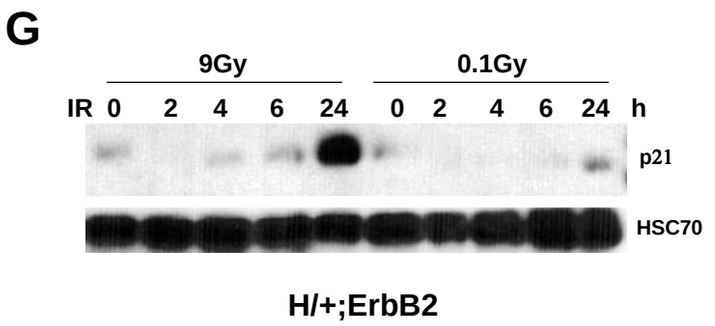
G
9Gy
0.1Gy
IR 0 2 4 6 24 0 2 4 6 24 h
p21
HSC70
H/+;ErbB2

Figure 3

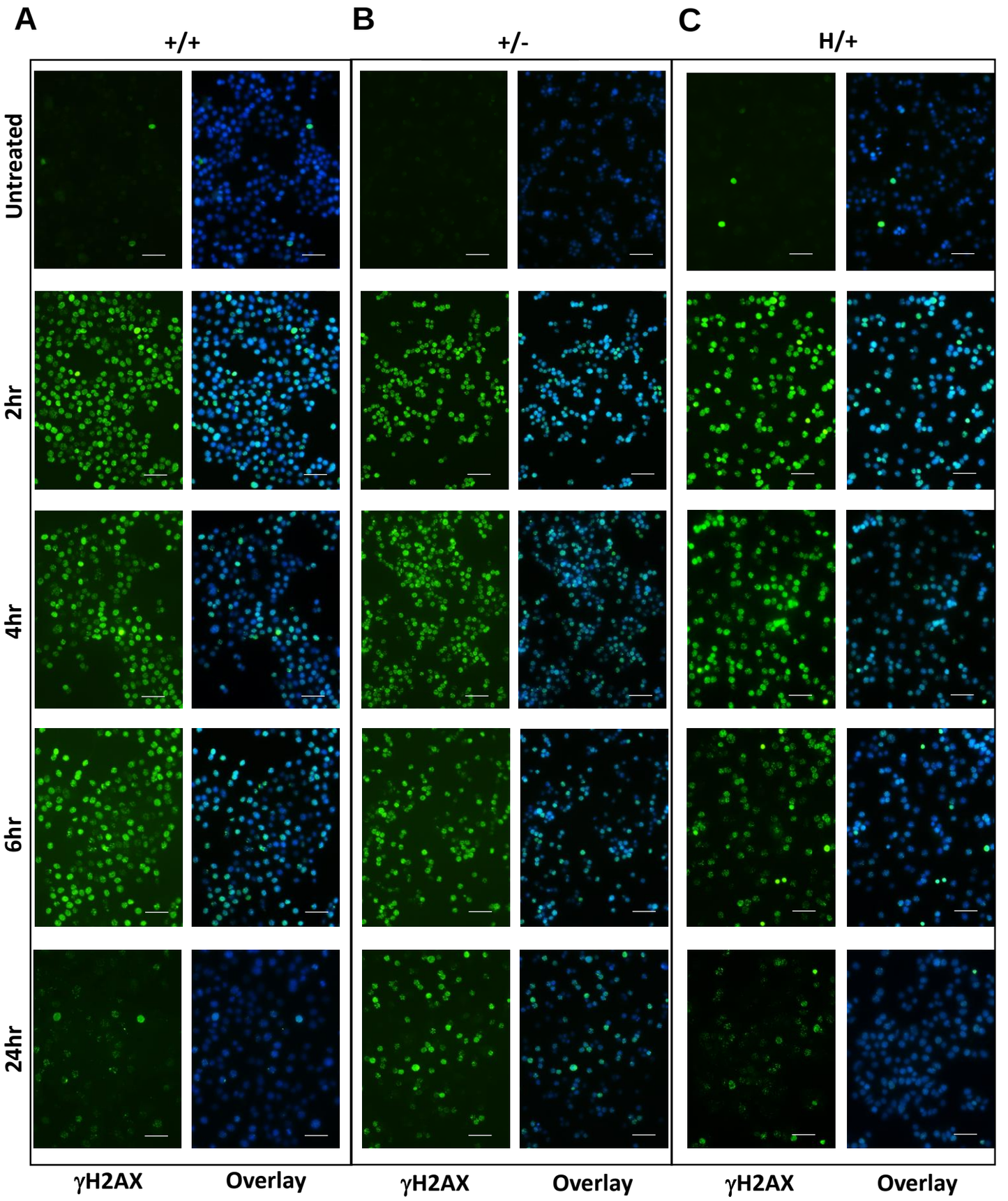
A
+/+
B
+/-
C
H/+
Untreated
2hr
4hr
6hr
24hr
γH2AX
Overlay
γH2AX
Overlay
γH2AX
Overlay

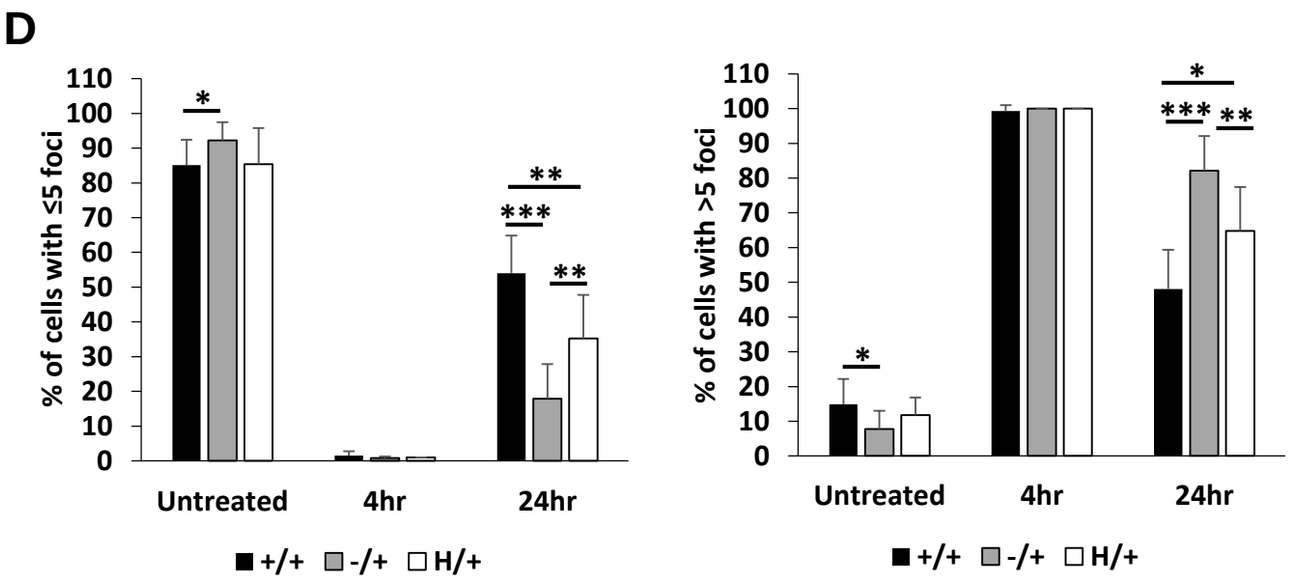
D
% of cells with ≤5 foci
110
100
90
80
70
60
50
40
30
20
10
0
*
**
***
**
Untreated
4hr
24hr
+/+
-/+
H/+
% of cells with >5 foci
110
100
90
80
70
60
50
40
30
20
10
0
*
*
***
**
Untreated
4hr
24hr
+/+
-/+
H/+

Figure 4

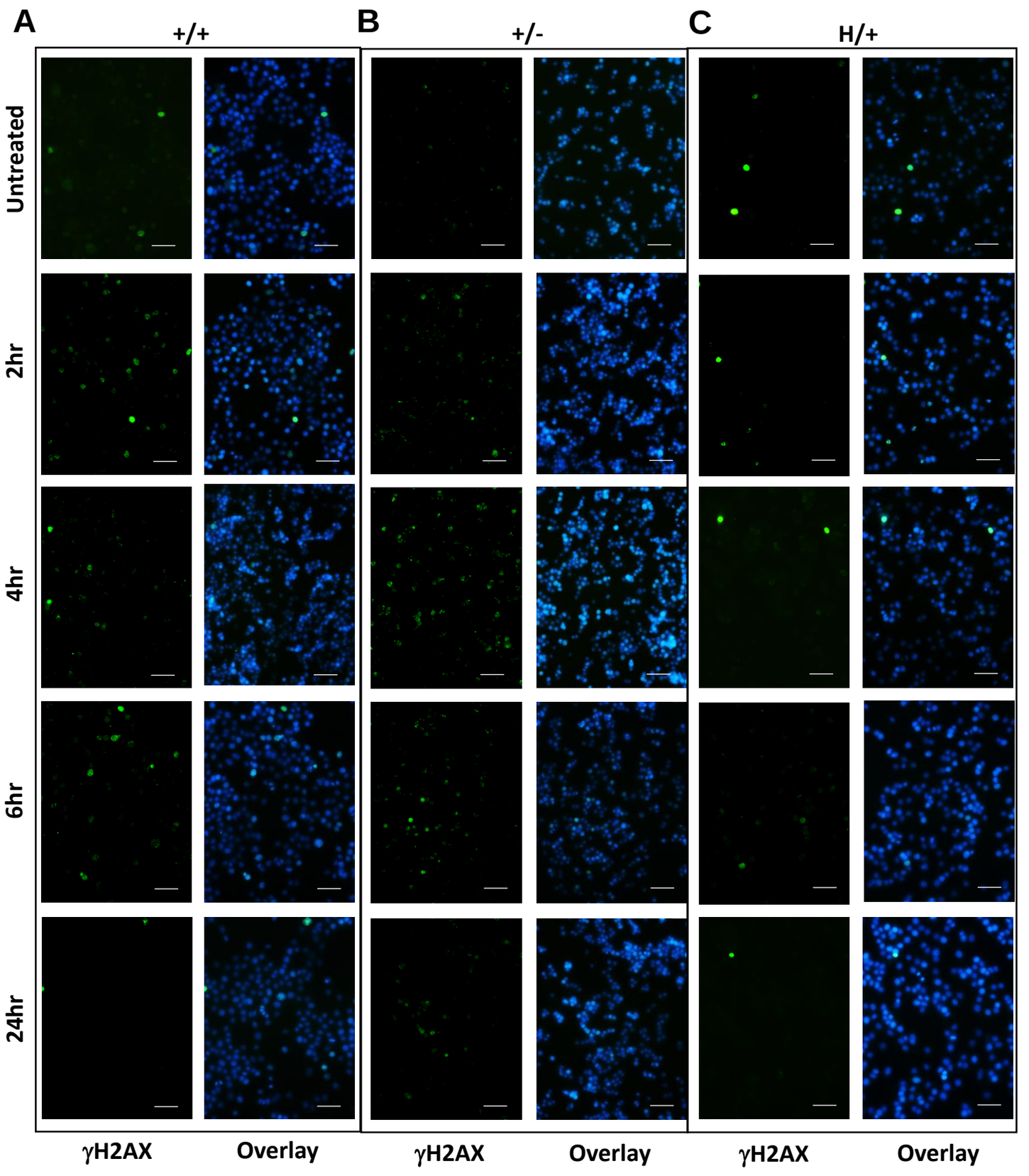
A
+/+
B
+/-
C
H/+
Untreated
2hr
4hr
6hr
24hr
γH2AX
Overlay
γH2AX
Overlay
γH2AX
Overlay

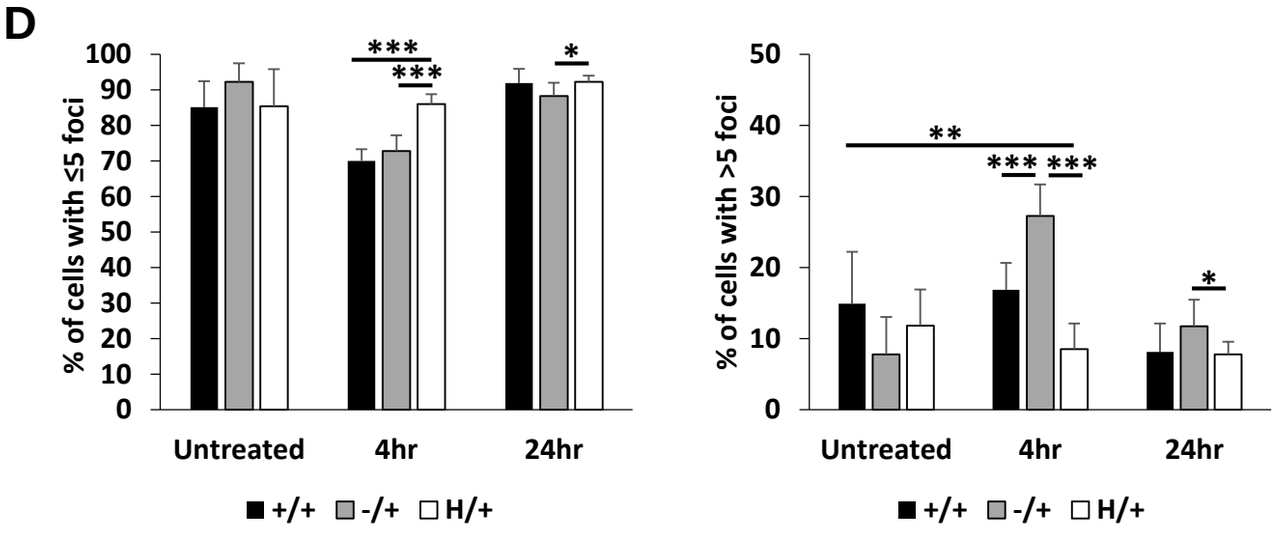
D
% of cells with ≤5 foci
100
90
80
70
60
50
40
30
20
10
0
***
***
*
Untreated
4hr
24hr
+/+
-/+
H/+
% of cells with >5 foci
50
40
30
20
10
0
**
***
***
*
Untreated
4hr
24hr
+/+
-/+
H/+

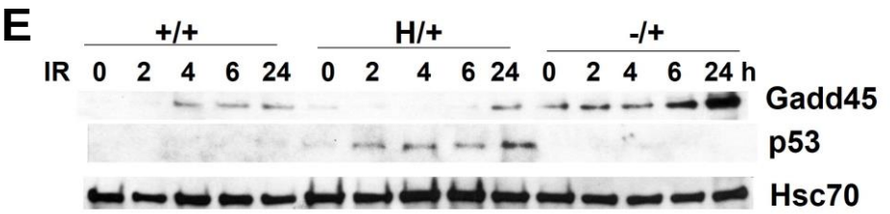
E
+/+
H/+
-/+
IR 0 2 4 6 24 0 2 4 6 24 0 2 4 6 24 h
Gadd45
p53
Hsc70

Figure 5

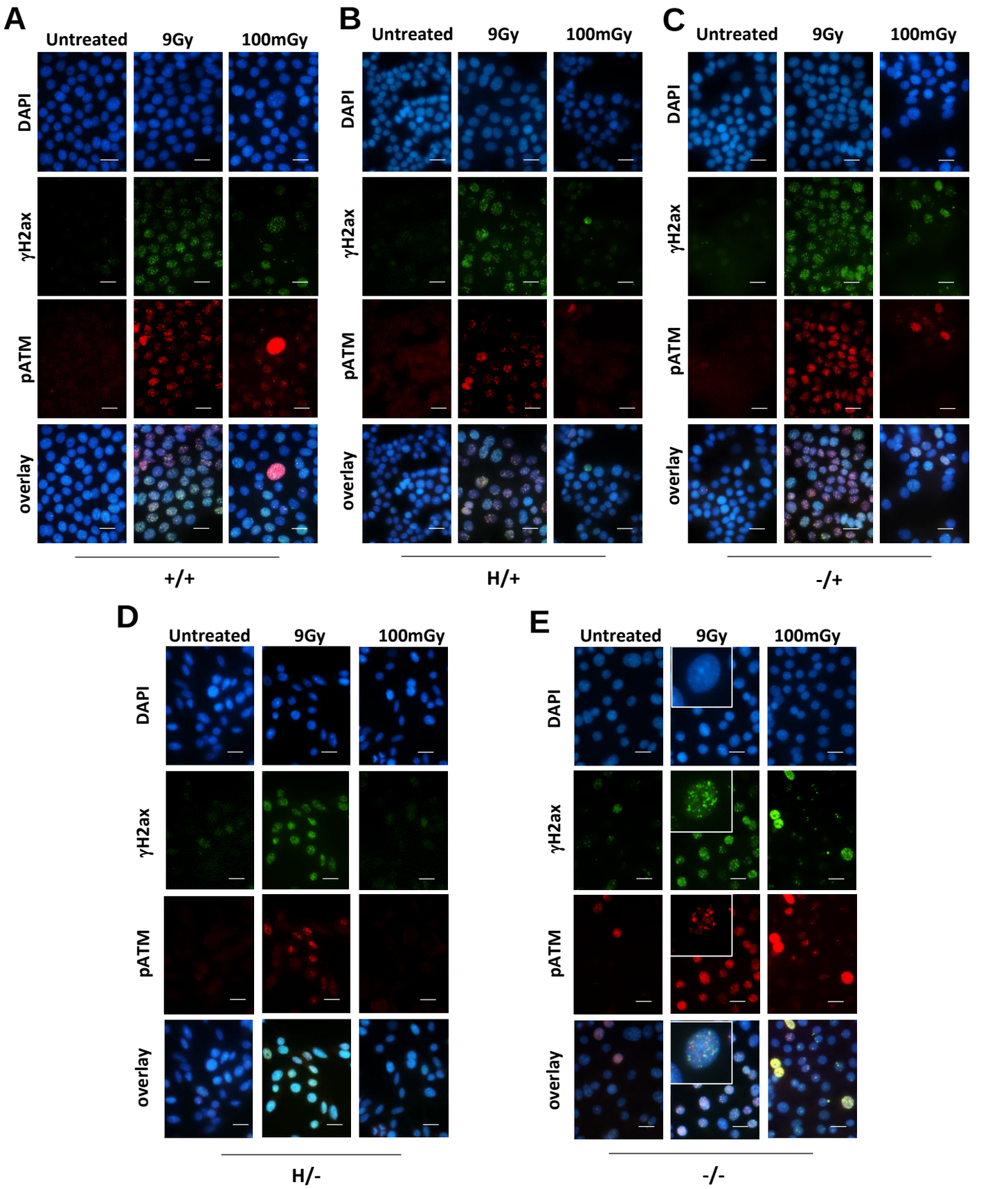
A
B
C
Untreated
9Gy
100mGy
DAPI
γH2ax
pATM
overlay
+/+
H/+
-/+
D
E
H/-
-/-
F
pATM
% of cells
100
80
60
40
20
0
***
$$$
&&&
###
$
*
+/+
-/+
H/+
H/-
-/-
Untreated
4hr-HDR
4hr-LDR
G
H/+
-/-
H/-
IR
0
2
4
6
24
6 h
γH2AX
HSC70

Figure 6

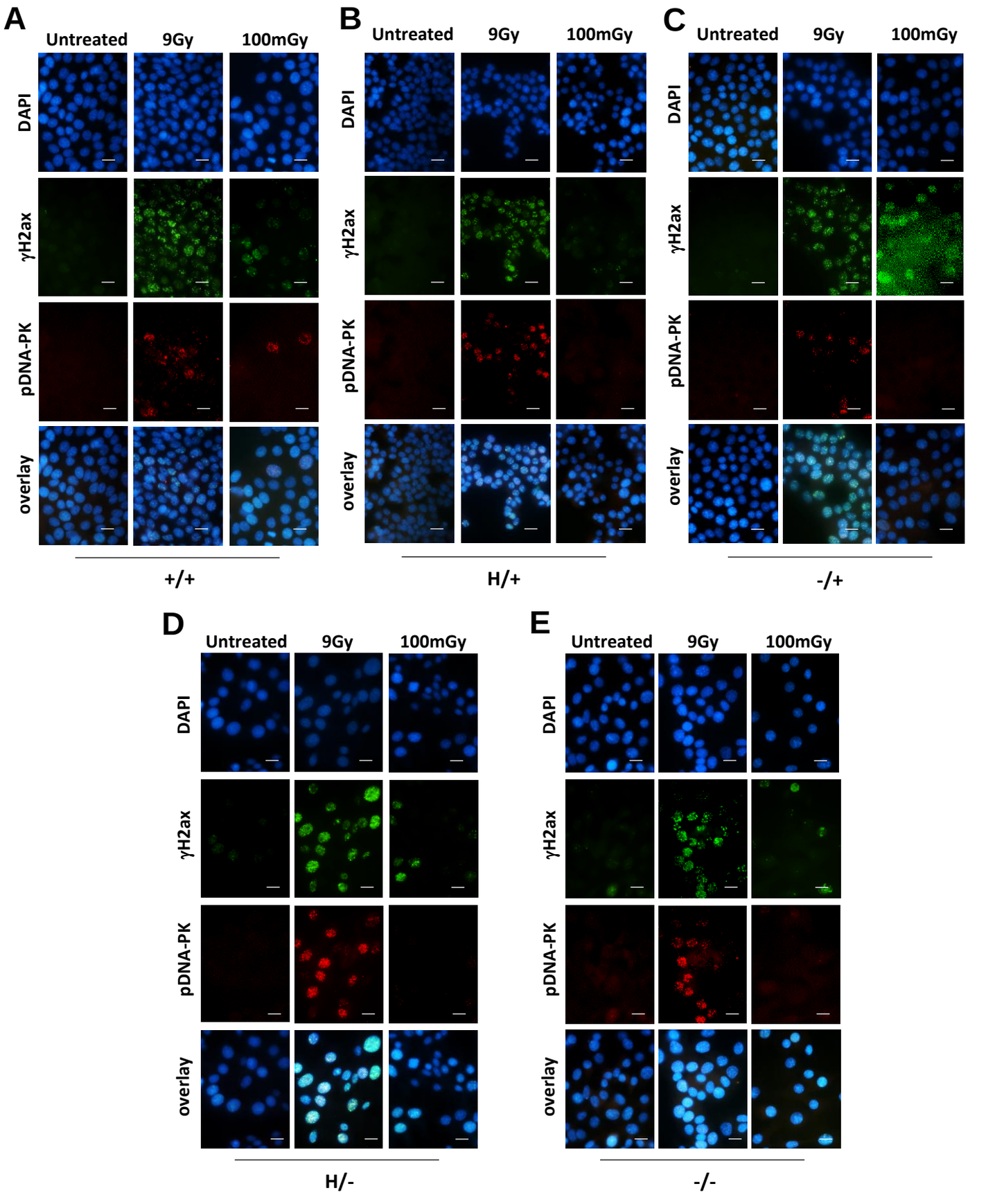
A
B
C
D
E
Untreated
9Gy
100mGy
DAPI
γH2ax
pDNA-PK
overlay
+/+
H/+
-/+
H/-
-/-

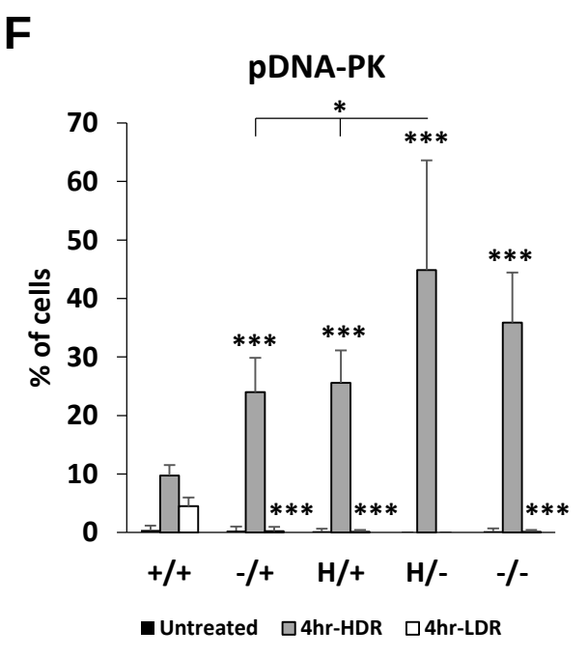
F
pDNA-PK
% of cells
70
60
50
40
30
20
10
0
*
***
+/+
-/+
H/+
H/-
-/-
Untreated
4hr-HDR
4hr-LDR

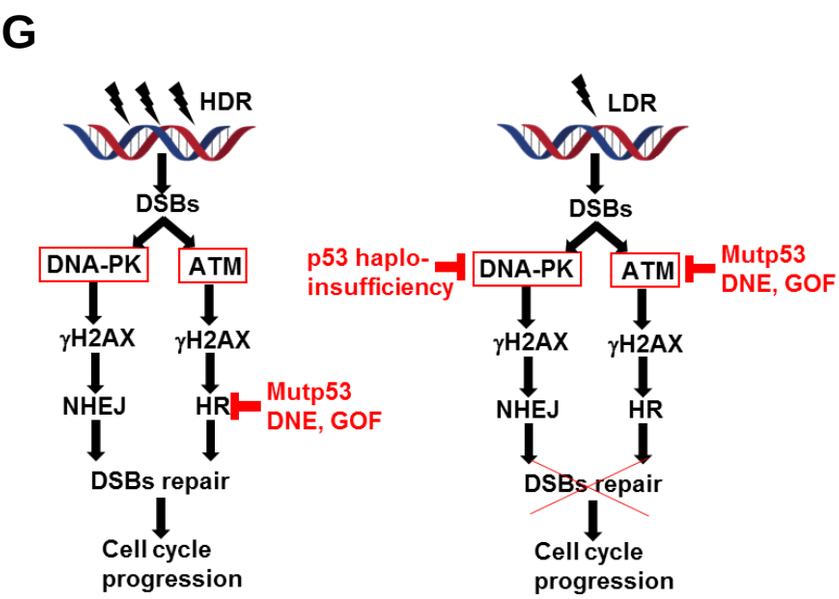
G
HDR
DSBs
DNA-PK
ATM
γH2AX
NHEJ
HR
Mutp53
DNE, GOF
DSBs repair
Cell cycle
progression
LDR
p53 haplo-
insufficiency

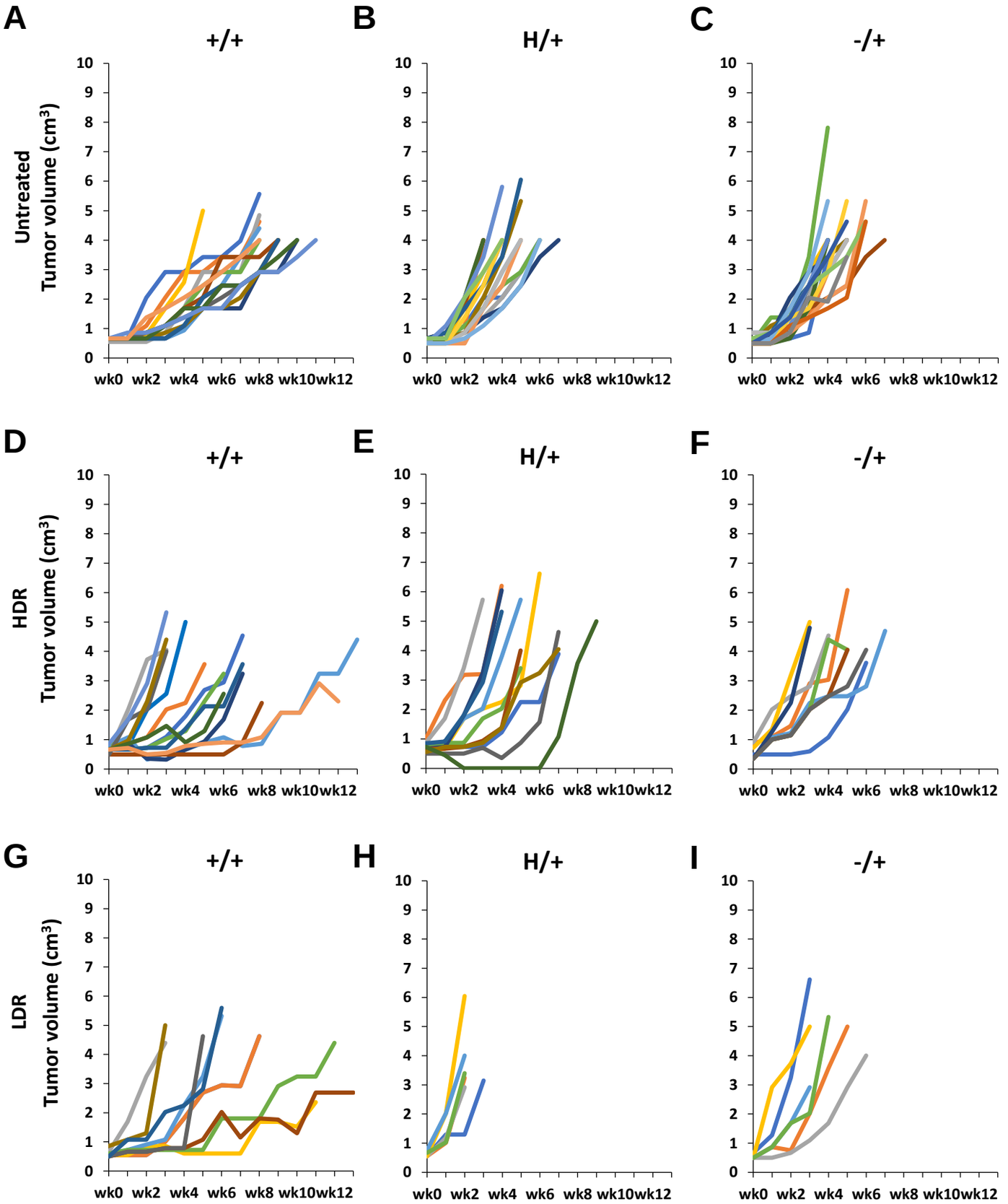

Supplemental Figure 1